The Eurasia Proceedings of Science, Technology, Engineering & Mathematics

EPSTEM

ICRETS 2022 SEPTEMBER

Volume 17, Pages 1-174 (September 2022)

The Eurasia Proceedings of Science, Technology, Engineering & Mathematics (EPSTEM)

e-ISSN: 2602-3199

©2022 Published by the ISRES Publishing

Address: Istanbul C. Cengaver S. No 2 Karatay/Konya/TURKEY

Website: www.isres.org

Contact: isrespublishing@gmail.com

Conference: ICRETS2022: International Conference on Research in Engineering, Technology and Science
Conference website: https://www.2022.icrets.net
Dates: July 01 – 04, 2022
Location: Baku, Azerbaijan
Edited by: Mehmet Ozaslan

About Editor(s)
Prof Dr. Mehmet Ozaslan
Department of Biology, Gaziantep University, Turkey
Website: http://mehmetozaslan.com/
Email: ozaslanmd@gantep.edu.tr

Language Editor(s)
Assoc. Prof. Dr. Kagan Buyukkarci
Department of English Language Education, Suleyman Demirel University, Turkey
Email: kaganbuyukkarci@sdu.edu.tr

Gabriel Delgado-Toral - Universidad Nacional Autónoma de México, Mexico
Gordana Savıc - University of Belgrade, Serbia
Irina Andreeva - Peter The Great St. Petersburg Polytechnic University, Russia
Isti Hıdayah - Semarang State University, Indonesia
Jose Manuel Lopez Guede - University of Basque Country, Spain
Kamil Yurtkan - Cyprus International University, Cyprus
Katsina Christopher Bala - Federal University of Technology, Minna, Nigeria
Khitam Shraim - Palestine Technical University, Palestine
Marija Stanıć - University of Kragujevac, Serbia
M. Hanefi Calp - Karadeniz Technical University, Turkey
Mohamed Ahmed - Mansoura University, Egypt
Mousa Attom- American University of Sharjah, U.A.E.
Nicu Bızon - Pitesti University, Romania
Pandian Vasant - Teknology Petronas University, Romania
Rajnalkar Laxman - Gulbarga University, India
Sanaa Al-Delaımy - Mosul University, Iraq
Shadi Aljawarneh - Jordan University of Science and Technology, Jordan
Shynar Baımaganbetova - Nazarbayev University, Kazakhstan
Svetlana Khan - Almaty University of Power Engineering and Telecommunications, Kazakhstan
Tunde Anifowose-Kelani, Siegener Sabithos College of Health Science & Technology, Nigeria
Yiyang Chen - Soochow University (CN), China
Zipporah Pewat Duguryil - Federal College of Education, Nigeria

ORGANIZING COMMITTEE

Aynur Aliyeva - Institute of Dendrology of Anas, Azerbaijan
Besnik Hajdari - University "isa Boletini" Mitrovica, Kosovo
Cemil Aydogdu - Hacettepe University, Turkey
Danielle Gonçalves de Oliveira Prado-Federal Technological University of Paraná, Brazil
Dariusz Jacek Jakóbczak - Technical University of Koszalin, Poland
Elman Iskender - Central Botanical Garden of Anas, Azerbaijan
Halil Snopce - South East European University, Macedonia
Ishtar Imad - Uruk University, Iraq
Jaya Bishnu Pradhan-Tribhuvan University, Mahendra Ratna Campus, Nepal
Mohammad Sarwar - Scialert, Dubai, United Arab Emirates
Murat Beytur - Kafkas University, Turkey
Samire Bagırova - Institute of Dendrology of Anas, Azerbaijan
Shafag Bagirova - Baku State University, Azerbaijan
Suhail Bayati - Hadi University College, Iraq
Tunde Anifowose-Kelani, Siegener Sabithos College of Health Science & Technology, Nigeria

Editorial Policies

ISRES Publishing follows the steps below in the procdings book publishing process.
In the first stage, the papers sent to the conferences organized by ISRES are subject to editorial oversight. In the second stage, the papers that pass the first step are reviewed by at least two international field experts in the conference committee in terms of suitability for the content and subject area. In the third stage, it is reviewed by at least one member of the organizing committee

for the suitability of references. In the fourth step, the language editor reviews the language for clarity.

Review Process

Abstracts and full-text reports uploaded to the conference system undergo a review procedure. Authors will be notified of the application results in three weeks. Submitted abstracts will be evaluated on the basis of abstracts/proposals. The conference system allows you to submit the full text if your abstract is accepted. Please upload the abstract of your article to the conference system and wait for the results of the evaluation. If your abstract is accepted, you can upload your full text. Your full text will then be sent to at least two reviewers for review**. The conference has a double-blind peer-review process**. Any paper submitted for the conference is reviewed by at least two international reviewers with expertise in the relevant subject area. Based on the reviewers' comments, papers are accepted, rejected or accepted with revision. If the comments are not addressed well in the improved paper, then the paper is sent back to the authors to make further revisions. The accepted papers are formatted by the conference for publication in the proceedings.

Aims & Scope

Engineering, technology and basic sciences are closely related fields. Developments and innovations in one of them affect the others. Therefore, **the focus of the conference** is on studies related to these three fields. Studies in the fields of engineering, technology and basic science are accepted to the conference even if they are not associated with other fields. The conference committee thinks that a study in only one field (for example, mathematics, physics, etc.) will contribute to other fields (for example, engineering, technology, etc.) in future studies, even if it is not associated with the presentation at the conference. In line with this perspective, studies in the following fields are accepted to the conference: Biology, Chemistry, Engineering, Mathematics, Physics and Technology. The aim of the conference is to bring together researchers and administrators from different countries, and to discuss theoretical and practical issues in all fields of Engineering, Technology and Basic Sciences.

Articles: 1-17

CONTENTS

Synthesis and Characterization of Gold/Silver Bimetallic Nanoparticles Using Trastuzumab: An Enhanced Anti-Cancer Activity

Muhammad SAFDAR
Gaziantep University

Mehmet OZASLAN
Gaziantep University

Abstract: Bimetallic nanoparticles are getting a lot of attention in medicine and society because they might have interesting physical and synthetic properties, such as higher affinity, a lower molecular weight, and a larger surface area. Trastuzumab capped gold/silver bimetallic nanoparticles (Au/Ag-BNPs) were prepared for the purpose of enhancing the effects of Au/Ag-BNPs on SKBR3 breast cancer cells in order to reduce trastuzumab resistance. Au/Ag-BNPs were produced chemically. These Au/Ag-BNPs were characterized using various techniques. UV-Visible (UV-Vis) spectroscopy were used to monitor Plasmon absorption maxima at 462 nm. X-ray powder diffraction (XRD) pattern was utilized to confirm the crystalline nature of the BNPs. Lastly, Fourier transformed infrared (FT-IR) spectroscopy was used to investigate the bonding patterns of the NPs. In SKBR3 human breast cancer cells, the biological characteristics of these NPs were exemplary. Based on the results, we concluded that these gold/silver bimetallic nanoparticles have anticancer potential and can serve as an alternative to decrease the trastuzumab resistance of SKBR3 breast cancer cells. However, additional research is required to corroborate these results.

Keywords: Bimetallic nanoparticles, Trastuzumab resistance, SKBR3 cells, Apoptosis

Introduction

Nanotechnology has gotten people interested in engineering, farming, medicine, and other fields (Safdar & Ozaslan, 2022; Safdar et al., 2021; Safdar et al., 2022; Safdar, Ozaslan, et al., 2019). In order to protect human and environmental health, research will concentrate on safer synthetic processes that use green methods, such as renewability, the use of non-toxic chemicals, the use of less energy, and time-conserving approaches (Mageswari et al., 2016). Nanoparticles with different sizes between 1 and 100 nm have been found to be very effective and have better results in a wide range of areas (Mejia et al., 2021). This is because they are very potent, have a wide base, can act as catalysts, absorb light, and have a robust compatibility. Metal NPs have also been shown to have good attributes in the areas of catalysis, mechanics, magnetism, temperature, light, photoelectrochemistry, and biology (Safdar & Ozaslan, 2022; Safdar et al., 2021; Safdar et al., 2022; Safdar, Ozaslan, et al., 2019). Metal NPs have been used as bacteriostatic agents, drug carriers, drug delivery, to treat cancer, for biosensing, and to speed up chemical reactions (Surapaneni et al., 2018). Scientists have used many different ways to make nanoparticles such as physical, chemical, and biological methods (Uzma et al., 2020). In the past, bimetallic nanoparticles have been developed and employed for a variety of biomedical applications, such as imaging, luminous tagging, labelling, and drug transporters (Smith et al., 2013). By regulating the diffusion of Cu into Au, atomically ordered intermetallic nanocrystals have been prepared using Au-Cu nanoparticles (Sra & Schaak, 2004). This concept offers a novel method for the fabrication of one-of-a-kind bimetallic nanoparticles. Au-Ni nanorods have been engineered as selectively functionalized DNA vehicles (Salem et al., 2003). Bimetallic silver/nickel nanoparticles excelled common catalysts owing to their relatively small size, novel physicochemical properties, and electrostatic impacts (Karaman, 2022). Trastuzumab

(Herceptin) is a monoclonal antibody that is used to treat breast cancer and stomach cancer (Rebischung et al., 2005). It is only used to treat cancers that have HER2 receptors. It can be used by itself or with other medicines for chemotherapy (Safdar et al., 2020; Safdar et al., 2019). One of the major problems with using trastuzumab to treat people with breast cancer is trastuzumab resistance (Maximiano et al., 2016). In the last ten years, many tests have been done to figure out how trastuzumab resistance happens with or without extra drugs, but they failed yet (Maximiano et al., 2016). To best our knowledge, there is no study related to synthesize and characterize trastuzumab capped gold/silver bimetallic nanoparticles (Au/Ag BNPs) to target HER2 receptors via MTT, relative gene and protein expressions on SKBR3 breast cancer cells. The aimed of this study was to synthesize, characterize and analyze novel trastuzumab capped gold/silver bimetallic nanoparticles (Au/Ag BNPs) to target HER2 receptors via MTT and relative gene expressions on SKBR3 breast cancer cells.

Methods

Bimetallic Au/Ag nanoparticles

In order to generate 1.5 mM solutions of gold and silver salt, 0.021 g of $AuSO_4$ and 0.022 g of $AgNO_3$ were dissolved in 100 mL of deionized water in two separate measuring flasks. A 500 mL flask was filled with 40 mL of a binary salt aqueous solution (1.5 mM) and 1 mL of trastuzumab solution. The flask was set on a hot plate at 55-50 °C and 1300 rpm for an hour, and a magnetic stirrer was used to keep the mixture moving. Because metal salts were quickly broken down, bimetallic nanoparticles were made, and the colour of Ag/Au BNPs changed from light yellow to dark yellow as they formed. Several analytical techniques were used to find out about the size, shape, form, crystallinity, and potential of dried bimetallic nanoparticles. The Ag/Au BNPs were used as a nanomedicine for SKBR3 breast cancer cell treatment. These nanoparticles were characterized by various techniques such as UV Visible, FTIR, SEM, TEM and XRD.

Cell culture

Breast cancer cell line (SKBR3) and immortal breast epithelial cell line (CRL-4010) were cultured and grown in the petri dished under laboratory optimized conditions. When they reached on the optimum condition, then they were harvested and RNA was extracted (Safdar & Ozaslan, 2022).

Cell Viability

Cell viability was assessed using the MTT assay according to the protocol mentioned on the kit. Cells grown at a density of 3000 cells/well were exposure to Au/AgNPs, for 24 h in a 96 well plate. Absorbance was measured at 505 nm wavelength using a microplate spectrophotometer (Molecular Devices).

Analysis of gene expression

A reverse transcription assay kit was used to obtain cDNA (Qiagen, Germany). HER2, and GAPDH gene expression levels (housekeeping gene). 2.5 Statistical analysis Corbet Rotor-Gene software was used to examine the data collected. Considerable downregulation was defined as a fold change (2Ct) value of 0.1 to 0.5, whereas significant upregulation was defined as a value of >2.0.

Results and Discussion

After treatment with Au/AgNPs, the expression level of HER2 and cell survival of both cell lines were assessed using the MTT test and quantitative Real-time PCR (qRT-PCR). It was shown that Au/Ag bimetallic NPs reduced the levels of HER2 expression in the SKBR3 breast cancer cell line. However, prior to receiving therapy with Au/AgNPs, the SKBR3 breast cancer cell line had significant high levels of HER2 expression. Additionally, the downregulation of NF-kB and simultaneous overexpression of p53 following Au/AgNPs therapy revealed that HER2 receptors were downregulated through reduced Trastuzumab resistance. This study is one of the first of its kind since it shows a connection between the NF-B, p53, and HER2 following treatment with Au/Ag bimetalic NPs (Fig. 1 & 2).

CRL-4010 VS SKBR3
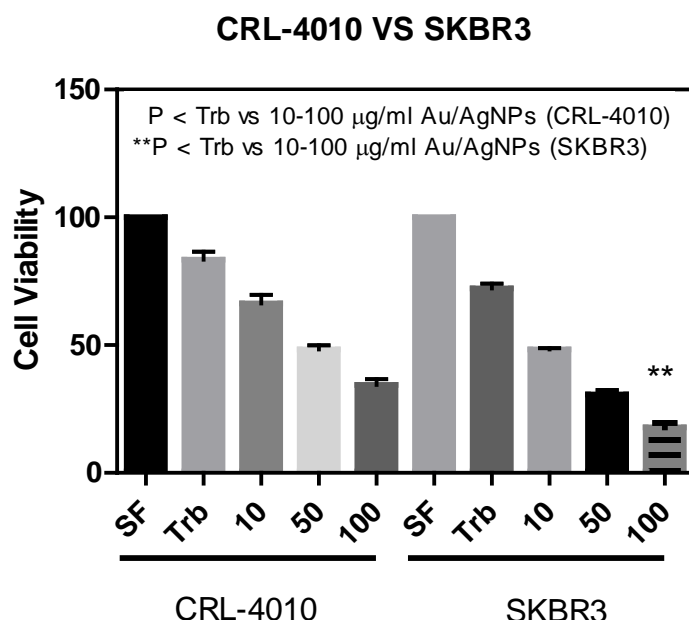
Figure 1. Au/AgNPs has decreased significantly the living cells in SKBR3 when compared with CRL-4010 cells. The 10-100µg/mL Au/AgNPs concentrations were exposed to both cell lines via MTT assay. The results have been expressed as *$P \leq 0.01$, and **$P \leq 0.001$.

CRL-4010 VS SKBR3
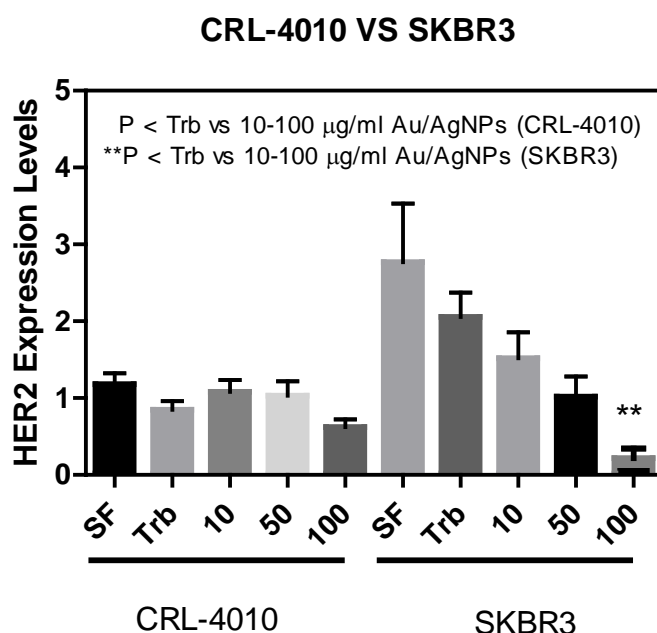
Figure. 2. HER2 expression levels are overexpressed in SKBR3 cell lines. Au/AgNPs has decreased HER2 gene expression levels significantly in SKBR3 when compared with CRL-4010 cells. The 10-100µg/mL Au/AgNPs concentrations were exposed to both cancer and normal cell lines via qRTPCR assay. The results have been expressed as *$P \leq 0.01$, and **$P \leq 0.001$.

HER2-positive breast cancer cells have been targeted with metallic nanoparticles (Dziawer et al., 2019; Maximiano et al., 2016; Rebischung et al., 2005). However, because of the focus on cellular absorption, we deemed the same results as (Kulhari et al., 2016) to be noteworthy and worth addressing in this study. The cellular absorption of trastuzumab was investigated in parallel (Kulhari et al., 2016). The results were compared to the SKBR3 HER2-positive breast cancer cell line and the CRL4010 cell line (Wege et al., 2014). The uptake efficiency of nanoparticles in combination with trastuzumab was compared. The fluorescence intensity was higher in the nanoparticles, indicating that increased uptake occurred due to the targeting mechanism, which

could lead to a reduction in SKBR3 malignancies in women (Mi et al., 2012). As a result, these bimetallic nanoparticles are crucial for future use in nanomedicine applications.

Conclusion

The expression levels of HER2 in breast cancer cell line (SKBR3) were increased/decreased on a particular concentration (10-100μg/mL) of gold and silver bimetallic nanoparticles. In addition, the downregulation of HER2 after Au/AgNPs treatment displayed a particular pathway. These results showed that expression levels of NFκB, p53 and HER2 genes were modified via Au/Ag bimetallic treatments.

Recommendations

This article will lead the scientists to focus on HER2 overexpression control via newly synthesized bimetallic nanoparticles.

Scientific Ethics Declaration

The authors declare that the scientific ethical and legal responsibility of this article published in EPSTEM journal belongs to the authors.

Acknowledgements or Notes

References

Dziawer, Ł., Majkowska-Pilip, A., Gaweł, D., Godlewska, M., Pruszyński, M., Jastrzębski, J., . . . Bilewicz, A. (2019). Trastuzumab-modified gold nanoparticles labeled with 211At as a prospective tool for local treatment of HER2-positive breast cancer. *Nanomaterials*, *9*(4), 632.

Karaman, C. (2022). Engineering of N, P, S-Triple doped 3-dimensional graphene architecture: Catalyst-support for "surface-clean" Pd nanoparticles to boost the electrocatalysis of ethanol oxidation reaction. *International Journal of Hydrogen Energy*. https://doi.org/10.1016/j.ijhydene.2022.02.093

Kulhari, S., Bharti, N., Bala, I., Arora, S., & Singh, G. (2016). Efficacy of pectoral nerve block versus thoracic paravertebral block for postoperative analgesia after radical mastectomy: a randomized controlled trial. *BJA: British Journal of Anaesthesia*, *117*(3), 382-386.

Mageswari, A., Srinivasan, R., Subramanian, P., Ramesh, N., & Gothandam, K. M. (2016). Nanomaterials: classification, biological synthesis and characterization. In *Nanoscience in Food and Agriculture 3* (pp. 31-71). Springer.

Maximiano, S., Magalhaes, P., Guerreiro, M. P., & Morgado, M. (2016). Trastuzumab in the treatment of breast cancer. *BioDrugs*, *30*(2), 75-86.

Mejia, S. P., Sánchez, A., Vásquez, V., & Orozco, J. J. F. i. p. (2021). Functional nanocarriers for delivering itraconazole against fungal intracellular infections. *12*.

Mi, Y., Liu, X., Zhao, J., Ding, J., & Feng, S.-S. (2012). Multimodality treatment of cancer with herceptin conjugated, thermomagnetic iron oxides and docetaxel loaded nanoparticles of biodegradable polymers. *Biomaterials*, *33*(30), 7519-7529.

Rebischung, C., Barnoud, R., Stéfani, L., Faucheron, J.-L., & Mousseau, M. (2005). The effectiveness of trastuzumab (Herceptin) combined with chemotherapy for gastric carcinoma with overexpression of the c-erbB-2 protein. *Gastric Cancer*, *8*(4), 249-252.

Safdar, M., & Ozaslan, M. (2022). Enhanced Catalytic, Antibacterial and Anti-cancer Activities of Erythromycin Capped Gold Nanoparticles. *Journal of Inorganic and Organometallic Polymers and Materials*, 1-9.

Safdar, M., Ozaslan, M., & Junejo, Y. (2021). Synthesis, Characterization and Employed Doxycycline Capped Gold Nanoparticles on TRP Channel Expressions in SKBR3 Breast Cancer Cells and Antimicrobial Activity. *Journal of Cluster Science*, 1-8.

Safdar, M., Ozaslan, M., Junejo, Y., & Channa, I. S. (2022). Cytotoxic and anticancer activity of a novel synthesized tet-AuNPs simultaneously activates p53 and inhibits NF-kB signaling in SKBR3 cell line. *Toxicology and Environmental Health Sciences*, *14*(1), 69-76.

Safdar, M., Ozaslan, M., Khailany, R. A., Latif, S., Junejo, Y., Saeed, M., . . . Kanabe, B. O. (2019). Synthesis, Characterization and Applications of a Novel Platinum-Based Nanoparticles: Catalytic, Antibacterial and Cytotoxic Studies. *Journal of Inorganic and Organometallic Polymers and Materials*. https://doi.org/10.1007/s10904-019-01387-7

Safdar, M., Ozaslan, M., Khailany, R. A., Latif, S., Junejo, Y., Saeed, M., . . . Kanabe, B. O. (2020). Synthesis, characterization and applications of a novel platinum-based nanoparticles: catalytic, antibacterial and cytotoxic studies. *Journal of Inorganic and Organometallic Polymers and Materials*, *30*(7), 2430-2439.

Safdar, M., Qumar, G. M., Saravanan, M., Khailany, R. A., Ozaslan, M., Gondal, M. A., . . . Junejo, Y. J. J. o. C. S. (2019). Synthesis and characterization of Cefditoren capped silver nanoparticles and their antimicrobial and catalytic degradation of Ibuprofen. *Journal of Cluster Science, 30*(6), 1663-1671.

Salem, A. K., Searson, P. C., & Leong, K. W. (2003). Multifunctional nanorods for gene delivery. *Nature materials*, *2*(10), 668-671.

Smith, D. M., Simon, J. K., & Baker, J. R., Jr. (2013). Applications of nanotechnology for immunology. *Nat Rev Immunol*, *13*(8), 592-605. https://doi.org/10.1038/nri3488

Sra, A. K., & Schaak, R. E. (2004). Synthesis of atomically ordered AuCu and AuCu3 nanocrystals from bimetallic nanoparticle precursors. *Journal of the American Chemical Society*, *126*(21), 6667-6672.

Surapaneni, S. K., Bashir, S., & Tikoo, K. (2018). Gold nanoparticles-induced cytotoxicity in triple negative breast cancer involves different epigenetic alterations depending upon the surface charge. *Sci Rep*, *8*(1), 12295. https://doi.org/10.1038/s41598-018-30541-3

Uzma, M., Sunayana, N., Raghavendra, V. B., Madhu, C. S., Shanmuganathan, R., & Brindhadevi, K. (2020). Biogenic synthesis of gold nanoparticles using Commiphora wightii and their cytotoxic effects on breast cancer cell line (MCF-7). *Process Biochemistry*, *92*, 269-276.

Wege, A. K., Schmidt, M., Ueberham, E., Ponnath, M., Ortmann, O., Brockhoff, G., & Lehmann, J. (2014). Co-transplantation of human hematopoietic stem cells and human breast cancer cells in NSG mice: a novel approach to generate tumor cell specific human antibodies. MAbs, In MAbs (Vol. 6, No. 4, pp. 968-977). Taylor & Francis.

Author Information

Muhammad Safdar
Department of Biology, Division of Molecular Biology and Genetics, Gaziantep University, Gaziantep 27310, Turkey
Contact e-mail: *drmuhammadsafdar8@gmail.com*

Mehmet Ozaslan
Department of Biology, Gaziantep University
Gaziantep 27310, Turkey

To cite this article:

Synthesis of Iron-containing Nanoparticles from Iron-Steel Industrial Waste for Adsorption of Malachite Green

Deniz UZUNOGLU
Mersin University

Ayla OZER
Mersin University

Abstract: For the synthesis of iron-containing nanoparticles (FeNPs), the iron ions were recovered from iron-steel industrial waste by leaching method followed by the chemical precipitation of ferric hydroxide with NH_3. The ferric hydroxide was reduced pyrometallurgical to iron-containing nanoparticles by the reducing agent of CO generated from charcoal. FeNPs were characterized by XRD and SEM analysis. XRD results showed that FeNPs had predominantly face-centered cubic Fe_3O_4 structure, besides, the peaks of Fe_2O_3 and Fe^0 structures were also observed. The particle size of FeNPs was calculated as 57.75 nm using Williamson–Hall equation. According to SEM images, FeNPs had homogeneous and spherical-like structures; also, the structures partially decomposed and the particle size increased due to the agglomeration of the particles after adsorption. FeNPs were used as an adsorbent for the removal of Malachite Green (MG). The experimental design and the optimization of experimental conditions were investigated by using response surface methodology (RSM) according to central composite design (CCD). The optimum experimental conditions were determined as 180 min contact time, 75 °C temperature, and 300 mg/L initial MG concentration. The agreement between the adsorbed MG concentrations at the equilibrium (q_e) calculated from the model (148.43 mg/g) and determined experimentally (146.63 mg/g) under the optimum conditions showed that the selected model was suitable for MG adsorption by FeNPs. Langmuir isotherm model had higher R^2 and lower ARE values than Freundlich isotherm model, showing that the equilibrium data of MG adsorption with FeNPs was the best agreement to Langmuir isotherm model with the maximum monolayer coverage capacity of 175.44 mg dye/g FeNPs. The thermodynamic studies suggested that the adsorption process was endothermic, spontaneous at the optimum conditions, and the positive ΔS value indicated the increased disorder at the solid-solution interface during the adsorption.

Keywords: Iron-containing nanoparticles, Pyrometallurgical nanoparticle synthesis, Response surface methodology, Adsorption, Malachite Green

Introduction

Textile industries consume large quantities of water and so large quantities of wastewater containing synthetic dyes causing significant environmental pollution due to their toxic, carcinogenic, teratogenic or mutagenic nature were discharged into receiving water environment (Deb et al., 2021). These dyes have a non-biodegradable and stable against oxidizing agents structure, which makes them difficult to remove from the aqueous solutions. Color is the first detectable contaminant in this type of wastewaters and should be removed before it is discharged into receiving water environment. There are several physical, chemical, biological, and advanced separation methods for color removal, which is listed in Table 1 (Gadekar & Ahammed, 2019). Among the methods listed in Table 1, adsorption has a long-standing background and still continues to attract great attention due to some advantages such as low cost, a wide variety of adsorbents, high removal efficiency, regeneration possibility, and lower energy requirement (Harja et al., 2022).

Table 1. Color removal methods

Physical methods	Chemical methods	Biological methods	Advanced methods
Sedimentation Float (Flotation) Membrane processes	Oxidation Chemical Precipitation Electrochemical degradation Chemical reduction/oxidation	Aerobic/anaerobic treatment Activated sludge process	Improved ultrafiltration Electrodialysis Integrated chemical-biological degradation Reverse osmosis Ion exchange Adsorption

The types and properties of adsorbents affect adsorption processes. There are various adsorbent types used in the adsorption of dyes from wastewaters and they are listed in Table 2 (Harja et al., 2022). Among them, nanomaterials have higher adsorption capacities than the others due to their higher surface/volume ratio. Nanomaterials can be synthesized by physical, chemical, and biological methods or hybrid methods that are combinations of several of them (Patra & Baek, 2014). The synthesis costs of nanomaterials with high adsorption capacity are relatively high and this cost can be reduced by using agricultural or industrial waste. The iron-steel industry produces tons of waste materials containing iron oxides, heavy metals, and other different contaminants. Disposing of them in landfills causes environmental pollution because they release toxic substances to soil and groundwater (Kargin et al., 2022). Iron-steel slag has the most significant industrial waste volumes and more than 400 million tons of iron and steel slag were produced worldwide in 2017. If such a large volume of waste materials is effectively recycled, not only the environmental pollution and disposal costs would reduce, but also new cheap technologies would assert for developing advanced materials such as micro/nano materials (Schoeman et al., 2021). With this viewpoint, in this study, iron-containing nanoparticles, a synthetic adsorbent, were synthesized via chemical precipitation followed by pyrometallurgical reduction with the intent of converting an industrial waste to a value-added advanced product. In addition to these studies, the experimental design, the optimization of experimental conditions, and the two-way interaction between the independent variables were investigated by using response surface methodology (RSM) according to central composite design (CCD) for the adsorption of MG by FeNPs. Response surface methodology (RSM) is a widely-used statistical technique applied in order to optimize independent variables to achieve maximum or minimum response through a series of experiments. There are some limitations of the conventional optimization technique of the one-factor variable approach such as the requirement of a large number of experimental data and inadequate explanation of the interactive relation between multiple process parameters. These limitations of the conventional technique can be overcome by optimizing all the independent variables collectively by central composite experimental design via RSM, which reduces the runs of experiments resulting in cost and timesaving. So, RSM has been frequently used in the optimization of the adsorption process in recent years (Deb et al., 2021; Nguyen et al., 2022).

Table 2. Adsorbent types

Natural adsorbents	Synthetic adsorbents	Agricultural waste	Industrial waste
Algae Clays Zeolites Silicon ores Iron oxides	Activated carbon Fullerenes Hydrochar Chitin/chitosan Hydroxyapatite Polymers Micro/nano materials Micro/nano composites	Sawdust Wood splinter Tree bark Cone Fruit and vegetable peels Nut shells Wheat straw Rice husk Corncob Sugarcane pulp Animal pulp	Waste paper Cotton linter waste Waste cigarette filters Fly ash Iron-steel industrial waste Red mud Metal hydroxide waste Aluminum sulphate waste Treatment sludge waste tire Blast furnace slag

Method

Synthesis and Characterization of Iron-containing Nanoparticles

For the synthesis of iron-containing nanoparticles (FeNPs); the components in the iron-steel industrial waste were firstly leach out by treatment with HCl, then a precipitation was formed by NH_3 solution, and finally FeNPs were synthesized via the pyrometallurgical reduction using charcoal as the reductant agent. Accordingly;

the iron-steel industrial waste and concentrated HCl solution (35 wt%) were mixed in an Erlenmeyer-flask at a ratio of solid:liquid=1:6 and this mixture was magnetically stirred for 1 h at 80 °C for leaching out the components in the waste into HCl. After cooling of the resulting mixture, the acid insoluble residue was separated by centrifuge at 3460 RCF for 5 min and the obtained leach solution was analyzed by Inductively Coupled Plasma-Mass Spectrometer (ICP-MS, Agilent, Japan). Then, the desired amount of concentrated NH_3 solution (25 wt%) was added to the leach solution until the precipitate formation was over. The formed precipitate as a result of the reaction between NH_3 and the leach solution was separated by centrifuge at 3460 RCF for 5 min, washed with 1.0% HCl followed by distilled water to remove the excess NH_3 and soluble impurities and finally dried in the stove at 105°C for 12 h. After that, FeNPs were synthesized via pyrometallurgical reduction method using charcoal and the obtained precipitate. Accordingly, certain amounts of the precipitate and charcoal were taken into porcelain crucibles separately, and they were heated in the muffle furnace at 1200 ºC for 4 h. FeNPs formed as a result of the reaction between the precipitate and CO generated from the charcoal. Finally, the obtained FeNPs were washed with distilled water and dried in the stove at 105°C for 12 h (Giri et al., 2011). The synthesized FeNPs were characterized with X-ray diffractometer (XRD) and scanning electron microscopy (SEM). The XRD pattern was collected on a Rigaku (Japan) diffractometer with CuKα radiations in diverse angle range (2θ) of 10–90°, operating at the tube voltage of 40 kV and a tube current of 30 mA. The morphological examination was performed on Zeiss (Germany) field emission scanning electron microscopy.

Experimental Design and Optimization using Response Surface Methodology

The experimental design and the optimization of experimental conditions of the adsorption of MG by FeNPs were investigated by using response surface methodology (RSM) according to central composite design (CCD). The independent variables were chosen as contact time, temperature, and initial dye concentration; and the adsorbed dye amount per gram of adsorbent at the predetermined contact time (Y:mg dye/g adsorbent) was set down as dependent response variable. The ranges and the levels of the independent variables for the adsorption of MG by FeNPs are presented in Table 3.

Table 3. The ranges and the levels of the independent variables for the adsorption of MG by FeNPs

Symbol	Independent variable	Coded ranges and levels		
		Low (−1)	Center (0)	High (+1)
A	Contact time (min)	10	95	180
B	Temperature (°C)	25	50	75
C	Initial dye concentration (mg/L)	100	200	300

Table 4. The experimental design and the responses for the adsorption of MG by FeNPs

Run order	Independent variables and responses				Run order	Independent variables and responses			
	A	B	C	Y		A	B	C	Y
1	95	25	200	39.21	21	10	25	300	0.43
2	95	50	200	79.48	22	10	25	300	0.45
3	180	50	200	85.84	23	10	75	100	4.82
4	95	50	300	93.37	24	180	25	100	25.96
5	95	75	200	91.27	25	10	75	100	4.75
6	95	50	100	47.37	26	95	50	200	79.33
7	95	25	200	39.50	27	180	25	100	25.81
8	95	75	200	89.19	28	95	50	200	78.53
9	180	50	200	85.82	29	95	50	200	78.69
10	95	50	200	78.66	30	180	25	300	95.40
11	95	50	200	78.63	31	10	25	100	0.33
12	95	50	200	78.84	32	180	25	300	92.65
13	95	50	300	94.00	33	95	50	200	78.56
14	10	50	200	2.77	34	10	25	100	0.32
15	95	50	100	47.43	35	10	75	300	40.51
16	10	50	200	2.83	36	95	50	200	79.15
17	95	50	200	79.74	37	180	75	100	51.42
18	180	75	300	146.94	38	10	75	300	40.52
19	95	50	200	78.80	39	180	75	100	51.28
20	180	75	300	146.86	40	95	50	200	79.15

The experimental design as well as the responses for the effect of three independent variables in 40 runs of experiments were given in Table 4. The obtained responses were treated to develop an empirical model which correlated the response to the independent variables using a second-degree polynomial equation as given by the following equation (Dargahi et al., 2021):

$$Y = \beta_0 + \sum_{i=1}^{k} \beta_i x_i + \sum_{i=1}^{k} \beta_{ii} x_i^2 + \sum_{i=1}^{k-1} \sum_{j=i+1}^{k} \beta_{ij} x_i x_j + \varepsilon \qquad \text{Eq. (1)}$$

where Y is the predicted response, β_0 is the constant coefficient, β_i is the linear coefficient, β_{ij} is the interaction coefficient, β_{ii} is the quadratic coefficient, x_i and x_j are the coded values of the adsorption of MG by FeNPs. The interaction between the independent variables and the responses were tested by using ANOVA and the effect of the variables was also evaluated with response surface graphs.

Adsorption of Malachite Green by FeNPs

The experiments of the adsorption of MG by FeNPs were carried out according to the central composite design matrix given in Table 4. The adsorption experiments were performed out in Erlenmeyer flasks (250 mL) containing 100 mL of MG dye solutions. 1.0 g/L of the adsorbent (FeNPs) was blended with MG dye solution at natural pH and known initial MG concentration (100−300 mg/L). Then, the flasks were shaken in the agitation vessel at desired temperatures and constant shaking rate. The samples were taken at the predetermined contact time and then were separated from the adsorbent by centrifugation at 3460 RCF for 5 min. The unadsorbed MG dye concentration in supernatant was analyzed at 618 nm wavelength with UV–vis spectrophotometer. Experiments were repeated for different contact time, temperature, and initial dye concentration values (Karacabey et al., 2019). The adsorbed dye amount per gram of adsorbent at the predetermined contact time, q_t (mg/g), was calculated as follows:

$$q_t = (C_0 - C_t)/X_0 \qquad \text{Eq. (2)}$$

where C_0 is the initial dye concentration (mg/L), C_t is the dye concentration at the predetermined contact time (mg/L), and X_0 is the adsorbent concentration (g/L).

Results and Discussion

Synthesis Steps of FeNPs

The illustration of the synthesis steps of FeNPs was presented in Figure 1. In order to explain the formation of FeNPs, the prepared leach solution was analyzed by ICP-MS and the results were given in Table 5. The results of ICP-MS showed that the obtained leach solution was in the form of $FeCl_3$ in view of the mole ratio between Fe and Cl ions. In the formation step of $FeCl_3$, the ferric iron (Fe^{3+}) was firstly recovered from the iron-steel industrial waste, and then the experiment was continued for the reaction between Fe^{3+} and HCl to take place resulting in $FeCl_3$. After that, NH_3 solution was added to $FeCl_3$ solution until the precipitate formation was over; in this step, the reaction took place between NH_3 and $FeCl_3$ resulting in ferric hydroxide. In the last synthesis step, the pyrometallurgical reduction was carried out in the muffle furnace. Accordingly, CO formed as a result of the combustion of coal, and the resulting CO reduced the ferric hydroxide to form FeNPs.

Table 5. ICP-MS results of the leach solution

Element	mg/L	Number of Moles
Cl	170.2	
Mg	104.3	
Fe	89.37	
Cr	74.83	Base: 1 L solution
Ca	68.79	Number of Moles (n): (Mass)/(Molar Mass)
Na	42.87	n_{Cl}: (170.2 mg) / (35.5 mg/mmole) = 4.79 mmole
Al	10.77	n_{Fe}: (89.37 mg) / (55.84 mg/mmole) = 1.60 mmole
Si	1.132	Empirical formula: $Fe_{1.6}Cl_{4.79} \sim FeCl_3$
Zn	1.093	
Ti	0.773	
Cu	0.489	

Figure 1. The synthesis steps of FeNPs

Characterization of FeNPs

XRD analysis was carried out to determine the crystal structure and phase state of FeNPs. The characteristic peaks in XRD pattern of FeNPs (Figure 2) belong to the phases of Fe_3O_4, Fe_2O_3, and Fe^0 (Gandha et al., 2016; Khuyen et al., 2018) were given in Table 6.
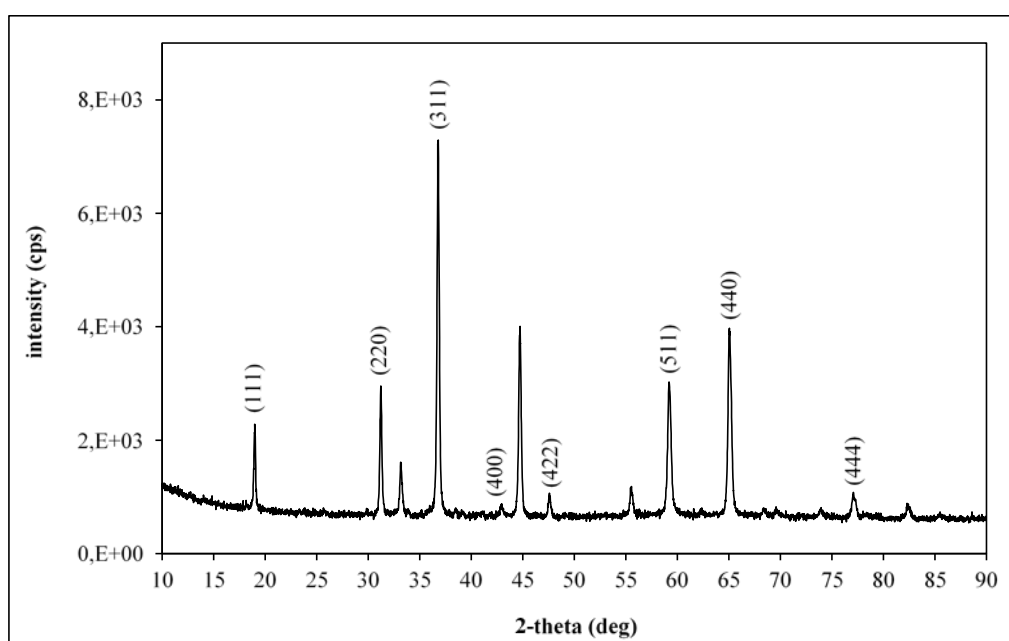
Figure 2. XRD pattern of FeNPs

Table 6. The characteristic peaks of the different phases of FeNPs

Phase	Plane	2-theta (deg)
Fe$_3$O$_4$	(111)	18.99°
	(220)	31.22°
	(311)	36.77°
	(400)	42.98°
	(422)	55.49°
	(511)	59.19°
	(440)	65.05°
	(444)	77.08°
Fe$_2$O$_3$	(104)	33.14°
	(110)	36.77°
	(024)	47.57°
	(116)	55.49°
Fe^0	(110)	44.69°
	(211)	82.36°

The particle size of FeNPs was calculated using the obtained characteristic XRD peaks according to Williamson–Hall equation given below (Irfan et al., 2018; Kahouli et al., 2015):

$$\beta.\cos\theta = (K\lambda/D) + 4\,\varepsilon.\sin\theta \qquad\qquad \text{Eq. (3)}$$

where β is the expanded diffraction peak measured at FWHM (in radians), θ is the diffraction angle of Bragg, K is the shape factor (K=0.9), λ is the X-ray wavelength (CuK$_\alpha$=0.154 nm), D is the crystallite size (nm), and ε is the average strain.

By plotting $4.\sin\theta$ vs $\beta.\cos\theta$, the crystalline size and the average strain can be found by the Y-intercept extrapolation and the slope of the line given in Figure 3. Accordingly, the crystalline size of FeNPs and the average strain were calculated to be 57.75 nm and 0.0065.
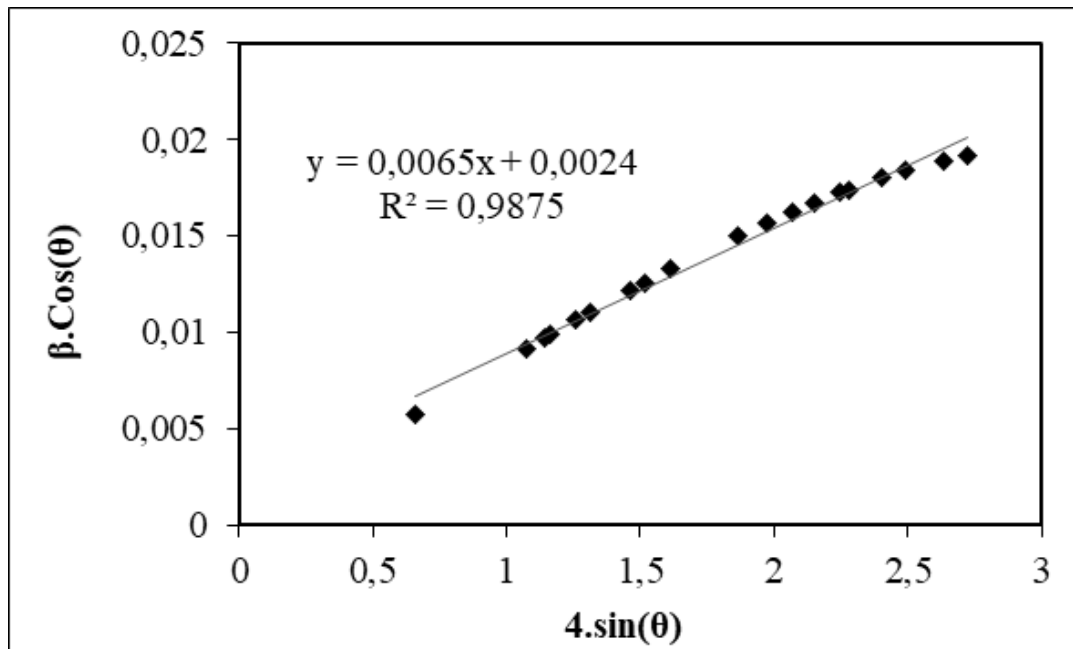
Figure 3. Williamson–Hall plot

The morphology of FeNPs was investigated with SEM, and SEM images before and after adsorption were presented in Figure 4. (a) and (b). According to Figure 4. (a), FeNPs had a homogeneous appearance and their structures were similar to spherical. It was observed that large structures were formed due to the agglomeration. In addition, the average particle size of FeNPs was calculated as 54.83 nm with Image-J program, that was consistent with the value calculated using Williamson–Hall equation (57.75 nm). According to SEM image of FeNPs after adsorption Figure 4. (b), it was observed that the structure of FeNPs partially deteriorated after adsorption and the particle size increased due to the agglomeration.
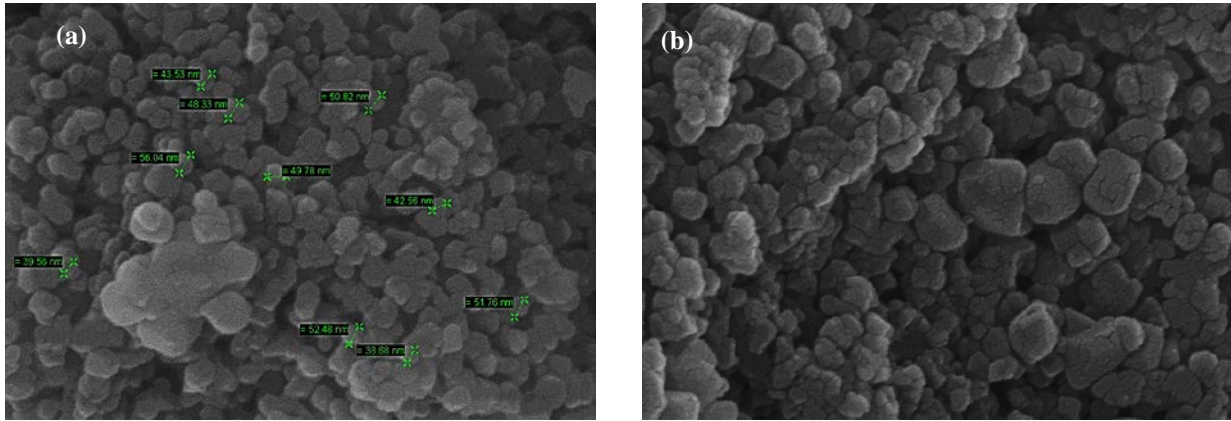
Figure 4. SEM images of FeNPs (a) before adsorption and (b) after adsorption

Adsorption Studies

Optimization of the Experimental Conditions of the Adsorption of MG by FeNPs

The effects of experimental conditions such as contact time, temperature, and initial dye concentration on the adsorption of MG by FeNPs were investigated by using RSM according to CCD. The second-degree polynomial equation expressing the relation between the independent variables and the response for this study was given below.

$$Y = -33.8 + 0.6574\,A + 0.949\,B - 0.0520\,C - 0.003763\,A^2 - 0.01073\,B^2 - 0.000096\,C^2 + 0.001989\,AB + 0.001880\,AC + 0.003151\,BC \qquad \text{Eq. (4)}$$

The F-test was used for statistical significance analysis of variance (ANOVA) of the quadratic model equation and the ANOVA results were given in Table 7. Accordingly, the F values of linear, square, and two-way interaction models were found to be 573.84, 111.27, and 71.02, respectively, also all P values of the models were lower than 0.0001.

Table 7. ANOVA results of the quadratic model

Source	Degree of freedom	Sum of squares	Mean square	F-value	P-value	Remarks
Model	11	57733.5	5248.5	208.45	<0.0001	Significant
Linear	3	43346.2	14448.7	573.84	<0.0001	Significant
A	1	25223.3	25223.3	1001.76	<0.0001	Significant
B	1	6037.9	6037.9	239.80	<0.0001	Significant
C	1	12084.9	12084.9	479.96	<0.0001	Significant
Square	3	8404.9	2801.6	111.27	<0.0001	Significant
AA	1	3968.7	3968.7	157.62	<0.0001	Significant
BB	1	241.5	241.5	9.59	0.004	-
CC	1	4.9	4.9	0.20	0.662	-
Two-way interaction	3	5364.7	1788.2	71.02	<0.0001	Significant
AB	1	285.8	285.8	11.35	0.002	-
AC	1	4086.0	4086.0	162.28	<0.0001	Significant
BC	1	992.9	992.9	39.43	<0.0001	Significant
Error	28	705.0	25.2	*	*	*
Lack of fit	5	697.2	139.4	409.16	<0.0001	Significant
Pure error	23	7.8	0.3	*	*	*
Total	39	58438.5	*	*	*	*

$R^2=0.9879$; $R^2_{adj}=0.9832$; $R^2_{pred}=0.9760$

It revealed that linear, quadratic, and two-way interaction models were statistically significant. The variance analysis of the experimental design showed that the terms of A, B and C in linear model; the term of AA in the

quadratic model; the terms of AC and BC in the two-way interaction model were significant. The regression coefficient (R^2) was found to be 0.9879, showing that 98.79% of the variability in response was explained by the model. Figure 5 represented the relationship between predicted Y values (theoretically calculated transformed values) and actual Y values (experimentally transformed values). The data points were found to be close to linear (R^2=0.9879), indicating the good correlation between the predicted and the experimental responses. Also, the difference between R^2_{pred}= 0.9760 and R^2_{adj}=0.9832 was acceptable. As a result, the quadratic model provided an adequate estimate of the adsorption of MG by FeNPs.
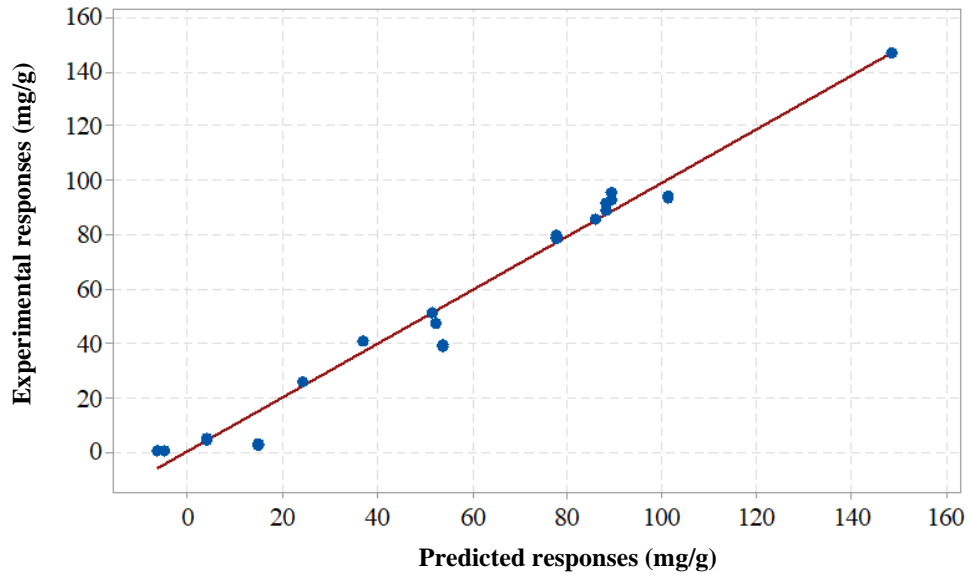
Figure 5. The plot of experimental responses vs predicted responses

The normal probability plot is a graphical technique used to identify important distinctions from normality. In this graph, it is desired that the points are distributed on a straight line (Dargahi et al., 2021). The normal probability graph obtained in this study was presented in Figure 6. It was seen in Figure 6 that the data were normally distributed in this study.
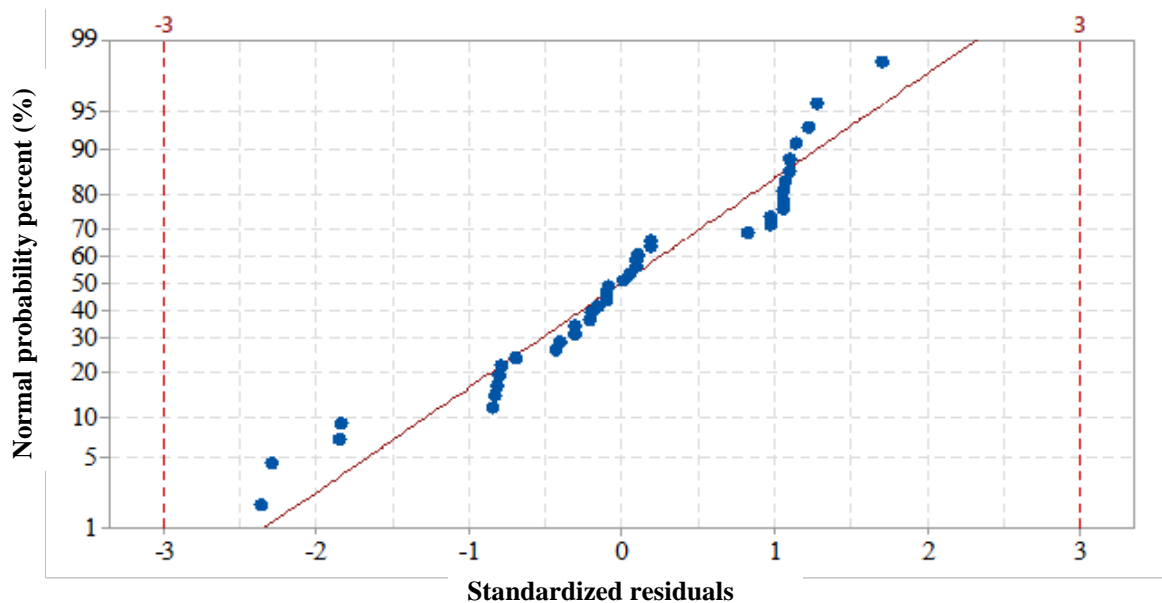
Figure 6. Normal probability plot

The optimum experimental conditions were determined to be 180 min contact time (A), 75°C temperature (B), and 300 mg/L initial MG concentration (C). Under these conditions, the maximum adsorbed MG amount per gram of adsorbent (Y:mg MG/g adsorbent) was determined as 148.43 mg/g from the quadratic model. In order

to prove the accuracy of the model, an experiment was conducted under the optimum experimental conditions and Y value was found to be 146.63 mg/g experimentally. The agreement between the Y values calculated from the model and determined experimentally showed that the selected model was suitable for the adsorption of MG by FeNPs.

In order to investigate the two-way interactions between the independent variables, 3D response surface graphs (Figure 7. (a-c)) were drawn based on the second-degree polynomial equation. In Figure 7. (a), the variation of Y with temperature and initial MG concentration was shown when the other variables were kept constant at the center points. Accordingly, Y values increased with increasing temperature and initial dye concentration. For this reason, the optimum temperature and initial dye concentration were determined as 75°C and 300 mg/L, respectively. As seen in Figure 7. (b), Y values increased with increasing contact time; so, the optimum contact time was determined as 180 min. It was observed in Figure 7. (c) that Y values increased as the contact time and temperature increased.

The increase in Y values as the temperature increases can be attributed to the endothermic nature of the process. On the other hand, as the initial dye concentration increases, more dye molecules are adsorbed on the adsorbent surface and the adsorbed dye amounts increases due to the increase in the driving force (ΔC) in the adsorbate solution. With the increase in the contact time, the active sites of the adsorbent are filled with more dye cations and thus the adsorbed dye amounts increases.

It could be seen in 3D response surface graphs that the two-way interactions in Figure 7. (a) and Figure 7. (b) were more effective on the response than that of Figure 7. (c), as well as the F values of the two-way interactions in Table 7. The F values of the contact time-initial dye concentration (AC) and temperature-initial dye concentration (BC) were greater than that of the contact time-temperature (AB). In addition, while the two-way interactions of the contact time-initial dye concentration (AC) and temperature-initial dye concentration (BC) were significant, the contact time-temperature (AB) two-way interaction was not significant.
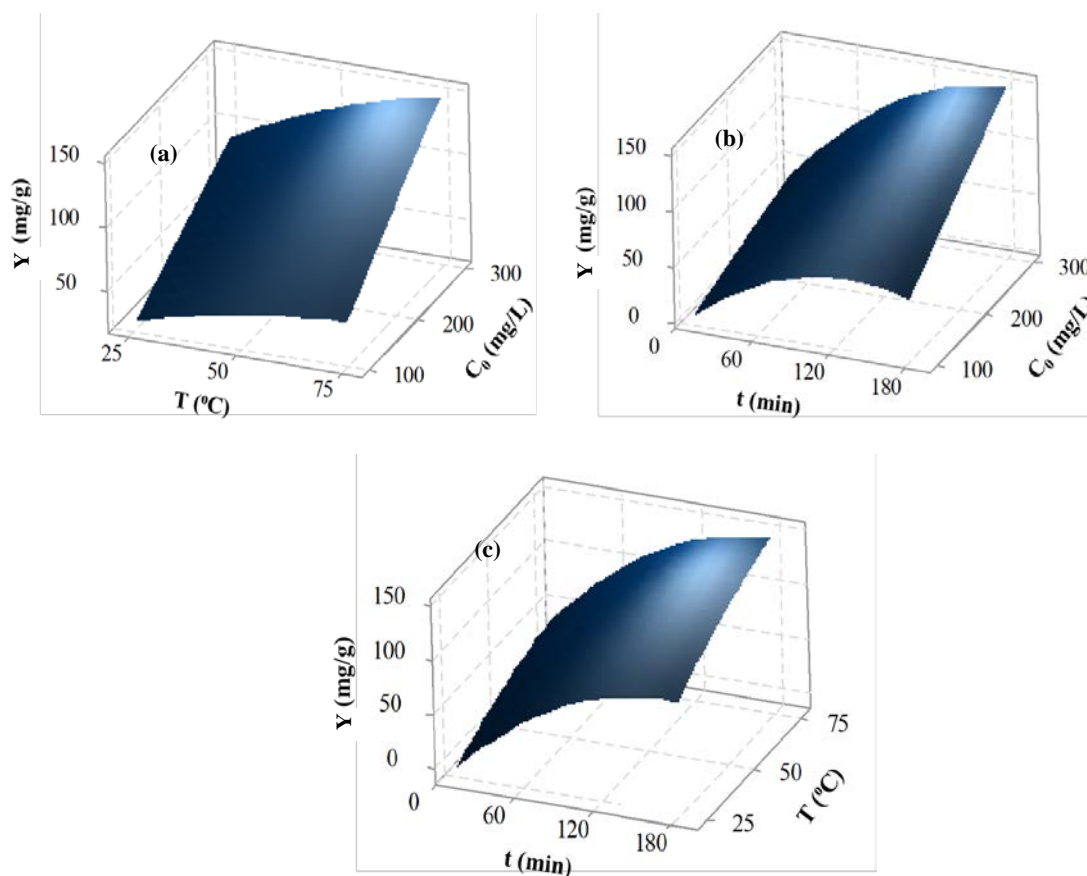

Figure 7. 3D response surface graphs **(a)** T; Temperature (°C)- C_o; Initial dye concentration (mg/L), **(b)** t; Contact time (min)- C_o; Initial dye concentration (mg/L), **(c)** t; Contact time (min)- T; Temperature (°C)

Equilibrium Modelling

Information about the surface properties of the adsorbent, the design of the adsorption process, and the adsorption behavior can be obtained by applying the adsorption isotherms to the equilibrium data. The linear equations of Langmuir and Freundlich isotherm models, which are the most used isotherm models, were given below:

$$[1/q_e] = [1/(Q^o.b.C_e)] + [1/Q^o] \qquad \text{Eq. (5)}$$
$$[\ln q_e] = [\ln K_f] + [(1/n).(\ln C_e)] \qquad \text{Eq. (6)}$$

where q_e (mg/g) and C_e (mg/L) are the adsorbed dye amount per gram of adsorbent and unadsorbed dye concentration in solution at equilibrium, respectively; Q^o is the maximum monolayer coverage capacity (mg/g) and b is a constant related to the affinity of the binding sites (L/mg); K_f and $1/n$ are the Freundlich constants indicating adsorption capacity and intensity, respectively.

The values of Q^o and b were calculated from intercept and slope of the linear plot of $1/q_e$ vs. $1/C_e$ (Eq. 5), and the values of K_f and $1/n$ were determined from intercept and slope of the linear plot of $\ln q_e$ vs. $\ln C_e$ (Eq. 6). In this study, the equilibrium data were evaluated with Langmuir and Freundlich isotherm models for different temperatures. The obtained isotherm constants as well as regression coefficients and ARE values were presented in Table 8. Accordingly, the higher R^2 values and the lower ARE values indicated that the equilibrium data could be represented with Langmuir isotherm model than Freundlich isotherm model. It indicated the monolayer adsorption of MG on the homogeneous surface of FeNPs with identical binding sites. In addition, the increase in Q^o values with the increase in temperature confirmed that the adsorption process was endothermic. The maximum monolayer adsorption capacity (Q^o) of FeNPs was found to be 175.44 mg/g at the optimum temperature of 75°C and compared with the other adsorbents in the literature (Table 9). It could be concluded that FeNPs could be evaluated as an efficient adsorbent for the adsorption of MG due to its relatively high adsorption capacity (Q^o) compared to the other adsorbents in the literature.

Table 8. Isotherm model constants with the values of R^2 and ARE

T (°C)	Langmuir Isotherm Model				Freundlich Isotherm Model			
	Q^o (mg/g)	b (L/mg)	R^2	ARE	K_f (mg/g)/(L/mg)$^{1/n}$	$1/n$	R^2	ARE
25	89.29	0.006401	0.9997	1.1639	1.39	0.6908	0.9916	4.08
50	92.59	0.864000	0.9995	1.5559	39.65	0.2239	0.8614	15.27
75	175.44	0.438462	0.9996	1.8395	48.70	0.4782	0.9133	16.36

Table 9. The maximum monolayer adsorption capacities (Q^o) of different adsorbents for MG adsorption

Adsorbent	Q^o (mg/g)	Reference
Corn straw-derived biochar supported nZVI magnetic composite	515.77	(Eltaweil et al., 2020)
Magnetic activated carbon (Fe_3O_4-AC)	311.40	(Altintig et al., 2018)
FeNPs	175.44	This work
Gold nanoparticles loaded on activated carbon	172.20	(Roosta et al., 2014)
Zinc sulfide:copper nanoparticle loaded on activated carbon	168.07	(Dastkhoon et al., 2015)
Halloysite nanotubes	99.6	(Kiani et al., 2011)
β-cyclodextrin polymer coated Fe_3O_4 magnetic nanoparticles	88.49	(Liang et al., 2018)
Nanoscale zero-valent iron supported by carbonized pomegranate peel	32.47	(Gunduz & Bayrak, 2018)
Bimetallic Fe–Zn nanoparticles	21.74	(Gautam et al., 2015)

Thermodynamic Evaluation

In order to define the thermodynamic behavior of the adsorption of MG by FeNPs, the thermodynamic parameters of Gibb's free energy change (ΔG), enthalpy change (ΔH), and entropy change (ΔS) were calculated using the following equations:

$$\Delta G = -RT.\ln K_c \qquad \text{Eq. (7)}$$
$$K_c = C_{ad,e}/C_e \qquad \text{Eq. (8)}$$
$$\ln K_c = (\Delta S/R) - (\Delta H/RT) \qquad \text{Eq. (9)}$$

where K_c is the equilibrium constant at temperature T, $C_{ad,e}$ is the adsorbed dye concentration at equilibrium (mg/L), C_e is the unadsorbed dye concentration at equilibrium (mg/L), ΔG (J/mole) is the Gibb's free energy change, ΔH (J/mole) is the enthalpy change of the adsorption process, ΔS (J/(mole.K)) is the entropy change of the adsorption process.

The values of ΔH and ΔS can be calculated from the slope and intercept of the linear plot of $\ln K_c$ vs $1/T$, respectively. The calculated thermodynamic parameters were given in Table 10. Accordingly, the adsorption of MG by FeNPs was spontaneous ($\Delta G < 0$) at optimum temperature, increasing in the randomness of adsorbed species ($\Delta S > 0$), and endothermic ($\Delta H > 0$) as predicted in the sections of adsorption studies and equilibrium modeling (Shalaby et al., 2021).

Table 10. The calculated thermodynamic parameters

T (K)	Kc	ΔG (J/mole)	ΔH (J/mole)	ΔS (J/mole.K)
298	0.1193	5267.71		
323	0.8840	331.02	75104.52	233.45
348	9.4639	−6502.57		

Conclusion

This work revealed an applicable method for the evaluation of iron-steel industrial waste in the pyrometallurgical synthesis of a value-added product, iron-containing nanoparticles (FeNPs), for an environmental application of MG adsorption. The crystal and morphological structure of FeNPs synthesized via this route was proved by XRD and SEM analysis. The particle sizes of FeNPs were calculated with Williamson–Hall equation and Image-J program as 57.75 nm and 54.83 nm, respectively. The usability of the synthesized FeNPs in the adsorption of MG was investigated. The experimental design, the effect of independent variables on the response, and the optimization of experimental conditions were investigated with RSM according to CCD by significantly reducing the number of experiments. The optimum experimental conditions were found to be 180 min contact time, 75 °C temperature, and 300 mg/L initial MG concentration. The all independent variables were found to have significant effects on the adsorption of MG by FeNPs at the individual level. The results of ANOVA indicated that the two-way interaction between the contact time and initial dye concentration had the highest effect on the response due to the highest F-value. RSM based optimization revealed that the maximum adsorbed dye amount per gram of adsorbent was determined as 148.43 mg/g at the optimum conditions which was close to the value found experimentally as 146.63 mg/g. It was found that the equilibrium adsorption data were better fitted to the Langmuir isotherm model than the Freundlich isotherm model. The monolayer adsorption capacity obtained at optimum condition (Q^o=175.44 mg/g) was competitive with the values reported for the adsorption of MG. Thermodynamic data showed that the adsorption process was endothermic and spontaneous, and the randomness of adsorbed species increased during the adsorption of MG by FeNPs. These results showed that the low-cost FeNPs synthesized from iron-steel industrial waste can be efficiently applied for the adsorption of industrial wastewater containing of MG.

Scientific Ethics Declaration

The authors declare that the scientific ethical and legal responsibility of this article published in EPSTEM journal belongs to the authors.

Acknowledgements or Notes

References

Altintig, E., Onaran, M., Sari, A., Altundag, H., & Tuzen, M. (2018). Preparation, characterization and evaluation of bio-based magnetic activated carbon for effective adsorption of malachite green from aqueous solution. *Materials Chemistry and Physics*, *220*(January), 313–321.

https://doi.org/10.1016/j.matchemphys.2018.05.077

Dargahi, A., Samarghandi, M. R., Shabanloo, A., Mahmoudi, M. M., & Nasab, H. Z. (2021). Statistical modeling of phenolic compounds adsorption onto low-cost adsorbent prepared from aloe vera leaves wastes using CCD-RSM optimization: effect of parameters, isotherm, and kinetic studies. *Biomass Conversion and Biorefinery*. https://doi.org/10.1007/s13399-021-01601-y

Dastkhoon, M., Ghaedi, M., Asfaram, A., Goudarzi, A., Langroodi, S. M., Tyagi, I., … Gupta, V. K. (2015). Ultrasound assisted adsorption of malachite green dye onto ZnS:Cu-NP-AC: Equilibrium isotherms and kinetic studies - Response surface optimization. *Separation and Purification Technology*, *156*, 780–788. https://doi.org/10.1016/j.seppur.2015.11.001

Deb, A., Debnath, A., & Saha, B. (2021). Sono-assisted enhanced adsorption of eriochrome Black-T dye onto a novel polymeric nanocomposite: kinetic, isotherm, and response surface methodology optimization. *Journal of Dispersion Science and Technology*, *42*(11), 1579–1592. https://doi.org/10.1080/01932691.2020.1775093

Eltaweil, A. S., Ali Mohamed, H., Abd El-Monaem, E. M., & El-Subruiti, G. M. (2020). Mesoporous magnetic biochar composite for enhanced adsorption of malachite green dye: Characterization, adsorption kinetics, thermodynamics and isotherms. *Advanced Powder Technology*, *31*(3), 1253–1263. https://doi.org/10.1016/j.apt.2020.01.005

Gadekar, M. R., & Ahammed, M. M. (2019). Modelling dye removal by adsorption onto water treatment residuals using combined response surface methodology-artificial neural network approach. *Journal of Environmental Management*, *231*(October 2018), 241–248. https://doi.org/10.1016/j.jenvman.2018.10.017

Gandha, K., Mohapatra, J., Hossain, M. K., Elkins, K., Poudyal, N., Rajeshwar, K., & Liu, J. P. (2016). Mesoporous iron oxide nanowires: Synthesis, magnetic and photocatalytic properties. *RSC Advances*, *6*(93), 90537–90546. https://doi.org/10.1039/c6ra18530d

Gautam, R. K., Rawat, V., Banerjee, S., Sanroman, M. A., Soni, S., Singh, S. K., & Chattopadhyaya, M. C. (2015). Synthesis of bimetallic Fe-Zn nanoparticles and its application towards adsorptive removal of carcinogenic dye malachite green and Congo red in water. *Journal of Molecular Liquids*, *212*, 227–236. https://doi.org/10.1016/j.molliq.2015.09.006

Giri, S. K., Das, N. N., & Pradhan, G. C. (2011). Magnetite powder and kaolinite derived from waste iron ore tailings for environmental applications. *Powder Technology*, *214*(3), 513–518. https://doi.org/10.1016/j.powtec.2011.09.017

Gunduz, F., & Bayrak, B. (2018). Synthesis and performance of pomegranate peel-supported zero-valent iron nanoparticles for adsorption of malachite green. *Desalination and Water Treatment*, *110*, 180–192. https://doi.org/10.5004/dwt.2018.22185

Harja, M., Buema, G., & Bucur, D. (2022). Recent advances in removal of Congo Red dye by adsorption using an industrial waste. *Scientific Reports*, Vol. 12. https://doi.org/10.1038/s41598-022-10093-3

Irfan, H., Mohamed Racik, K., & Anand, S. (2018). Microstructural evaluation of CoAl2O4 nanoparticles by Williamson–Hall and size–strain plot methods. *Journal of Asian Ceramic Societies*, *6*(1), 54–62. https://doi.org/10.1080/21870764.2018.1439606

Kahouli, M., Barhoumi, A., Bouzid, A., Al-Hajry, A., & Guermazi, S. (2015). Structural and optical properties of ZnO nanoparticles prepared by direct precipitation method. *Superlattices and Microstructures*, *85*, 7–23. https://doi.org/10.1016/j.spmi.2015.05.007

Karacabey, P., Döven, S., Uzunoglu, D., & Özer, A. (2019). Synthesis of 3D Hierarchical Flower-like MgO Microstructure: Investigation of its Adsorption and Antibacterial Properties. *Arabian Journal for Science and Engineering*, *44*(12). https://doi.org/10.1007/s13369-019-03959-8

Kargin, J., Valladares, L. D. L. S., Borja-Castro, L. E., Xize, J., Mukhambetov, D. G., Konyukhov, Y. V., … Barnes, C. H. W. (2022). Characterization of iron oxide waste scales obtained by rolling mill steel industry. *Hyperfine Interactions*, *243*(1), 1–11. https://doi.org/10.1007/s10751-022-01800-7

Khuyen, H. T., Huong, N. T., Huong, T. T., Lien, P. T., Chi, T. K., Thi, V., Tung, D. K. (2018). Luminescent – Magnetic Nanoparticle and Their Properties. *IEEE Transactions on Magnetics*, *54*(6), 4–7.

Kiani, G., Dostali, M., Rostami, A., & Khataee, A. R. (2011). Adsorption studies on the removal of Malachite Green from aqueous solutions onto halloysite nanotubes. *Applied Clay Science*, *54*(1), 34–39. https://doi.org/10.1016/j.clay.2011.07.008

Liang, W., Li, D., Ma, X., Dong, W., Li, J., Wu, R., … Dong, Q. (2018). Surface β-cyclodextrin polymer coated Fe 3 O 4 magnetic nanoparticles: Synthesis, characterization and application on efficient adsorption of malachite green. *Journal of Nano Research*, *54*, 54–65. https://doi.org/10.4028/www.scientific.net/JNanoR.54.54

Nguyen, V. T., Vo, T. D. H., Nguyen, T. B., Dat, N. D., Huu, B. T., Nguyen, X. C., … Bui, X. T. (2022). Adsorption of norfloxacin from aqueous solution on biochar derived from spent coffee ground: Master variables and response surface method optimized adsorption process. *Chemosphere*, *288*(P2), 132577.

https://doi.org/10.1016/j.chemosphere.2021.132577

Patra, J. K., & Baek, K. H. (2014). Green Nanobiotechnology: Factors Affecting Synthesis and Characterization Techniques. *Journal of Nanomaterials*, *2014*. https://doi.org/10.1155/2014/417305

Roosta, M., Ghaedi, M., Shokri, N., Daneshfar, A., Sahraei, R., & Asghari, A. (2014). Optimization of the combined ultrasonic assisted/adsorption method for the removal of malachite green by gold nanoparticles loaded on activated carbon: Experimental design. *Spectrochimica Acta - Part A: Molecular and Biomolecular Spectroscopy*, *118*, 55–65. https://doi.org/10.1016/j.saa.2013.08.082

Schoeman, Y., Oberholster, P., & Somerset, V. (2021). A zero-waste multi-criteria decision-support model for the iron and steel industry in developing countries: A case study. *Sustainability (Switzerland)*, Vol. 13, pp. 1–23. https://doi.org/10.3390/su13052832

Shalaby, S. M., Madkour, F. F., El-Kassas, H. Y., Mohamed, A. A., & Elgarahy, A. M. (2021). Green synthesis of recyclable iron oxide nanoparticles using Spirulina platensis microalgae for adsorptive removal of cationic and anionic dyes. *Environmental Science and Pollution Research*, *28*(46), 65549–65572. https://doi.org/10.1007/s11356-021-15544-4

Author Information

Deniz Uzunoglu
Department of Chemical Engineering, Faculty of
Engineering, Mersin University, Mersin, 33343, Turkey
Contact e-mail: *denizuzunoglu4@gmail.com*

Ayla Ozer
Department of Chemical Engineering, Faculty of
Engineering, Mersin University, Mersin, 33343, Turkey

To cite this article:

On Tzitzeica Curves According to Q-Frame in Euclidean 3-Space

Muhammed Talat SARIAYDIN
Selcuk University

Aziz YAZLA
Selcuk University

Abstract: *Tzitzeica curve* is a special spatial curve, which introduced Gheorghe Tzitzeica in 1911. Gheorghe Tzitzeica defined this curve as follows; for a spatial curve ϕ, "if the ratio of its torsion τ and the square of the distance d from the origin to the osculating plane at an arbitrary point of the curve is constant, then this spatial curve is a *Tzitzeica curve* in Euclidean space." Moreover Gheorghe Tzitzeica defined a special surface which is named *Tzitzeica surface* in 1907. In this surface, the asymptotic lines of *Tzitzeica surfaces* with negative Gaussian curvature are *Tzitzeica curves*. Also, the ratio of its Gaussian curvature K and the distance d from the origin to the tangent plane at any arbitrary point of the surface is constant. In this paper, we study the *Tzitzeica curve* via q-frame in $\mathbb{E}^3$. Firstly, we redefine the *Tzitzeica curve* q-frame in Euclidean 3- space. Then, it is obtained some conditions for the *Tzitzeica curve* as a spherical curve. Finally, we investigate harmonic vector cases of the *Tzitzeica curve* according to q- frame in Euclidean space.

Keywords: Tzitzeica curve, q-frame, Spherical curve

Introduction

Tzitzeica curve satisfies the following condition

$$\frac{\tau}{d_{osc}^2} = a,$$

where $a \neq 0 \in \mathbb{R}$, and $d_{osc} = \langle \mathbf{B}, \phi \rangle$ and Tzitzeica surface satisfies the following condition

$$\frac{K}{d_{osc}^4} = a,$$

where $a \neq 0 \in \mathbb{R}$, (Bayram et al., 2018, Bila, 2012 and Crâsmareanu, 2002). Then, these curves and surfaces are often used in scientific research from the past to the present with geometric properties. For example, Crâsmareanu studied the cylindrical form of Tzitzeica curves in (Crâsmareanu, 2002), Karacan gave the elliptic cylindrical form of Tzitzeica curves in (Karacan & Bukcu, 2009), Agnev computed the effect of a general centro-affine transformation on *Tzitzeica surface* in (Agnew et al.,2010) and finally, Bayram characterized *Tzitzeica curves* in $\mathbb{E}^3$ in terms of their curvatures, (Bayram et al., 2018). See more details (Bobe et al., 2012, Yazici et al., 2022)

Although there are many studies on these curves and surfaces in Euclidean space and Minkowski space, it is almost never studied according to q- frame in Euclidean space. We redefine the *Tzitzeica curve* q-frame in Euclidean 3- space. Then, it is obtained some conditions for the *Tzitzeica curve* as a spherical curve. Finally, we give harmonic vector cases of the *Tzitzeica curve* according to q- frame in Euclidean space.

Preliminaries

Let $\phi: I \subseteq \mathbb{R} \to \mathbb{E}^3$ be an unit speed curve. The q-frame of the curve ϕ is obtained as follows

$$\mathbf{t} = \phi', \ \mathbf{n}_q = \frac{\mathbf{t} \times z}{\|\mathbf{t} \times z\|}, \ \mathbf{b}_q = \mathbf{t} \times \mathbf{n}_q, \tag{1}$$

where $\mathbf{n}_q$ is the quasi-normal vector, $\mathbf{b}_q$ is the quasi-binormal vector, and z is the projection vector. The q formulas are expressed as

$$\begin{bmatrix} \nabla_{\phi'}\mathbf{t} \\ \nabla_{\phi'}\mathbf{n}_q \\ \nabla_{\phi'}\mathbf{b}_q \end{bmatrix} = \begin{bmatrix} 0 & k_1 & k_2 \\ -k_1 & 0 & k_3 \\ -k_2 & -k_3 & 0 \end{bmatrix} \begin{bmatrix} \mathbf{t} \\ \mathbf{n}_q \\ \mathbf{b}_q \end{bmatrix}, \tag{2}$$

where k_i are called q-curvatures ($1 \leq i \leq 3$),

$$\begin{aligned} k_1 &= \kappa\cos\gamma = \langle \mathbf{t}', \mathbf{n}_q \rangle, \\ k_2 &= -\kappa\sin\gamma = \langle \mathbf{t}', \mathbf{b}_q \rangle, \\ k_3 &= d\gamma + \tau = -\langle \mathbf{n}_q, \mathbf{b}_q' \rangle, \end{aligned} \tag{3}$$

and γ is the angle between the principal normal vector and the quasi normal vector. In this paper, it will be assumed that the projection vector $z = (0,0,1)$. If ϕ and z are parallel, the vector z can be chosen as $z = (0,1,0)$, (Dede & Ekici, 2018).

On the other hand, let ϕ be a space curve with the arclength parameter s, and $\nabla_{\phi'} = \frac{d}{ds}$. The Laplacian operator $\triangle$ of ϕ can write as, (Kocayigit et al., 2016),

$$\triangle = -\nabla_{\phi'}\nabla_{\phi'}.$$

Definition 2.1 *Let* $\phi: I \subset \mathbb{R} \to \mathbb{E}^3$ *be a unit speed curve. The curve* ϕ *is called a harmonic tangent vector if*

$$\triangle \mathbf{t} = 0.$$

Also, *The curve* ϕ *is called a harmonic 1-type tangent vector if*

$$\triangle \mathbf{t} = \lambda\mathbf{t},$$

where $\lambda \in \mathbb{R}$, (Kocayigit et al., 2016).

Definition 2.2 *Let* $\phi: I \subset \mathbb{R} \to \mathbb{E}^3$ *be a unit speed curve. The curve* ϕ *is called a harmonic principal vector if*

$$\triangle \mathbf{n} = 0.$$

Also, *The curve* ϕ *is called a harmonic 1-type principal normal vector if*

$$\triangle \mathbf{n} = \lambda\mathbf{n},$$

where $\lambda \in \mathbb{R}$, (Kocayigit et al., 2016).

Definition 2.3 *Let* $\phi: I \subset \mathbb{R} \to \mathbb{E}^3$ *be a unit speed curve. The curve* ϕ *is called a harmonic binormal vector if*

$$\triangle \mathbf{b} = 0.$$

Also, *The curve* ϕ *is called a harmonic 1-type binormal vector if*

$$\triangle \mathbf{b} = \lambda\mathbf{b},$$

where $\lambda \in \mathbb{R}$, (Kocayigit et al., 2016).

Some Characterizations of Tzitzeica Curves

In this chapter, we will define *Tzitzeica curves* according to q-frame in $\mathbb{E}^3$. Then, we will do some characterizations of *Tzitzeica curves* with q-curvatures.

Definition 3.1 *Let* $\phi: I \subset \mathbb{R} \to \mathbb{E}^3$ *be a unit speed curve,* $\{\mathbf{t}, \mathbf{n}_q, \mathbf{b}_q\}$ *be its q-frame, and* k_1, k_2, k_3 *be q-curvatures. If the inner product of the two vectors* α *and* β *in Euclidean space is denoted by* $g(\alpha, \beta)$, *the curve* ϕ *that provides the following condition is called the Tzitzeica curve:*

$$k_3 = \ell g(\mathbf{b}_q, \phi), \tag{4}$$

where $k_3 \neq 0$, $k_1 > 0$, *and* $k_2 > 0$.

Proposition 3.2 *Let* $\phi: I \subset \mathbb{R} \to \mathbb{E}^3$ *be a unit speed Tzitzeica curve,* $\{\mathbf{t}, \mathbf{n}_q, \mathbf{b}_q\}$ *be its q-frame. Then, the Tzitzeica curve* ϕ *provides the following equality*

$$k_2 k_3 g(\phi, \mathbf{t}) + k_3^2 g(\phi, \mathbf{n}_q) + k_3' g(\phi, \mathbf{b}_q) = 0. \tag{5}$$

Proof. Because the *Tzitzeica curve* ϕ provides eq. (4), $\ell \neq 0$. In this case, the proof is clear.

Theorem 3.3 *Let* $\phi: I \subset \mathbb{R} \to \mathbb{E}^3$ *be a unit speed Tzitzeica curve,* $\{\mathbf{t}, \mathbf{n}_q, \mathbf{b}_q\}$ *be its q-frame, and* k_1, k_2, k_3 *be q-curvatures. The Tzitzeica curve* ϕ *is a spherical curve if and only if*

$$(-k_1^2 - k_2^2)g(\phi, \mathbf{t}) + (k_1' - k_2 k_3)g(\phi, \mathbf{n}_q) + (k_1 k_3 + k_2')g(\phi, \mathbf{b}_q) = 0. \tag{6}$$

Proof. If the *Tzitzeica curve* ϕ is a spherical curve, we can write

$$\|\phi\| = r.$$

Take the derivative last equation, it is obtained as

$$g(\phi, \mathbf{t}) = 0.$$

If the last equation is taken again derivative, we can write as

$$(-k_1^2 - k_2^2)g(\phi, \mathbf{t}) + (k_1' - k_2 k_3)g(\phi, \mathbf{n}_q) + (k_1 k_3 + k_2')g(\phi, \mathbf{b}_q) = 0.$$

In this case, the proof is completed.

Proposition 3.4 *Let* $\phi: I \subset \mathbb{R} \to \mathbb{E}^3$ *be a unit speed spherical Tzitzeica curve,* $\{\mathbf{t}, \mathbf{n}_q, \mathbf{b}_q\}$ *be its q-frame, and* k_1, k_2, k_3 *be q- curvatures. The following equations can be written for the curvatures of the spherical Tzitzeica curve;*

$$
\begin{aligned}
k_1 &= \frac{k_3' - k_2'}{k_3}, \\
k_2 &= \frac{k_1' - k_3^2}{k_3}, \\
k_3 &= -\frac{k_1^2 + k_2^2}{k_2}.
\end{aligned}
\tag{7}
$$

Proof. The proof is completed considering the Proposition 3.2 and the Theorem 3.3 together.

Theorem 3.5 *Let* $\phi: I \subset \mathbb{R} \to \mathbb{E}^3$ *be a unit speed Tzitzeica curve,* $\{\mathbf{t}, \mathbf{n}_q, \mathbf{b}_q\}$ *be its q-frame, and* k_1, k_2, k_3 *be q-curvatures. If the position vector of the Tzitzeica curve is*

$$\phi(s) = \pi_1(s)\mathbf{t}(s) + \pi_2(s)\mathbf{n}_q(s) + \pi_3(s)\mathbf{b}_q(s),$$

the following equations can be written

$$\pi_1' - \pi_2 k_1 - \pi_3 k_2 = 1,$$
$$\pi_1 k_1 + \pi_2' - \pi_3 k_3 = 0,$$
$$\pi_1 k_2 + \pi_2 k_3 + \pi_3' = 0.$$

Theorem 3.6 *Let* $\phi: I \subset \mathbb{R} \to \mathbb{E}^3$ *be a unit speed Tzitzeica curve,* $\{\mathbf{t}, \mathbf{n}_q, \mathbf{b}_q\}$ *be its q-frame, and* k_1, k_2, k_3 *be q-curvatures. The differential equation characterizing Tzitzeica curve according to its tangent vector is obtained*

$$\mu_1 \nabla_{\phi'}^3 \mathbf{t} + (k_1 \eta_2 - k_2 \eta_1) \nabla_{\phi'}^2 \mathbf{t} + (\lambda_3 \eta_1 + \lambda_2 \eta_2) \nabla_{\phi'} \mathbf{t} \qquad (8)$$
$$+ (\mu(\lambda_3 k_2 + \lambda_2 k_1 - \lambda_1') + \eta_1 k_2 \lambda_1 - \eta_2 k_1 \lambda_1) \mathbf{t} = 0,$$

where

$$\lambda_1 = -k_1^2 - k_2^2,$$
$$\lambda_2 = k_1' - k_2 k_3,$$
$$\lambda_3 = k_1 k_3 + k_2',$$
$$\mu_1 = k_2 \lambda_2 - k_1 \lambda_3$$
$$\eta_1 = \lambda_1 k_1 + \lambda_2' - \lambda_3 k_3,$$
$$\eta_2 = \lambda_1 k_2 + \lambda_3' + \lambda_2 k_3.$$

Proof. Assume that ϕ is the *Tzitzeica curve* and $\{\mathbf{t}, \mathbf{n}_q, \mathbf{b}_q\}$ is its q-frame. Then, the following equations can be written

$$\nabla_{\phi'} \mathbf{t} = k_1 \mathbf{n}_q + k_2 \mathbf{b}_q, \qquad (9)$$

$$\nabla_{\phi'}^2 \mathbf{t} = (-k_1^2 - k_2^2) \mathbf{t} + (k_1' - k_2 k_3) \mathbf{n}_q + (k_1 k_3 + k_2') \mathbf{b}_q, \qquad (10)$$

And

$$\nabla_{\phi'}^3 \mathbf{t} = (\text{-}2k_1 k_1' \text{-} 3k_2 k_2' \text{-} k_1' k_2 + k_2^2 k_3 \text{-} k_1 k_2 k_3) \mathbf{t} \qquad (11)$$
$$+ (-k_1^3 - k_1 k_2^2 + k_1'' - 2k_2' k_3 - k_2 k_3' - k_1 k_3^2) \mathbf{n}_q$$
$$+ (-k_1^2 k_2 - k_2^3 + 2k_1' k_3 - k_2 k_3^2 + k_1 k_3' + k_2'') \mathbf{b}_q$$

Considering eq. (9) and eq. (10) together, q-normal vector and q-binormal vector of the *Tzitzeica curve* obtained as

$$\mathbf{n}_q = \frac{1}{k_2 \lambda_2 - k_1 \lambda_3} \left(k_2 \nabla_{\phi'}^2 \mathbf{t} - \lambda_3 \nabla_{\phi'} \mathbf{t} - k_2 \lambda_1 \mathbf{t} \right),$$

and

$$\mathbf{b}_q = \frac{1}{k_2 \lambda_2 - k_1 \lambda_3} \left(-k_1 \nabla_{\phi'}^2 \mathbf{t} + \lambda_2 \nabla_{\phi'} \mathbf{t} + k_1 \lambda_1 \mathbf{t} \right).$$

Then, we can write

$$L_1 \nabla_{\phi'}^3 \mathbf{t} + L_2 \nabla_{\phi'}^2 \mathbf{t} + L_3 \nabla_{\phi'} \mathbf{t} + L_4 \mathbf{t} = 0,$$

where

$$L_1 = 2k_1 k_2 \lambda_2 \lambda_3 - k_1^2 \lambda_3^2 - k_2^2 \lambda_3^2,$$
$$L_2 = -(k_2 \eta_1 + k_1 \eta_2),$$
$$L_3 = \lambda_3 \eta_1 + \lambda_2 \eta_2,$$
$$L_4 = (2k_1 k_2 \lambda_2 \lambda_3 - k_1^2 \lambda_3^2 - k_2^2 \lambda_3^2)(\lambda_3 k_2 + \lambda_2 k_1 - \lambda_1')$$
$$+ \eta_1 k_2 \lambda_1 + \eta_2 k_1 \lambda_1.$$

Corollary 3.7 *Let $\phi: I \subset \mathbb{R} \to \mathbb{E}^3$ be a unit speed Tzitzeica curve, $\{\mathbf{t}, \mathbf{n}_q, \mathbf{b}_q\}$ be its q-frame, and k_1, k_2, k_3 be q-curvatures. The Tzitzeica curve ϕ is not both harmonic tangent vector and harmonic 1-type tangent vector.*

Proof. Assume that ϕ is a the *Tzitzeica curve*. Considering the Definition 2.1 and the Corollary 3.7 together, If the curve ϕ is a harmonic 1-type tangent vector, The following equations can be written

$$k_1^2 + k_2^2 = 0,$$
$$k_1' - k_2 k_3 = 0,$$
$$k_1 k_3 + k_2' = 0.$$

In this case, we can write $k_1 = k_2 = 0$, but the last equations conflict the Definition 3.1. That is, the *Tzitzeica curve ϕ i*s not harmonic 1-type tangent vector according to q-frame in Euclidean space.
The other case can be shown similarly. That is, the *Tzitzeica curve ϕ i*s not harmonic tangent vector according to q-frame in Euclidean space.

Theorem 3.8 *Let $\phi: I \subset \mathbb{R} \to \mathbb{E}^3$ be an unit speed Tzitzeica curve, $\{\mathbf{t}, \mathbf{n}_q, \mathbf{b}_q\}$ be its q-frame, and k_1, k_2, k_3 be q-curvatures. The differential equation characterizing Tzitzeica curve according to its q-normal vector is obtained*

$$\mu_2 \nabla_{\phi'}^3 \mathbf{n}_q - (\eta_3 k_3 + \eta_4 k_1) \nabla_{\phi'}^2 \mathbf{n}_q + (\eta_3 \lambda_3 - \eta_4 \lambda_1) \nabla_{\phi'} \mathbf{n}_q \qquad (12)$$
$$+ (\eta_3 k_3 \lambda_2 - \mu_2 (\lambda_1 k_1 + \lambda_2' - \lambda_3 k_3) + \eta_4 k_1 \lambda_2) \mathbf{n}_q = 0,$$

where

$$\lambda_4 = -k_1' - k_2 k_3,$$
$$\lambda_5 = -k_1^2 - k_3^2,$$
$$\lambda_6 = -k_1 k_2 + k_3',$$
$$\mu_2 = k_1 \lambda_3 + \lambda_1 k_3$$
$$\eta_3 = \lambda_1' + \lambda_2 k_1 - \lambda_3 k_2,$$
$$\eta_4 = \lambda_1 k_2 + \lambda_2 k_3 + \lambda_3'.$$

Proof. Assume that ϕ is the *Tzitzeica curve* and $\{\mathbf{t}, \mathbf{n}_q, \mathbf{b}_q\}$ is its q-frame. Then, the following equations can be written

$$\nabla_{\phi'} \mathbf{n}_q = -k_1 \mathbf{t} + k_3 \mathbf{b}_q, \qquad (13)$$

$$\nabla_{\phi'}^2 \mathbf{n}_q = (-k_1' - k_2 k_3) \mathbf{t} + (-k_1^2 - k_3^2) \mathbf{n}_q + (-k_1 k_2 + k_3') \mathbf{b}_q, \qquad (14)$$

and

$$\nabla_{\phi'}^3 \mathbf{n}_q = \left(-k_1'' - k_2' k_3 - 2k_2 k_3' - k_1^3 - k_1 k_3^2 + k_1 k_2^2 \right) \mathbf{t} \qquad (15)$$
$$+ (-3k_1 k_1' - k_1 k_2 k_3 + k_1 k_2 k_3 - 3k_3 k_3') \mathbf{n}_q$$
$$+ (-2k_1' k_2 - k_2^2 k_3 - k_1^2 k_3 - k_3^3 - k_1 k_1' + k_3'') \mathbf{b}_q.$$

The proof is completed.

Corollary 3.9 *Let $\phi: I \subset \mathbb{R} \to \mathbb{E}^3$ be a unit speed Tzitzeica curve, $\{\mathbf{t}, \mathbf{n}_q, \mathbf{b}_q\}$ be its q-frame, and k_1, k_2, k_3 be q-curvatures. The Tzitzeica curve ϕ is not both harmonic q-normal vector and harmonic 1-type q-normal vector.*

Proof. The proof is clear from the proof of the Corollary 3.7.

Theorem 3.10 *Let $\phi: I \subset \mathbb{R} \to \mathbb{E}^3$ be an unit speed Tzitzeica curve, $\{\mathbf{t}, \mathbf{n}_q, \mathbf{b}_q\}$ be its q-frame, and k_1, k_2, k_3 be q- curvatures. The differential equation characterizing Tzitzeica curve according to its q-binormal vector is obtained*

$$\mu_3 \nabla_{\phi'}^3 \mathbf{b}_q - (\eta_5 k_3 + \eta_6 k_2) \nabla_{\phi'}^2 \mathbf{b}_q - (\eta_5 \lambda_8 + \eta_6 \lambda_7) \nabla_{\phi'} \mathbf{b}_q \qquad (16)$$
$$+ \left(\eta_5 k_3 \lambda_9 + \eta_6 k_2 \lambda_9 - \mu_3 (\lambda_7 k_2 - \lambda_8 k_3 + \lambda_9') \right) \mathbf{b}_q,$$

where

$$
\begin{aligned}
\lambda_7 &= -k_2' + k_1 k_3, \\
\lambda_8 &= -k_1 k_2 - k_3', \\
\lambda_9 &= -k_2^2 - k_3^2, \\
\mu_3 &= \lambda_8 k_2 - \lambda_7 k_3, \\
\eta_5 &= \lambda_7' - \lambda_8 k_1 - \lambda_9 k_2, \\
\eta_6 &= \lambda_7 k_1 + \lambda_8' - \lambda_9 k_3.
\end{aligned}
$$

Proof. Assume that ϕ is the *Tzitzeica curve* and $\{\mathbf{t}, \mathbf{n}_q, \mathbf{b}_q\}$ is its q-frame. Then, the following equations can be written

$$\nabla_{\phi'} \mathbf{b}_q = -k_2 \mathbf{t} - k_3 \mathbf{n}_q, \tag{17}$$

$$\nabla_{\phi'}^2 \mathbf{b}_q = (-k_2' + k_1 k_3)\mathbf{t} + (-k_1 k_2 - k_3')\mathbf{n}_q + (-k_2^2 - k_3^2)\mathbf{b}_q, \tag{18}$$

and

$$
\begin{aligned}
\nabla_{\phi'}^3 \mathbf{b}_q = &(\lambda_7' - \lambda_8 k_1 - \lambda_9 k_2)\mathbf{t} + (\lambda_7 k_1 + \lambda_8' - \lambda_9 k_3)\mathbf{n}_q \\
&+ (\lambda_7 k_2 - \lambda_8 k_3 + \lambda_9')\mathbf{b}_q.
\end{aligned}
$$

Corollary 3.11 *Let* $\phi: I \subset \mathbb{R} \to \mathbb{E}^3$ *be a unit speed Tzitzeica curve,* $\{\mathbf{t}, \mathbf{n}_q, \mathbf{b}_q\}$ *be its q-frame, and* k_1, k_2, k_3 *be q-curvatures. The Tzitzeica curve* ϕ *is not both harmonic q-binormal* vector *and harmonic 1-type q-binormal* vector.

Proof. The proof is clear from the proof of the Corollary 3.7.

Conclusion

Tzitzeica curve is a special spatial curve which is introduced by Gheorghe Tzitzeica in 1911. We redefine the *Tzitzeica curve* according to q-frame in Euclidean 3-space. We obtain the necessary and sufficient condition for a *Tzitzeica curve* to be a spherical curve. Then, we give some curvature properties satisfied by these curves. Finally, we obtain differential equations that characterize *Tzitzeica curves* according to q-frame and we determine if the *Tzitzeica curve* can both be harmonic and harmonic 1-type vector for three cases according to q-frame in Euclidean 3-space.

Scientific Ethics Declaration

The authors declare that the scientific ethical and legal responsibility of this article published in EPSTEM journal belongs to the authors.

Acknowledgements or Notes

References

Agnew, A., Bobe, A., Boskoff, W., & Suceava, B. (2010). Tzitzeica curves and surfaces. *The Mathematica Journal, 12*, 1-18.

Bayram, B., Tunc, E., Arslan, K., & Ozturk, G. (2018). On Tzitzeica curves in Euclidean 3-space, *Facta Universitatis, Series: Mathematics and Informatics*, 409-416.

Bila, N. (2012). *Symmetry reductions for the Tzitzeica curve equation*, Math and Computer Science Faculty Working Papers.

Bobe, A., Boskoff, W. G., & Ciucă, M. G. (2012). Tzitzeica-Type centro-affine invariants in Minkowski spaces. *Analele Universitatii" Ovidius" Constanta-Seria Matematica, 20*(2), 27-34.

Crâsmareanu, M. (2002). Cylindrical Tzitzeica curves implies forced harmonic oscillators. *Surfaces, 1*, 32.

Dede, M., & Ekici, C. (2018). Directional Bertrand curves. *Gazi University Journal of Science, 31*(1), 202-211.

Karacan, M. K., & Bukcu, B. (2009). On the elliptic cylindrical Tzitzeica curves in Minkowski 3-space. *Sci. Manga, 5*, 44-48.

Kocayigit, H., Kazaz, M., & Ari, Z. (2016). *Some Characterizations of space curves according to Bishop frame in Euclidean 3-space E3*. Ankara Matematik Gunleri, TOBB Ekonomi ve Teknoloji Universitesi Matematik Bolumu, Ankara, 3-4.

Yazici, B. D,. Karakus, S. O., & Tosun, M. (2022). On framed Tzitzeica curves in Euclidean space. *Facta Universitatis, Series: Mathematics and Informatics*, 313-325.

Author Information

Muhammed Talat Sariaydin	**Aziz Yazla**
Selcuk University, Department of Mathematics, 42130, Konya, TURKEY. ORCID: 0000-0002-3613-4276	Selcuk University, Department of Mathematics, 42130, Konya, TURKEY. ORCID: 0000-0003-3720-9716
Contact e-mail:*talatsariaydin@gmail.com*	azizyazla@gmail.com

To cite this article:

ICRETS 2022: International Conference on Research in Engineering, Technology and Science

The Role of Project Management in Cyber Warfare with the Support of Artificial Intelligence

Oszkar DOBOS
Obuda University

Agnes CSISZARIK-KOCSIR
Obuda University

Abstract: Cyberspace has a large number of actors and technologies involved that are parts of civil society. The ICT sector professionals and their applied and RDI project technologies are integral and indispensable parts of cyberspace. Project management doctrines and methods can significantly improve the effectiveness of projects, driving organizations towards success. Asymmetric or hybrid warfare clearly extends to the civil sector, and the reverse of this relationship raises interesting questions. The aim of the study is to examine, that what is the role of civilian professionals and technologies in cyber warfare? Narrowing down the question, the focus of this article is on what role project managers and methodologies have in cyber warfare, and in what ways can AI support them? Shall the PM knowledge help and support the efforts. The paper helps to present the issues raised through the eyes of project management by providing a systematic literature review through different aspect of the topic.

Keywords: Project Management, Cyber security, Artificial intelligence

Introduction

The aim of this paper is to determine whether project management has a role in cyber warfare. If there is one, to what extent does artificial intelligence support project management to operate effectively in cyber warfare? We think the ICT sector has surpassed, or at least caught up with, the defence industry in terms of RDI projects. This is understandable, as global skills shortages and capital-intensive developments are concentrating high value-added RDI activity to where large pools of highly skilled personnel and adequate funding is available. These are clearly concentrated in global technology companies, which have a vested interest in continuous improvement, gaining a competitive advantage and achieving ever higher market penetration. This has resulted in an almost unimaginable pace of technological development and the widespread adoption of global products and services. These enable civil society to enter cyberspace and become an active player in it. In response to the impact of digitalisation, global services are also bringing other economic and political actors into cyberspace, so that critical infrastructure and critical information infrastructure owned and operated by civilians also become parts of the network.

In this paper, we will first demonstrate that a significant part of cyber warfare takes place in the civil sector, not only through civilian targets, but also through professionals who take an active role in this activity. Using the structure of the ICT sector, we will illustrate the role of project management in the operation of the sector and in the relevant areas of cyber warfare. We also present ICT technologies and their links to artificial intelligence, and will examine the most commonly used project methodologies in terms of current and potential applications of AI.

Systematic Literature Review

1. Interpreting and Positioning Cyber Warfare

In order to introduce cyber warfare and link it to project management, we first need to define and characterise the concept of cyberspace. There are many definitions and historical overviews available to describe cyberspace, and we will mention only those, which we consider to be definitive and which we think can be applied practically and scientifically, based on our current knowledge and understanding. Therefore, in this article we will present modern approaches through which we illustrate the relationship of cyber warfare with the civil sector and project management. Haig's (2018) detailed, yet concise definition is a good starting point for our present work, which states that "cyberspace is the man-made, dynamically changing artificial domain in which interconnected infocommunication devices and systems operate using the electromagnetic spectrum to collect, store, process, transmit and use information, enabling continuous and global connectivity between people and devices. The above definition corresponds to:

- the need for new forms of interconnectability between people
- the connectivity of physical devices, in line with the Internet of Things principle, and
- the use of the electromagnetic spectrum."

It places a strong emphasis on information as the fundamental driving force of cyberspace. It describes well the technological and logical links between machine-to-machine, human-to-human and human-to-machine, and the flow of information through these links, i.e. the virtual dimension. It also points to the networkisation that is a prerequisite for today's knowledge and technology-based world (Haig, 2018). Taking and strengthening this idea further, it is worth to mention the approach of Laszlo Kovacs, which also suggests a viewpoint appropriate to the modern ICT era. According to Kovacs, cyberspace is an umbrella term that includes everything that comes into contact with information, i.e. processes, actors of these processes, technical and software tools, the systems involved; all of these are directly or indirectly connected to a computer network (Kovacs, 2018a). Having summarized the two definitions, cyberspace is best described as any element, device, process, system, activity, and actor that is networked and directly or indirectly related to the production, processing, transformation, transport, storage or use of data and/or information.

Warfare, as defined, will not be addressed in this article, because one of the characteristics of cyberspace and the virtual world is that it completely blurs the boundaries in the areas that are the defining parameters of this type of action. Thus war and peace cannot be precisely defined in the dimensions of time, space and actors. In terms of actors, in cyberspace warfare, be it defence or counter-insurgency, the actors who carry out actions and those who are targeted are not necessarily military actors. It is safe to say that the majority of potential targets in cyberspace can be identified in civil, economic or political domains. Elements of critical infrastructure or critical information infrastructure, social media systems or events involving large crowds, such as elections or sporting events, are all high-risk areas of cyberspace that do not belong to a country's military forces. This is why civilians and civilian-military cooperation in cyberspace operations have an important role to play in NATO's understanding of cyberspace. Joint activities are complemented by, among other things, joint competence building and capability development (NATO, 2009).

The time horizon is also blurred and it is not possible to separate war or warfare from peace, as cyberspace is characterised by the fact that cyber incidents, whether caused by malicious software robots or human actions, can occur at any time, both on the offensive and defensive. The civilian population, accessible through cognitive operations and internet techniques, is a potential target at every moment. As with the previous analogy, the location of a war zone or a specific area of operation cannot be separated or delimited. Anything that exists in cyberspace, i.e. is connected to a network, is accessible from any point on the network regardless of geographical location or distance.

To summarise the above, cyber warfare, given the specificities of cyberspace, is an activity that is constant in time and space, and in which everyone who is directly or indirectly connected to the information network becomes an actor. In line with Laszlo Kovacs, we understand this activity as a deliberate act of military, political, and economic defence in cyberspace. In our interpretation, the use of the word "warfare" is justified because this activity is carried out in pursuit of national interests and, where appropriate, threatening the interests and security of other nations. The fact that NATO identified cyberspace as the fifth theatre of war at the Warsaw Summit in 2016 complements and completes this line of thought (NATO, 2016).

Warfare involves the use of offensive and defensive capabilities alike, and in this case, cyber weapons and cyber defence assets as well. Thus, we should not think of devices that operate in the physical dimension, similar to the mechanism of action of real devices, but of software and hardware tools and their application in cyberspace that inflict some degree of damage on designated targets (Kovacs, 2018b). Indirectly, of course, this damage can be physical, material or even cognitive, but overall, the first target is always some kind of information and the carrying out of an operation involving it. Since this paper aims to focus on the role of civil development project managers in cyber warfare, herein it is appropriate to focus on the information-related areas of cyber warfare, therefore we examine the ICT sector's link to that field.

2. ICT and Cyber Warfare

The definition of cyberspace illustrates the link with the infocommunications industry: networks, especially the internet, information operations, actors, the IoT principle, or wireless communications. Given that the environment for cyber warfare is cyberspace, an indirect link between cyber warfare and ICT can be demonstrated. By interpreting cyber warfare, direct links can also be proven, which is why we consider it necessary to briefly address this issue. Focusing on the ICT sector and civilian use, I will only examine certain cyber-operational capabilities of cyber warfare (Haig, 2018).

- Computer network operations
- Deception
- Psychological operations
- Civilian-military cooperation
- Mass information / mass media.

Computer network operations are operations involving the physical and logical layers of the network. They target network elements, software, hardware, and databases, and include detection, attack, defence, and data manipulation within the network. The term "deceptiveness" covers the communication of any information that is not true, meaning that it can be physical deception, be it electronic or software induced, or even psychological - e.g. social engineering. Deception can occur in all layers of cyberspace. Psychological operations affect people specifically, in the sense of some form of influence, cooperation, or contact. This can apply to any kind of communication channel in cyberspace.

Civil-military cooperation is a capability that is closely related to psychological operations, using the same tools and techniques for communication between the civilian population and the administrative authorities. Mass media is specifically aimed at bringing information to the general public: information via the internet, social media, and news portals. The cyber information capabilities listed above are of course carried out in cyberspace, but it is clear that they have an impact through the products and services of ICT organisations, and in many cases they are the targets themselves.

3. The Technologies and Development of Cyberspace

It is not possible to cover all current and foreseeable technologies due to physical constraints and the dynamics of the ICT sector, so we will focus on those areas that best illustrate the role of ICT and civilians in cyber warfare, and of course, those related to artificial intelligence.The world wide web, or internet, is the basis for all digitisation and data collection: it is virtually what makes cyberspace exist on such a large scale and allows information to be shared quickly and efficiently. Although the Internet was not designed for civilian use, it is now an indispensable tool in the ICT market. Its main purposes and characteristics are (O'Reagen, 2012):

- there is no central management or supervisory body,
- no central control computer,
- billions of computers are connected to each other,
- it is not in a single physically well-defined location,
- not a physically tangible thing.

The role of the internet in networking and the technologies that build on it is important. It is therefore also important in areas such as machine learning and artificial intelligence, which rely on it for data processing and transmission. The next level of networking among Internet-based technologies is cloud technology. As bandwidth has increased, a new approach has become possible. Data is no longer stored and processed on

networked devices, but in a central location in the network. This is an important shift in approach as it fundamentally changes the way digital operations work, enabling complex data processing and the interconnection of independent systems. Another benefit for users is scalability, always using as many resources as needed, so the devices used do not need extreme capacity to meet the infrequently occurring performance peaks. Information and services can be accessed from multiple devices, without the need for duplication/multiplication across them. Tech companies in the ICT sector are constantly developing new technologies based on existing ones through RDI projects. Cloud computing and evolving mobile communications, in contrast to the smart device networks of the past, allow almost any electronic device to be networked and then remotely monitored or even controlled. This means that the condition is reversed and networking can transform anything into a smart device. We call this the Internet of Things (IoT). In many cases with IoT, everything regarding information is actually happening in the cloud. A networked device contains just a sensor and a microchip that enables network connectivity. This is an important milestone for cyberspace, as much of the real physical world can be converted into data through sensors and thus moved into cyberspace. IoT technology forms the basis for the entire smart ecosystem, such as smart cities, smart homes, smart cars and their further development into connected vehicles and the resulting self-driving vehicle technology.

This is a huge amount of data, which is growing exponentially as infocommunications technologies take over. According to Cisco's 2018-2023 projections, the number of internet users will grow from 3.9 billion to 5.3 billion, and the number of networked devices will increase from 18.4 billion to 29.3 billion (Cisco, 2020). This of course implies an increase in data volume, based on a year earlier projections, with personal data traffic rising from 13 gigabytesto to 35 gigabytes from 2017 to 2021. The classical data processing methods used and structured databases are not suitable for processing such volumes and, more importantly, such complexity of data sets, and therefore a new technological development is underway, called Big Data. Big Data works differently from traditional data operations; there is no data processing on the networked device or sensor, it is done in the cloud, where huge amounts of data are collected and connected. Then servers, also with huge resources, have the capacity to perform the operations issued at the endpoints. This, in addition to the advantages of cloud computing, gives the possibility of linking completely independent data, thus making it possible to use and visualise information in ways that have not been used or even known before.

The technologies presented so far allow data to be collected, transformed and processed. Thanks to digitalisation, IoT and broadband communication technology, a lot of data is being accumulated that could not be processed by earlier methods or only with great inefficiency. The trend to address this is Big Data. Along with this, another very important technology is also coming to the fore - artificial intelligence (AI). AI is designed to perform tasks automatically, without human intervention. In the first wave, human knowledge and skills are taught to software, parameterised and, based on certain information and feedback, machines can perform complex tasks, such as making decisions, in a given environment. Data-intensive operations in the last few years have pushed research in a more dynamic, adaptive direction than the earlier approach. This means that, in addition to decisions and predictions made from historical data, these algorithms can also work based on real-time information obtained from the environment. Recent research results go beyond this to endow AI with the ability to learn. This ability called machine learning allows the results of the analysis of incoming data to be incorporated into further operations, i.e. to improve operations - in other words, learning. This is currently a complex and complicated operation, requiring a very large amounts of data, which in many cases is not available, so synthetic data is produced, which makes the process of learning very expensive and time consuming (Negyesi, 2019).

In addition to the technologies already in use and widely accepted, the future is of course also about developing these and similar technical solutions. Although, according to the technological singularity defined by Raymond Kurzweil, we cannot accurately predict the technologies of the future, because we will reach a point in our development where, due to the rapid pace of development, we will not be able to grasp the workings of tomorrow (Kurzweil, 2013). There are estimates, however, and various research institutes are trying to identify trends that show the future in a few years' time. The Gartner research institute is constantly analysing and using a hype curve to identify and determine future trends. The latest available hype curve for 2019 identifies five areas, of which we will only discuss those related to AI in more detail (Gartner, 2019):

- Sensors and mobility: this trend brings together technologies that increasingly enable mobility and the management of associated devices, including 3D sensor cameras and advanced autonomous driving. With advances in sensors and AI, autonomous robots can operate more consciously in the environment around them. For example, new technologies such as lightweight transport drones (both flying and taxiing) will be more advanced in navigating and taking account of objects. This technology is currently hampered by the legal environment, but technological development will continue.

Technologies covered include cloud-based augmented reality (AR), fourth and fifth level self-driving and flying self-driving vehicles.
- Human robotic technologies is a trend to improve human physical and psychological capabilities with biochips and emotional artificial intelligence.
- Post classical computing and communication: classical or binary computing, which uses binary bits, is evolving by modifying existing traditional architectures.
- Digital ecosystems, which are sharing platforms connecting cyberspace actors.
- High-level artificial intelligence (AI) and analytics. Next-generation analytics is the autonomous or semi-autonomous analysis of data or content using sophisticated tools, beyond traditional business aspects. Technologies based on machine learning models will enable the further development of AI and, through it, data analytics. This trend includes adaptive machine learning, AI, and graph analytics.

In addition to the benefits, the new technologies and developments described above also pose increased risks, as they ensure that the entire society and economy is connected to the cyberspace.

4. Extending Cyber Warfare to the Civil Sector

Cyber warfare naturally includes reconnaissance and counter-intelligence activities, but from the perspective of ICT organisations and civilian experts, it is reasonable to narrow the analysis to defence, because in peacetime it is illegal to conduct any kind of reconnaissance or counter-intelligence. To show the civilian dimension of cyber defence, it is also necessary to understand both critical infrastructure and critical information infrastructure as entities that are important for the country, but are operated by civilians, such as telecommunication companies, the banking sector, media, and transport, with a special focus on logistics. Infrastructure elements critical to national security. Article 1, point f. of Act CLXVI of 2012 defines critical infrastructure as follows. *"An asset, facility or system element belonging to one of the defined sectors that is essential for the performance of vital societal functions, in particular health, safety and security of people and property, and the provision of economic and social public services, the loss of which would have significant consequences due to the lack of continuity in the performance of these functions, but which has also become critical information infrastructure as a consequence of digitalisation and the data-driven society."* (CLXVI Act)

It is not possible to give a detailed and comprehensive list in this publication, but one of the main sectors and its sub-sectors is an important part of the subject, and a large part of it also operates in the NGO/civil sector:

Table 1. The types of info communication technologies

Infocommunications technologies	Internet infrastructure and Internet access services
	fixed and wireless electronic communications services, fixed and wireless communications networks
	radio telecommunications
	space telecommunications
	broadcasting
	postal services
	government information technology, electronic networks

Critical Information Infrastructure is defined in a government decree for the following year, the Decree on the Implementation of the Critical Infrastructure Protection Act. *"The networked, physical or virtual systems, devices and methods of society which, due to the need to ensure the continuity of information and the continuity of IT conditions, are essential for the operation of vital system elements by themselves or other identified vital system elements."* (Government Act, 2013).

Critical Information Infrastructure has been defined in a government decree for the following year, the Decree on the Implementation of the Critical Infrastructure Protection Act. *"The networked, physical or virtual systems, devices and methods of society which, due to the need to ensure the continuity of information and the continuity of IT conditions, are essential for the operation of vital system elements by themselves or other identified vital system elements."* (Government Act, 2013).

Beyond these systems, cybersecurity is important for ICT companies' products and services, as high internet penetration puts citizens' data, and through it their assets, at risk. Taking this further, ICT organisations and professionals are indispensable actors in cyberspace and should therefore be an important part of cyber defence. According to Alexander Klimburg, ICT actors are also an integral part of information security. The products and

services of ICT companies, which are accepted and globally distributed, are also a source of vulnerability. Because of the products and services used worldwide, no country is able to secure the entire ICT supply chain on its own, from sources it can entirely trust and control. Areas where the products of multiple suppliers need to be integrated pose a fundamental risk, compounded by cases where products that are unreliable or uncontrollable for the organisation or even the country, are incorporated. The figure below illustrates the role of ICT security in information security (Klimburg, 2012).
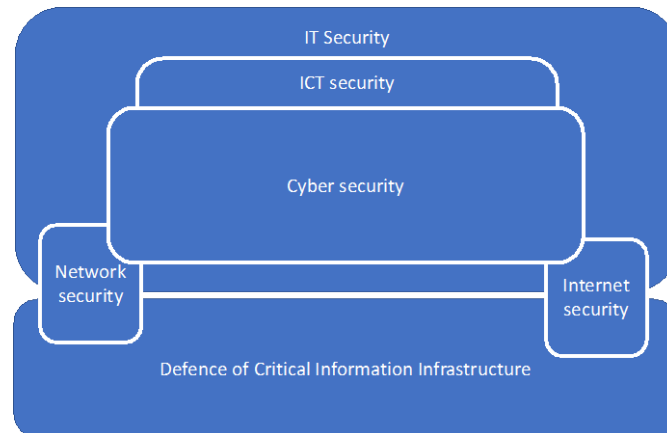

Figure 1. The role of ICT security in information security

So the main link between cyber warfare and the ICT sector is cyber defence and cyber security. In summary, the above shows that a significant part of cyber warfare is taking place in the civilian part of the ICT sector. The majority of civil actors are targets of cyber warfare in relation to the total number of citizens, but professionals in the field appear in important defensive roles. The experts required to develop models, hardware and software tools for defence, their implementation, integration with each other, customisation to the organisation and response and recovery to a given incident are the following:

- technical specialist, typically from several fields
- project manager
- business analyst
- technical analyst/responsible person
- other specialists (legal, economic, political, and communication skills may be required for a specific issue)

A technical specialist and project manager are included in all of the projects listed, while the need for a business analyst, a technical officer or other specialists depends on the type and size of the project and the organisation's processes.

Results and Discussion

1. Project Management in the AI and ICT Sectors

The organizational structure of today's organisations in the ICT sector is generally twofold. The first is the project organisation, which is explicitly project-based, so the organisation is built around projects, which are at the heart of its operations. The management typically follows the "management by project school", and therefore takes project management to a strategic level: the whole organisation works on a project basis and there is full alignment between project objectives and corporate objectives (strategic goals). Outside the project, colleagues only participate in training, education and internal efficiency improvement projects. Typically, after a project is completed, employees are placed in a so-called resource pool, from where they can be freely involved in a new or ongoing project. In IT, this model is typically used by organisations involved in custom development, systems integration, high value-added RDI consultancy and implementation, and by research laboratories.

Another form of organisation is the matrix organisation, where, if we imagine a matrix, the columns are the functional units and the rows are the projects. Both the functional unit and the project have a manager. In a matrix organisation, the functional unit has core tasks that need to be performed. Projects, on the other hand, are

built up by "hiring" colleagues from several functional units across the organization. Projects form the rows in the matrix. Project approach and project-function are also important in this organisation, which is why temporary organisations and project managers are identified by name within the structure. Between projects, colleagues carry out the core activities of the unit in their respective departments. This model is used by large organisations that have other ongoing core activities, services or products in addition to project activities. Typical examples are multinational companies, centralised international groups and large public organizations (Gaal & Szabo, 2013).

With the proliferation of agile methodologies, a third organisational structure is coming to the fore, similar to a project organisation, however, in this methodology, the project team does not split up after completing a task, but stays together and is dedicated to the next task as a team. This is only possible in a highly agile, flexible environment, which is why even fewer organisations opt for it; these are typically small to medium-sized development companies or organisations with a product of their own that need to respond quickly to customer needs, e.g. start-ups and innovative companies that develop new technologies. Both main organizational structures focus on effective project management, and the vast majority of their operations and work is project-based. In addition to the organisational structure, these bodies strengthen their operations with professional project management at the organisational level. In order to measure and improve this, they use existing methodologies and measure the maturity of the organisation in order to see where it stands in its development.

According to the Project Management Institute (PMI) 2018 survey, 93% of companies use some form of standard project management (PMI, 2018). An earlier survey by Price Waterhouse Coopers in 2007 found a similarly high proportion, with 77% of businesses using some form of documented, company-wide project management methodology (PwC, 2007). The maturity models look at different aspects of project management in an organisation, using different methods, which are described in more detail in the description of the models below.

Paul, one of the researchers of the CMM(R) model, defines PM maturity as "how clearly a specific process is defined, managed, measured, controlled, and how effective it is" (Paul et.al, 1993). According to Skumolski, project management maturity is both a measure of the organisation's receptiveness and openness to project management, and a measurement of the extent to which the organisation is able to fully support and enable its project managers to take the steps necessary for the success of the project (Skumolski, 2001).

In the following, only the most common project management maturity models will be presented, as Pennypacker collected more than 30 existing models in the early 2000s, and their number has been increasing ever since (Pennypacker & Grant, 2003). The three best-known and most used project management models are currently PMI - OPM3, PRINCE2 and the International Project Management Association (IPMA) model. However, the PMI, Prince2 and CMMI models are those that will be presented in this publication, as CMMI was specifically developed for ICT developments and therefore I believe it has more relevance than the IPMA model, and I also think that its penetration is not lower either when looking specifically at the IT domain.

The models are presented without being exhaustive, focusing on areas where they can or could be connected to AI. The main reason for the creation of this model was to manage projects in IT organisations, but it is now considered a much more widespread, almost universal project management methodology. This project management technique, based on a 'de facto' standard, has become a common and frequently used methodology not only in the UK but also in Europe (OGC, 2005).

PRINCE2 is a process-based approach to project management. It describes how a project can be divided into different, separately manageable processes, each with well-defined inputs, outputs, and objectives. The method is based on quality management, which allows the organisation to control the project from its inception to its completion.

Four key elements of the PRINCE2 methodology:

- 8 defined processes that provide the framework for project management
- 8 principles and guidelines used under the different processes
- 3 methods that support the processes
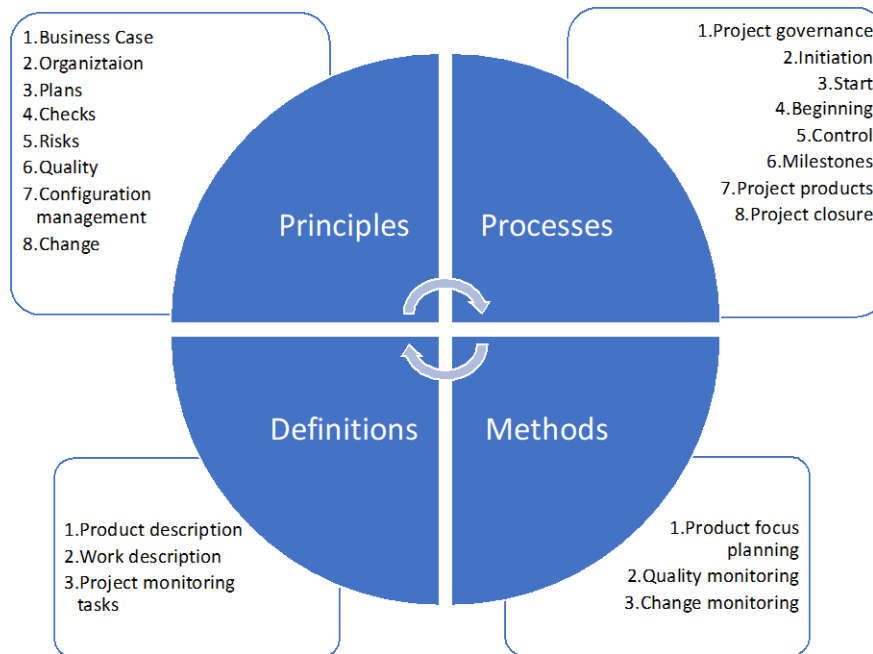- Precise definition of the components for project verification

Figure 2. PRINCE2 key features

If an organization chooses this methodology, it allows its managers and project managers to take a unique approach to different projects. The PRINCE2 methodology assumes that the organisation already has well-established project management techniques in place, so it encourages participants to continue using and developing them. The model itself has five levels of maturity, as follows:

Figure 3. Levels of the PRINCE2 maturity model

On the first and second levels there aren't any controlled processes or procedures, although it is not even neccesary for the execution of ad-hoc tasks. There are agreed guidelines for processes and procedures at the defined level, which apply to all projects. Depending on the organisation, there may even be guidelines on the use of artificial intelligence or related tools. At the managed and at the optimal levels, most processes operate within a controlled framework, but there are procedures in place as well. Here, the organisation performs project management tasks at a professional level.

The PRINCE2 methodology, a tool for effective operational project management, does not currently place primary emphasis on the use of artificial intelligence or any related IT tools. Its general process is to enable a specific/individual focus on the use of AI-based techniques or tools, with a strong mandate from the project manager, there are no specific recommendations or good practices dedicated within the framework of the methodology. By its very design, the model is about providing the project manager with a wealth of accurate

data. Due to digitalisation and strong authorisation, organisations and project managers using the methodology can quickly adopt AI logic and support even for ongoing projects.

2. Capability Maturity Model Integration

The CMMI model can basically be described as a "hybrid" model that has been created by incorporating the strengths of several maturity models. The aim was to develop a model to support the development of processes and products. It consists of two parts, an organisational maturity test part and a process maturity part. The organisational maturity part, known as the "gradual" part, examines groups of key organisational processes that need to be improved in order for the organisation to move to a higher level of maturity. The latter area is the continuum approach, which identifies capability levels for each process [22]. In the case of the CMMI model, we can also speak of 5 maturity levels, with key processes identified at each level. Its creators have also collected tools to help organisations at lower levels to move to higher levels.

- development of organisational rules
- process design
- identifying and making free resources available
- establishing areas of responsibility
- training of employees
- applying performance management to processes
- identification and involvement of relevant stakeholders
- monitoring and controlling processes
- gathering information for development

The highly process-oriented and integrative nature of the CMMI model emphasises the close intertwining of organisational processes and standards with project management, thus facilitating the extension of the artificial intelligence tools and good practices applied by the organisation to the projects. It places less emphasis on identifying and analysing them, thus hiding the potential for their application beyond the organisational use. Project managers are less empowered due to mature and planned processes, and therefore have less opportunity to independently implement new AI applications unknown to the organisation. The methodology focuses on the technical part of project management, on development tasks, and adopts the additional areas and processes from within the organisation.

3. Organization Project Management Maturity Model – OPM3

The Project Management Institute aimed to create a 'good practice' resource in the area of project/programme/portfolio management, which could also be used to standardise and assess these capabilities of the organisation. OPM3 is also a generic model that can be implemented across different industries, sizes and geographies.

With the model, users will be able to identify which good practice belongs to which area, and thus match theory with practice, increasing the efficiency of implementation. Hundreds of case studies are available in the field of organisational project management, showing which specific skills need to be developed and how to develop them to reach the desired level of maturity. Furthermore, OPM3 supports the organisation in its self-assessment. Based on these results, the strategic prioritisation and resources of the organisation, it helps to create a development plan. This plan enables the development of the necessary project management skills, thus leading to a higher level of maturity.

The basic components of OPM3 (PMI, 2003):

- A collection of good practices
- Collection of skills
- Observable outputs
- Key performance indicators.
- Development plan.

The structure of OPM3 (PMI, 2003):

- Standardisation: repeatable processes and activities are used by the organisation.
- Measurement: it can measure its processes, activities and their effectiveness.
- Management: it can analyse and evaluate measurements. It can react to them and thus control the output, i.e. the efficiency.
- Continuous development: the need for improvement is established. The emphasis shifts from reactive to proactive behaviour, with problems and performance issues not aimed to be solved but to be prevented and eliminated.

In addition to the maturity levels, there are three levels of management that make up project management at the organisational level: project, programme, and portfolio. These areas are divided into five project life cycles: identification, design, implementation, monitoring and management, and closure. From this we can draw the structure of the OPM3. These good practices (represented by arrows) lead through the maturity levels, which are broken down into project lifecycle (rings). The rings contain the skills required for the level (points within the rings).
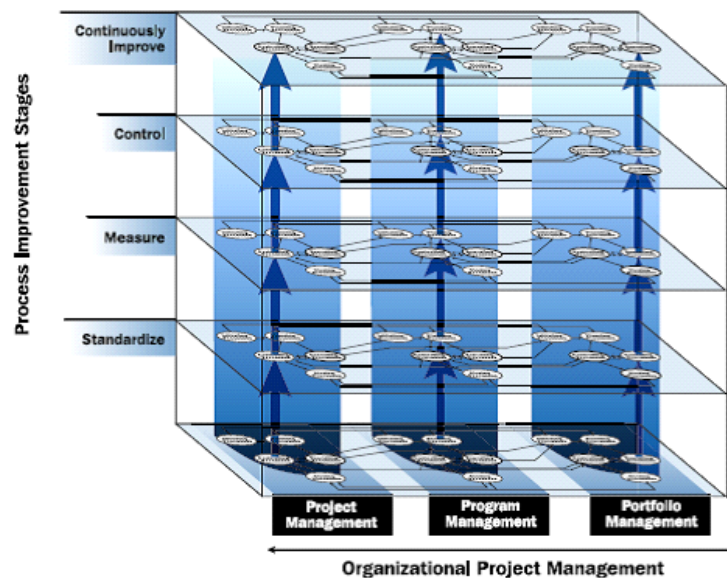

Figure 4. OPM3 structure

3. OPM3 model summary

The PMI model, while often referring to organisational policies and processes in general, does not mention AI as a specific area of maturity or project management. It is important to note, however, that PMI in his recent research names AI as an important and indispensable organisational capability. [24] It relies on a strong matrix or project-oriented organization for its operation, a very strong empowerment for project management. It provides the opportunity to identify areas for improvement or even project risks where the application of MI could be a solution. This is important because it gives you the authority to allocate resources within the project. This could mean specialist staff, extra time for certain tasks, or even financial resources for tools or training for colleagues. So there is a certain degree of freedom for project management in this model, although the client's needs and risk apportionment must of course be taken into account. That said, it is of course not a sustainable method if each project needs to introduce MI individually, but the model is structured so that it can easily become good practice, then become legitimate to use and can be adopted by the whole organisation's project management in a spirit of continuous improvement.

Although current methodologies do not name and dedicate processes or tools for the use of AI, it is clear from the trends that, like all fields, project management will become data-driven as a result of digitalisation, and this also means the use of AI. Currently known AI applications could be used for data processing, decision making, forecasting based on data patterns, important reporting and administration tasks, risk occurrence and assessment, and of course instant status reporting. According to PMI's 2019 research, 85% of organisational leaders predict that AI will change the way they do business within five years. The organisation has defined PMTQ, project management technology quotient, as a capability for future project management. It summarises knowledge of technologies such as AI or cyber security (PMI, 2019).

Conclusion

The publication confirmed our hypothesis that the ICT sector has a very high involvement in cyberspace, and thus in cyber warfare. This means that ICT professionals, including project managers, can be active participants in cyber warfare. In this paper, this is only confirmed for cyber defence, but knowing the project characteristics, projects can also be considered as reconnaissance or counter-intelligence type tasks. As these are also carried out in the civilian part of cyberspace, and since the actors, environment and tools are the same, the methodology could be the same too.

The project management methodologies used do not currently use AI in a standardised way. Therefore, it cannot be stated formally that AI makes professional project methodologies more effective or in any way assists professional project methodologies in cyber governance. Developers of project management methodologies appear to be putting a lot of emphasis on moving towards AI, and companies producing various project management tools and software are currently using AI for certain tasks. While these facts somewhat nuance the picture, overall the use and integration of standardised AI into formal methodologies is still in its infancy.

Scientific Ethics Declaration

The authors declare that the scientific ethical and legal responsibility of this article published in EPSTEM journal belongs to the authors.

Acknowledgements or Notes

This article was presented as an oral presentation at the International Conference on Research in Engineering, Technology and Science (www.icrets.net) conference held in Baku/Azerbaijan on July 01-04, 2022.

References

Act CLXVI of 2012. *On the identification, designation and protection of critical systems and installations*. Wolters Kluwer. Retrieved June 28 2021 from https://net.jogtar.hu/jogszabaly?docid=a1200166.tv.

Cisco. (2020). *Cisco annual internet report (2018–2023).* White Paper. Retrieved June 28 2021 from https://www.cisco.com/c/en/us/solutions/collateral/executive-perspectives/annual-internet-report/white-paper-c11-741490.html,

Gaal, Z.. Szabo, L. (2013). *Segedlet a projektmenedzsmenthez II. Megoldasok, modszerek, technikak*. Veszpremi Egyetemi Kiado.

Gartner (2019). 5 trends appear on the gartner hype cycle for emerging technologies, Retrieved June 28 2021, from https://www.gartner.com/smarterwithgartner/5-trends-appear-on-the-gartner-hype-cycle-for-emerging-technologies-2019/.

Government Act. *Implementing Act CLXVI of 2012 on the Identification, Designation and Protection of Critical Systems and Installations*. Wolters Kluwer. Retrieved June 28 2021 from https://net.jogtar.hu/jogszabaly?docid=a1300065.kor.

Haig, Z. (2018). *Informacios Muveletek A Kiberterben*. Dialog Campus Kiado. https://nkerepo.uni-nke.hu/xmlui/bitstream/handle/123456789/12651/web_PDF_Informacios_muveletek_a_kiberterben.pdf;jsessionid=97D3B77EE69E4C11F4B0AE1A46544334?sequence=1,

Klimburg, A. (2012). *National cyber security framework manual*. NATO CCD COE Publication.

Kovacs, L. (2018a). *A kiberter vedelme.* Dialog Campus Kiado.

Kovacs, L. (2018b). *Kiberbiztonsag es –strategia.* Dialog Campus Kiado.

Kurzweil, G. (2013). *A szingularitas kuszoben.* Ad-Astra.

NATO. (2009). Allied Joint Doctrine for Information Operations, Retrieved June 22 2021, from https://info.publicintelligence.net/NATO-IO.pdf.

NATO. (2016). *Warsaw Summit Communique*, Retrieved June 22 2021, from https://www.nato.int/cps/en/natohq/official_texts_133169.htm.

Negyesi, I. (2019): A mesterseges intelligencia es a hadseregek, *Hadtudomany, 2019*/3., 71-79.

O'Reagen, G. (2012). *A brief history of computing*. 2nd ed. Springer.

Office of Government Commerce (2005). *Managing successful projects with PRINCE2*,

Paul, M.C.; Curtis, B.; Chrissis, M.B.; Weber, C.V. (1993). *Capability maturity model for software, version 1.1*, Software Engineering Institute, Carnegie Mellon University. Retrieved May 16 2021, from https://resources.sei.cmu.edu/asset_files/technicalreport/1993_005_001_16211.pdf,

Pennypacker, J.S.; Grant, K.P. (2003). Project management maturity: An industry benchmark. *Project Management Journal, 34*(1), 4-11.

PMI (2003). *Organizational project management maturity model, opm3 knowledge foundation*

PMI. (2018). P*ulse of profession – succes in disruptive times* Retrieved May 16 2021, from https://www.pmi.org/-/media/pmi/documents/public/pdf/learning/thought-leadership/pulse/pulse-of-the-profession-2018.pdf, downloaded: 16.05.2021.

PMI. (2019). *Pulse of profession – the future of work – leading the way with pmtq*, Retrieved May 16 2021, from https://www.pmi.org/-/media/pmi/documents/public/pdf/learning/thought-leadership/pulse/pulse-of-the-profession-2019.pdf?v=ff445571-0b23-4a2b-a989-44eb20df55bd&sc_lang_temp=en.

PwC. (2007). *Insights and trends: current programme and project management practices - the second global survey on the current state of project management maturity in organisations across the world*. Retrieved May 16 2021, from https://www.pwc.com/cl/es/publicaciones/assets/insighttrends.pdf.

Skumolski, G. (2001). Project maturity and competence interface. *Cost Engineering; Morgantown, 43*(6),11-18.

Author Information

Oszkar Dobos
Obuda University
1034 Budapest, Becsi út 96/b.
Contact e-mail:*dobos.oszkar@xiagency.hu*

Agnes Csiszarik-Kocsir
Obuda University
1034 Budapest, Becsi út 96/b.
kocsir.agnes@uni-obuda.hu

To cite this article:

Dobos, O. & Csiszarik-Kocsir, A. (2022). The role of project management in cyber warfare with the support of artificial intelligence, *The Eurasia Proceedings of Science, Technology, Engineering & Mathematics (EPSTEM), 17, 26-37.*

Efficiency Evaluation of Cyber Security Based on EBM-DEA Model

Van Thanh Tien NGUYEN
National Kaohsiung University

Chia-Nan WANG
National Kaohsiung University

Fu-Chiang YANG
National Kaohsiung University

Thi Minh Nhut VO
Thu Dau Mot University

Abstract: Cyber security aims to protect against the unlawful use of systems, networks, and technologies by lowering the likelihood of cyberattacks and thwarting their execution. The comparatively low degree of security, which plays an essential part in the activities of any nation, has been a primary contributor to the low overall operational efficiency. In addition, implementing machine learning and artificial intelligence would make the network vulnerable to several severe vulnerabilities in terms of cybersecurity, which could lead to disastrous results. Therefore, research into the efficacy of cyber security is essential to ensure the future safety of the whole world. An EBM evaluation approach was utilized in this research project so that the production efficiency of firms on a micro level could be assessed. After that, it analyzed the effectiveness of cybersecurity organizations' input and output variables by using financial data for 2020 from sources in the US market. It was found that DMU 1, DMU 7, DMU 9, and DMU 10 had the highest performance levels. After doing an efficiency analysis of the ten most prominent organizations now functioning in the cybersecurity sector, we realized that three of those companies required significant modifications. However, four of the other businesses were typically more efficient.

Keywords: EBM (Epsilon-based measure) Model, Cybersecurity, 5G security, AI security, Cyber security industry.

Introduction

All aspects of society are changing because of technology. We discover that technology is being used and relied upon more and more in our personal lives and incorporated into more and more activities at work."Industry 4.0 " or "the fourth industrial revolution" are both for this transition. Fourth Industrial Revolution, also known as Industry 4.0, is a theory that predicts rapid change to occur in the 21st century in the areas of technology, industries, and societal patterns and processes(Gan et al., 2021). This change is theorized to result from growing interconnectedness and intelligent automation.

Because of this, more cyber-attacks exist on computer systems, networks, programs, devices, and data as automation and 5G technologies become more widespread (Shrestha et al., 2021). Because of this, the efficiency of a nation's cyber security measures is crucial to developing all aspects of a country's infrastructure, including its financial, economic, agricultural, medical, and even national security systems. To enhance competitiveness, assure a sustainable future, and increase overall corporate efficiencies, it is essential to examine the efficiencies

in cyber security, from which the opportunities for improvement can be discovered at each company. These efficiencies can be found by looking at each company's improvement spaces in their cyber security practices.

Within the existing body of research on efficiency, which has been chiefly conducted from a more generalist vantage point, only a select few articles have taken a specific look at the efficiency of cybersecurity organizations. In addition, rather than focusing on how input and output indicators affect efficiency, most studies have broken down efficiency before analyzing the causes. To help fill in some of these research gaps, the authors of this work use the DEA methodology and an EBM (epsilon-based measure) model to conduct a statistical analysis of the operational efficiency of 10 different cyber security businesses.

Literature Review

Traditional, static DEA analyses separate the efficacy of an enterprise into three subcategories: scale performance, entire technical performance, and natural technical performance (Bian & Yang, 2010). The EBM technique analyzes manufacturing performance from an organization's dynamic factor of view (Bin Arfaj et al., 2022). In conclusion, the slack variables have no longer been considered in maximum cybersecurity performance analyses, which is inconsistent with accurate manufacturing. This is because natural technical performance is the first aspect affecting ordinary cybersecurity performance and whether a typical DEA method or the Malmquist index methodology is correct (Chen et al., 2022). To treat this deficiency, EBM models have been applied to discover the performance of the cybersecurity enterprise (Chen & He, 2017). Despite each favored and undesirable output, the performance remains vulnerable to being overvalued within the radial path distance characteristic version. This is because the goal characteristic is to maximize entry and output inefficiencies.

Although the EBM version has been applied to engage in studies on effectiveness, the version has been used to discover and expand usage handiest a small percent of the time (Chen et al., 2018). In conclusion, researchers have investigated the performance of the usage of monetary sources by using plenty of DEA models. Because there haven't been any studies on cybersecurity performance research the use of EBM models, this paper uses an EBM version to look at the performance of the cybersecurity business (Chen et al., 2019). This is due to the fact there haven't been any studies on cybersecurity performance research that have used each "radial and non-radial EBM model" (Tone & Tsutsui, 2010) (Tavana et al., 2013).

The Methodologies and Frameworks of Research

To assess the effectiveness of a range of inputs and outputs, Data Envelopment Analysis (DEA) models that are based on "radial measurements," such as the CCR and BCC (Bian & Yang, 2010) models, likewise models based on non-radial metrics, such as the SBM model, may be utilized to evaluate the efficiency of a variety of inputs and outputs (Chen & He, 2017). [CCR] and [BCC] are abbreviations for the CCR and BCC models, respectively (Chen et al.,2022). Radial measurements assume that all components vary proportionately, which is rarely the case. These measurements also ignore slack factors, such as excessive or inadequate output (Chen et al., 2018). The SBM models (non-radial slack variable efficiency), which are based on slack variable efficiency and do not employ radial estimate assumptions, aim to optimize input and output inefficiencies by selecting the points that are the farthest away from the frontier (Tone & Tsutsui, 2010). However, as a result, they lose the information regarding the original ratio used to calculate the efficiency front projection value. The results almost always differ from the estimates since the amount of room for improvement is so significant. As a potential answer to this issue, in 2010, Tone suggested three EBM (epsilon-based measure) models that contained both "radial and non-radial components" (Chen & He, 2017). These models were "input-oriented, output-oriented, and non-oriented," respectively. Both radial and non-radial properties were taken into consideration by the models (Chen et al., 2019).

The conventional "unguided EBM calculation model" can be summarized as follows when the input-oriented EBM (EBM I-C) for DMUo = (xo, yo) is provided:

$$\delta^* = \min_{\theta, \lambda, s^-} \theta - \varepsilon_x \sum_{i=1}^{m} \frac{\omega_i^- s_i^-}{x_{io}} \tag{1}$$

Subject to

$$\sum_{j=1}^{n} x_{ij}\lambda_j = \theta x_{io} - s_{i,}^{-} i = 1,\ldots,m$$

$$\sum_{j=1}^{n} y_{ij}\lambda_j \geq y_{ro,} r = 1,\ldots,s$$
$$\lambda_j \geq 0, j = 1,2,\ldots,n$$
$$s_{i,}^{-} \geq 0, i = 1,2,\ldots,n$$

Where λ_j shows the dominant direction of DMU's intensity, "o" indicates that DMU is being evaluated, $s_{i,}^{-}$ and ω_i^{-} reflect the amount of weight and slack that is present in the ith input, ε_x It is a parameter that relies on the degree of dispersion of inputs and represents the radial qualities. Whereas $s_{i,}^{-}$ and ω_i^{-} describe how much slack and weight are present in the input, respectively, ε_x is a variable demonstrating the radial characteristics and affects the amount of scattering present in the inputs. "o" indicates that DMU is being evaluated. (Wang et al., 2021)

Research and Analysis Based on Empirical Evidence

Data Sources

This report aims to assist decision-makers (Li et al., 2021; Moreira et al., 2021; Wang et al., 2021)in evaluating what kinds of security process changes are essential by analyzing the operational efficiencies of ten cybersecurity organizations in the year 2020. There is a wide range of sizes and technologies among cyber security companies. From a structural aspect, these ten organizations have enhanced their data and market-oriented operations. Therefore, the writers compiled a list of ten cyber security businesses on the US Stock Exchange in 2020. Table 1 contains the names of all DMUs.

Table 1. List of DMUs

Units	Companies Name	Stock ID
DMU 1	Synopsys	SNPS
DMU 2	Palo Alto Networks	PANW
DMU 3	Oracle	ORCL
DMU 4	Microsoft	MSFT
DMU 5	IBM	IBM
DMU 6	BlackBerry Ltd	BB
DMU 7	Cisco Systems, Inc.	CSCO
DMU 8	CyberArk	CYBR
DMU 9	Fortinet	FTNT
DMU 10	Juniper Networks	JNPR

Evaluation of DMUs' Performance

We use the EBM-I-C, input-oriented under the assumption of constant returns-to-scale in DEA (Alghassab, 2022; Alharbi et al., 2021; Bian & Yang, 2010; Bin Arfaj et al., 2022; Chen et al., 2022; Chen & He, 2017; Chen et al., 2018; Chen et al., 2019), to evaluate the effectiveness of each cybersecurity company. This part's financial data from 2020 is shown in Table 2. The 2020 efficiency will be shown in Tables 3 and 4 below. Before evaluating the DMUs' efficiency using EBM, one of the most crucial considerations was assessing whether a positive value for the data existed. Aside from that, there's an isotonic relationship between the input and output data. The coefficient of correlation (Wu et al., 2020), which ranges from 0 to +1, defines the link between two variables. The two variables were highly correlated if the index was close to +1. If the correlation coefficient is close to 0, the connection between the input and the output is not very strong.

The Pearson's correlation of the DMUs is shown in Table 4 for each year. The minimal correlation coefficient, as seen in the findings, was 0.4918, higher than 0. This demonstrates that all data variables were correlated in a meaningful sense, making it possible to carry out EBM.

Table 2. Data in 2020 (currency unit: million USD)

DMUs	(I)Assets	(I)Liabilities	(I)Operating Expenses	(O)Revenue	(O)Gross Profit
DMU 1	8,752	3,118	2,234	3,685	2,891
DMU 2	9,065	7,964	2,588	3,408	2,409
DMU 3	115,438	102,721	16,928	39,068	31,130
DMU 4	301,311	105,184	5,294	12,958	11,812
DMU 5	155,971	135,245	28,680	73,621	35,575
DMU 6	3,888	1,359	946	893	643
DMU 7	94,853	56,933	17,582	49,301	31,683
DMU 8	1,562	855	376	464	382
DMU 9	4,045	3,189	1,533	2,594	2,024
DMU 10	9,378	4,835	1,533	4,445	2,574

Table 3. Statistics on input/output data year 2020

	Assets	Liabilities	Operating Expenses	Revenue	Gross Profit
Max	301311	135245	28680	73621	35575
Min	1562.4	855.06	375.85	464.43	381.86
Average	70426	42140	7769.4	19044	12112
SD	93872	50497	9273.9	24435	13915

Table 4. Pearson's correlation coefficient year 2020

	Assets	Liabilities	Operating Expenses	Revenue	Gross Profit
Assets	1	0.8551	0.4924	0.4918	0.5557
Liabilities	0.8551	1	0.842	0.8254	0.8538
Operating Expenses	0.4924	0.842	1	0.9962	0.9657
Revenue	0.4918	0.8254	0.9962	1	0.9646
Gross Profit	0.5557	0.8538	0.9657	0.9646	1

An affinity index was used to establish two parameters incorporating the radial and nonradial models, as indicated in the EBM model. The Pearson's correlation coefficient was replaced with the affinity index between two vectors. The values they appropriated had to meet the criterion. $0 \leq P(a, b) \leq 1$. The deviation of variables was used to calculate the diversity index (Bian & Yang, 2010) of the vectors, and $0 \leq D(a,b) = D(b,a) \leq 1/2$. The only time it was equal to 0 was when the two vectors were proportionate. To guarantee that the input and output variables were in sufficient condition to assess the effectiveness of the DMUs using EBM, the affinity and diversity indicators were utilized (Li et al., 2021; Liang et al., 2020; Moreira et al., 2021; Tian et al., 2019; Tone & Tsutsui, 2010; Wang et al., 2021). Tables 5 and 6 show the diversity index and affinity indicator matrices used to ensure that the input and output variables corresponded to the criteria for measuring the effectiveness of the DMUs in the EBM model. According to the findings, the diversity matrix values vary from 0 to 0.2994, and the affinity matrix values range from 0.4013 to 1, as shown in Tables 5 and 6. Because the data variables matched the EBM model's criteria, the model may be used to rank the efficiency/inefficiency of DMUs.

Table 5. Diversity matrix in EBM model 2020

	Assets	Liabilities	Operating Expenses
Assets	0	0.2994	0.1619
Liabilities	0.2994	0	0.2059
Operating Expenses	0.1619	0.2059	0

Table 6. Affinity matrix in EBM model 2020

	Assets	Liabilities	Operating Expenses
Assets	1	0.4013	0.6762
Liabilities	0.4013	1	0.5883
Operating Expenses	0.6762	0.5883	1

The weight to input/output and epsilon indicator is crucial in eliminating the EBM score (Jin et al., 2021; Li et al., 2019; Liang et al., 2020; Tian et al., 2019; Wang et al., 2018; Wang et al., 2021; Yu et al., 2019) for each DMU. A weighted index (Li et al., 2021)specifies the degree to which input influences output. According to

Table 7, all weight indexes are positive, indicating that information changes will influence production, and if input values increase, output values will also increase.

Table 7. Weight to input/output and epsilon for EBM model year 2020.

Weight to Input/Output		
Assets	Liabilities	Operating Expenses
0.33	0.309	0.361753438

The efficiency of ten cybersecurity companies will be obtained based on EBM's factor weight and epsilon. The result of Epsilon for EBM of 2020 is approximately 0.441, which satisfies the condition: $0 <$ Epsilon index < 1.

Table 8. Efficiency Score of EBM model 2020

No.	DMU	Score	Rank
1	DMU 1	1	1
7	DMU 7	1	1
9	DMU 9	1	1
10	DMU 10	1	1
4	DMU 4	0.934	5
3	DMU 3	0.925	6
5	DMU 5	0.874	7
8	DMU 8	0.68	8
2	DMU 2	0.627	9
6	DMU 6	0.56	10

The efficiency score of DMUs is compared in Figure 1. It can be observed from the figure that in 2020, the performance scores of organizations vary. When they achieved the first rank in 2020, Synopsys, Cisco Systems, Inc., Fortinet, and Juniper Networks will be regarded as the most effective manufacturers of units and ideals suppliers. In contrast, DMU 2 and DMU 6- Palo Alto Networks and BlackBerry Ltd are the last four efficient units and ideal suppliers.

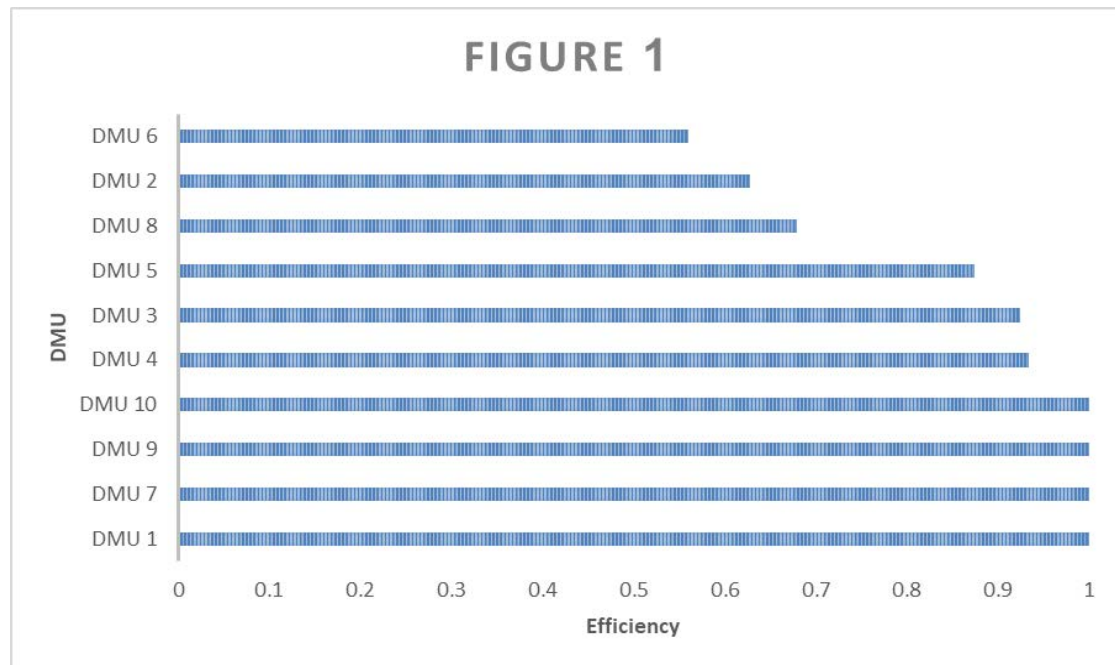

Figure 1. The efficiency score of DMUs

Conclusions and Recommendations

The following courses of action will be suggested following the original study direction if it is recommended that this line of investigation be continued in the future.

(i).   Many other topics and locations may be investigated, which brings us to the first strategy, which is to do the research with the only intention of using what was learned. The second strategy involves combining DEA models with other forecasting models, such as fuzzy or grey.

(ii).   The author suggests that future research on the same subject alter the input and output components and then compare the findings of these two different approaches. A more objective result can be attained by doing things in this manner. Other elements, such as the total units of production, undesired factors, such as recalled defective units, and non-financial variables, are all feasible to be considered.

Scientific Ethics Declaration

The authors declare that the scientific ethical and legal responsibility of this article published in EPSTEM journal belongs to the authors.

Acknowledgements or Notes

References

Alghassab, M. (2022). Analyzing the impact of cybersecurity on monitoring and control systems in the energy sector. *Energies, 15*(1). doi:ARTN 21810.3390/en15010218

Alharbi, A., Seh, A. H., Alosaimi, W., Alyami, H., Agrawal, A., Kumar, R., & Khan, R. A. (2021). Analyzing the impact of cyber security related attributes for intrusion detection systems. *Sustainability, 13*(22). doi:ARTN 1233710.3390/su132212337

Bian, Y., & Yang, F. J. E. P. (2010). Resource and environment efficiency analysis of provinces in China: A DEA approach based on Shannon's entropy. *38*(4), 1909-1917.

Bin Arfaj, B. A., Mishra, S., & AlShehri, M. (2022). Efficacy of unconventional penetration testing practices. *Intelligent Automation and Soft Computing, 31*(1), 223-239. doi:10.32604/iasc.2022.019485

Chen, K., Ren, X. T., Yang, G. L., & Qin, H. B. (2022). The other side of the coin: The declining of Chinese social science. *Scientometrics, 127*(1), 127-143. doi:10.1007/s11192-021-04208-2

Chen, L. L., & He, F. (2017). Measurements and factors of carbon emission efficiency. *Polish Journal of Environmental Studies, 26*(5), 1963-1973. doi:10.15244/pjoes/69939

Chen, L. L., He, F., & Wang, J. J. (2018). Allocative efficiency of carbon emission allowances among sectors in china. *Polish Journal of Environmental Studies, 27*(2), 557-563. doi:10.15244/pjoes/75821

Chen, Q., Ai, H. S., Zhang, Y. B., & Hou, J. X. (2019). Marketization and water resource utilization efficiency in China. *Sustainable Computing-Informatics & Systems, 22*, 32-43. doi:10.1016/j.suscom.2019.01.018

Gan, G. Y., Lee, H. S., & Liu, J. Y. (2021). A DEA approach towards to the evaluation of iot applications in intelligent ports. *Journal of Marine Science and Technology-Taiwan, 29*(3), 256-265.

Jin, S. Y., Zhou, X. L., & Chiu, Y. H. (2021). The parent-subsidiary knowledge transfer efficiency of Chinese-African multinational enterprises based on a metafrontier epsilon-based measure model. *Managerial and Decision Economics, 42*(2), 479-492. doi:10.1002/mde.3248

Li, M. J., & Wang, J. (2021). Spatial-temporal distribution characteristics and driving mechanism of green total factor productivity in china's logistics industry. *Polish Journal of Environmental Studies, 30*(1), 201-213. doi:10.15244/pjoes/121046

Li, Y. L., Lin, J., Cui, Z. H., Wang, C., & Li, G. J. (2021). Workforce productivity evaluation of the US construction industry from 2006 to 2016. *Engineering Construction and Architectural Management, 28*(1), 55-81. doi:10.1108/Ecam-07-2019-0366

Li, Y., Chiu, Y. H., & Lu, L. C. (2019). New energy development and pollution emissions in china. *International Journal of Environmental Research and Public Health, 16*(10). doi:ARTN 176410.3390/ijerph16101764

Liang, D., Tian, Z., Ren, F. R., & Pan, J. J. (2020). Installed hydropower capacity and carbon emission reduction efficiency based on the ebm method in china. *Frontiers in Energy Research, 8*. doi:ARTN 8210.3389/fenrg.2020.00082

Moreira, F. R., Da Silva, D. A., Nze, G. D. A., de Sousa, R. T., & Nunes, R. R. (2021). Evaluating the performance of nist's framework cybersecurity controls through a constructivist multicriteria methodology. *Ieee Access, 9*, 129605-129618. doi:10.1109/Access.2021.3113178

Shrestha, R., Omidkar, A., Roudi, S. A., Abbas, R., & Kim, S. (2021). Machine-learning-enabled intrusion detection system for cellular connected UAV networks. *Electronics, 10*(13). doi:ARTN 154910.3390/electronics10131549

Tavana, M., Mirzagoltabar, H., Mirhedayatian, S. M., Saen, R. F., & Azadi, M. (2013). A new network epsilon-based DEA model for supply chain performance evaluation. *Computers & Industrial Engineering, 66*(2), 501-513. doi:10.1016/j.cie.2013.07.016

Tian, Z., Ren, F. R., Xiao, Q. W., Chiu, Y. H., & Lin, T. Y. (2019). Cross-regional comparative study on carbon emission efficiency of china's yangtze river economic belt based on the meta-frontier. *International Journal of Environmental Research and Public Health, 16*(4). doi:ARTN 61910.3390/ijerph16040619

Tone, K., & Tsutsui, M. (2010). An epsilon-based measure of efficiency in DEA - A third pole of technical efficiency. *European Journal of Operational Research, 207*(3), 1554-1563. doi:10.1016/j.ejor.2010.07.014

Wang, C. N., Day, J. D., & Nguyen, T. K. L. (2018). Applying EBM model and grey forecasting to assess efficiency of third-party logistics providers. *Journal of Advanced Transportation*. doi:Artn 121287310.1155/2018/1212873

Wang, C. N., Nguyen, M. N., Nguyen, T. D., Hsu, H. P., & Nguyen, T. H. Y. (2021). Effective decision making: data envelopment analysis for efficiency evaluation in the cloud computing marketplaces. *Axioms, 10*(4). doi:ARTN 30910.3390/axioms10040309

Wang, C. N., Nguyen, N. A., Fu, H. P., Hsu, H. P., & Dang, T. T. (2021). Efficiency assessment of seaport terminal operators using DEA malmquist and epsilon-based measure models. *Axioms, 10*(2). doi:ARTN 4810.3390/axioms10020048

Wang, C.-N., Nguyen, N.-A.-T., Fu, H.-P., Hsu, H.-P., & Dang, T.-T. J. A. (2021). Efficiency assessment of seaport terminal operators using DEA Malmquist and epsilon-based measure models. *Axioms 10*(2), 48.

Wu, D. D., Wang, Y. H., & Qian, W. Y. (2020). Efficiency evaluation and dynamic evolution of China's regional green economy: A method based on the Super-PEBM model and DEA window analysis. *Journal of Cleaner Production, 264*. doi:ARTN 12163010.1016/j.jclepro.2020.121630

Yu, Y. T., Huang, J. H., & Zhang, N. (2019). Modeling the eco-efficiency of Chinese prefecture-level cities with regional heterogeneities: A comparative perspective. *Ecological Modelling, 402*, 1-17. doi:10.1016/j.ecolmodel.2019.03.012

Author Information

Van Thanh Tien Nguyen
National Kaohsiung University of Science and Technology,
415 Jiangong, Sanmin, Kaohsiung, Taiwan
Industrial University of Ho Chi Minh City
12, Nguyen Van Bao, Go Vap, Ho Chi Minh City, Vietnam
Contact e-mail: *thanhtienck@ieee.org*

Chia-Nan Wang
National Kaohsiung University of Science and Technology,
415 Jiangong, Sanmin, Kaohsiung, Taiwan

Fu-Chiang Yang
National Kaohsiung University of Science and Technology,
415 Jiangong, Sanmin, Kaohsiung, Taiwan

Thi Minh Nhut Vo
Thu Dau Mot University
Binh Duong, Vietnam

Examination of Energy Efficiency of Air Handling Unit with Integrated Air to Air Heat Exchanger in Cooling Mode

Slav VALCHEV
University of Food Technologies

Ivan MIHAILOV
University of Food Technologies

Abstract: Object of the present study is an experimental determination of parameters, showing efficiency of air handling unit with integrated air to air heat exchanger in cooling mode: effectiveness of supply side of air to air heat exchanger, coefficient of performance and specific fan power of air handling unit. A daily performance of air handling unit in cooling mode is conducted. Effectiveness of supply side of air to air heat exchanger in range of 50.5 % to 74.3 % is received. Coefficient of performance in range of 0.88 to 2.99 and specific fan power of air handling unit in range of 1.77 kW/(m^3/s) to 3.06 kW/(m^3/s) are received. A relation between effectiveness of supply side of air to air heat exchanger and ratio of heat capacity rates of supply and exhaust air is received. Effectiveness of supply side of air to air heat exchanger depends on values of mass flow of supply and the exhaust air. High values of mass flow of exhaust air responds to high effectiveness of supply side of air to air heat exchanger.

Keywords: Air handling unit, air to air heat exchanger, effectiveness, coefficient of performance, specific fan power

Introduction

Air handling units are equipment used for air conditioning of large office and commercial buildings. These units need to provide cooling, heating and required amount of fresh air in conditioned space of the building. A necessary amount of supply fresh air must be with high purity and required temperature, so that it does not affect negative to the people in an air-conditioned room. To minimize energy costs, air handling units has an integrated air to air heat exchanger and heating (cooling) section with direct evaporation of refrigerant (heat pump). (Kolev et al, 2020). The initial heating (cooling) of supply air in air handling unit is realized by passing it through air to air exchangers, in which it accepts (takes away) heat with exhaust air, taken away from the room. The heat exchangers used in air handling unit can be different types - plate heat exchangers, rotary heat wheel or heat pipe. (Masitah et al., 2015). The main heating (cooling) of supply air is performed by heating (cooling) section of air handling units, where energy of supply air is delivered by electric power, hot or cold fluid. High energy efficiency of these units is guaranteed by use of efficiency heat exchangers, cooling and heating sections with low energy costs for air cooling and heating, as well as the use of fans with low electrical energy consumption. Energy efficiency of air handling units is based on the values of three parameters: effectiveness of air to air heat exchanger, coefficient of performance and specific electric fan power, consumed by fans of air handling unit.

Cross flow air to air plate heat exchangers have high efficiency in small sizes. Main advantages of aluminium plate heat exchangers are also: corrosion resistance, fire safety, no moisture and odor transfer between supply and exhaust air. Effectiveness of these heat exchanger can be calculated by supply side and exhaust side.

Energy efficiency class of heat pumps in air handling units is determined according to Delegated Regulation (EU) 626/2011, supplementing Directive 2010/30/EU with regard to energy labelling of air conditioners. Energy efficiency class of air handling units is determined according to Regulation (EU) 1253/2014, implementing Directive 2009/125/EC of the European Parliament and of the Council with regard to ecodesign requirements for ventilation units. High values of effectiveness of air to air heat exchanger and coefficient of performance of air handling unit and low values of specific electric fan power of air handling unit indicate high energy efficiency of the system. (Bobilov et al., 2011), (Kolev et al., 2017).

In this study a daily performance of air handling unit in cooling mode is conducted. Temperatures of supply air on outlet and inlet of air to air heat exchanger and temperature of exhaust air on inlet of air to air heat exchanger are measured. Room temperature, outdoor temperature and velocities of supply and exhaust air of air handling unit are measured and mass flow rates through heat exchanger are calculated. Heat capacity rates of the supply and exhaust air are determined. Effectiveness on a supply side of air to air heat exchanger is determined. Electrical power of refrigeration compressor, supply and exhaust fan of air handling unit are measured. Heat flux exchanged in cooling section, coefficient of performance in cooling section (heat pump) are calculated. Heat flux exchanged in air to air heat exchanger, total cooling capacity of air handling unit and coefficient of performance of air handling unit are calculated. Specific fan power of air handling unit is determined. A relation between effectiveness of supply side of air to air heat exchanger and ratio of heat capacity rates of the supply and exhaust air is received.

Materials and Methods

The installation is located in science laboratory of University Of Food Technology – Plovdiv, Bulgaria. Schematic diagram of air handling unit is shown on Figure 1.
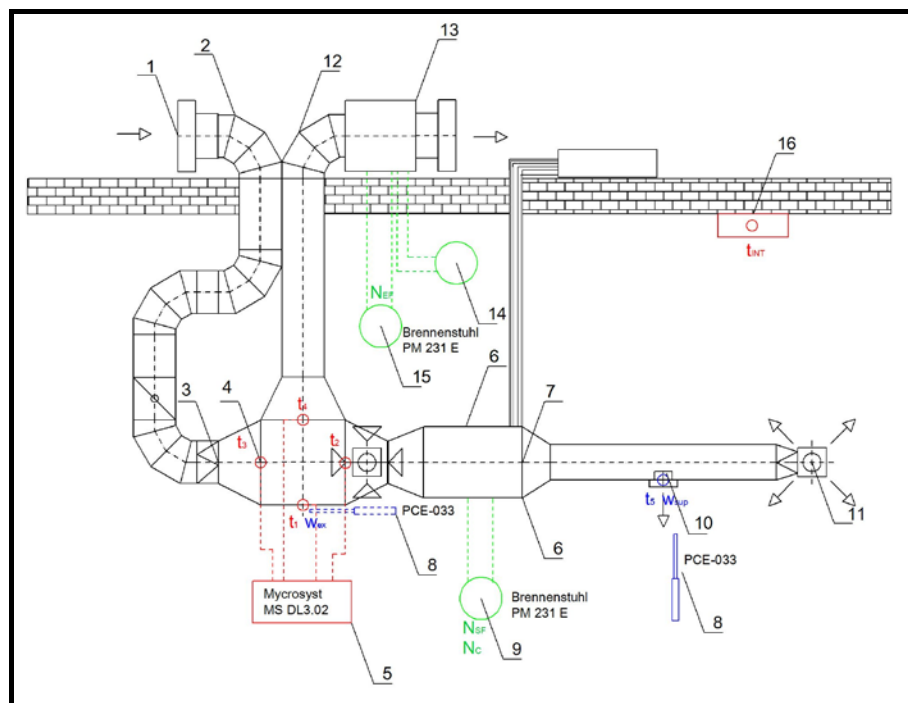

Figure1. Schematic diagram of air handling unit

Through external grill 1 supply air (100 % fresh air) goes to supply air duct 2. Supply fan 7 trasport supply air to conditioned room and enters the room from grills 10 and 11. The fan is mounted in cooling section of air handling unit (HP unit) 6. To air duct 2 supply air passes through filter section 3 and enters to air to air plate heat exchanger HE 4, where it is precooled by exhaust air from the room. The temperatures of supply air on inlet and outlet of HE 4 t_3 and t_2 is measured with temperature sensors, connected to controller 5. Precooled supply air from air to air plate heat exchanger HE 4 passes through HP unit 6, where is additionally cooled. The temperature of supply air on outlet of HP unit t_5 and his velocity w_{sup} are measured by thermo-anemometer 8. Energy power consumption of HP unit and supply fan are measured by digital wattmeter 9. The exhaust air is transported on exhaust air duct 12 by exhaust fan 13, mounted in ventilation box. Exhaust fan is equipped with

fan speed controller 14. The temperatures of exhaust air on inlet and outlet of HE 4 t_1 and t_4 is measured with temperature sensors, connected to controller 5. The velocity of exhaust air on inlet of HE 4 w_{ex} is measured by thermo-anemometer 8. The energy power consumption of exhaust fan are measured by digital wattmeter 15.The temperature of air in the room t_{int} is measured with remote controller 16. General appearance of air handling unit are shown in Figure 2. (Valchev et al., 2019)

Figure 2. General appearance of air handling unit

Measuring devices and measured parameters of air handling unit are shown in Table 1.

Table 1. Measuring devices and measured parameters of air handling unit

Measuring device	Measured parameter	Designation	Precision measuring	Measuring range
Remote controller Fujitsu General UTY-RNNYM 1	Set point of room temperature	t_{int}, ºC	±1.0 ºC	10-30 ºC
Controller Mycrosyst Data Logger GSM Dialer MS DL3.02 – 2 – 4 channel	Air temperatures in control point of air handling unit	t_1, t_2, t_3, t_4 ºC	±0.1 ºC	10-60 ºC
Thermo-anemometer PCE-033	Air temperatures and velocities in control point of air handling unit	t_5, ºC w_{sup}, w_{ex}, m/s	Temperature: ±0.1 ºC Velocity: ±0.1 m/s	Temperature: 0.0-50 ºC Velocity: 0.2-20 m/s
Digital wattmeter Brennenstuhl PM 231 E	Current power consumption of electrical energy spent by refrigeration compressor and supply air fan;	N_{SF}, N_C, W	±0.2W	0-9999.9 kWh
Digital wattmeter Brennenstuhl PM 231 E	Current power consumption of electrical energy spent by exhaust air fan	N_{EF}, W	±0.2W	0-9999.9 kWh

Results and Discussion

A daily performance of air handling unit is conducted. The temperatures of supply air on outlet t_2 and inlet t_3 of air to air heat exchanger and temperature of exhaust air on inlet t_1 of air to air heat exchanger are measured three times for one hour. The velocities of supply air w_{sup} and exhaust air w_{ex} of air handling unit are measured three times for one hour. Respective arithmetical mean values of measured temperatures and velocities are calculated. Mass flow rates of supply air and exhaust air through heat exchanger are determined by equations:

$$\dot{m}_{sup} = \rho_{air}.w_{sup}.f_{sup}$$

$$\dot{m}_{ex} = \rho_{air}.w_{ex}.f_{ex}$$

where: - ρ_{air} – density of air for average temperature of air on inlet and outlet of air to air heat exchanger, kg/m^3;

w_{sup} – velocity of supply air on outlet of grill of rectangular duct, m/s;

w_{ex} – velocity of exhaust air on inlet of air to air heat exchanger, m/s;

f_{sup} – effective area of grill on rectangular duct, m^2.

f_{ex} – effective area of ait to air heat exchanger, m^2.

The results are shown in Table 2.

Table 2. Experimental data – Temperatures and mass flow rates heat exchanger

№	t_1	t_2	t_3	t_5	w_{sup}	$\dot{m}_{sup}$	w_{ex}	$\dot{m}_{ex}$
	°C	°C	°C	°C	m/s	kg/s	m/s	kg/s
1	28.8	28.9	29.0	12.2	5.6	0.0869	0.3	0.0815
2	28.6	28.8	29.0	12.2	5.5	0.0853	0.3	0.0815
3	28.2	29.0	29.8	12.0	5.3	0.0822	0.3	0.0815
4	27.4	28.9	30.5	12.2	5.1	0.0791	0.3	0.0815
5	26.5	27.7	30.6	10.9	5.0	0.0776	0.4	0.1086
6	26.3	28.5	33.1	10.4	4.6	0.0714	0.4	0.1086
7	26.3	28.5	33.2	10.5	4.5	0.0698	0.4	0.1086
8	26.0	27.9	33.3	10.8	4.4	0.0683	0.5	0.1358
9	26.1	28.0	33.5	11.3	4.0	0.0621	0.5	0.1358
10	26.0	27.5	31.4	11.5	3.9	0.0605	0.5	0.1358

Heat capacity rate of the supply air C_s and heat capacity rate of the exhaust air C_e are determined by equations:

$$C_s = \dot{m}_{sup}.C_{air}$$

$$C_e = \dot{m}_{ex}.C_{air}$$

where: - $\dot{m}_{sup}$ – mass flow rate of supply air through the heat exchanger, kg/s;

$\dot{m}_{ex}$ - mass flow rate of exhaust air through the heat exchanger, kg/s;

C_{air} – specific heat capacity of the supply air, kJ/kg.K, (C_{air} =1,0 kJ/kg.K).

Effectiveness on a supply side of air to air heat exchanger ε_s is determined as follows (Larson & Pihlquist, 2011), (Pisarev et al., 2016):

$$\varepsilon_s = \frac{C_s}{C_{min}}.\left(\frac{t_2 - t_3}{t_1 - t_3}\right).100$$

where: - C_{min} – minimum of C_s and C_e, kW/K.

t_2 – temperature of supply air on outlet of air to air heat exchanger, ℃;

t_3 – temperature of supply air on inlet of air to air heat exchanger, ℃;

t_1 – temperature of exhaust air on inlet of air to air heat exchanger, ℃.

t_4 – temperature of exhaust air on outlet of air to air heat exchanger, ℃.

The results are shown in Table 3.

Table 3. Experimental data – Effectiveness supply side heat exchanger

№	$\dot{m}_{sup}$	$\dot{m}_{ex}$	C_s	C_e	C_s/C_e	ε_s
	kg/s	kg/s	kW/K	kW/K	-	%
1	0.0869	0.0815	0.0869	0.0815	1.07	53.3
2	0.0853	0.0815	0.0853	0.0815	1.05	52.4
3	0.0822	0.0815	0.0822	0.0815	1.01	50.5
4	0.0791	0.0815	0.0791	0.0815	0.97	51.6
5	0.0776	0.1086	0.0776	0.1086	0.71	70.7
6	0.0714	0.1086	0.0714	0.1086	0.66	67.6
7	0.0698	0.1086	0.0698	0.1086	0.64	68.1
8	0.0683	0.1358	0.0683	0.1358	0.50	74.0
9	0.0621	0.1358	0.0621	0.1358	0.46	74.3
10	0.0605	0.1358	0.0605	0.1358	0.45	72.2

Heat flux exchanged in heat pump unit $\dot{Q}_{HP}$ and coefficient of performance in cooling section (heat pump unit) COP_{HP} are calculated by equations:

$$\dot{Q}_{HP} = \dot{m}_{sup} . C_{air} (t_2 - t_5)$$

where: - t_5 – temperature of supply air on outlet of heating section (HP unit), ℃;

$$COP_{HP} = \frac{\dot{Q}_{HP}}{|N_C|}$$

where: - N_C – electrical power for refrigeration compressor of heat pump unit, W.

Electrical power of refrigeration compressor N_C is measured three times in one hour and respective arithmetical mean values of this power are calculated. The results are shown in Table 4.

Table 4. Experimental data – Coefficient of performance on heat pump unit

№	t_2	t_5	w_{sup}	$\dot{m}_{sup}$	$\dot{Q}_{HP}$	N_C	COP_{HP}
	℃	℃	m/s	kg/s	W	W	-
1	28.9	12.2	5.6	0.0869	1451	302	4.80
2	28.8	12.2	5.5	0.0853	1417	361	3.92
3	29.0	12.0	5.3	0.0822	1398	558	2.51
4	28.9	12.2	5.1	0.0791	1321	696	1.90
5	27.7	10.9	5.0	0.0776	1303	799	1.63
6	28.5	10.4	4.6	0.0714	1292	922	1.40
7	28.5	10.5	4.5	0.0698	1257	955	1.32
8	27.9	10.8	4.4	0.0683	1167	1088	1.07
9	28.0	11.3	4.0	0.0621	1036	1193	0.87
10	27.5	11.5	3.9	0.0605	968	1188	0.81

Heat flux exchanged in air to air heat exchanger $\dot{Q}_{HE}$, total cooling capacity of air handling unit $\dot{Q}_{AHU}$ and coefficient of performance of air handling unit COP$_{AHU}$ are calculated by the equations (Michalak, 2021), (Zhou et al.,2018), (Gendebien et al., 2018):

$$Q_{HE} = \dot{m}_{sup} . C_{air} (t_3 - t_2)$$

$$\dot{Q}_{AHU} = \dot{Q}_{HP} + \dot{Q}_{HE}$$

$$COP_{AHU} = \frac{\dot{Q}_{AHU}}{|N_{TOT}|}$$

Total power consumption of air handling unit N$_{TOT}$ is calculated by equation:

$$N_{TOT} = N_C + N_{SF} + N_{EF}$$

Power consumption of supply N$_{SF}$ and exhaust fan of N$_{EF}$ of air handling unit is measured three times in one hour and respective arithmetical mean values of this power are calculated. The results are shown in Table 5.

Table 5. Experimental data – Coefficient of performance of air handing unit

№	t_2	t_3	$\dot{m}_{sup}$	$\dot{Q}_{HE}$	$\dot{Q}_{AHU}$	N$_{TOT}$	COP$_{AHU}$
	˚C	˚C	kg/s	W	W	W	-
1	28.9	29.0	0.0869	9	1460	489	2.99
2	28.8	29.0	0.0853	17	1434	548	2.62
3	29.0	29.8	0.0822	66	1464	751	1.95
4	28.9	30.5	0.0791	127	1448	876	1.65
5	27.7	30.6	0.0776	225	1528	980	1.56
6	28.5	33.1	0.0714	328	1620	1108	1.46
7	28.5	33.2	0.0698	328	1585	1144	1.39
8	27.9	33.3	0.0683	369	1536	1274	1.21
9	28.0	33.5	0.0621	341	1378	1381	1.00
10	27.5	31.4	0.0605	236	1204	1375	0.88

Specific fan power of air handling unit SFP, volume flow rate of exhaust air $\dot{V}_{ex}$ and total power consumption of supply and exhaust fan of air handling unit N$_F$ are determined by equations:

$$SFP = \frac{N_F . \rho_{air}}{\dot{m}_{MAX}},$$

where:- $\dot{m}_{MAX} = \dot{m}_{ex}$ – maximum mass flow rate throw air to air heat exchanger, equal to mass flow rate of exhaust air throw air to air heat exchanger, kg/s.

$$\dot{V}_{ex} = \frac{\dot{m}_{ex}}{\rho_{air}}$$

$$N_F = N_{SF} + N_{EF}$$

where: - N$_{SF}$ – electrical power for supply fan of air handling unit, W;

N$_{EF}$ – electrical power for exhaust fan of air handling unit, W.

The results are shown in Table 6.

Table 6. Experimental data – Specific fan power of air handling unit

№	$\dot{m}_{ex}$ kg/s	$\dot{V}_{ex}$ m³/s	N_{SF} W	N_{EF} W	N_C W	N_{TOT} W	SFP kW/(m³/s)
1	0.0815	0.0630	22	165	302	489	2.97
2	0.0815	0.0630	21	166	361	548	2.97
3	0.0815	0.0630	21	172	558	751	3.06
4	0.0815	0.0630	20	160	696	876	2.86
5	0.1086	0.0840	20	161	799	980	2.15
6	0.1086	0.0840	25	161	922	1108	2.21
7	0.1086	0.0840	24	165	955	1144	2.25
8	0.1358	0.1050	22	164	1088	1274	1.77
9	0.1358	0.1050	23	165	1193	1381	1.79
10	0.1358	0.1050	22	165	1188	1375	1.78

In Figure 3 a correlation between effectiveness of supply side of air to air heat exchanger and ratio of heat capacity rates of supply and exhaust air is shown.
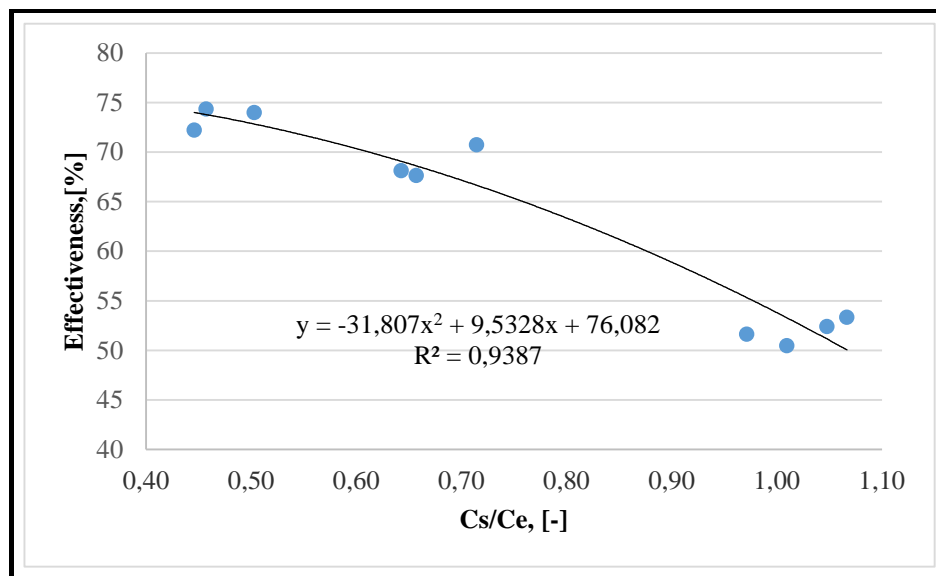

Figure 3. Correlation between effectiveness of supply side of air to air heat exchanger and ratio of heat capacity rates of supply and exhaust air

Conclusions

A daily performance of air handling unit in cooling mode is conducted. Effectiveness of supply side of air to air heat exchanger in range of 50.5 % to 74.3 % is received. Coefficient of performance in range of 0.88 to 2.99 and specific fan power of air handling unit in range of 1.77 kW/(m³/s) to 3.06 kW/(m³/s) are received. It was found experimentally that effectiveness of supply side of air to air heat exchanger depends on values of mass flow of supply and the exhaust air. High values of mass flow of exhaust air responds to high effectiveness of supply side of air to air heat exchanger.

Scientific Ethics Declaration

The authors declare that the scientific ethical and legal responsibility of this article published in EPSTEM journal belongs to the authors.

Acknowledgements or Notes

References

Bobilov, V., Genchev, G., Mushakov, P., Zlatev, P., Kolev, Z. (2011). Methodology for investigation the coefficient of performance of reversible heat pump water-water. *Proceedings of University of Ruse – Bulgaria, 50 (1.2)*, 8-12.

Gendebien, S., Martens, J., Prieels, L., Lemort, V. (2018). Designing an air-to-air heat exchanger dedicated to single room ventilation with heat recovery. *Building Simulation, 11*, 103–113.

Kolev, Z., Kadirova, S., Nenov, T., (2017). Research on reversible heat pump installation for greenhouse heating. *INMATEH - Agricultural Engineering, 52(2)*, 77-84.

Kolev, Z., Mushakov P., Kadirova, S. (2020). Experimental investigation of the refrigeration cycle of water to water heat pump. *IOP Conference Series: Materials Science and Engineering, 1032, 012031.*

Larson, K., Pihlquist, F. (2011). *Methods of increasing thermal efficiency of a counter flow air to air heat exchanger.* (Master of Science Thesis, Chalmers University of Technology, Goteborg, Sweden).

Masitah, A.R.S., M. I Ahmad and Y.M. Yatim. (2015). Heat transfer and effectiveness analysis of a cross- flow heat exchanger for potential energy recovery applications in hot-humid climate. *Energy Research Journal, 6(1)*, 7-14.

Michalak, P. (2021). Annual energy performance of an air handling unit with a cross-flow heat exchanger. *Energies, 14(6), 1519.*

Pisarev, V., Rabczak, S., Nowak, K. (2016).Ventilation system with ground heat exchanger. *Journal of Ecological Engineering, 17(5)*, 163–172.

Valchev, S., Minchev, M., Arnaudov, M. (2019). Air conditioning installation with direct evaporation of refrigerant with air to air heat exchanger. (in Bulgarian). *Scientific Works of Union of Scientist Bulgaria – Plovdiv, XVII (C),* 14-17.

Zhou, G., Ye, Y., Zuo, W.,Wang, J. (2018). Modeling air to air plate-fin heat exchanger without dehumidification. *Applied Thermal Engineering, 143*, 137-148.

Author Information

Slav Valchev	**Ivan Mihailov**
University of Food Technology	University of Food Technology
Plovdiv, Bulgaria, 26 Maritza Boulevard	Plovdiv, Bulgaria, 26 Maritza Boulevard
Contact e-mail: *slav_vul4ev@abv.bg*	

To cite this article:

Valchev, S.E. & Mihailov, I.M. (2022). Examination of energy efficiency of air handling unit with integrated air to air heat exchanger in cooling mode. *The Eurasia Proceedings of Science, Technology, Engineering & Mathematics (EPSTEM), 17,* 45-52.

Synthesis and Fluorimetric Application of Novel Schiff Base Compound Containing Imidazole

Onder ALICI
Selcuk University

Duygu AYDIN
Karamanoglu Mehmetbey University

Abstract: This study describes the synthesis and application of 2-(2-hydroxy-5-(1H-phenanthro [9,10-d]imidazol-2-yl)benzylidene)-N-phenylhydrazine-1-carboxamide (**TC**) as a fluorogenic chemosensor toward for Zn^{2+} sensing in EtOH-H_2O (9:1, v/v) media. The chemosensor **TC** could sensitively determine Zn^{2+} ions with a low detection limit (LOD) and LOD value was found to be 5.73 nM. The fluorogenic titration spectrum indicated that the Zn^{2+} concentration was proportional to emission and gave a good linear alteration in emission in response to the equivalent of Zn^{2+}, the complexation ratio between chemosensor TC and Zn^{2+} was calculated as 1:1 by the method of continuous variation (Job's plot) from the obtained titration study. Moreover, the Ka value for the TC-Zn^{2+} complexation was found as 6.7×10^{-3} M^{-1} according to the Benesi–Hildebrand value of the changess in the titration of the chemosensor TC against Zn^{2+} ions. As a result of obtained data, chemosensor TC could be utilized to be an effective fluorogenic chemosensor for recognizing Zn^{2+} ions.

Keywords: Fluorogenic chemosensor, Schiff base, Zn^{2+}

Introduction

The design and construction of high performance fluorogenic chemosensors for sensitive and selective recognition of cations (such as Zn2+ recognition) have a significant value. Zinc metal in the human body after Fe is the second essential and most abundant transition element and zinc ions have a key role in neural signal transmission, regulating the immune system, cell nucleic acid and protein and a lot of molecular mechanisms. Zinc in the cell membrane plays an important role in preventing damage to the cell via the oxidative reactions. However, a lot of investigations displayed that an excess value of Zn2+ in the human body can gradually cause a lot of diseases, for example epilepsy, osteoporosis, prostate and breast cancers, and neurodegenerative diseases like Alzheimer's disease (Sethupathi et al., 2020; Erdemir & Malkondu, 2020; Ghaedi et al., 2009). Hence, it is very important to control and monitor the amount of Zn2+ to prevent the side effects of Zn2+ ions for the human body.

In the past few years, a lot of conventional analytical methodologies such as differential pulse stripping anodic voltammetry, electrochemical analysis, atomic absorption spectroscopy, flame atomic absorption spectrometry, isotope chromatography, and chromatography have been generally applied for the recognition of Zn2+ ions. Conversely, these conventional detection methods have some issues such as the necessity of time-consuming recognition, complex pretreatment, the necessity of sophisticated and high expensive equipment, and cumbersome operation, which make them not convenient for real-time and large-scale monitoring of samples. Compared with conventional analytical methodologies for the recognition of Zn2+ ions, fluorescence-based recognition technique is highly sensitive and selective. Additionally, this recognition technology has a lot of advantages for example, fast response time, easy sample preparation and so on (Sethupathi et al., 2020; Erdemir, & Malkondu, 2020; Ghaedi et al., 2009). In addition, fluorescence-based technique is superior sensitive and

selective, and it has a simple operation. Therefore, fluorescence-based recognition technique for cations detection has been extensively employed in medicine, chemistry, life science, environmental science, and many other research areas. There are a lot of synthesized fluorescence-based molecules for the fluorescence recognition of Zn2+ ions in the literature. These molecules are generally coumarin, fluorescein, calixarene, and thiazole based molecules (Erdemir & Malkondu, 2020; Aydin et al., 2021). Many of them have high detection limits or low selectivity behavior for the recognition of Zn2+ ions. Hence, it is exceedingly meaningful to construct novel fluorogenic chemosensors for effect and fast fluorescence analysis of Zn2+ recognition in environmental waste.

In this study, phenanthro imidazol based fluorogenic sensor TC (2- (2-hydroxy 5-(1H-phenanthro [9,10-d] imidazol-2-yl) benzylidene) N-phenyl hydrazine 1-carboxamide) was designed and constructed for the sensitively and selectively determination of environmentally significant Zn2+ ions. Preparation fluorogenic probe TC was characterized by 1H and 13C NMR spectroscopy. The fluorogenic sensing of Zn2+ ions with fluorogenic chemosensor TC in EtOH: H2O (9/1, v/v) medium has been accomplished with a great alteration in fluorescence emission spectra. The binding stoichiometry for TC and Zn2+ was computed to be 1:1 by Job's plot method. Furthermore, the binding constant between the TC and Zn2+ ions was found to be 6.7×10^{-3} M^{-1} from the Benesi–Hildebrand graph. In addition, the calculated limit of the detection (from the formula of 3σ/s) value of fluorogenic sensor TC for the recognition of Zn2+ ions in EtOH: H2O (9/1, v/v) medium was as low as 5.73 nM and this obtained value was lower than the determined value in drinking water by WHO (World Health Organization). As a result of obtained results, newly designed and synthesized fluorogenic chemosensor TC could be successfully utilized to be a fluorogenic chemosensor for the recognition of Zn2+ ions in environmental samples and solution.

Method

Chemicals and Instruments

All necessitated chemicals are analytical grade and were obtained from Sigma-Aldrich Chemicals (Zwijndrecht, The Netherlands) and utilized with no further processing. The perchlorate salts of the cations were utilized in this study. 1H and 13C-NMR spectral studies were measured by a Spinsol and Magritek NMR spectrometer and emission spectra of the chemosensor TC were recorded in a Varian Cary Eclipse Fluorescence Spectrophotometer (Agilent Technologies Inc, Santa Clara, CA, USA).

Synthesis of 2-hydroxy-5-(1H-phenanthro[9,10-d]imidazol-2-yl)benzaldehyde (1)

Compound (1) was prepared according in the literature (Kutluca Alici, 2020).

Synthesis of the chemosensor TC

Absolute ethanolic solutions (10 mL) of compound(1) (0.1 g, 0.295 mmol) was added to 4-phenylsemicarbazide(0.05 g, 0.33 mmol) in absolute EtOH and stirred under reflux for 20 hours. After completion of the reaction, the precipitate formed was filtered off. The precipitate was washed three times with water and ethanol, and dried in a vacuum oven. Finally, the Schiff base compound (TC) was recrystallized with hot ethanol to obtain white crystals.

Yield: 75 %, Melting Point: 225 0C, FTIR (ATR-cm-1): 3054 (N-H), 1658 (HC=N) 1H-NMR (400 MHz, DMSO-d6) δ 11.27 (s, 1H), 11.06 (s, 1H), 9.04 (s, 1H), 8.89 (d, J = 8.4 Hz, 2H), 8.78 (s, 1H), 8.58 (d, J = 7.9 Hz, 2H), 8.36 (s, 1H), 8.13 (d, J = 8.6 Hz, 1H), 7.81 (t, J = 7.5 Hz, 2H), 7.72 (t, J = 8.3 Hz, 4H), 7.33 (t, J = 7.6 Hz, 2H), 7.20 (d, J = 8.5 Hz, 1H), 7.03 (t, J = 7.3 Hz, 1H). 13C NMR (100 MHz, DMSO-d6) δ 176.2, 158.13, 149.78, 139.57, 130.28, 128.67, 127.94, 127.53, 125.86, 125.76, 125.58, 124.37, 122.54, 122.33, 121.01, 117.23, 66.82.

Results and Discussion

Preparation of the chemosensor TC

The synthesis routes of TC include three steps: the preparation of compound 4-(1H-Phenanthro[9,10-d]imidazol-2-yl)phenol was prepared by the reaction of 9,10-Phenanthrenedioneand 4-Hydroxybenzaldehyde,

and 2-hydroxy-5-(1H-phenanthro[9,10-d]imidazol-2-yl)benzaldehydesynthesized by the Duff reactionwith HMTA in trifluoroacetic acid. The chemosensor TC was easily prepared by the condensation reaction of2-hydroxy-5-(1H-phenanthro[9,10-d]imidazol-2-yl)benzaldehyde (1) and 4-phenylsemicarbazide (2) in ethanol with 75 % yield as illustrated in Scheme 1. 1H-NMR, 13C-NMRand FT-IR were utilized to verify the structure of newly proposed chemosensor TC.
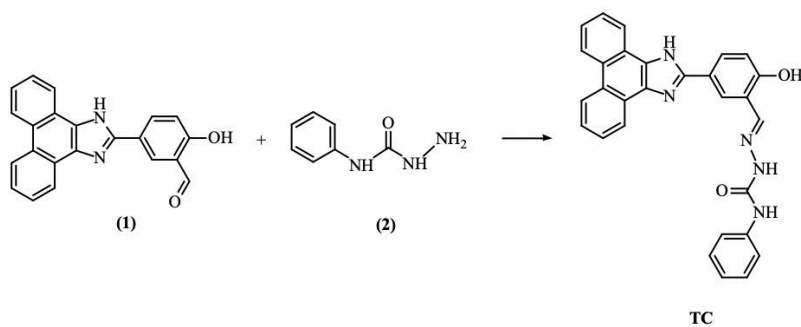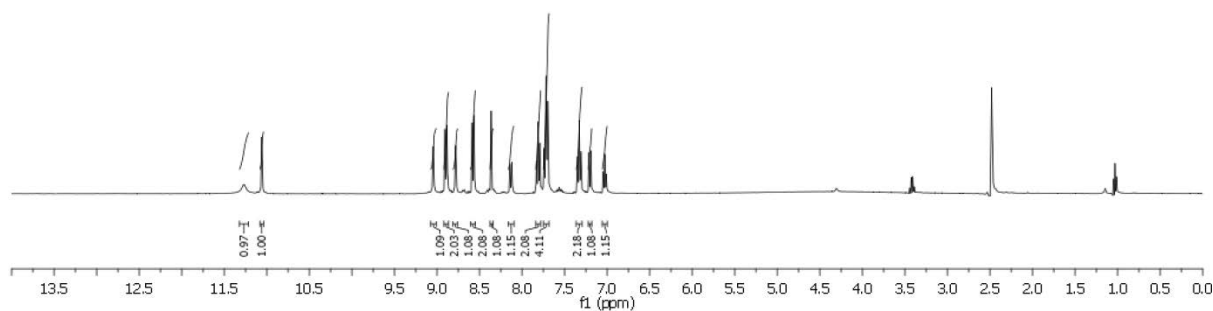

Figure 1. Synthesis of Compound TC
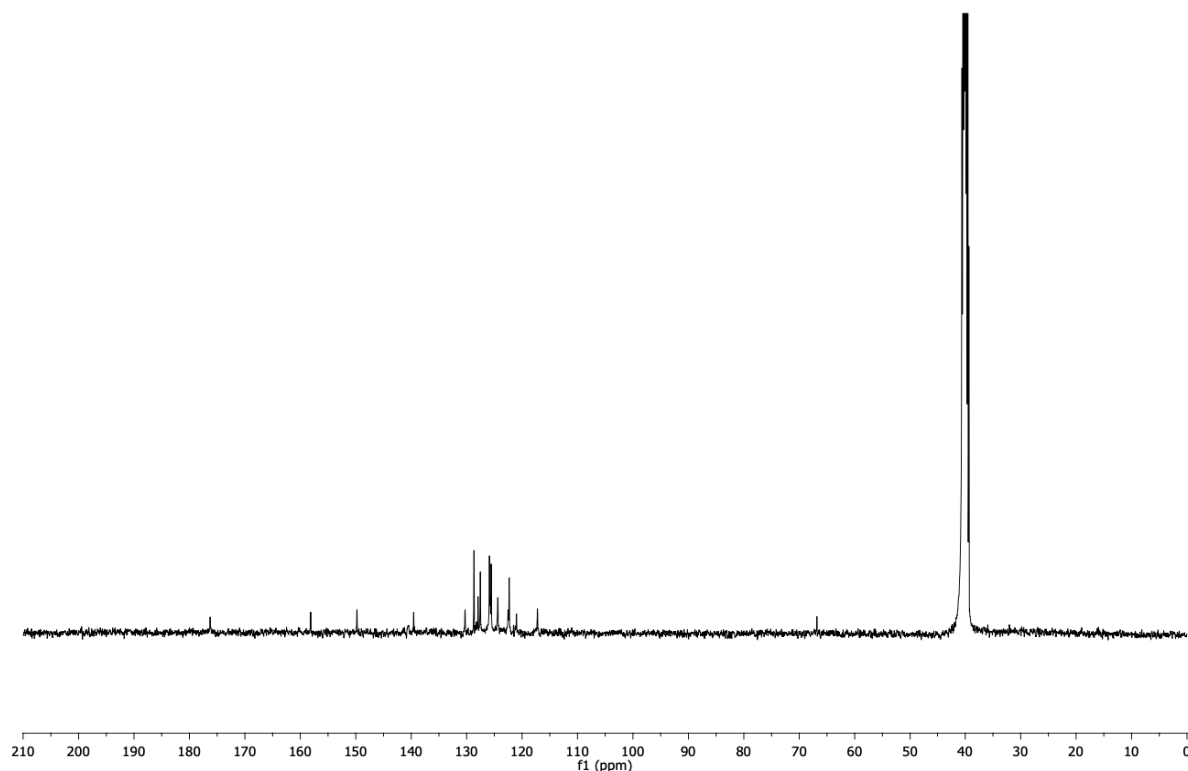

Figure 2. ^{1}H-NMR spectrum of Compound TC

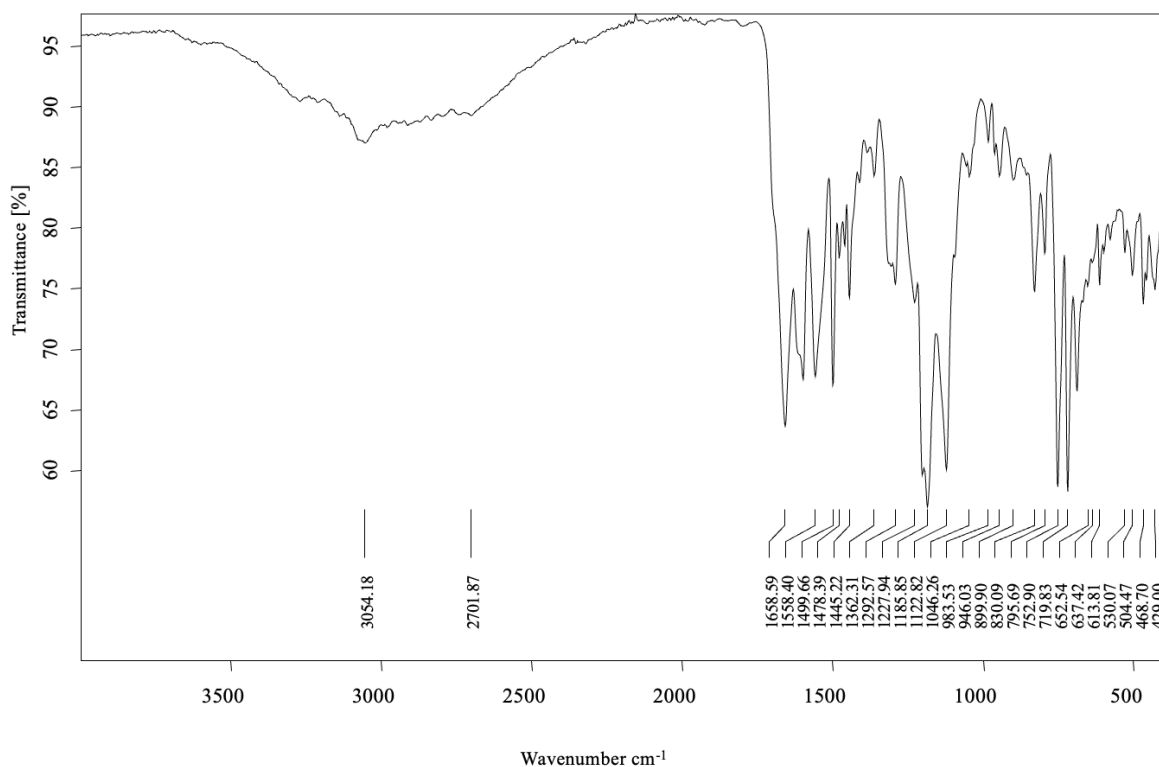Figure 3. ^{13}C-NMR spectrum of Compound TC

Figure 4. FT-IR spectrum of Compound TC

Emission study

The stock solution of TC (10 mM) was prepared in DMSO and then diluted 50 µM in EtOH/H2O (9/1, v/v). The tested metal perchlorate salts were utilized as (10-2 M).

Photophysical Studies of TC toward Zn^{2+}

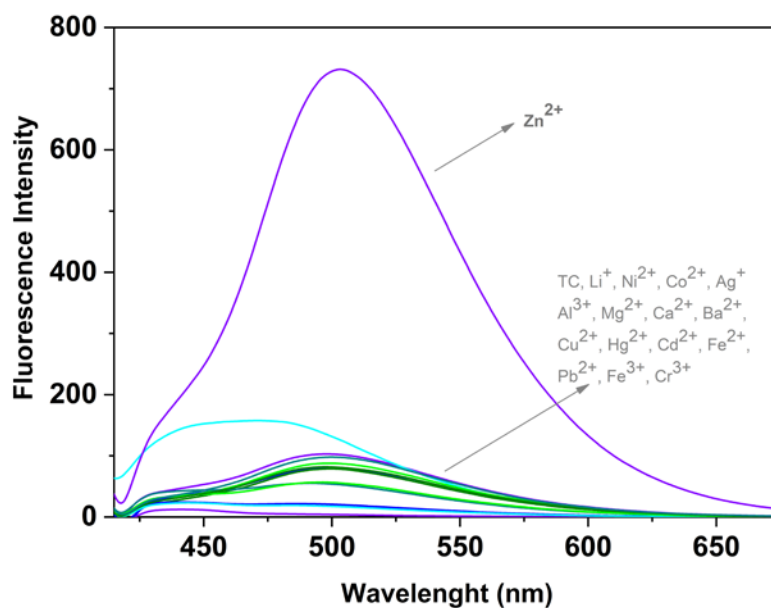Figure 5. Emission intensity alterations of TC (50 µM) in the presence of various tested cations.

The fluorescent study of TC was carried out in EtOH−H$_2$O (9:1, v/v) with Li$^+$, Ni^{2+}, Co^{2+}, Ag$^+$, Al^{3+}, Mg^{2+}, Ca^{2+}, Ba^{2+}, Cu^{2+}, Hg^{2+}, Cd^{2+}, Fe^{2+}, Pb^{2+}, Fe^{3+}, Cr^{3+} ve Zn^{2+}. Initially, TC had no emission at 512 nm and then the adding of Zn^{2+} in TC led to significant intensity enhancement at 512 nm. Other mentioned cations introduced into the TC solution did not produce any spectral alteration at 512 nm (Fig 4). The corresponding change in This remarkable enhancement of the intensity exhibits the strong interaction between TC and Zn^{2+}.

To evaluate the sensitivity and quantitative appraisal of TC toward Zn^{2+}, the standard titration analysis was utilized as depicted in Fig. 2. The TC intensity at 512 nm enhanced with the increasing of the concentration of Zn^{2+}. The fluorescent spectral trend of the solution of TC with the addition of increasing concentration of Zn^{2+} was performed as illustrated in Fig 5. The TC intensity enhanced with the increasing Zn^{2+} concentration.
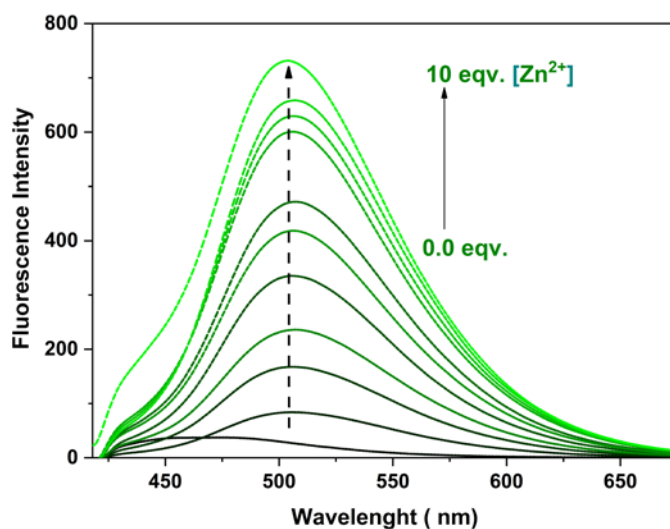

Figure 6. Emission spectra of TC with various concentrations of Zn^{2+}

The emission values were plotted as a function of the concentrations of Zn^{2+} Fig 6a to investigate the limit of detection (LOD) value of TC for Zn^{2+} determination The LOD value of compound **TC** was determined as 5.73 nM according to the equation: LOD = 3σ/k (σ: symbolizes the root-mean-square of blank measurements, k: the slope of the linear calibration curve). Furthermore, the Ka value for the TC-Zn^{2+} system was 6.7×10^{-3} M^{-1} in accordance with the Benesi–Hildebrand plot of the alterations in the titration of the TC toward Zn^{2+}.

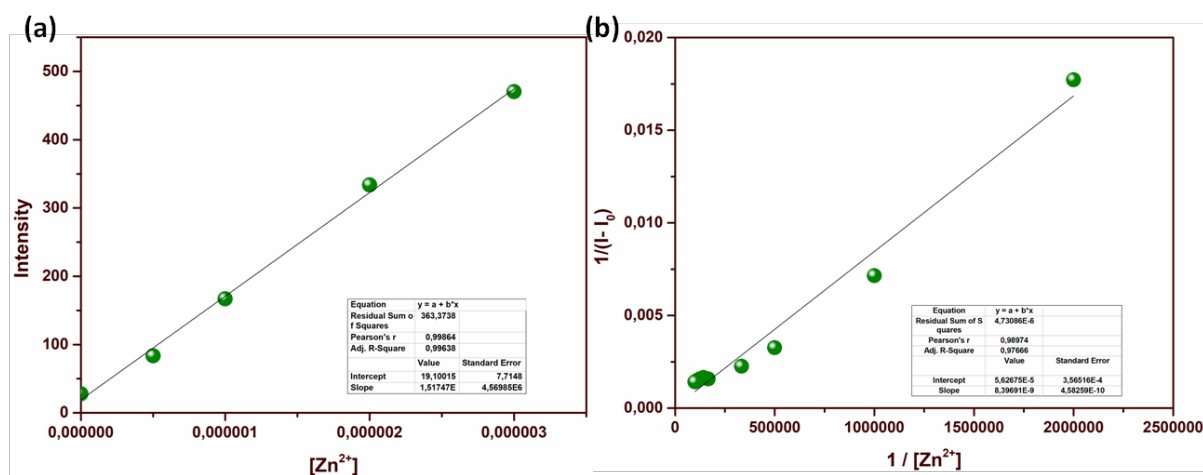Figure 7. (a) The plot of emissions of TC versus with various Zn^{2+} concentration, (b) Benesi–Hildebrand plot of TC- Zn^{2+}

The complexation ratio between TC-Zn^{2+} was investigated by the method of continuous variation (Job's plot). As depicted in Fig. 7, the turning point happened at 0.5 of Zn^{2+} concentration ratio, indicating that the stoichiometric ratio of TC-Zn^{2+} was 1:1.
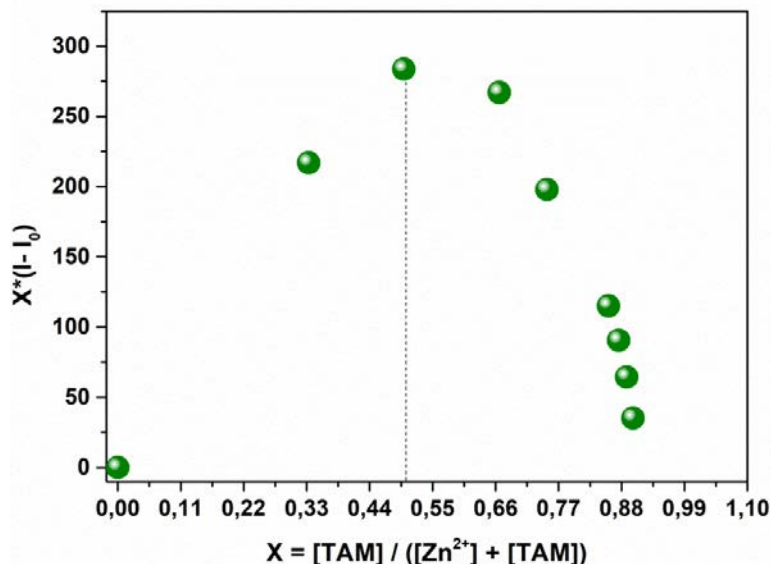

Figure 8. Job's plots of TC with Zn^{2+}

Conclusion

In conclusion, a novel imidazole-derived fluorogenic chemosensor for Zn^{2+} sensing has been developed. As a result of the coordination of the TC with Zn^{2+}, the intensity alteration of TC solution has occurred because of the strong affinity between TC and Zn^{2+}. This proposed fluorogenic chemosensor TC can become an easy recognition tool for Zn^{2+} in solutions and can reveal the design of various fluorogenic probes for Zn^{2+} recognition.

Scientific Ethics Declaration

The authors declare that the scientific ethical and legal responsibility of this article published in EPSTEM journal belongs to the authors.

Acknowledgements or Notes

References

Aydin, D., Karuk Elmas, S. N., Savran, T., Arslan, F. N., Sadi, G., & Yilmaz, I. (2021). An ultrasensitive "off–on" fluorogenic sensor based on thiazole derivative for zn2+: Food supplement, water and Bio–Imaging Applications. *Journal of Photochemistry and Photobiology A: Chemistry*, *419*, 113459. https://doi.org/10.1016/j.jphotochem.2021.113459

Erdemir, S., & Malkondu, S. (2020). Calix[4]arene based a NIR-fluorescent sensor with an enhanced stokes shift for the real-time visualization of Zn(ii) in living cells. *Sensors and Actuators B: Chemical*, 306, 127574. https://doi.org/10.1016/j.snb.2019.127574

Ghaedi, M., Shokrollahi, A., Niknam, K., & Soylak, M. (2009). Cloud point extraction of copper, zinc, iron and nickel in biological and environmental samples by flame atomic absorption spectrometry. *Separation Science and Technology, 44(*3), 773–786. https://doi.org/10.1080/01496390802437164

Kutluca Alici, M. (2020). Phentroimidazole based fluorescence "turn on" sensor for highly sensitive detection of Zn^{2+} ions. *Journal of Fluorescence, 30*(2), 269–273. https://doi.org/10.1007/s10895-020-02498-y

Sethupathi, M., Jayamani, A., Muthusankar, G., Sakthivel, P., Sekar, K., Gandhi, S., Sengottuvelan, N., Gopu, G., & Selvaraju, C. (2020). Colorimetric and fluorescence sensing of Zn^{2+} ion and its bio-imaging applications based on macrocyclic "Tet a" derivative. *Journal of Photochemistry and Photobiology B: Biology*, *207*, 111854. https://doi.org/10.1016/j.jphotobiol.2020.111854

Author Information

Onder Alici	Duygu Aydin
Selcuk University Science Faculty, Department of Chemistry, Konya/Turkey	Karamanoglu Mehmet Bey University, Kamil Ozdag Faculty of Science, Department of Chemistry, Karaman/Turkey
Contact e-mail: *onderkimya@gmail.com*	

To cite this article:

Alici, O. & Aydin, D. (2022). Synthesis and fluorimetric application of novel schiff base compound containing imidazole. *The Eurasia Proceedings of Science, Technology,Engineering & Mathematics (EPSTEM), 17*, 53-59.

Analysis of the Performance and Emission Characteristics of Biokerosene with 2-Ethylhexyl Nitrate Additive

Ayhan UYAROGLU
Selcuk University

Mahmut UNALDI
Selcuk University

Abstract: The increase in population and living standards has sparked to mobility of people. Therefore, mobility of the people who enhanced welfare causes a raising in travel activities. Such a demand growth results in the accumulation of the energy requirement. In parallel, leads to developing greenhouse gas (GHG) reduction strategies. To decrease the GHG in the aviation sector comes into prominence nowadays. Emissions from the aircrafts that using as the transportation medium are related to the fuel characteristics. In this sense, growing attention of using biokerosene instead of the fossil based kerosene is encountered in some air carriers. In this study, biodiesel produced via transesterification manner and obtained from waste frying oil was blended with fossil based kerosene in volumetrically (B60K40: 60% waste frying oil methyl ester and 40% fossil based kerosene). Then, 1000 ppm, 2000 ppm, 3000 ppm and 4000 ppm amount of 2-Ethylhexyl nitrate *(*2-EHN) cetane improver have been added to the biokerosene mixture of B60K40. These fuels have been scrutinized emission and engine parameters in 4 cylinder, 4 stroke, turbocharged, direct injection compression ignition (CI) engine with the volume of 3.908 liters and 17/1 compression ratio at full load at 1400, 1600, 1800, 2000, 2200, 2400 and 2600 rpm. In consequence of the present study, biokerosene fuel (B60K40) with additive 2-EHN improves the emissions.

Keywords: Biokerosene, Emissions, Kerosene, Performance, 2-EHN

Introduction

The interest in alternative fuels have been increasing with the effect of environmental awareness and oil scarcity. Biodiesel, which is used as an alternative to petrol based diesel fuel, is derived from vegetable oils or animal fats as a fuel consisting of monoalkylesters of long-chain fatty acids (Cıldır & Canakcı, 2006). Transesterification, which is the most spread method of biodiesel generating methods, is also called alcoholysis, is the process of formation of fatty esters and glycerine by the reaction of triglyceride molecule with alcohol and base (Arslan & AlibaS, 2015). In terms of sustainability, the use of fatty acid methyl esters as biodiesel by blending with diesel fuel is a very common method, while the use of fatty acid methyl esters as biokerosene by blending with fossil-based kerosene fuel is not widespread. On the other hand, studies on the use of bio kerosene fuel are increasing. Kerosene i.e. white oil includes paraffin and naphtha, is obtained from crude oil distillation. Researchers from oil importing countries more particularly have studied about performance and emissions of blending kerosene-vegetable oils and kerosene-diesel fuels, because of the kerosene has lower price than gasoline and diesel fuels (Ekaab et al., 2019). Kerosene not only improves ignition characteristics at low temperatures, but also improves cold starting. Thanks to the low viscosity of kerosene, the injection duration is longer than diesel fuel, and it completes the combustion by improving atomization and injection (Gad et al., 2020). Bayindir et al., (2017) reported a decrease in NOx and CO emissions, while an increase in HC emissions, by using canola biodiesel and kerosene in B80&K20 and B80&K10&D10 fuel mixtures. They also stated that

by adding kerosene or kerosene diesel fuel to biodiesel to reduce the density of biodiesel and similar properties to diesel fuel can be obtained (Bayındır et al., 2017).

Aydın et al., (2010) explained that, in terms of environmental pollution, biodiesel-kerosene mixture can be used as an alternative because its emissions are lower than fossil-based diesel and biodiesel-diesel mixtures. By adding kerosene to biodiesel fuel, engine power increased slightly and specific fuel consumption decreased compared to biodiesel-diesel mixtures, they explained that BK20 fuel has similar properties with fossil-based diesel fuel and that the low viscosity and high calorific value of kerosene, and the high cetane number and thermal efficiency of the mixture cause the increase in effective pressure and power of this fuel (Aydın et al., 2010). Aydın, (2016) determined that, among S90&K10, S75&K25 and S50&K50 safflower biodiesel and kerosene mixtures, the highest Pmax value and maximum heat release rate, the lowest specific fuel consumption and exhaust temperature were obtained with S50&K50 mixtures. In addition to this, as the kerosene ratio increases, NOx emissions decrease and there was a slight increase in CO and HC emissions compared to diesel fuel (Aydın, 2016). Roy et al., (2014), have investigated biodiesel–diesel and biodiesel–diesel-additive blends of 0, 5, 10, 20, 50 and 100 volume percent, and kerosene–biodiesel blends of 0, 5, 10, 20, 50 and 100 volume percent, and specific fuel consumption have increased in biodiesel–diesel and biodiesel–diesel-additive mixtures by increasing biodiesel ratio. With regard to emissions, they stated that CO emissions decreased with biodiesel-diesel and biodiesel-diesel additive blends at low and medium loads. As the biodiesel amount increases in biodiesel-diesel and biodiesel-diesel mixtures HC emissions decrease, but in kerosene-biodiesel mixtures, HC emissions only reduce under heavy loads. With the increment of biodiesel ratio in biodiesel-diesel and biodiesel-diesel additive mixtures, NOx emissions increase at medium loads, while in kerosene-biodiesel mixtures have lower NOx emissions at all loads (Roy et al., 2014).

Fuel additives are chemical compounds used to improve fuel properties, if less than <1% is added in refineries, they are called refinery (functional) additives, while if they are added in more than 1%, they are called blending components (Uyaroglu & Unaldı, 2021a). Ali et al., (2016) indicated that DTBP and EHN cetane improvers reduce NOx emission by 4% in B20 mixtures (Ali et al., 2016). Imdadul et al., (2016) NO emissions tend to decrease as the EHN ratio increases. They found that the addition of EHN increased the HC emissions while reducing the smoke emissions (Imdadul et al., 2016). Atmanlı, (2016) determined that the EHN cetane improver Diesel n-butanol mixture decreased the specific fuel consumption and NOx emissions by 1.07%, while increasing the CO and HC emissions by 15.7% and 11.10%, respectively. With the addition of EHN to the diesel fuel 1-pentanol mixture, NOx emissions decreased by 2.23%, HC emissions decreased by 17.25%, and CO emissions increased by 10.49% (Atmanlı, 2016). İleri, (2016) conducted the engine performance and emissions at 0%, 25%, 60%, 98% and 100% engine loads at 2200 rpm with the addition of 500, 1000 and 2000 ppm EHN to 70% diesel fuel, 10% sunflower oil and 20% n butanol or 1-pentanol mixtures. Thanks to the adding EHN to D70S20B10 and D70S20P10 fuels reduced NOx emissions by 2.28%-5.26% and 0.26-2.90%, respectively, while increasing CO emissions by 11.85-23.46% and 7.16%-23.41%, respectively. It was stated that while the addition of EHN to D70S20B10 fuel increased HC emission a little, the addition of EHN to D70S20P10 fuel reduced HC emission by 28.23%, 21.63% and 17.70% compared to D70S20P10 (İleri, 2016). Zhang et al., (2013) the addition of EHN slightly increases NOx emissions and significantly reduces THC emissions. The addition of EHN has little effect on CO emissions, but offers a better match between combustion noise and soot emissions (Zhang et al., 2013). Hess et al., (2004) determined that the addition of 1000 ppm 2-EHN reduced NOx emissions by 4.5% (Hess et al., 2004).

In this study, B60K40 mixture, that optimum biodiesel-kerosene mixture obtained previous work (Uyaroglu & Unaldı, 2021b), was added 1000 ppm, 2000 ppm, 3000 ppm ve 4000 ppm of EHN (Ethylhexyl Nitrate). These fuels (B60K40/1000, B60K40/2000, B60K40/3000, B60K40/4000) are tested under full engine load with 1400, 1600, 1800, 2000, 2200, 2400 and 2600 engine speeds in terms of the performance and emission characteristics.

Method

Methyl ester production and test fuel specification

In the transesterification reaction, 0.45% NaOH and 6:1 alcohol/oil molar ratio MeOH were used. The reaction took place for 60 minutes and at 60 °C. After the transesterification reaction is finished, ester was left to rest for 6-8 hours to separate the glycerin and then esters were washed with hot distilled water (85 °C) several times till the water and ester became clear. At the end of the washing process, it was dried at 120 °C for 30 minutes. Various properties of fuels that used in the tests were shown at Table 1.

Table 1. Fuel properties

Fuels	Kinematic viscosity (40 °C mm^2/s)	Density @15 °C (g/cm^3)	Lower Heating Value (kJ/kg)
B100	5.17	0.8831	37953
Diesel	3.02	0.8342	43524
Kerosene	1.42	0.7898	44407
B60K40	3.08	0.8464	40388
B60K40-3000	3.09	0.8479	40346

The engine and test devices specifications

Engine tests were conducted at full load in a brand of Tumosan 4-cylinder, 4-stroke, compression ratio 17/1, 3.908 liters turbocharged direct injection compression ignition (CI) engine at full load and at 1400, 1600, 1800, 2000, 2200, 2400 and 2600 rpm. The technical specifications of the Tumosan brand engine are shown in Table 2.

Table 2. Engine specification

Technical specification	Engine specification
Number of cylinder	4
Diameter of cylinder	104 mm
Stroke	115 mm
Total cylinder volume	3908 cm^3
Compression ratio	17:1
Maximum torque	295 Nm (at 1600 1/min)
Maximum power	62.5 kW (at 2500 1/min)
Maximum speed	2700 1/min
Cooling system	Water cooled
Injection advance	18 (CA°)
Injection pressure	230 Bar
Fuel pump	Bosch - Distributor Type

Table 3 has shown the specifications of the hydraulic dynamometer used in the tests.

Table 3. Engine dynamometer specification

Technical specification	Dynamometer specification
Max. Brake power	160 (HP)
Max. Brake moment	750 (Nm)
Max. speed	6000 (min^{-1})
Water amount	2.4 (m^3)
Direction of rotation	One direction
Engine Mounting Flange	Double

Table 4 consists of the features of the devices used for emission measurements.

Table 4. Emission devices

Emission	Measuring range	Precision
CO (% volume)	0-10	0.01
CO_2 (%volume)	0-20	0.01
HC (ppm)	0-2000	1
O_2 (%volume)	0-21	0.01
NOx (ppm)	0-5000	1
Lambda	0.5-2	0.001
k	0-20	1/m

Table 5 indicates the flowmeter specifications while Table 6 indicates the flowmeter indicator specifications.

<div align="center">Table 5. Flowmeter specifications</div>

Flowmeter	Specifications
Measuring range (min^{-1})	0.005-1.5
Maximum pressure (bar)	100
Body, gear and shaft	AISI316
Precision	±%0.5
Output	NPN, signal output
Operating voltage (VDC)	5-24

<div align="center">Table 6. Flowmeter indicator</div>

Flowmeter indicator	Specifications
Indicator	2x6 digit
Outputs (Vac)	2 relay output 8A@250
Supply voltage (Vac)	220

Engine performance characteristics calculation method

Effective power is calculated by the effective motor torque (Me) value and the motor speed (n) at which this torque is obtained. Equation 1 used to calculate the effective power (Pe) is shown below.

$$P_e = \frac{M_e . n}{9549.3} \text{ (kW)} \tag{1}$$

Effective specific fuel consumption (be) determines the amount of fuel spent (m_y) over an hour to obtain unit power (P_e), and calculated with equation 2.

$$b_e = \frac{\dot{m}_y . 3600}{P_e} \text{ (gr/kWh)} \tag{2}$$

The thermal efficiency (η_{th}) of the engine represents the conversion rate of the fuel energy taken into the cylinder to power. H_u represents lower heating value. The thermal efficiency is calculated using Equation 3.

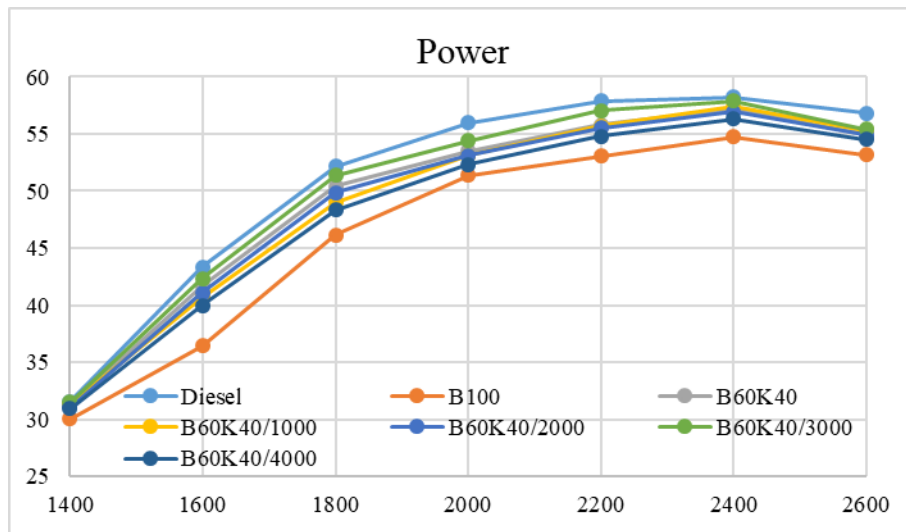$$\eta_{th} = \frac{P_e \times 3600}{m_y \times H_u} \times 100 \tag{3}$$

Figure 1. Engine power

Results and Discussion

Engine speed and power changes of the test fuels have shown at Figure 1. While the highest engine power was reached with diesel fuel at 58.2495 kW at 2400 rpm, the lowest engine power was reached with B100 fuel at 30.031 kW at 1400 rpm. This situation can be explained from the low calorific value of biodiesel In Figure 2, the torque changes with the speed of the test fuels are shown. Diesel fuel gives the highest torque value, and the B60K40/3000 fuel mixture has the highest torque value after diesel fuel. The highest torque value was realized with diesel fuel at 276.58 Nm at 1800 rpm, and the lowest torque value was realized with B100 fuel at 2600 rpm with 195.27 Nm. The fact that the torque values are lower than diesel is due to the high viscosity and lower heating value compared to diesel (Aksoy et al., 2018).
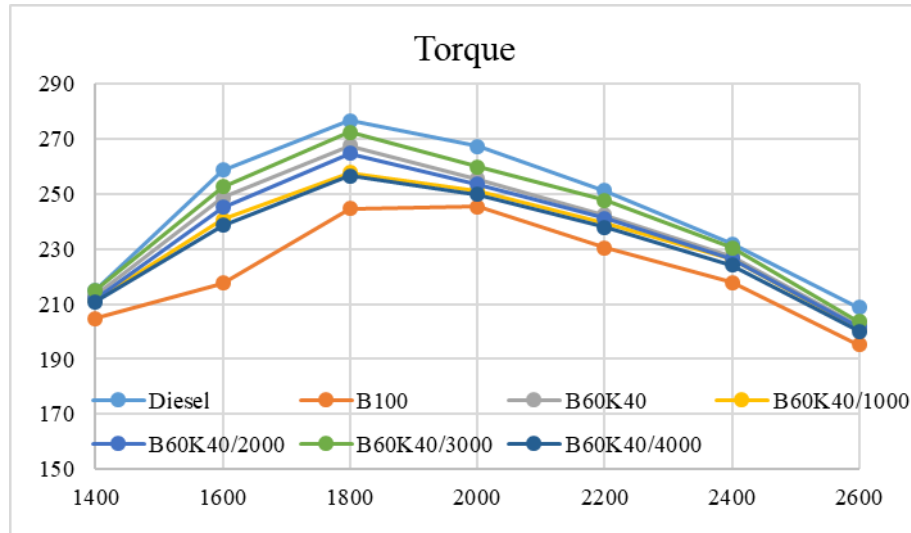

Figure 2. Engine Torque

The variation of brake specific fuel consumption (BFSC) according to engine speed is shown in Figure 3. Looking at the figure, it is seen that the lowest values are obtained with standard diesel fuel, while the highest values are obtained with B100, that is, 100% biodiesel fuel. It is known that the heating value causes this difference.
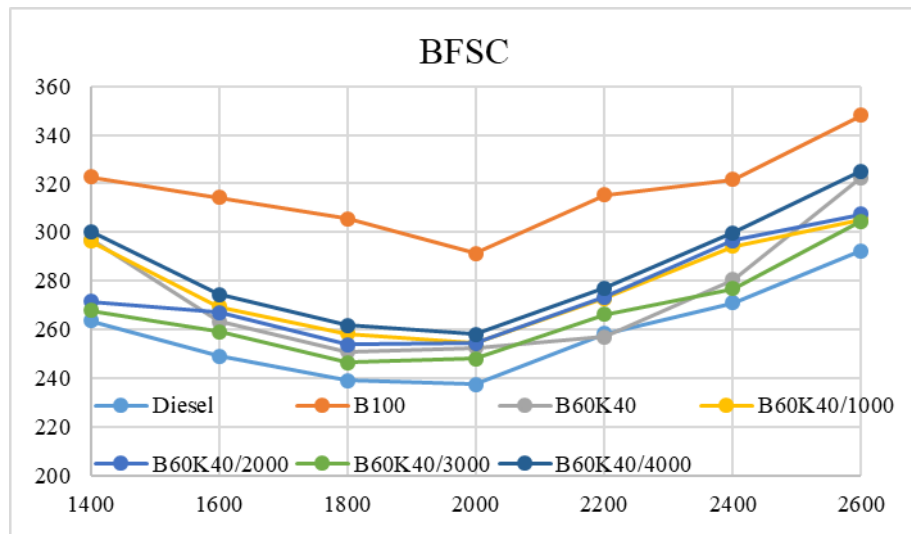

Figure 3. Brake specific fuel consumption

The relationship between thermal efficiency and engine speed is given in Figure 4. While the highest thermal efficiency was 36% with B60K40/3000 with 60% biodiesel-40% kerosene and 3000 ppm 2-EHN additive added, the lowest thermal efficiency was realized in B100 fuel with approximately 27%.
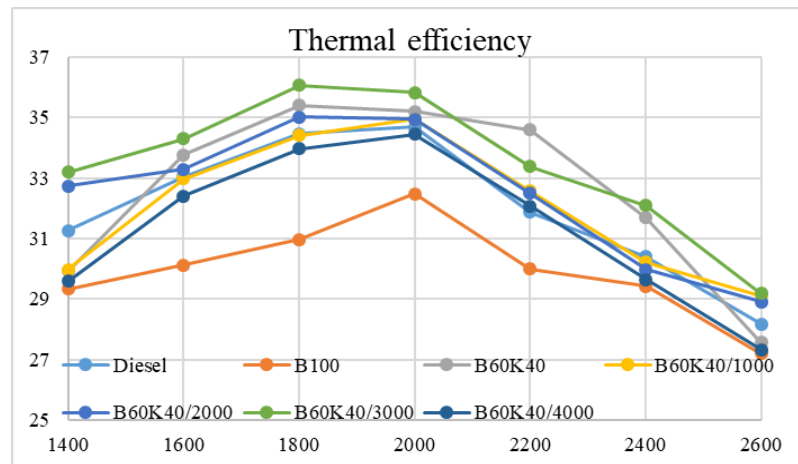
Figure 4. Thermal efficiency

Figure 5 shows the variation between exhaust gas temperature (EGT) and engine speed. While the highest exhaust gas temperature was measured at 470 °C and 2600 rpm in B100 fuel, the lowest value was measured at 370 °C at 1400 rpm in standard diesel fuel.
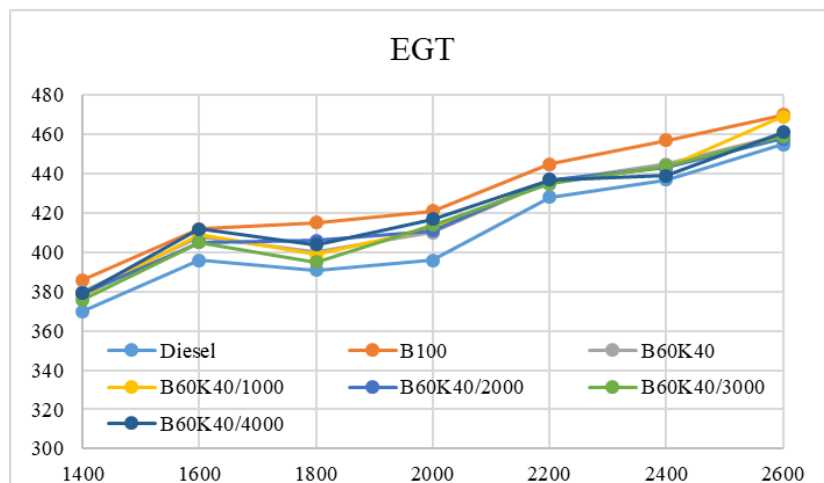
Figure 5. Exhaust gas temperature
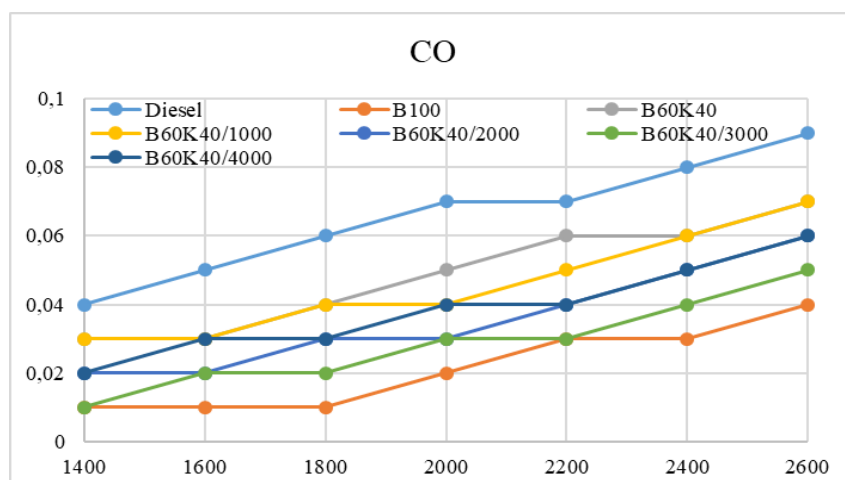
Figure 6. CO emissions

The variation of carbon monoxide (CO) emission depending on engine speed is given in Figure 6. The CO emission values of diesel fuel were higher than the other test fuels at the engine speeds indicated in the graph. Carbon monoxide is formed from incomplete combustion caused by insufficient oxygen (Sugozu, 2016). Owing to the oxygen content of biodiesel, CO emissions are less. The changing of hydrocarbon (HC) emissions at

various engine speeds is shown in Figure 7. It is seen in the graph that the amount of HC emission of standard diesel fuel at various engine speeds is higher than that of other test fuels. Oxygen content in biodiesel is effective in reducing HC emissions.
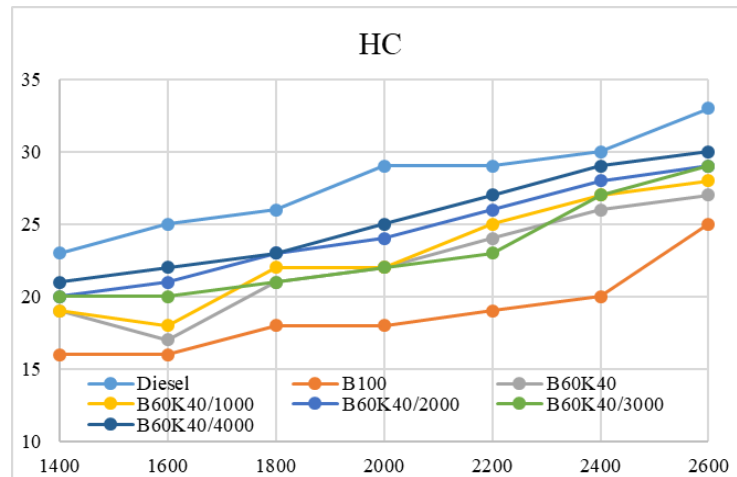
Figure 7. HC emissions
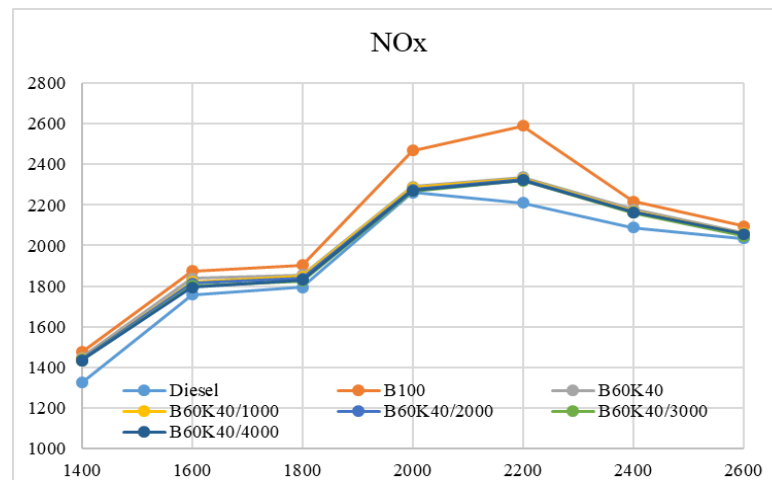
Figure 8. NO$_x$ emissions
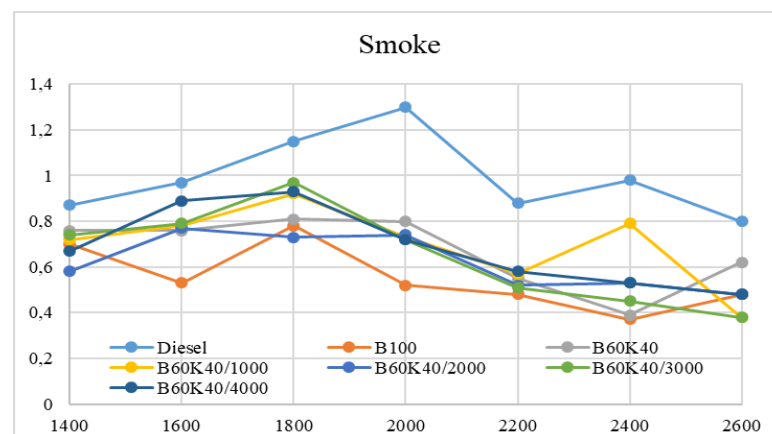
Figure 9. Smoke emissions

Figure 8 shows the nitrogen oxides (NOx) emission changes of the test fuels depending on the engine speed. The highest NOx emission values were determined in B100 fuel, and the lowest NOx emission values were determined in standard diesel fuel. By means of the N and O atoms reacting at elevated temperatures, NOx emission is emanated (Ors, 2020). According to Sathiyamoorthi et al. (2018), biodiesel blends with 2-EHN additives reduce NOx emissions by emitting less heat as they reduce the in-cylinder temperature

(Sathiyamoorthi et al., 2018). Ciniviz et al., (2017) 2-EHN reduces NOx emissions by increasing the cetane number (Ciniviz et al., 2017).

The changes in smoke emission were determined as in figure 9. While the highest soot emission value was seen in standard diesel fuel, the lowest value was observed in B100 fuel. The fact that biodiesel contains more oxygen improves oxidation reactions and prevents soot formation. According to Calam (2020), soot emissions are the result of thermal decomposition of long-chain hydrocarbons in regions where oxygen is scarce for combustion, and the oxygen content of biodiesel is effective in reducing soot emissions (Calam 2020).

Conclusion

In a Tumosan brand direct injection compression ignition (CI), 4-cylinder, 4-stroke, turbocharged engine with a compression ratio of 17/1, with an engine capacity of 3.908 liters, at full load at 1400, 1600, 1800, 2000, 2200, 2400 and 2600 rpm. 2-EHN that is a cetane improver, was added to B60K40 biodiesel-kerosene mixture at rates of 1000 ppm, 2000 ppm, 3000 ppm and 4000 ppm. Among these test fuels, the mixture with B60K40 and 3000 ppm 2-EHN; in terms of specific fuel consumption, engine power, engine torque and thermal efficiency, it showed values close to diesel fuel, and it was observed that it had lower emission values than diesel fuel in terms of emissions. In this respect, it is thought that it is possible to use B60K40-3000 ppm 2-EHN fuel mixture as an alternative fuel in diesel engines.

Scientific Ethics Declaration

The authors declare that the scientific ethical and legal responsibility of this article published in EPSTEM journal belongs to the authors.

Acknowledgements or Notes

References

Aksoy, F., Mutlu, İ., İnal, A., Uyumaz, A., Solmaz, H., Yilmaz, E., ... & Calam, A. (2018). *Dizel ve hashas yagı biyodizel yakıt karısımlarının motor performansı ve egzoz emisyonları uzerindeki etkilerinin deneysel incelenmesi.* 14th International Combustion Sysmposium Proceedings Book

Ali, O. M., Mamat, R., Abdullah, N. R., Abdullah, A. A., Khoerunnisa, F., & Sardjono, R. E. (2016). Effects of different chemical additives on biodiesel fuel properties and engine performance. A comparison review. In *MATEC Web of Conferences* (Vol. 38, p. 03002). EDP Sciences.

Arslan, M., & AlibaS, K. (2015). Laboratuvar olcekli biyodizel uretim tesisinin projelendirilerek imal edilmesi ve bu tesiste ceSitli bitkisel yag kaynaklarından biyodizel uretimi. *Uludag Universitesi Ziraat Fakultesi Dergisi, 29*(1), 107-114.

Atmanlı, A. (2016). Effects of a cetane improver on fuel properties and engine characteristics of a diesel engine fueled with the blends of diesel, hazelnut oil and higher carbon alcohol. *Fuel, 172*, 209-217.

Aydın, H. (2016). Scrutinizing the combustion, performance and emissions of safflower biodiesel–kerosene fueled diesel engine used as power source for a generator. *Energy Conversion and Management, 117*, 400-409.

Aydin, H., Bayindir, H., & Ilkilic, C. (2010). Emissions from an engine fueled with biodiesel-kerosene blends. *Energy Sources, Part A: Recovery, Utilization, and Environmental Effects, 33*(2), 130-137.

Bayındır, H., ISık, M. Z., Argunhan, Z., Yucel, H. L., & Aydın, H. (2017). Combustion, performance and emissions of a diesel power generator fueled with biodiesel-kerosene and biodiesel-kerosene-diesel blends. *Energy, 123*, 241-251.

Calam, A. (2020). Atık kızartma yagı biyodizeliyle calısan direkt enjeksiyonlu bir dizel motorun yanma performans ve emisyon ozellikleri. *Dokuz Eylul Universitesi Muhendislik Fakultesi Fen ve Muhendislik Dergisi, 22*(64), 97-106.

Cildir, O., & Canakci, M. (2006). Ceşitli bitkisel yaglardan biyodizel uretiminde katalizor ve alkol miktarinin yakit ozellikleri uzerine etkisinin incelenmesi. *Gazi Universitesi Muhendislik Mimarlık Fakultesi Dergisi, 21*(2), 367-372

Ciniviz, M., İlker, O. R. S., & Kul, B. S. (2017). The effect of adding EN (2-ethylhexyl nitrate) to diesel-ethanol blends on performance and exhaust emissions. *International Journal of Automotive Science and Technology, 1*(1), 16-21.

Ekaab, N. S., Hamza, N. H., & Chaichan, M. T. (2019). Performance and emitted pollutants assessment of diesel engine fuelled with biokerosene. *Case Studies in Thermal Engineering, 13*, 100381.

Gad, M. S., El-Fakharany, M. K., & Elsharkawy, E. A. (2020). Effect of HHO gas enrichment on performance and emissions of a diesel engine fueled by biodiesel blend with kerosene additive. *Fuel, 280*, 118632.

Hess, M. A., Haas, M. J., Foglia, T. A., & Marmer, W. N. (2004). The effect of antioxidant addition on NOx emissions from biodiesel. Prepr. Pap.-*Am. Chem. Soc., Div. Fuel Chem, 49*(2), 852-853.

İleri, E. (2016). Experimental study of 2-ethylhexyl nitrate effects on engine performance and exhaust emissions of a diesel engine fueled with n-butanol or 1-pentanol diesel–sunflower oil blends. *Energy Conversion and Management, 118*, 320-330.

Imdadul, H. K., Masjuki, H. H., Kalam, M. A., Zulkifli, N. W. M., Alabdulkarem, A., Rashed, M. M., & Ashraful, A. M. (2016). Influences of ignition improver additive on ternary (diesel-biodiesel-higher alcohol) blends thermal stability and diesel engine performance. *Energy Conversion and Management, 123,* 252-264.

Ors, İ. (2020). Experimental investigation of the cetane improver and bioethanol addition for the use of waste cooking oil biodiesel as an alternative fuel in diesel engines. *Journal of the Brazilian Society of Mechanical Sciences and Engineering, 42*(4), 1-14.

Roy, M. M., Wang, W., & Alawi, M. (2014). Performance and emissions of a diesel engine fueled by biodiesel–diesel, biodiesel–diesel-additive and kerosene–biodiesel blends. *Energy Conversion and Management, 84*, 164-173.

Sathiyamoorthi, R., Babu, S. C., Rajangam, V., & Tamizhselvan, L. S. (2018). Evaluation of neem oil biodiesel with 2-ethyl hexyl nitrate (2-EHN) as cetane improver on performance and emission characteristics of a DI diesel engine. *Int J Eng Res, 6*(2), 1-4.

Sugozu, B. (2016). Influence of diesel fuel and soybean oil ethyl ester blends on the performance and emission characteristics of a diesel engine. *International Journal of Automotive Engineering and Technologies, 5*(1), 1-7.

Uyaroglu, A., & Unaldi, M. (2021a). The influences of gasoline and diesel fuel additive types. *International Journal of Energy Applications and Technologies, 8*(3), 143-153.

Uyaroglu, A., Unaldı M. (2021b). *Performance and emission characteristics of biodiesel and kerosene mixtures.* International Symposium on Automotive Science and Technology, Ankara/TURKEY, 8-10 September 2021.

Zhang, Q., Yao, M., Luo, J., Chen, H., & Zhang, X. (2013). Diesel engine combustion and emissions of 2, 5-dimethylfuran-diesel blends with 2-ethylhexyl nitrate addition. *Fuel, 111*, 887-891.

Author Information

Ayhan Uyaroglu
Selcuk University Cihanbeyli High Vocational School, Konya, Turkey
Contact e-mail: *ayhan.uyaroglul@selcuk.edu.tr*

Mahmut Unaldi
Selcuk University Cihanbeyli High Vocational School, Konya, Turkey

To cite this article:

ICRETS 2022: International Conference on Research in Engineering, Technology and Science

Efficient Decolorization of Anionic Dye (Methyl Blue) by Natural-Based Biosorbent (nano-Magnetic *Sophora Japonica* Fruit Seed Biochar)

Okan BAYRAM
Suleyman Demirel University

Elif KOKSAL
Suleyman Demirel University

Emel MORAL
Suleyman Demirel University

Fethiye GODE
Suleyman Demirel University

Erol PEHLIVAN
Konya Technical University

Abstract: Today, various methods are used to remove the dye pollution in the increasing water. Adsorption is a fast and effective method that has been used since the past. The value of the obtained adsorption capacity varies according to the type of biosorbent material used. The seeds of the fruit of *Sophora Japonica* (SJfs), a tree commonly found in nature, were pyrolyzed at 450°C to produce biochar (SJfsB) in this study. Iron nanoparticles were immobilized into the SJfsB structure to form a more active biosorbent matrix. The obtained SJfsB and nM-SJfsB were used in the removal of methyl blue, an anionic dye. SJfsB and nM-SJfsB used for dye removal were characterized by FT-IR and SEM instruments. The obtained results revealed that the adsorption process occurred in the pseudo-second-order and was consistent with the Langmuir model. The maximum adsorption capacity for MB removal was 434.783 mg/g for nM-SJfsB and 76.923 mg/g for SJfsB, respectively.

Keywords: Nanomagnetic-*Sophora Japonica* fruits seed biochar, Methyl blue, isotherm, kinetics

Introduction

Water pollution in the world has become a serious environmental problem that has gained importance with the development of many industries. Clean, drinkable water resources are gradually decreasing. Most industrial and domestic processes produce wastewater containing toxic substances (Amari et al. 2019). Pollutants that threaten the environment and human health, such as dyes and heavy metals, are often mixed with industrial wastewater and water sources in nature. Many industries such as cosmetics, leather, paper, textiles use dyes, and non-biodegradable dyes in these areas that use large amounts of water harm the environment with wastewater (Jawad et al. 2020). Dyes cause color pollution in water even at low concentrations, and this pollution delays photosynthesis by preventing light transmission. According to their ionic structure, dyes are divided into three as non-ionic, cationic and anionic dyes. Methyl blue is an anionic dye in the triphenylmethane group (Mouni et al. 2018). The treatment of wastewater and the use of purified water in industrial processes are gaining importance today. Many physical and chemical processes are applied for water purification. To treat dye-contaminated wastewater, various chemical, biological, and physical methods such as biodegradation, membrane filtration, ion exchange, electrochemical oxidation, and adsorption are used and many of them are

costly (Arunachalam et al. 2018). Adsorption is one of the most effective and simple methods and it is used to detoxify and purify wastewater by removing its color and odor (Mohammed et al. 2022).
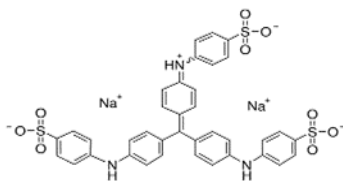
Adsorption occurs as a result of the formation of chemical and physical bonds between a porous solid surface and a liquid phase (Al-Ghouti & Da'ana, 2020). Biomass, agricultural wastes and natural minerals are at the forefront of environmentally friendly, low cost, easily available, high capacity, renewable biosorbents that do not form harmful by-products. Adsorption rate and selectivity are the most important properties of biosorbents. Researches on high selectivity biosorbents with fast adsorption and desorption rates are continuing (Kadhom et al. 2020). Biomass from plants contains oxygen-rich functional groups such as hydroxyl and carboxyl. The surface properties and adsorption capacity of these carbon-containing biosorbents are improved by chemical activation method (Jawad et al. 2020). As the specific surface area, pore volume, and surface chemical functional groups increase and the pore size decreases, the adsorption capacity of biosorbents increases. Biochar is obtained by pyrolysis of biomass in the presence of low oxygen. Surface area and porosity are two important physical and chemical properties of biochar. Biochar is rich in carbon content. It has a stable structure, large surface area and cation exchange capacity. Biochar is an biosorbent widely used to remove organic pollutants, toxic metals from industrial wastewater, agricultural wastewater, municipal wastewater (Wang & Wang 2019). Nanomaterials have been employed as a feasible choice of pollutant removal processes due to their unique qualities such as good recovery and high specific surface area. To protect human health and the natural environment, there is a need for nanobiosorbent materials to remove dyes from industrial wastes. The morphological and chemical properties of biological wastes can be enhanced by a wide variety of modification procedures (Bayram et al. 2022). One of them involves the inclusion of the magnetic form of nanomaterials matching the original structure. As biosorbents for dye removal, magnetically sensitive inexpensive biological materials were used. Recently, metals such as iron and their oxides have been used to obtain magnetic biochar. We created a magnetically modified biosorbent (nM-SJfsB) as a low-cost biosorbent for the removal of organic pollutants from an aqueous system in this study. SJfsB and nM-SJfsB were investigated and characterized for the removal of MB as anionic dye.

Materials and methods

Reagents and Instrumentation

The chemical materials ($FeSO_4.7H_2O$, $FeCl_3.6H_2O$, NaOH, HCl) used were obtained from Merck Company. Methyl blue (MB) was provided from Isolab Company. A 0.05 M HCl and 0.05 M NaOH solution was used to adjust the pH of the solutions. Table 1 shows the chemical formula, properties, and structures of MB.

Table 1. Some properties of methyl blue dye

Name	Molecular Formula	Molecular Weight	λnm	2D Structure
Methyl blue	$C_{37}H_{27}N_3Na_2O_9S_3$	799.81 g/mol	595-605 nm	

The samples for the FT-IR measurements were prepared using the KBr technique and peaks were recorded by Perkin Elmer Spectrum BX FT-IR spectrometer. The SEM FEI QUANTA 250 FEG was used for SEM images of the produced biosorbents.

Preparation methods

Wavelength Scan

In the wavelength scan, the highest absorbance value was measured at 600 nm. The wavelength scan for methyl blue is shown in Figure 1.
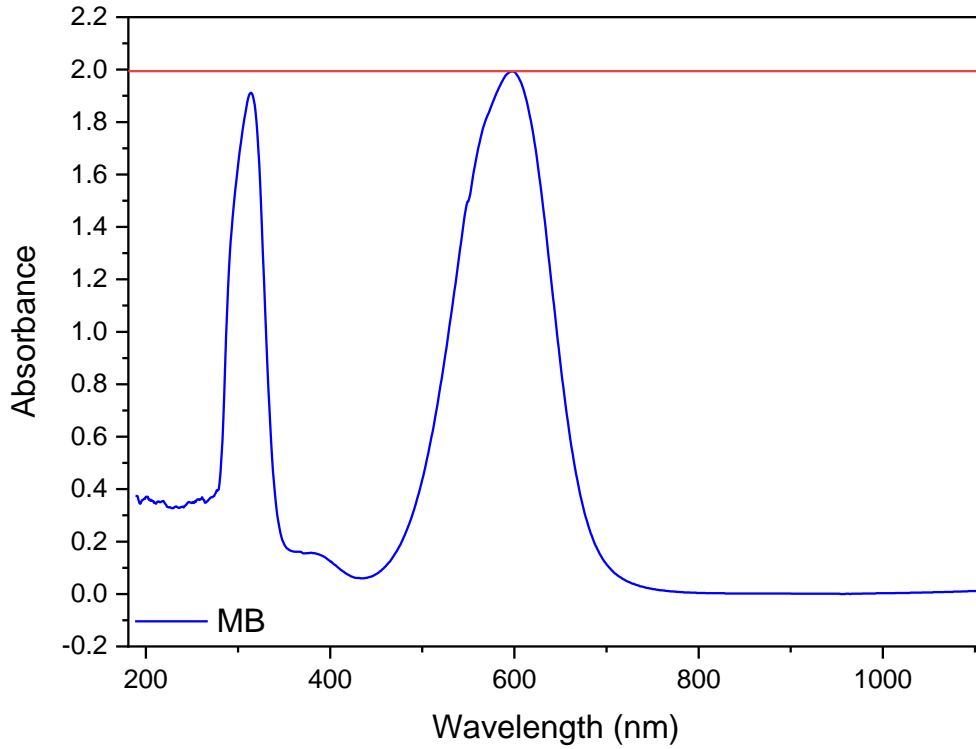
Figure 1. Wavelength of methyl blue

Preparation of Biochar (SJfsB)

SJfs were burned for 4.30 hours at 450 °C in a Carbolite ELF 11/6B brand muffle furnace. The produced SJfsB biochar and modified nM-SJfsB were used in the adsorption experiments.

Preparation of the nM-SJfsB

SJ seeds were cleaned and stored at room temperature for one day. It was then dried again for one more day at 60 °C. The co-precipitation method, which had previously been described in the literature, was used to prepare nM-SJfsB (Fig. 1) (Song et al. 2022). A volumetric flask was filled with 10 g of dried biosorbent. $FeCl_3.6H_2O$ (1 M, 25 mL) and $FeSO_4.7H_2O$ (1 M, 25 mL) solutions were added to a reactor containing 100 mL pure water, and the mixture was stirred at room temperature for one hour to dissolve the iron salt completely. After adding the biochar, the solution was stirred for another 30 minutes. The bottle is then filled with a 30% ammonia solution, which is added drop by drop to adjust the pH of the slurry, and the resulting yellow solution quickly turns into black precipitates. A color change revealed the production of the nM-SJfsB. The nM-SJfsB was filtered using a vacuum. The black precipitates were washed several times with deionized water and dried in an oven at 50 °C for one day after being separated from the solution phase using an external permanent magnet. For the adsorption experiments, the nM-SJfsB was stored in desicator. The reactions that occur during the generation of nM-SJfsB are depicted below (Zhao et al. 2022):

$$2FeCl_3.6H_2O + FeSO_4.7H_2O + 8NH_4OH \xrightarrow{yields} 6NH_4Cl + (NH_4)_2SO_4 + Fe_3O_4 + 17H_2O \qquad (1)$$

$$SJfsB + Fe_3O_4 + H_2O \xrightarrow{yields} nM - SJfsB \qquad (2)$$

Figure 2. The FT-IR spectral characteristics of SJfsB, SJfsB-MB, nM-SJfsB and nM-SJfsB-MB

Figure 3. SEM images of SJfsB and nM-SJfsB before and after MB removal

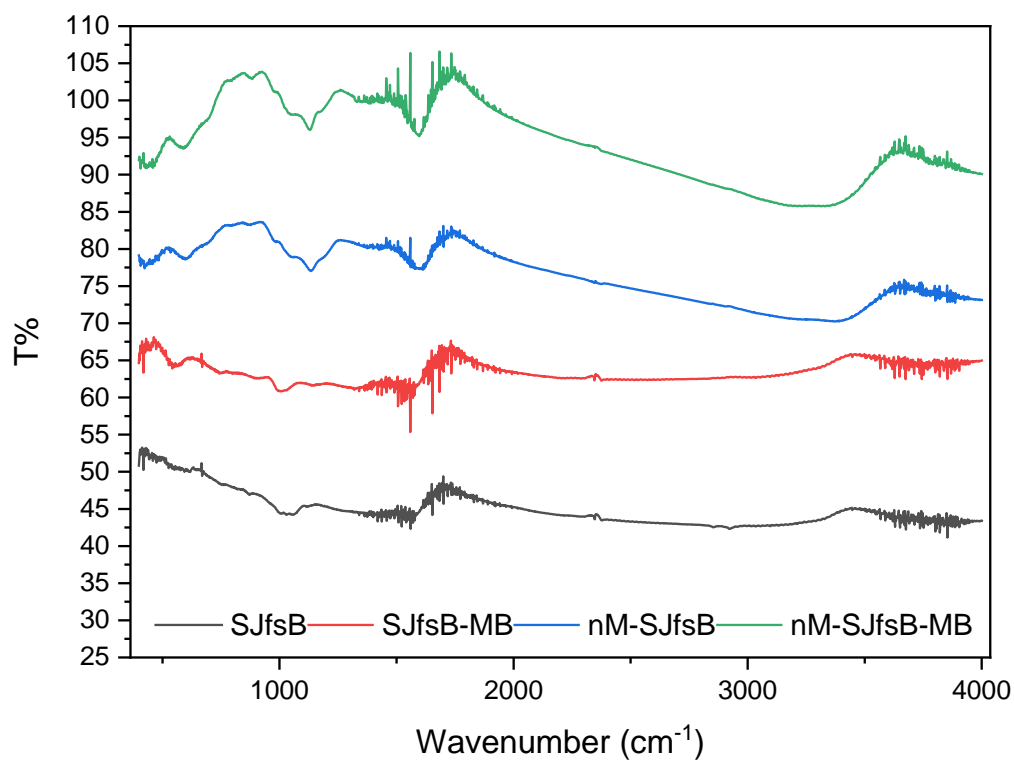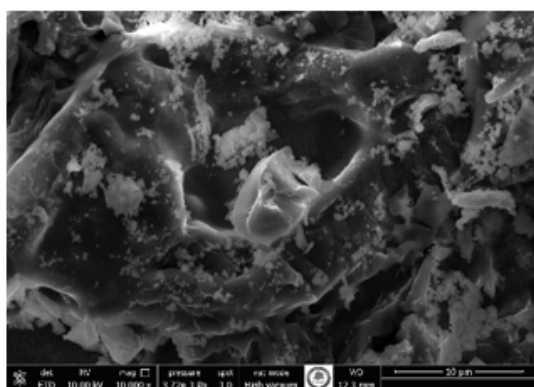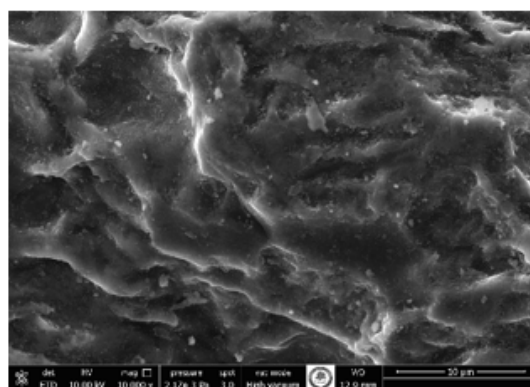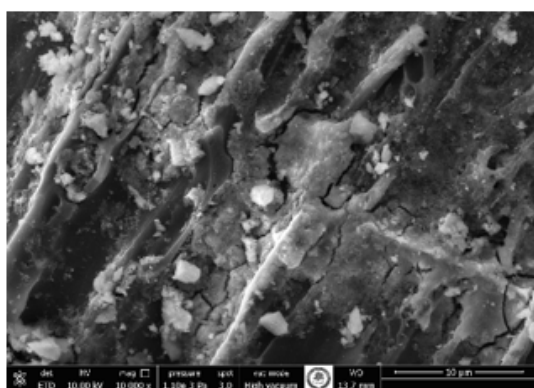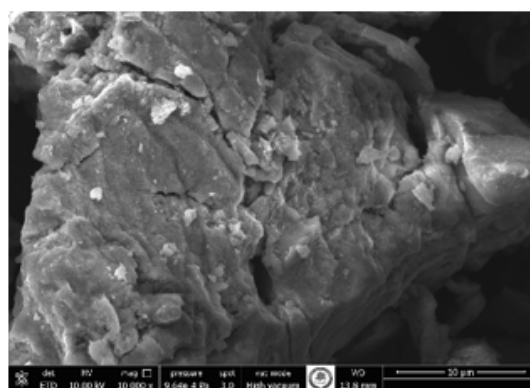FT-IR spectra for SJfsB, nM-SJfsB and SJfsB, MB absorbed on nM-SJfsB were analyzed FT-IR spectrometer (in the infrared region of 4000–400 cm^{-1}. FT-IR spectroscopy was used to observe the chemical structures of SJfsB and chemically modified nM-SJfsB and to determine their functional groups. The spectra are given in Figure 3. When the spectra were examined, broadbands were observed at approximately 3516 cm^{-1} for SJfsB and 3583 cm^{-1} for nM-SJfsB. These bands correspond to the OH stretching vibration. Similar bands were observed in the FT-IR spectra of nM-SJfsB-MB around 3584 cm^{-1} (Bayram et al. 2022). The bands seen around 2989 cm^{-1} in the spectra in Figure 3. correspond to the C–H stretching vibrations in the structure. Similar band was seen around 3010 cm^{-1} in modified nM-SJfsB, nM-SJfsB-MB spectra. The FT-IR spectrum showed that nM-SJfsB's generally consisted of functional groups such as alcohol, phenol, carboxylic groups (O–H groups, C=O and –C–O bonds). The formation of these groups is thought to be due to complexation reactions with MB (Khan et al. 2022; Deng et al. 2022). Stretching vibrations of the C=O bond in the spectra of SJfsB (1774 cm^{-1}) and nM-SJfsB (1757 cm^{-1}) were observed in similar bands in the FT-IR spectra of SJfsB-MB and nM-SJfsB-MBs. This result demonstrated that both SJfsB and chemically modified nM- SJfsBs interacted with dyes as expected. The bands at 786 and 654 cm^{-1} in nM-SJs have been assigned to Fe-O vibrational bonds, confirming the presence of Fe components (Bayram et al. 2022; Wang et al. 2018). The changes and intensities in the bands observed following MB adsorption in nM- SJfsBs suggested that they could be indicative of MB adsorption with functional groups present in nM- SJfsBs.

The surface morphology of both SJfsB and nM-SJfsB was investigated using scanning electron microscopy (SEM) before and after dye adsorption. SEM images were taken on a Quanta FEG250 (Thermo Fisher Scientific) brand device and a magnitude of 10000x was used. SEM examination at various magnifications revealed morphological changes before and after MB biosorbent. Figure 4 depicts the surface morphology results from SEM images, and the surface of SJfsB was discovered to be very porous and amorphous. These spherical granules have a brilliant, noticeable appearance. SEM analysis of nM-SJfsB revealed a wide range of voids on the surface that can be beneficial for MB removal, as well as a significant change in the structure of the biosorbent (Bayram et al. 2022).

Adsorption experiments of MB with the biosorbents

The batch method was used to investigate dye adsorption on the nM-SJfsB with different parameters such as temperature, concentration, pH, and time. To confirm the equilibrium at 25 ℃, the following MB batch adsorption experiments were designed: The saturation of biosorbent by MB was investigated using 0.2 g dosages of SJfsBs and nM-SJfsB in solutions containing 200 mg/L MB. The beaker was removed from the shaker and was placed in an incubator shaker (250 rpm) at 25 ℃ for different contact times (15 minutes, 30 minutes, 60 minutes, 90 minutes, 120 minutes, 180 minutes, and 240 minutes), and then removed from the shaker. The effect of SJfsB and nM-SJfsB biosorbent amount on MB removal was tested by mixing 200 mg/L MB solutions with the certain amount of the biosorbent for 60 minutes. In each vessel, the amount of nM-SJfsB in the dye solution was 0.05 g, 0.1 g, 0.2 g, 0.5 g and 0.75 g. The pH of the solution phase was adjusted from 2 to 9 by including 0.2 g of nM-SJfsB in serious beakers containing 200 mg/L of MB solution. Different starting concentrations of MB (25 mg/L-300 mg/L) were investigated at a stationary pH value of the dye solution. The experiments were repeated to ensure the data's dependability and accuracy. Following the adsorption process, nM-SJfsB was separated from the solution medium with a magnetic bar, and the remaining dye concentration was determined with a UV-Vis spectrometer set to 600 nm for MB. The following equation was used to calculate the adsorption capacity (q_e) of biosorbents. (Eq. (3 and 4)):

$$q_e = \frac{(C_o - C_e)V}{W} \qquad (3)$$

where C_o (mg/L) is initial dye concentration and C_e (mg/L) is equilibrium dye concentration. V (L) is the volume of the dye solution and m (g) is the amount of biosorbent.
The color removal efficiency was calculated using the following formula.

$$Colour(\%) = \frac{100(C_o - C_e)}{C_o} \qquad (4)$$

where C_o is initial MB concentration and C_e is the equilibrium MB concentration. The volume of the solution is denoted by V (mL), and the amount of SJfsBs and nM-SJfsB is denoted by W (g). Eq. (3) was used to calculate the q_e (mg/g) of the SJfsBs and nM-SJfsB. In an equilibrium study, each trial is repeated twice.

Results and Discussion

Effect of different parameters on MB removal

Effect of contact time

0.2 g biosorbent was added to 30 mL of the prepared 200 mg/L MB (pH: ~5.0-5.5) solution. The dyes were adsorbed at various times ranging from 15 to 240 minutes, and the effect of contact time on adsorption was investigated. Figure 5 depicts the effect of contact time on MB adsorption. Adsorption experiments measuring the effect of contact time revealed a slower phase in which MB adsorption began rapidly and tended to the horizontal asymptote in the first 30 minutes. Figure 5 shows that nM-SJfsB has significantly greater adsorption ability than SJfsB. The experiment found that 40-80 minutes of contact time was sufficient to achieve the biosorbent substance-MB equilibrium.

Figure 4. Effect of time change on adsorption (conditions: biosorbent amount: 0.2 g; concentration of dyes: 200 mg/L MB, temperature: 25 ± 1 °C, pH: solution pH 5.0–5.5 for MB; time: 30 min, 45 min, 60 min, 90 min, 120 min, 180 min, 240 min).

Effect of pH on Biosorption

The adsorption process is controlled by pH, which affects the surface charge of the biosorbent, the strength of ionization, the division of functional groups, the specification of the adsorbate, and the degree of ionization. Traditional biosorbents remove decolorization primarily through adsorption, and they may be effective if the concentration of dye in the solution is quite low. It is known that properties such as physical, mechanical, and chemical properties are effective in the interaction of dyes with biosorbent. In adsorption studies, the effect of pH is an important factor in the adhesion interactions of dye to the biosorbent surface. The adsorption of dyes is significantly affected by the surface charge on the biosorbent (nM-SJfsB). The pH is an effective factor in the ionization of MB and the chemical properties of nM-SJfsB in adsorption studies. The pH range of 5.0-5.5 provided the best dye adsorption for both biosorbents.
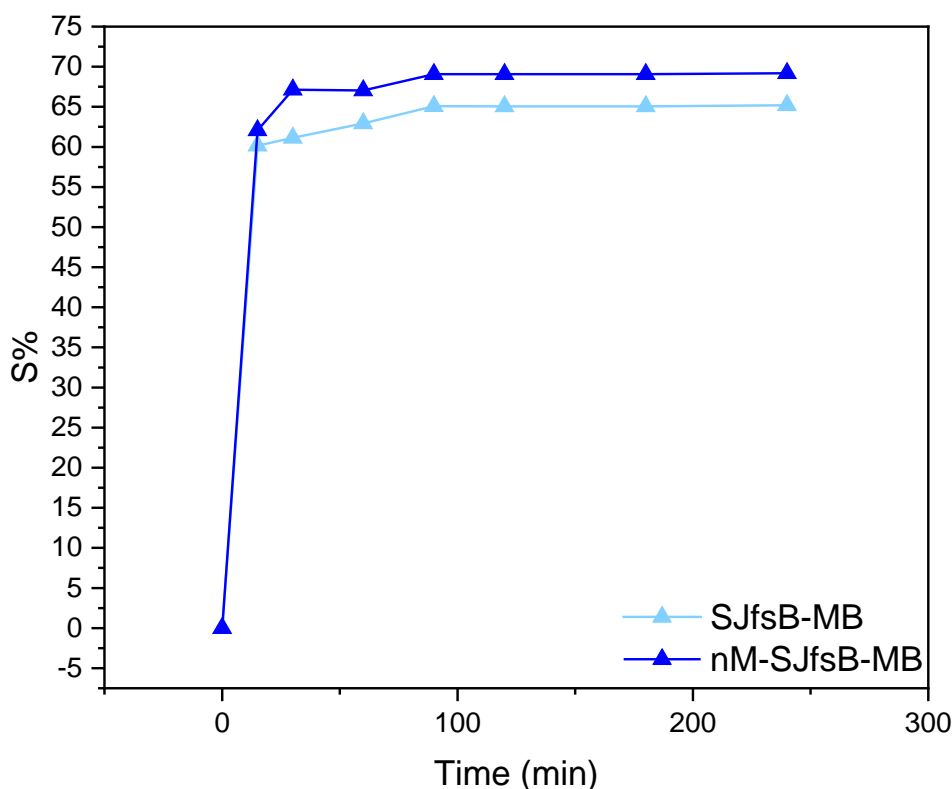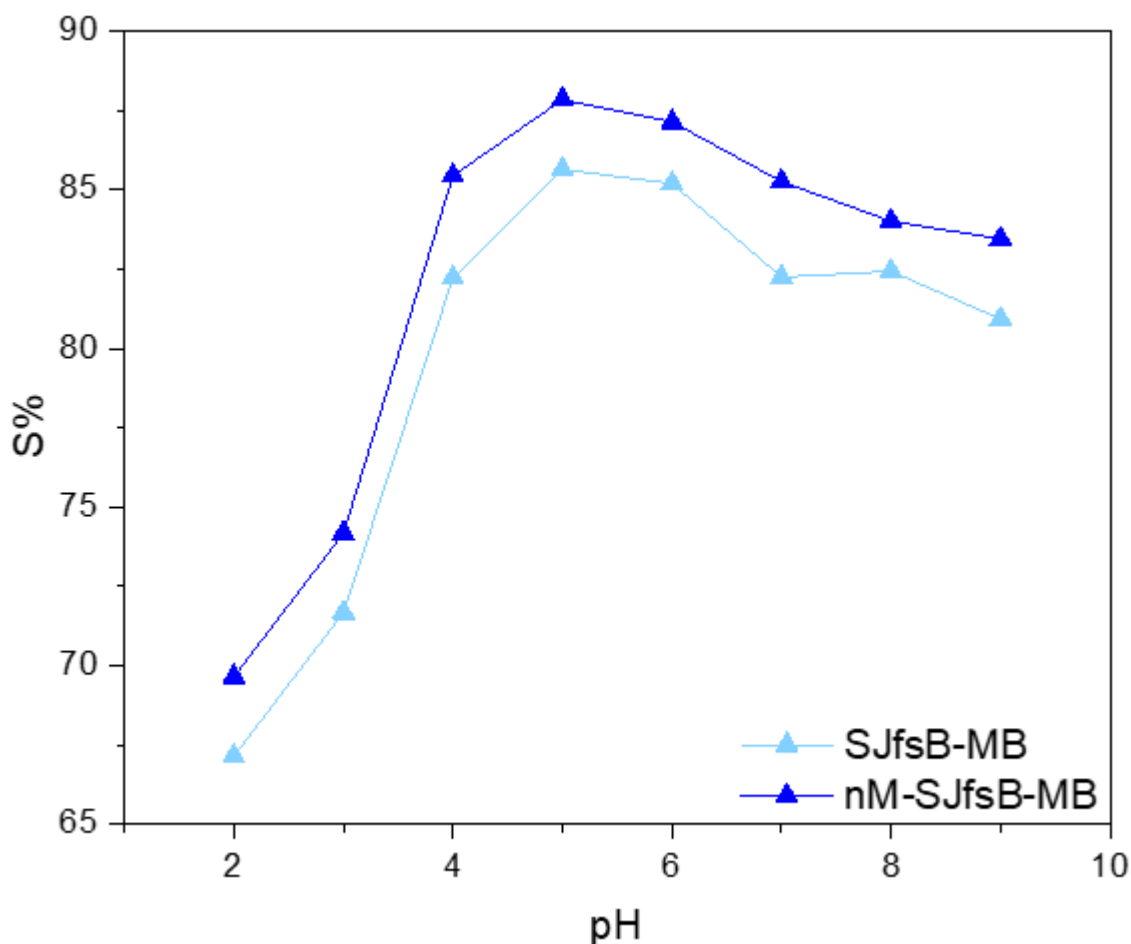
Figure 5. Effect of time change on adsorption (conditions: biosorbent amount: 0.2 g; concentration of dyes: 200 mg/L MB, temperature: 25 ± 1 °C, pH: solution pH 2.0–9.0 for MB; time: 60 min).

Effect of MB Initial Concentration (Adsorption Isotherms)

Adsorption isotherm models are used to explain the distribution of adsorbate molecules on the biosorbent surface when the solid and liquid phases are in equilibrium. Figure 7 shows the adsorption values obtained for equilibrium studies at various MB concentrations. Adsorption capacity SJfsBs and nM-SJfsB by changing the dye concentrations to 25 mg/L-300 mg/L were calculated. It indicates that the percent adsorption of MB reaches a horizontal equilibrium after the initial concentration of 300 mg/L. This is because MB saturation of active sites in SJfsBs and nM-SJfsB coats the surfaces of the biosorbents with sufficient dyes, causing the adsorption rate to slow down until equilibrium is reached. Over time, the surface of the biosorbents becomes saturated and thus the rate of adsorption slows down. Langmuir, Freundlich, Temkin, Dubinin and Radushkevich and Scathard isotherms were used to correlate experimental equilibrium adsorption data (Zhang et al. 2022, Jain et al. 2022). The isotherm equations and the obtained calculation results are shown in Table 2. Compared with other isotherms, Langmuir isotherm was found to be more suitable for dye adsorption. If the calculated R_L value is between 0 and 1, the sorption is considered sufficient. SJfsB and nM-SJfsB strongly absorbed MB dyes from the solution phase with R_L values ranging from 0.016 to 0.290 in our study (Table 2) (Bayram et al. 2022). For SJfsB and nM-SJfsB, the Langmuir isotherm model's high correlation coefficient range (R^2: 0.949-0.979) is more suitable (Table 2). The results showed that the adsorption process occurred in the pseudo-second order, which was consistent with the Langmuir model. The maximum adsorption capacity for MB removal for SJfsB was 434.783 mg/g for nM-SJfsB and 76.923 mg/g for SJfsB, respectively. The Freundlich isotherm was used to predict the adsorption process occurring on the heterogeneous biosorbent surface (Giri et al., 2022). The K_f and n parameters of the Freundlich equation were calculated and the n values were found to be 1.257 for MB adsorption by nM-SJfsB and 1.658 for MB adsorption by SJfsBs. If n is between 1 and 10, adsorption is considered suitable. The Freundlich isotherm model calculated K_f values of 19,173 mg/g for SJfsB-MB and 17,721 mg/g for nM-SJfsB-MB.
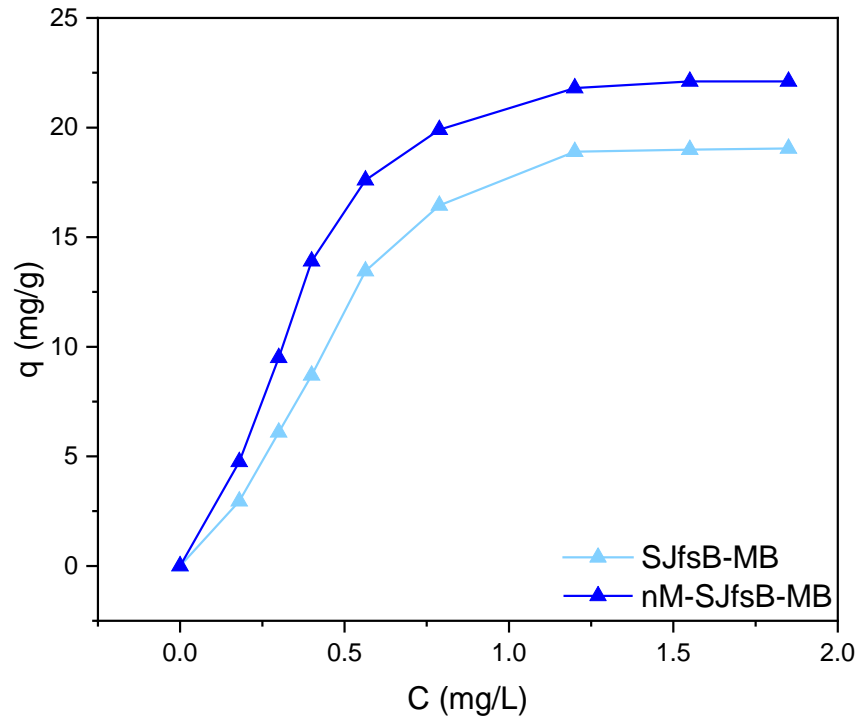
Figure 6. Effect of concentration change on adsorption (conditions: biosorbent amount: 0.2 g; concentration of dyes: 25 mg/L, 50 mg/L, 75 mg/L, 100 mg/L, 150 mg/L, 200 mg/L, 250 mg/L, 300 mg/L MB, temperature: 25 ± 1 °C, pH: solution pH 5.0–5.5 for MB; time: 60 min).

Table 2. Adsorption isotherm parameters and results

	Equation	Eq. no.	Biosorbent	Dye	Parameters for dye			
Langmuir (1916)	$\frac{1}{q_e} = \frac{1}{K_{L_{qmax}}} x \frac{1}{C_e} + \frac{1}{q_{max}}$	(5)			q_{max}	K_L	R^2	R_L
			SJfsB	MB	76.923	0.405	0.929	0.047
			nM-SJfsB	MB	434.783	0.049	0.949	0.290
Freundlich (1907)	$Log q_e = Log K_f + \frac{1}{n} Log C_e$	(6)			K_f	n	R^2	
			SJfsB	MB	19.173	1.658	0.831	19.173
			nM-SJfsB	MB	17.721	1.257	0.899	17.721
Dubinin and Radushkevich (1947)	$ln q_e = ln q_m - \beta\, \varepsilon^2$	(7)			X_m	K	E	R^2
			SJfsB	MB	3.071	4×10^{-8}	4082.482	0.992
			nM-SJfsB	MB	2.582	3×10^{-8}	3535.533	0.984
Scatchard (1949)	$\frac{q_e}{C_e} = Q_s K_s - q_e K_s$	(8)			Q_s	K_s	R^2	
			SJfsB	MB	26.608	3.552	0.960	
			nM-SJfsB	MB	19.315	39.815	0.997	
Temkin and Pyzhev (1940)	$q_e = B \ln K_T + B \ln C_e$	(9)			BT	K_t	R^2	
			SJfsB	MB	8.452	8.776	0.980	
			nM-SJfsB	MB	10.684	8.655	0.989	

Effect of SJfsB and nM-SJfsB dosage

In adsorption studies, the amount of nM-SJfsB that will provide maximum dye adsorption should be determined. Figure 8 shows the relationship between the amount of nM-SJfsB and its biosorption capacity. Between 0.05 g and 0.75 g of SJfsB and nM-SJfsB were added to the reactor bottles and 30 mL of 200 ppm MB was placed on it. At the end of 60 minutes of shaking, the optimal biosorbent amount was determined. Approximately 70.0% of MB could be removed with 0.2 g SJfsB and nM-SJfsB and further addition of biosorbents did not alter dye adsorption (Figure 8.), which quickly reached equilibrium. The high dye uptake could be attributed to the high adsorption displayed on the surface of the biosorbents. This could be due to the amorphous and porous structure of biosorbents (Chen et al. 2022, Liu et al. 2022). The optimum amount of biosorbent was determined in the equilibrium study to be 0.2 g. By increasing the amount of biosorbent, the biosorbent was able to have more surface contact area. As a result, the adsorption percentage increased. Aggregation of the biosorbent material may occur as the amount of biosorbent used in the experiments increases. As a result, the surface area is reduced. This was seen with 0.75 g of nM-SJfsb.
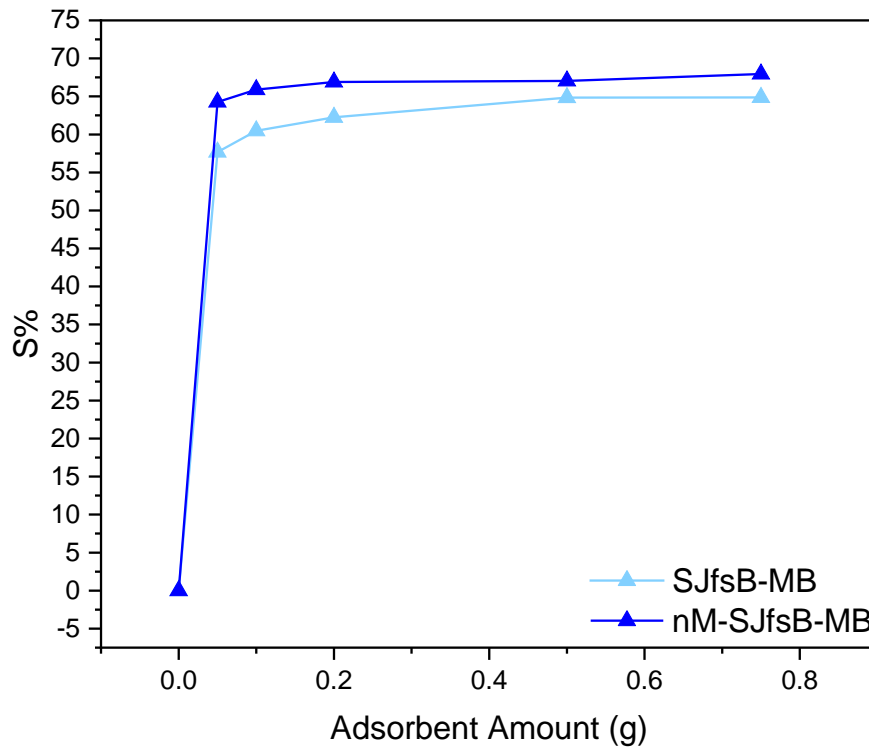
Figure 7. Effect of biosorbent amount change on adsorption (conditions: biosorbent amount: 0.05 g, 0.1 g, 0.2 g, 0.5 g, 0.75 g; concentration of dyes: 200 mg/L MB, temperature: 25 ± 1 °C, pH: solution pH 5.0–5.5 for MB; time: 60 min).

Kinetic Models

The many adsorptions kinetics, developed according to various physical and chemical conditions, are used to determine which mechanisms the adsorbed material fits during its adsorption onto the biosorbent surface. Adsorption kinetic modelling was used to explain dye transfer from solution phase to the solid phase (Huang et al. 2022, Srikhaow et al. 2022), with the observed data fitted to pseudo-first-order and pseudo-second-order kinetic models. To determine the mechanism of retention of dyes on the surface of nM-SJFSB and to understand the speed control step, kinetic data were equipped with these kinetic models. The pseudo-first-order kinetic model and pseudo-second-order kinetic equations are written as follows (Eq. 10 and Eq. 11):

$$q_t = q_e(1 - e^{-k_1 t}) \tag{10}$$

$$\frac{1}{q_t} = \frac{1}{k_2} \frac{1}{q_e^2} + \frac{1}{q_e} t \tag{11}$$

Table 3. Rate constants for the biosorption of MB with original and modified biosorbent (Pseudo-first-order kinetic equation and Pseudo-second-order kinetic equation)

	Sorbent	$q_{e\text{-}cal}$ (mg/g)	k_1(1/min)	$q_{e\text{-}exp.}$(mg/g)	R^2
First Order	SJfsB	17.995	1.25×10^{-09}	20.036	0.955
	nM-SJfsB	18.013	1.25×10^{-08}	20.157	0.907
	Sorbent	$q_{e\text{-}cal}$ (mg/g)	k_2(g/mg. min.)	$q_{e\text{-}exp.}$(mg/g)	R^2
Second Order	SJfsB	19.700	0.013	20.036	0.998
	nM-SJfsB	20.200	0.464	20.157	1.000

$q_{e\text{-}cal}$=calculated, $q_{e\text{-}exp}$=experimentally found)

The reaction order of dye adsorption on biosorbents was investigated. Table 3 shows the parameters of the kinetic models for MB adsorption. As shown in Table 3, the adsorption process for MB showed the pseudo-second-order rate model. Despite this, the calculated value (q_e) for the pseudo-second-order model deviated significantly less from the pseudo-first-order experimental data. The fact that the pseudo-second-order model has a higher R^2 value indicates that this model equation is more effective for adsorption kinetic studies (Yagnamurthy et al. 2022, Isik et al. 2022).

Thermodynamic Studies

The adsorption capacity of nM-SJfsB increased with increasing temperature of the system. This shows that the adsorption is endothermic. (Fig. 9). To determine the process, the following thermodynamic parameters must be considered: changes in standard enthalpy ΔH^o and standard entropy ΔS^o caused by the transfer of a unit mole of dye from solution to the biosorbent-liquid interface. Using the Van't Hoff equation, the values of ΔH^o and ΔS^o can be calculated from adsorption data at different temperatures (Saeed et al. 2022). Thermodynamic studies have been completed at various temperatures (25 °C, 35 °C, 45 °C, and 55 °C) and ΔH^o, ΔS^o and ΔG^o values were calculated (Table 4.). In equilibrium studies, when the ambient temperature of the solution is raised from 25 °C up to 55 °C, the capacity of SJfsB decreased slightly, while the capacity of nM-SJfsB increased slightly. This is the situation that demonstrates a weakening or slight strengthening of the binding relationship between the dyes and biosorbent's active sites (Kayalvizhi et al. 2022).
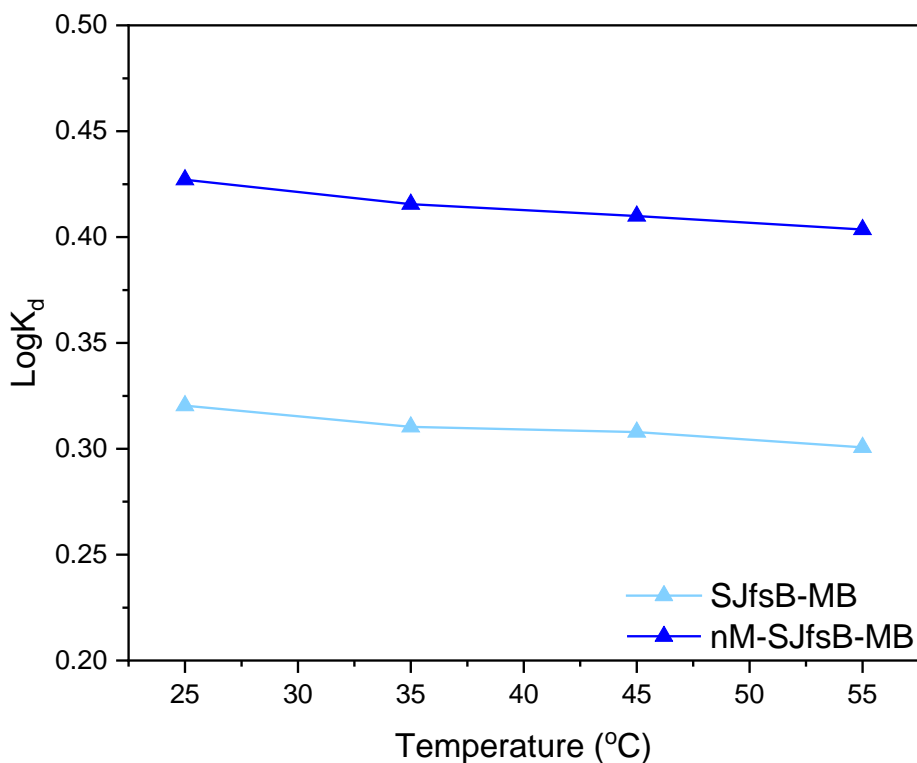

Figure 8. Effect of temperature change on adsorption (conditions: biosorbent amount: 0.2 g; concentration of dyes: 200 mg/L MB, temperature: 25 ± 1 °C, 35 ± 1 °C, 45 ± 1 °C, 55 ± 1 °C pH: solution pH 5.0–5.5 for MB; time: 60 min).

Table 4. Thermodynamic parameters for MB removal with SJfsB and nM-SJfsB

Dye	T(K)	ΔS^o (kJmol^{-1})	ΔH^o (kJmol^{-1})	ΔG^o (kJmol^{-1})
SJfsB-MB	298.150	2.262	-1.147	-1.827
	308.150			-1.830
	318.150			-1.875
	328.150			-1.888
nM-SJfsB-MB	298.150	3.348	-1.431	-2.437
	308.150			-2.450
	318.150			-2.496
	328.150			-2.534

The equilibrium constant is calculated in relation to temperature change using the following equation (Eq 12, Eq 13):

$$\ln K_L = -\frac{\Delta H^o}{RT} + \frac{\Delta S^o}{R} \tag{12}$$

where, K_L equilibrium constant, T temperature (K); R, ideal gas constant. The changes in the free energy ($\Delta G°$, kJ/mol) values were calculated from Equation (13).

$$\Delta G^o = \Delta H^o - T\Delta S^o \tag{13}$$

SJfsB-MB and nM-SJfsB-MB excothermic responses are indicated by negative ΔH^o values. The positive ΔS^o values indicates that the biosorbent-solution boundary is disordered during dye absorption of SJfsB-MB and nM-SJfsB-MB. Negative ΔG^o values indicate that the adsorption technique is applicable, and that dye adsorption is self-executing and spontaneous. Adsorption processes were exothermic and spontaneous. Thermodynamic parameters indicate that physisorption is the primary mechanism of dye adsorption to SJfsB-MB, nM-SJfsB-MB.

Recycling and Reusability of nM-SJfsB

The adsorption process used in wastewater treatment is a simple, low-cost, and highly efficient method in which pollutants are absorbed on biosorbent surfaces, without by-products. The desorption of dyes is an important in the adsorption process. Considering whether biosorbents can be reused is important in determining the adsorption mechanism. In the experiment, 0.1 mol/L diluted HCl was used as a desorption agent to examine the reuse of biosorbents (Ghaedi et al. 2022, Wu et al. 2022). The biosorbent still has a high adsorption efficiency after three cycles (respectively 92.0 %, 91.2%, 90.1% removal). These good results show that biosorbents can be used to remove MB effectively.

Comparison of MB removal with different biosorbents reported in the literature

Table 5 compares the biosorption capacity of dyes to various biosorbents studied in the literature. Because of its unique properties, nM-SJfsB has a higher dye adsorption capacity than others. This previously unpublished biosorbent may be useful for removing dyes from aqueous solutions.

Table 5. Comparison of maximum biosorption capacities of literature results with our results for MB dyes

Types of biosorbents	Dye	Biosorption capacities (mg/g)	Reference
TPP–PP	MB	159.80	He et al. 2022
Na–BaLa$_4$Ti$_4$O$_{15}$	MB	37.6	Chang et al. 2022
Zn–BaTiO$_3$/BaLa$_2$Ti$_3$O$_{10}$	MB	33.0	Chang et al. 2022
BMNPs	MB	136	Wang et al. 2017
Nanoporous Carbon	MB	555.56	Han et al. 2018
ZnCo$_2$O$_4$	MB	2400	Lin et al. 2018
SJfsB	MB	76.923	Present work
nM- SJfsB	MB	434.783	Present work

Conclusion

The adsorption efficiency of modified SJfsB in the removal of MB from the aqueous environment was investigated in this study. The results revealed that dye removal was sped up in the early stages of the biosorbent's contact with the dye, then increased and slowed when it reached equilibrium. The experiments were carried out over a period of 240 minutes. After examining the various dye concentration options, the MB was removed with high capacity by nM-SJfsB, and equilibrium was reached in a very short time, and the biosorbent efficiently adsorbed most of the dyes in the solution phase. The adsorption model fit to the Langmuir isotherm. The maximum adsorption capacity for SJfsB-MB was 76.923 mg/g, and the maximum adsorption capacity for nM-SJfsB was 434.783 mg/g. Negative ΔG^0 values calculated from thermodynamic studies indicated that the adsorption technique is applicable and dyes adsorption occur spontaneously. The biosorbents demonstrated reusability and a high adsorption capacity during the sequential adsorption cycle. This research demonstrates that the nM-SJfsB can be replaced with a green synthesis approach to create a biochar/nano iron composite with good dye removal capacity. The proposed nM-SJfsB provides a new solution for the long-term, cost-effective removal of harmful contaminants from toxic dyes. The results show that using a green synthesis approach to create nM-SJfsB is an effective way to improve the properties and potential practical applications of this nano-biosorbent for toxic dye environmental remediation.

Scientific Ethics Declaration

The authors declare that the scientific ethical and legal responsibility of this article published in EPSTEM journal belongs to the authors.

Acknowledgements or Notes

References

Al-Ghouti, M. A., & Da'ana, D. A. (2020). Guidelines for the use and interpretation of adsorption isotherm models: A review. *Journal of hazardous materials*, *393*, 122383.

Amari, A., Alalwan, B., Eldirderi, M. M., Mnif, W., & Rebah, F. B. (2019). Cactus material-based biosorbents for the removal of heavy metals and dyes: a review. *Materials Research Express*, *7*(1), 012002.

Arunachalam, A., Chaudhuri, R. G., Iype, E., & Prakash Kumar, B. G. (2018). Surface modification of date seeds (Phoenix dactylifera) using potassium hydroxide for wastewater treatment to remove azo dye. *Water Practice & Technology*, *13*(4), 859-870.

Bayram, O., Koksal, E., Gode, F., & Pehlivan, E. (2022). Decolorization of water through removal of methylene blue and malachite green on biodegradable magnetic Bauhinia variagata fruits. *International Journal of Phytoremediation*, *24*(3), 311-323.

Chang, A. L., Nguyen, B. S., Nguyen, V. H., & Hu, C. (2022). Adsorption kinetics of methyl blue using metal-modified barium lanthanum titanate as an effective absorbent. *Materials Chemistry and Physics*, *276*, 125363.

Chen, W. H., Hoang, A. T., Nižetić, S., Pandey, A., Cheng, C. K., Luque, R., ... & Nguyen, X. P. (2022). Biomass-derived biochar: From production to application in removing heavy metal-contaminated water. *Process Safety and Environmental Protection*, *160*, 704-733.

Deng, Z., Gu, S., Cheng, H., Xing, D., Twagirayezu, G., Wang, X., ... & Mao, M. (2022). Removal of Phosphate from Aqueous Solution by Zeolite-Biochar Composite: Adsorption Performance and Regulation Mechanism. *Applied Sciences*, *12*(11), 5334.

Dubinin, M. M. (1947). The equation of the characteristic curve of activated charcoal. In *Dokl. Akad. Nauk. SSSR.* (Vol. 55, pp. 327-329).

Freundlich, H. (1907). Uber die adsorption in losungen. *Zeitschrift fur physikalische Chemie*, *57*(1), 385-470.

Ghaedi, S., Seifpanahi-Shabani, K., & Sillanpää, M. (2022). Waste-to-Resource: New application of modified mine silicate waste to remove Pb2+ ion and methylene blue dye, adsorption properties, mechanism of action and recycling. *Chemosphere*, *292*, 133412.

Giri, B. S., Sonwani, R. K., Varjani, S., Chaurasia, D., Varadavenkatesan, T., Chaturvedi, P., ... & Pandey, A. (2022). Highly efficient bio-adsorption of Malachite green using Chinese Fan-Palm Biochar (Livistona chinensis). *Chemosphere*, *287*, 132282.

Han, X., Wang, H., & Zhang, L. (2018). Efficient removal of methyl blue using nanoporous carbon from the waste biomass. *Water, Air, & Soil Pollution*, *229*(2), 1-10.

He, Y., Bao, W., Hua, Y., Guo, Z., Fu, X., Na, B., ... & Liu, H. (2022). Efficient adsorption of methyl orange and methyl blue dyes by a novel triptycene-based hyper-crosslinked porous polymer. *RSC Advances*, *12*(9), 5587-5594.

Huang, H., Zheng, Y., Wei, D., Yang, G., Peng, X., Fan, L., ... & Zhou, Y. (2022). Efficient removal of pefloxacin from aqueous solution by acid–alkali modified sludge-based biochar: adsorption kinetics, isotherm, thermodynamics, and mechanism. *Environmental Science and Pollution Research*, *29*(28), 43201-43211.

Isik, Z., Saleh, M., M'barek, I., Yabalak, E., Dizge, N., & Deepanraj, B. (2022). Investigation of the adsorption performance of cationic and anionic dyes using hydrochared waste human hair. *Biomass Conversion and Biorefinery*, 1-14.

Jain, M., Khan, S. A., Sahoo, A., Dubey, P., Pant, K. K., Ziora, Z. M., & Blaskovich, M. A. (2022). Statistical evaluation of cow-dung derived activated biochar for phenol adsorption: Adsorption isotherms, kinetics, and thermodynamic studies. *Bioresource Technology*, *352*, 127030.

Jawad, A. H., Abdulhameed, A. S., & Mastuli, M. S. (2020). Acid-factionalized biomass material for methylene blue dye removal: a comprehensive adsorption and mechanism study. *Journal of Taibah University for Science*, *14*(1), 305-313.

Kadhom, M., Albayati, N., Alalwan, H., & Al-Furaiji, M. (2020). Removal of dyes by agricultural waste. *Sustainable Chemistry and Pharmacy*, *16*, 100259.

Kayalvizhi, K., Alhaji, N. M. I., Saravanakkumar, D., Mohamed, S. B., Kaviyarasu, K., Ayeshamariam, A., ... & Elshikh, M. S. (2022). Adsorption of copper and nickel by using sawdust chitosan nanocomposite beads–A kinetic and thermodynamic study. *Environmental Research*, *203*, 111814.

Khan, B. A., Ahmad, M., Iqbal, S., Bolan, N., Zubair, S., Shafique, M. A., & Shah, A. (2022). Effectiveness of the engineered pinecone-derived biochar for the removal of fluoride from water. *Environmental Research*, 113540.

Langmuir, I. (1916). The constitution and fundamental properties of solids and liquids. Part I. Solids. *Journal of the American chemical society*, *38*(11), 2221-2295.

Lin, K., Qin, M., Geng, X., Wang, L., & Wu, H. (2018). ZnCo2O4 nanorods as a novel class of high-performance biosorbent for removal of methyl blue. *Advanced Powder Technology*, *29*(8), 1933-1939.

Liu, Z., Zhen, F., Zhang, Q., Qian, X., Li, W., Sun, Y., ... & Qu, B. (2022). Nanoporous biochar with high specific surface area based on rice straw digestion residue for efficient adsorption of mercury ion from water. *Bioresource Technology*, 127471.

Mohammed Ali, N. S., Alalwan, H. A., Alminshid, A. H., & Mohammed, M. M. (2022). Synthesis and Characterization of Fe3O4-SiO2 Nanoparticles as Biosorbent Material for Methyl Blue Dye Removal from Aqueous Solutions. *Pollution*, *8*(1), 295-302.

Mouni, L., Belkhiri, L., Bollinger, J. C., Bouzaza, A., Assadi, A., Tirri, A., ... & Remini, H. (2018). Removal of Methylene Blue from aqueous solutions by adsorption on Kaolin: Kinetic and equilibrium studies. *Applied Clay Science*, *153*, 38-45.

Saeed, T., Naeem, A., Din, I. U., Farooq, M., Khan, I. W., Hamayun, M., & Malik, T. (2022). Synthesis of chitosan composite of metal-organic framework for the adsorption of dyes; kinetic and thermodynamic approach. *Journal of Hazardous Materials*, *427*, 127902.

Scatchard, G. D. (1949). The attractions of proteins for small molecules and ions. *Ann. NY Acad. Sci.*, *51*, 660-672.

Song, B., Cao, X., Gao, W., Aziz, S., Gao, S., Lam, C. H., & Lin, R. (2022). Preparation of nano-biochar from conventional biorefineries for high-value applications. *Renewable and Sustainable Energy Reviews*, *157*, 112057.

Srikhaow, A., Chaengsawang, W., Kiatsiriroat, T., Kajitvichyanukul, P., & Smith, S. M. (2022). Adsorption Kinetics of Imidacloprid, Acetamiprid and Methomyl Pesticides in Aqueous Solution onto Eucalyptus Woodchip Derived Biochar. *Minerals*, *12*(5), 528.

Temkin, M. J., & Pyzhev, V. (1940). Recent modifications to Langmuir isotherms.

Wang, H., Jia, S., Wang, H., Li, B., Liu, W., Li, N., ... & Li, C. Z. (2017). A novel-green biosorbent based on betaine-modified magnetic nanoparticles for removal of methyl blue. *Science Bulletin*, *62*(5), 319-325.

Wang, J., & Wang, S. (2019). Preparation, modification and environmental application of biochar: a review. *Journal of Cleaner Production*, *227*, 1002-1022.

Wang, Y., Zhang, Y., Li, S., Zhong, W., & Wei, W. (2018). Enhanced methylene blue adsorption onto activated reed-derived biochar by tannic acid. *Journal of Molecular Liquids*, *268*, 658-666.

Wong, S., Ngadi, N., Inuwa, I. M., & Hassan, O. (2018). Recent advances in applications of activated carbon from biowaste for wastewater treatment: a short review. *Journal of Cleaner Production*, *175*, 361-375.

Wu, T., Lin, Z., Wu, H., Wang, M., Zhu, C., Kanazawa, N., ... & Liang, R. (2022). Adsorption Studies on Ag (I) Using Poly (N-phenylglycine) Membrane and Application in Practical Silver Recycling. *ACS Applied Polymer Materials*, *4*(5), 3333-3342.

Yagnamurthy, S., Rakshit, D., Jain, S., Rocky, K. A., Islam, M. A., & Saha, B. B. (2022). Adsorption of difluoromethane onto activated carbon based composites: Adsorption kinetics, heat of adsorption, cooling performance and irreversibility evaluation. *Applied Thermal Engineering*, *210*, 118359.

Zhang, H., Tian, S., Zhu, Y., Zhong, W., Qiu, R., & Han, L. (2022). Insight into the adsorption isotherms and kinetics of Pb (II) on pellet biochar via in-situ non-destructive 3D visualization using micro-computed tomography. *Bioresource Technology*, 127406.

Zhao, F., Fang, S., Gao, Y., & Bi, J. (2022). Removal of aqueous pharmaceuticals by magnetically functionalized Zr-MOFs: Adsorption Kinetics, Isotherms, and regeneration. *Journal of colloid and interface science*, *615*, 876-886.

Author Information

Okan Bayram
Department of Chemistry, Graduate School of Applied and Natural Sciences, Suleyman Demirel University, Isparta, Turkey.
Contact e-mail: *okan.bayram.32@gmail.com*

Elif Koksal
Department of Chemistry, Graduate School of Applied and Natural Sciences, Suleyman Demirel University, Isparta, Turkey.

Emel Moral
Department of Chemistry, Graduate School of Applied and Natural Sciences, Suleyman Demirel University, Isparta, Turkey.

Fethiye Gode
Department of Chemistry, Faculty of Science and Arts, Suleyman Demirel University, Isparta, Turkey.

Erol Pehlivan
Department of Chemical Engineering, Faculty of Engineering and Natural Sciences, Konya Technical University, Konya, Turkey.

To cite this article:

Bayram, O., Koksal, E., Moral E., Gode, F., & Pehlivan, E. (2022). Efficient Decolorization of Anionic Dye (Methyl Blue) by Natural-Based Biosorbent (nano-Magnetic Sophora Japonica Fruit Seed Biochar. *The Eurasia Proceedings of Science, Technology, Engineering & Mathematics (EPSTEM), 17,* 69-82.

ICRETS 2022: International Conference on Research in Engineering, Technology and Science

Design and Experiments of a Foldable Wheeled-Mobile Robot

Turgay ERAY
Adnan Menderes University

Abstract: Mobile robots are used in a wide range of applications such as outdoor and indoor tasks. Even though, several design configuration exist for such applications, still extreme operations may require new type of design. An example for an extreme operations is that a mobile robot needs to be moved on a curved path in a confined space. In order to accomplish the task, mobile robot requires new type of body. This study proposes a new type of design of a mobile robot, which has a foldable chassis. The folding angle of the chassis could be adjusted according to the desired road conditions such as L-shaped road. After fabricating the proposed mobile robot, experiments are performed to determine the kinematic behavior capability of the foldable wheeled-mobile robot motion on a L-shaped path. The results demonstrate that the proposed design is feasible, and foldable wheeled-mobile robot can be used on curved paths.

Keywords: Design, Mobile robot, Foldable chassis, Curved path

Introduction

Mobile robots are used in a wide range of applications from human missions in hazardous areas (such as space research) to home care robots (such as autonomous vacuum cleaners). Mostly in mobile robotics, wheels are essential for the locomotion. Either changing the number of the wheels or the wheel geometry are the main design parameters of the mobile robots. This is because wheels yield a drawback on the mobile robots. That is the unbalanced motion when the mobile robots encounter rough roads or complex paths (Rubio et al. 2019). One way to overcome this problem is to design a deformable wheel (Lee et al., 2013a, 2013b, 2014) or customizable wheel (Guan et al. 2014). Although deformable or customizable wheel for the mobile robots exist for rough surface operations, still for extreme operations new types of mobile robots may be required. An example for such an application area is that a mobile robot could be able to move on a curved road. In order to be able to move on a curved road, mobile robot chassis should be able to fold with a customizable angle. We propose a structural design for a new type of mobile robot. This study deals with designing and fabricating a foldable mobile robot to be able to move on curved surfaces. The design comprises a foldable chassis where the folding angle could be adjusted according to the desired road conditions. Experiments are performed to show the kinematic behavior capability of the foldable wheeled-mobile robot motion on a curved surface. The results show that the proposed design is beneficial and feasible, and foldable wheeled-mobile robot can be used on curved paths instead of non-foldable mobile robots.

Structural Design

The structural design of the foldable wheeled-mobile robot and manufactured one are shown in Figure 1 and Figure 2, respectively. The mobile robot consists of four wheels where each wheel is connected to a direct-current (DC) motor. The motion of the mobile robot is achieved by driving the DC motors. The DC motors and the wheels are connected to the chassis with a rigid attachment. Two different chassis are designed to have a foldable configuration. The two chassis are connected to each other with revolute joints. Hence, one chassis can

be rotated with respect to the other one, which results in the allowable folding condition. Torsional springs are used to have a quick return from foldable configuration. Rotational motion of one chassis is achieved by a servo motor system, to which a pulley is attached. A rigid rope is used to make a connection between the pulley and the foldable chassis of the mobile robot. Therefore, with an activation of the servomotor, one chassis of the mobile robot can be rotated with a desirable angle. The maximum angle of the folding is approximately 70^0. A typical folding configuration and structural components of the foldable mobile robot are shown in Figure 1.b and Figure 1.c., respectively.
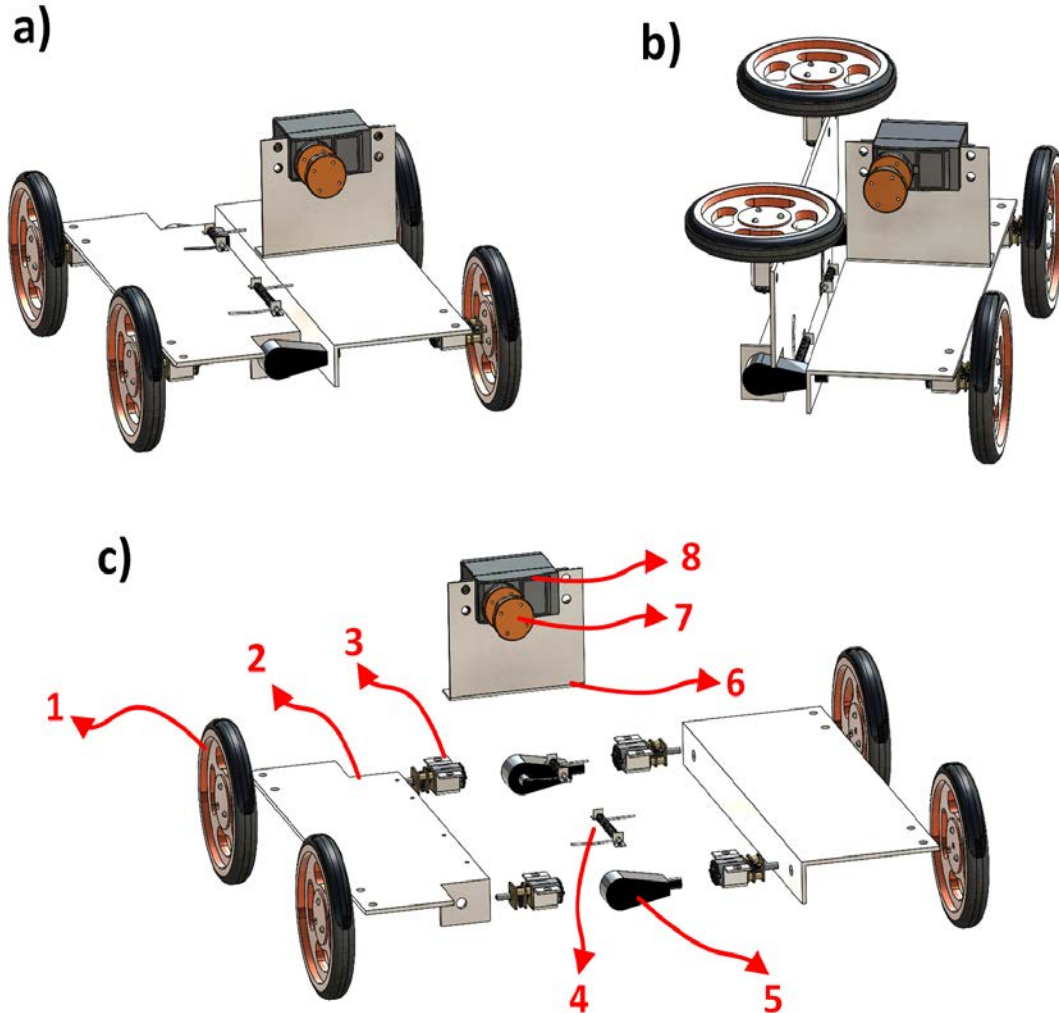
Figure 1. Structural design of the foldable mobile robot. a) General view, b) View of the folded condition, c) Components of the foldable mobile robot: 1- Wheels, 2- Chassis, 3- DC Motors, 4- Torsional spring, 5- Revolute joint, 6- Rigid support, 7- Pulley, 8- Servo motor.

Experiments

Two different kinds of experiments were performed. These are movements of the mobile robot on a flat road and on a curved road. The first experiment is to observe the similarity between a typical mobile robot and the foldable mobile robot kinematic behavior, even though two different chassis are coupled via revolute joints. The second experiment is to show the locomotion capability of the foldable wheeled-mobile robot on a L-shaped surface, where the two roads are perpendicular to each other. The snapshot of the videos of the first experiment was given in Figure 3. The results show that despite there being a foldable configuration of the mobile robot, still the kinematics of the foldable mobile robot is similar to the one with non-foldable one. This suggests that the foldable mobile robot can be used instead of a non-foldable one.
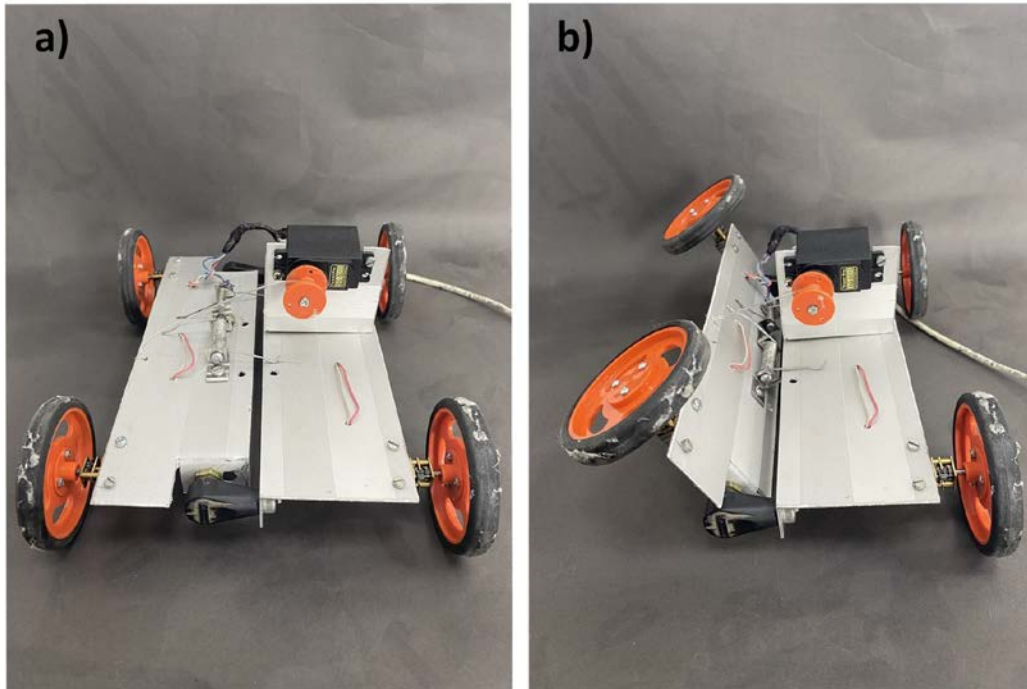
Figure 2. Manufactured foldable wheeled-mobile robot.
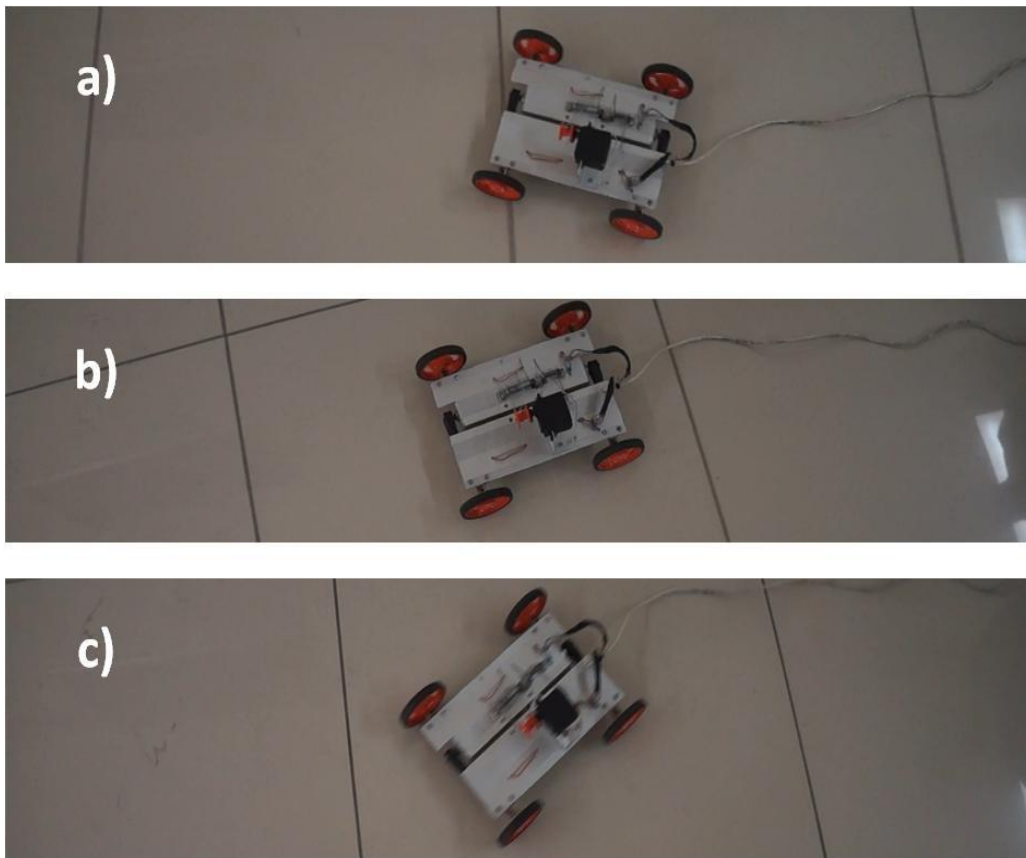
Figure 3. Snapshot of the first kind experiment. a) Translational motion, b) Beginning of the turning motion, c) End of the turning motion.

Figure 4, Figure 5 and Figure 6 show the results of the second kind experiment. Second kind of experiment was completed in three stages. The first stage corresponds to the transition of the foldable mobile robot motion from flat surface to curved surface. The second stage is to check the stability of the translational motion of the foldable mobile robot on the curved surface. In the final stage, this time, the kinematic stability of the

translational motion of the foldable mobile robot during its transition from the foldable configuration to the nominal (flat) configuration, while the mobile robot moves on the curved surface, is observed.

Figure 4 depicts the transition from nominal configuration to the foldable configuration to move on the L-shaped surfaces. The result demonstrates that the foldable configuration allows a stable kinematic behavior, which corresponds to the transition from flat surface to curved surface during translational motion of the foldable mobile robot. This yields that the proposed design is feasible for the motion of the mobile robot on a curved surface.

Figure 4. Snapshot of the first stage of the second kind experiment. a) Approach of the mobile robot to the curved surface, b) Transition from nominal to foldable configuration, c) Beginning of the movement on the curved surface, d) Translational motion on the curved surface.

Figure 5 shows the translational motion of the foldable mobile robot on the L-shaped curved surface. The results indicate that the foldable mobile robot can move on a straight path on the curved surface without loss of its kinematic stability. Hence, this yields that the foldable configuration of the mobile robot is feasible and beneficial in terms of the kinematic behavior capability of the mobile robot on the curved surface.
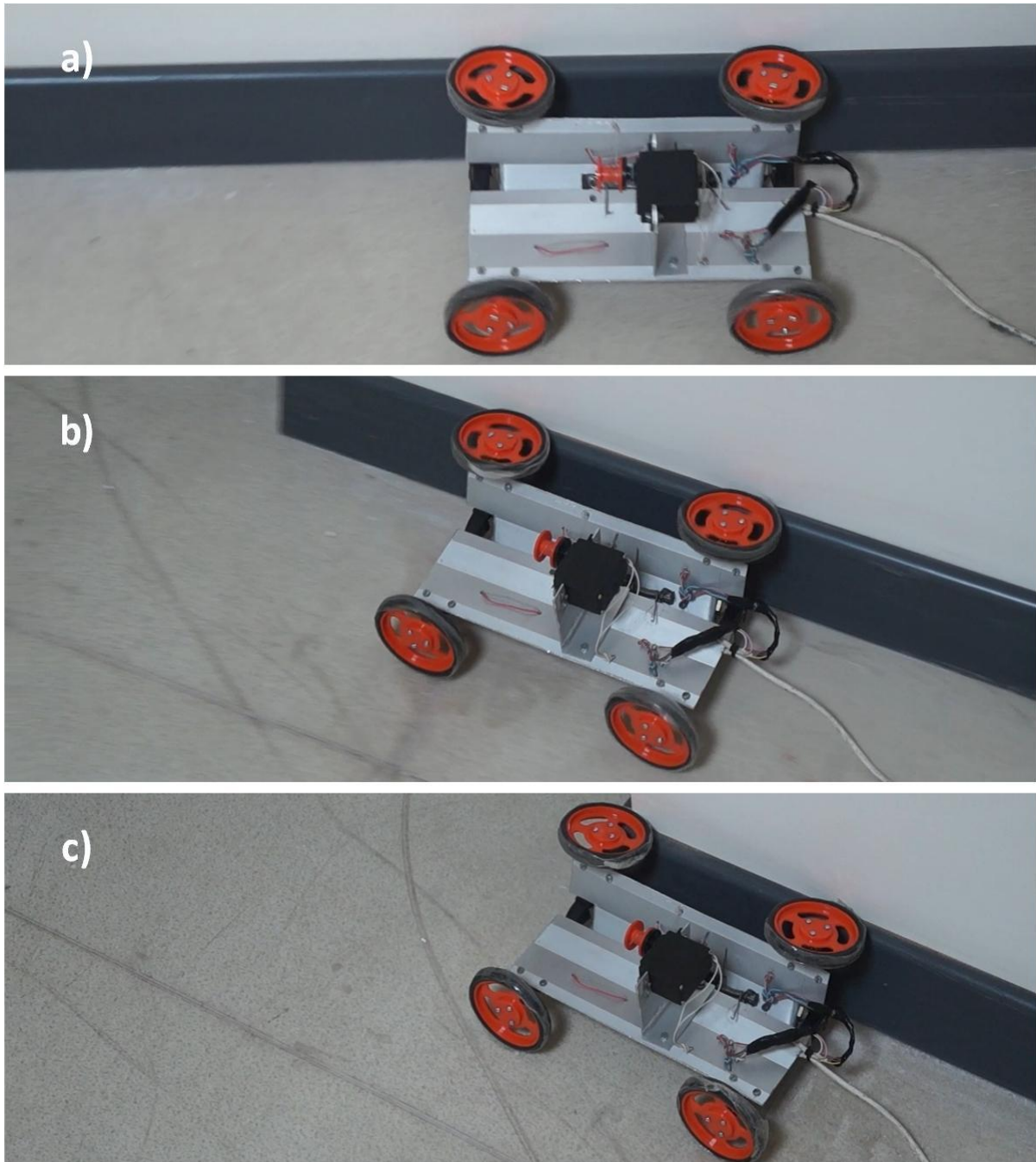
Figure 5. Snapshot of the second stage of the second kind experiment. a) Approach of the mobile robot to the curved surface, b) Transition from nominal to foldable configuration, c) Beginning of the movement on the curved surface, d) Translational motion on the curved surface.

Figure 6 gives the progress of change of the body of the foldable mobile robot from the foldable configuration to the nominal configuration during the crossing from the L-shaped curved surface to flat surface. The results demonstrate that there is no loss of kinematic stability of the foldable mobile robot while the path of the mobile robot shifts from the curved surface to the flat surface. As a result, the foldable configuration of the mobile robot has no effect on the stability of the translational motion of the mobile robot. This suggests that the foldable design of a mobile robot is attainable for the motion on the curved surfaces.
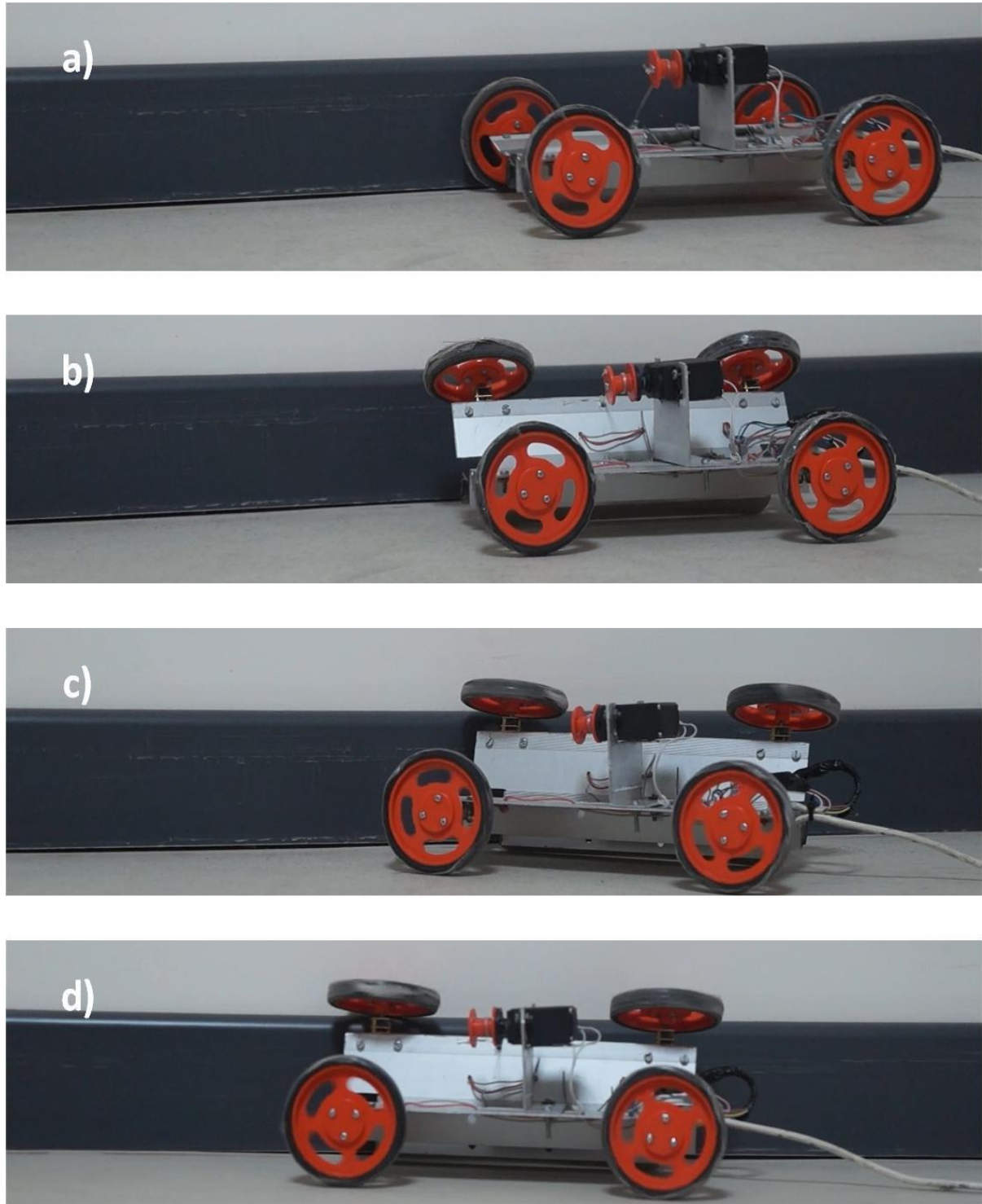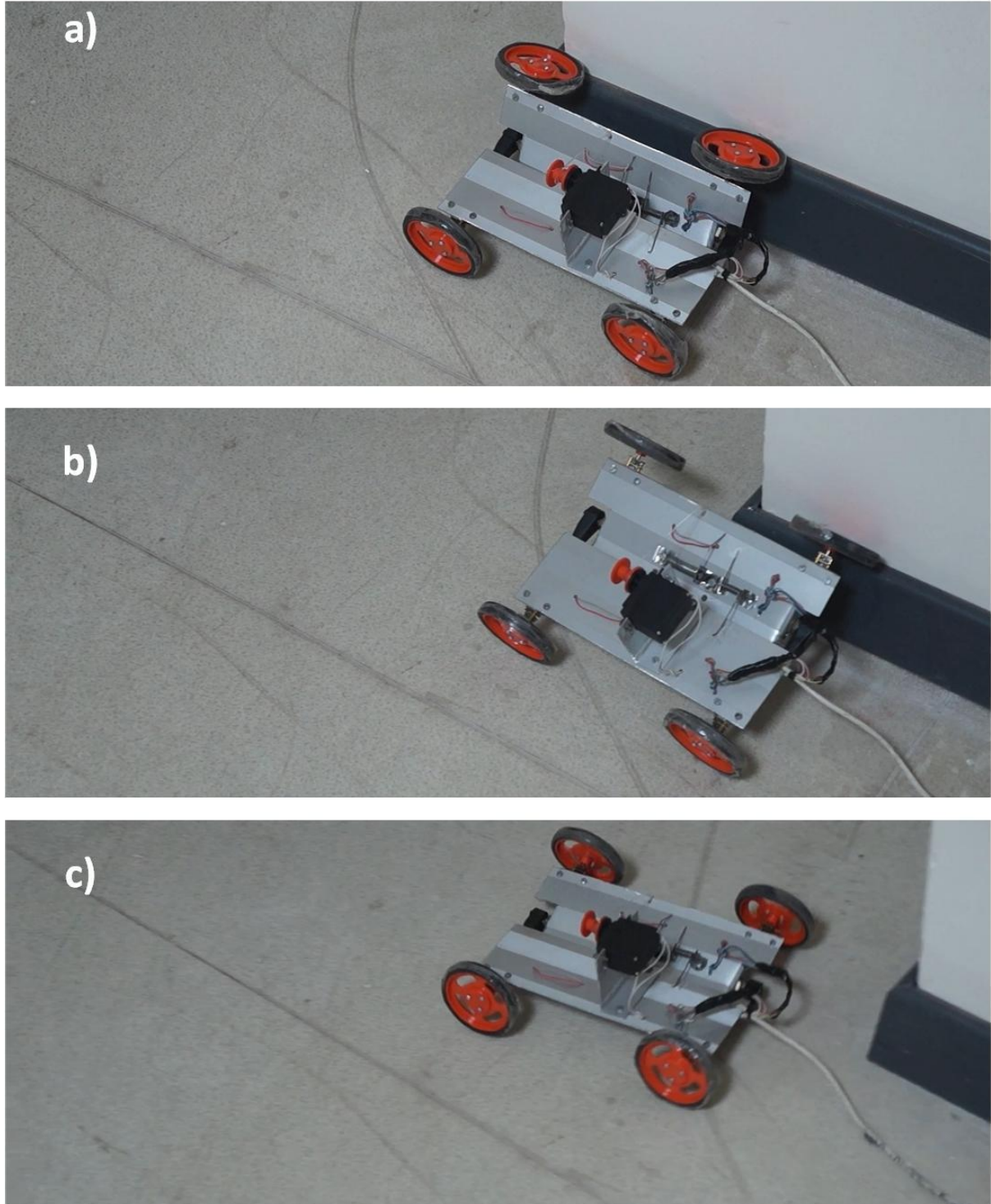
Figure 6. Snapshot of the final stage of the second kind experiment. a) Approach of the mobile robot to the edge of the curved surface, b) Transition from foldable to nominal configuration, c) Motion on the flat surface after the motion on the curved surface.

Conclusion and Recommendations

In this study, for extreme road conditions such confined spaces, a design for a mobile robot with a foldable configuration was proposed. After structural design was completed, the mobile robot was manufactured and kinematic performance of the foldable mobile robot was evaluated experimentally. The experimental results

show that the proposed design is feasible, and the foldable mobile robot can be used in complex paths. We recommend using the foldable mobile robot for confined spaces, which may have complex roads.

Scientific Ethics Declaration

The author declares that the scientific ethical and legal responsibility of this article published in EPSTEM journal belongs to the author.

Acknowledgements or Notes

This article was presented as an oral presentation at the International Conference on Research in Engineering, Technology and Science (www.icrets.net) conference held in Baku/Azerbaijan on July 01-04, 2022.

References

Guan, X., Zhang, P., Fang, M., Hu, Y., & Zhang, J. (2014). *The adaptive control for the Outdoor Mobile Robot with diameter-variable wheels*. 2014 IEEE International Conference on Information and Automation (ICIA), 2014, pp. 1096-1101.

Lee, D, Kim, J, Kim, S, Koh, J, & Cho, K. (2013). *The Deformable Wheel Robot Using Magic-Ball Origami Structure*. Proceedings of the ASME 2013 International Design Engineering Technical Conferences and Computers and Information in Engineering Conference. Volume 6B: 37th Mechanisms and Robotics Conference. Portland, Oregon, USA. August 4–7, 2013.

Lee, D., Jung, G., Sin, M., Ahn, S., & Cho, K. (2013). *Deformable wheel robot based on origami structure*. 2013 IEEE International Conference on Robotics and Automation, 2013, pp. 5612-5617.

Lee, D., Kim, J., Park, J., Kim, S., & Cho, K. (2014). *Fabrication of origami wheel using pattern embedded fabric and its application to a deformable mobile robot*. 2014 IEEE International Conference on Robotics and Automation (ICRA), 2014, pp. 2565-2565.

Rubio, F., Valero, F., & Llopis-Albert, C. (2019). A review of mobile robots: Concepts, methods, theoretical framework, and applications. *International Journal of Advanced Robotic Systems*, *16*(2), 1-22.

Author Information

Turgay Eray
Aydin Adnan Menderes University Faculty of Engineering,
Department of Mechanical Engineering,
Efeler - Aydin / TURKIYE
Contact e-mail: *turgay.eray@adu.edu.tr*

To cite this article:

Eray, T. (2022). Design and fabrication of a foldable wheeled-mobile robot *The Eurasia Proceedings of Science, Technology, Engineering & Mathematics (EPSTEM), 17,* 83-89.

Parametrical Analysis for Symmetrical Loading of a Single-Span Composite String Steel Structure

Edmundas BEIVYDAS

Vilnius Gediminas Technical University

Abstract: The article analyzes the string and composite string bridge behavior and compositional parameters. The derived parameters are calculated and presented by selecting the appropriate limit parameters. The main parameters for suspended structures are the cross-sectional area of the tensile element and the initial sag of the structure. The selection of different component parameters and assigning different prestressing to the string leads to the analysis: which cross-sectional areas meet the defined conditions, what is the effect of prestressing, of the lower cable initial sag and the axial stiffness ratios of the string and the lower cable on the weight of the structure.

Keywords: Steel bridge, Symmetrical load, Suspended cable, String, Nonlinear analysis, Displacements, Strain, parametrical analysis

Introduction

Suspension bridges are among the most rational types of bridges in terms of their construction and amount of materials used (Gimsing, 1997, Strasky, 2005, Chen et al., 2014, Greco et al., 2014). The main advantage of these structures is the minimal impact on the environment and its flexible structure with its graceful appearance conditioned by the extremely small height of the deck and amount of steel. However, there are also some negative aspects related to the minimal consumption of materials. The more lightweight these suspended structures are, the more deformable they are. (Katchurin, 1969; Juozapaitis et al., 2006). The alternative for suspended structures – string structures – are none the less elegant and lightweight (Linkute., 2015). They are pre-stressed and have no initial sag, making them completely insensitive to displacements of kinematic origin. The main disadvantage of the string structures is reflected in the high shear forces. Moreover, analytical methods as well as design and composition recommendations have not been developed for the design of these kinds of structures.

In order to reduce the shear forces and general displacements, the string can be transformed into a combined structure (Sandovic & Juozapaitis, 2012, Yunitskiy, 2019.) It is additionally supported by a suspended single-span structure (Beivydas, 2019). This solves the problem of shear forces and reduces excessive displacements. Compared to a single-span structure, this solves the problem of kinematic displacements, and the string creates a straight structure shape adapted to the vehicle traffic (Beivydas, 2018).

However, the design and composition of such composite string structures is complex. The publications on this subject matter are scarce. Most of the developed calculation methodologies are either designed for cables (Chen et al., 2014; Juozapaitis & Norkus 2005) and suspension bridges (Chen et al. 2014) or they are adapted for the calculation of individual elements. However, some methodologies have also been developed for double-span bridges, and their parameters as well as behavioral properties have been defined (Sandovic et al., 2011). However, such structures do not meet the functionality requirements, i.e. they do not create a straight line for the traffic.

Since the main design criterion for suspended structures is their deformability and stiffness (Kulbach, 1999; Schlaich et al., 2011), the structure is analyzed by choosing different composite parameters.

For the analysis of the structure, the limit stiffness conditions of the structure are selected and rational parameters are calculated with the use of analytical and numerical methods. The string structure and the combined string structure, which are presented in sections 2 and 3, are analyzed separately. The stresses and displacements of the structures depending on the limit deflections are analyzed.

String Structure Analysis
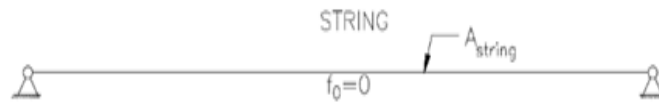
Figure 1. String structure

The well-known analytical expressions are used for the analysis of the string structure behaviour, their accuracy is confirmed by numerical methods (Linkute, 2015). The analysis is performed by applying the limits of the vertical displacements of the structure, and this condition is used for the calculation of the the required cross-sectional area of the string. The deflections of the analyzed structure are limited depending on the length of the span, i. e. three alternatives are investigated: $\Delta f_{\lim} = (\frac{L}{400}, \frac{L}{250}, \frac{L}{100})$, where L is the span length, equal to 25 and 50 m.

By using the familiar string displacement equation (Linkute, 2015), we can calculate the required cross-sectional area:

$$\Delta f = \sqrt[3]{\frac{3}{64} \cdot \frac{(p+q)L^4}{EA}};$$

We express the required cross-sectional area, taking into account the above stiffness condition in the following way:

$$A = \frac{3}{64} \cdot \frac{(p+q)L^4}{EA\Delta f_{\lim}^3};$$

This expression is used for the required cross-sectional area of the string to be calculated. Since the analyzed string is given an additional prestress T, the required area is calculated as follows:

$$A = \frac{3}{64} \cdot \frac{(p+q)L^4(1-\beta)}{EA\Delta f_{\lim}^3};$$

$$\beta = \frac{T}{H_1};$$

$$H_1 = T + H;$$

$$H = \sqrt[3]{\frac{1}{24} \cdot \frac{EA \cdot (p+q)^2L^2}{(1-\beta)}}.$$

where:

Δf — displacement in the middle of the span;
$p+q$ — dead and live loads (2,5+7,5 kN/m);
E — Elasticity module;
A — cross-sectional area;
H_1 — tension force, when the string is prestressed;
H — tension force, when the string is not prestressed;
T — prestressing force;
$\Delta f_{\lim}$ — displacement limit.

91

We can calculate the stresses in such a string as follows:

$$\sigma = \frac{H}{A} = \frac{\sqrt[3]{\frac{1}{24} \cdot E \cdot (p+q)^2 L^2}}{(1-\beta) \cdot A^{\frac{2}{3}}} \leq \sigma_u;$$

where:

σ — stresses in the string;

σ_u — stress limit in the string.

In order to identify the advantages and disadvantages of the string and the possible uses, 2 options are considered: the span equal to 25 m and 50 m. All parameters are calculated based on the analytical method provided. In Tables 1-3 below we see the results where L = 25 m, in Tables 4-6 with L = 50 m.

The results show that the string must always be pre-tensioned, otherwise its use becomes irrational due to the extremely large cross-sectional area. We also see that the prestress reduces the vertical displacements, and at the same time it increases the stresses in the string. At the minimum limiting deflection of the string, the string has to be composed of a large axial stiffness cross section. As a result, with the increasing axial stiffness of the string and minimal change in tensile force, we will have lower stresses in the string when designing the structure according to the service limit state. In this case, it is generally irrational to apply the string, since steel as a material is not used for its purpose, and additional prestressing, due to high shear forces, will require extremely massive foundations.

If we provide the strings with a larger limit bend according to the design norms, we also have to follow the safety limit state. In Table 3 we see that when the ultimate deflection is L / 100 and the prestress is 20 MN, the stresses in the string reach as high as 2189 MPA. In this case, it would now be necessary to apply strong steels or spiral cables. In the case of such materials, the material behavior should also be evaluated. In order to use structural steel for the string (for example, steel strips), in the case of a marginal displacement of L / 100, we can tension the string to a maximum of 4-6 MN with a span of 25 m.

Table 1. Dependence of the required cross-sectional area of the string on the limit displacements and prestressing force at L = 25 m

Prestressing force T, kN	L/400	L/250	L/100
	String cross-sectional area A, m2		
0	3.75	0.92	0.06
200	3.69	0.89	0.06
600	3.58	0.85	0.05
1000	3.47	0.81	0.04
1200	3.42	0.79	0.04
4000	2.84	0.59	0.02
8000	2.29	0.41	0.01
10000	2.08	0.36	0.01
30000	1.10	0.14	0.00
50000	0.75	0.10	0.00

Table 2. Dependence of cross-sectional diameter on ultimate deflection and prestressing with L = 25 m

Prestressing force T, kN	L/400	L/250	L/100
	The cross-sectional diameter of the string, m		
0	2.19	1.08	0.28
200	2.17	1.06	0.28
600	2.14	1.04	0.25
1000	2.10	1.02	0.23
4000	1.90	0.87	0.16
6000	1.80	0.79	0.16
8000	1.71	0.72	0.11
10000	1.63	0.68	0.11
30000	1.18	0.42	0.00
50000	0.98	0.36	0.00

Table 3. Dependence of stress in the string on the ultimate deflection and prestress at L = 25 m

Prestressing force T, kN	L/400	L/250	L/100
	Stresses in the string, MPa		
0	3.33	16.98	52.08
200	3.41	17.86	54.98
600	3.57	19.32	72.95
1000	3.74	20.94	99.98
4000	5.10	35.90	334.68
6000	6.20	49.42	426.71
8000	7.43	66.86	1040.00
10000	8.87	85.36	1228.53
30000	32.34	480.18	-
50000	72.58	1057.99	-

Table 4. Dependence of string cross-section on ultimate deflection and prestress at L = 50 m

Prestressing force T, kN	L/400	L/250	L/100
	String cross-sectional area, m2		
0	7,5	1,831	0,117
200	7,44	1,808	0,11
600	7,324	1,763	0,107
1000	7,212	1,721	0,101
4000	6,466	1,458	0,071
6000	6,048	1,232	0,06
8000	5,682	1,211	0,051
10000	5,357	1,116	0,045
30000	3,409	0,627	0,02
50000	2,50	0,436	0,013

Table 5. Dependence of cross-section diameter when the cross-section is round, on the ultimate deflection and prestressing with L = 50 m

Prestressing force T, kN	L/400	L/250	L/100
	The cross-sectional diameter of the string, m		
0	3.09	1.53	0.39
200	3.08	1.52	0.37
600	3.05	1.50	0.37
1000	3.03	1.48	0.36
4000	2.87	1.36	0.30
6000	2.78	1.25	0.28
8000	2.69	1.24	0.25
10000	2.61	1.19	0.24
30000	2.08	0.89	0.16
50000	1.78	0.75	0.13

As we can see from Table 4, with a span of 50 meters and when limiting the displacement of the string to L/400, an extremely large cross-sectional area of the string (7.5 m^2) is required. This means that strings using a spiral cable require a cable with a diameter as thick as 3.1 m or 10 cables with 1 m in diameter. If we limit the boundary deflection of the string to L/100, we will need a 0.4 m diameter cable. After prestressing it with a force of 4000 kN, we will need a 0.3 m diameter cable. Since one of the main goals in designing and composition of a structure is to minimize the use of materials, it appears that the string should be used for structures with a smaller span where its ultimate deflection is limited to L/400 and more.

Graph 2 shows the results of the cross-sectional area of the string required to satisfy the limit displacement conditions. Graph 1 and Table 6 show the magnitude of the stresses occurring in the string. We can see that when the limit displacement is L/100, more attention should be paid to the stresses generated in the string as the cross-section may simply no longer satisfy the safety limit state.

To show the differences more accurately, in Table 7 and Fig. 2 we can see how much the weight of the structure or the cross-section diameters will differ (in the case of a round shape cross-section) by comparing the spans of 25 and 50 meters. We can see that if the deflections of the structure should not exceed the limit values L/400,

depending on the prestressing the masses differ from 2 to 3.3 times. At the same time according to Table 5 we can assume that the use of a string is highly irrational when the stiffness L/400 is required, and the use of a string is rational only at limiting deflections L/100. As a result, the weight of 25-meter span and 50-meter span structures can vary from 2 to 7 times, while increasing the span of the structure. This leads us to a conclusion that it is recommended to design a span of 50 meters only by tensioning the string to at least 1200 kN and limiting the stiffness to no more than L/100.

Table 6. Dependence of the stress in the string on the ultimate deflection and prestress at L = 50 m

Prestressing force T, kN	L/400	L/250	L/100
	Stresses in the string, MPa		
-	3,33	8,53	53,33
200	3,36	8,64	55,04
600	3,41	8,86	58,45
1000	3,47	9,08	61,88
4000	3,87	10,72	87,47
6000	4,13	11,81	104,53
8000	4,40	12,90	121,60
10000	4,67	14,00	138,67
30000	7,33	24,92	309,33
50000	10,00	35,84	480,00

Table 7. Relative difference in string cross-sections when the spans are 25 and 50 m, respectively. (L = 50 / L = 25)

Prestressing force T, kN	L/400	L/250	L/100
	The ratio of the cross-sectional areas of the string where L = 50 m and L = 25 m		
0	2.0	2.0	2.0
200	2.0	2.0	2.0
600	2.0	2.1	2.1
1000	2.1	2.1	2.5
4000	2.3	2.5	3.6
6000	2.4	2.5	4.0
8000	2.5	3.0	5.1
10000	2.6	3.1	6.0
30000	3.1	4.5	7.0
50000	3.3	4.4	7.2
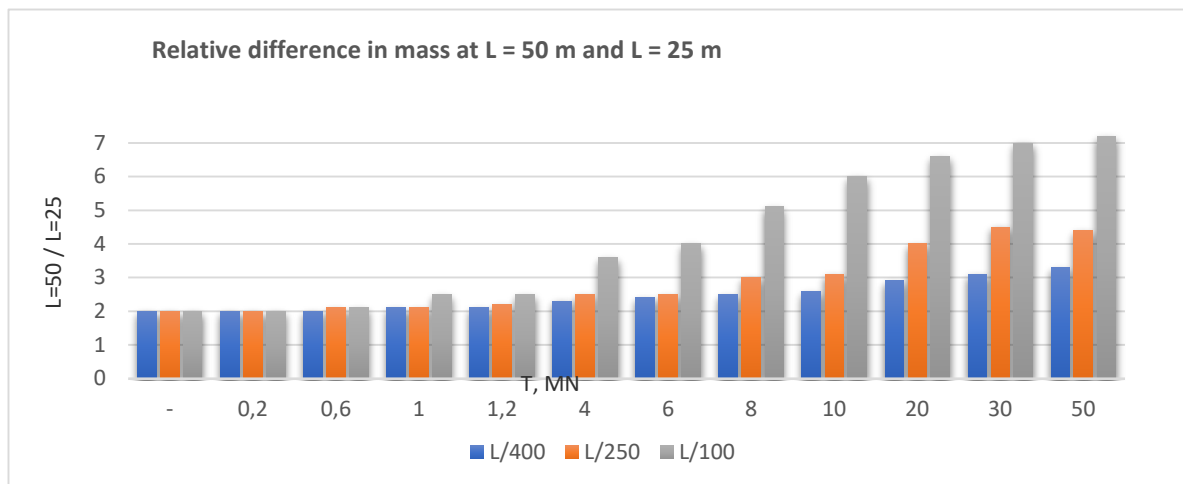
In order to overlap the larger spans and keep the advantages of the string, the string needs to be combined with an additional support cable to limit vertical displacements. When combined with a supporting cable, most of the symmetrical load is taken over by the lower cable and as a result we have smaller displacements from the symmetrical load. The string, meanwhile, operates under an asymmetrical load when it takes over the kinematic displacements caused by the cable and reduces the overall displacements of the entire system. The parametric analysis of the combined structure is presented in section 3.

Figure 2. Relative difference in mass at L = 50 m and L = 25 m

a) Dependence of string cross - section diameter on prestressing force

b) Dependence of string cross - sectional area on prestressing force

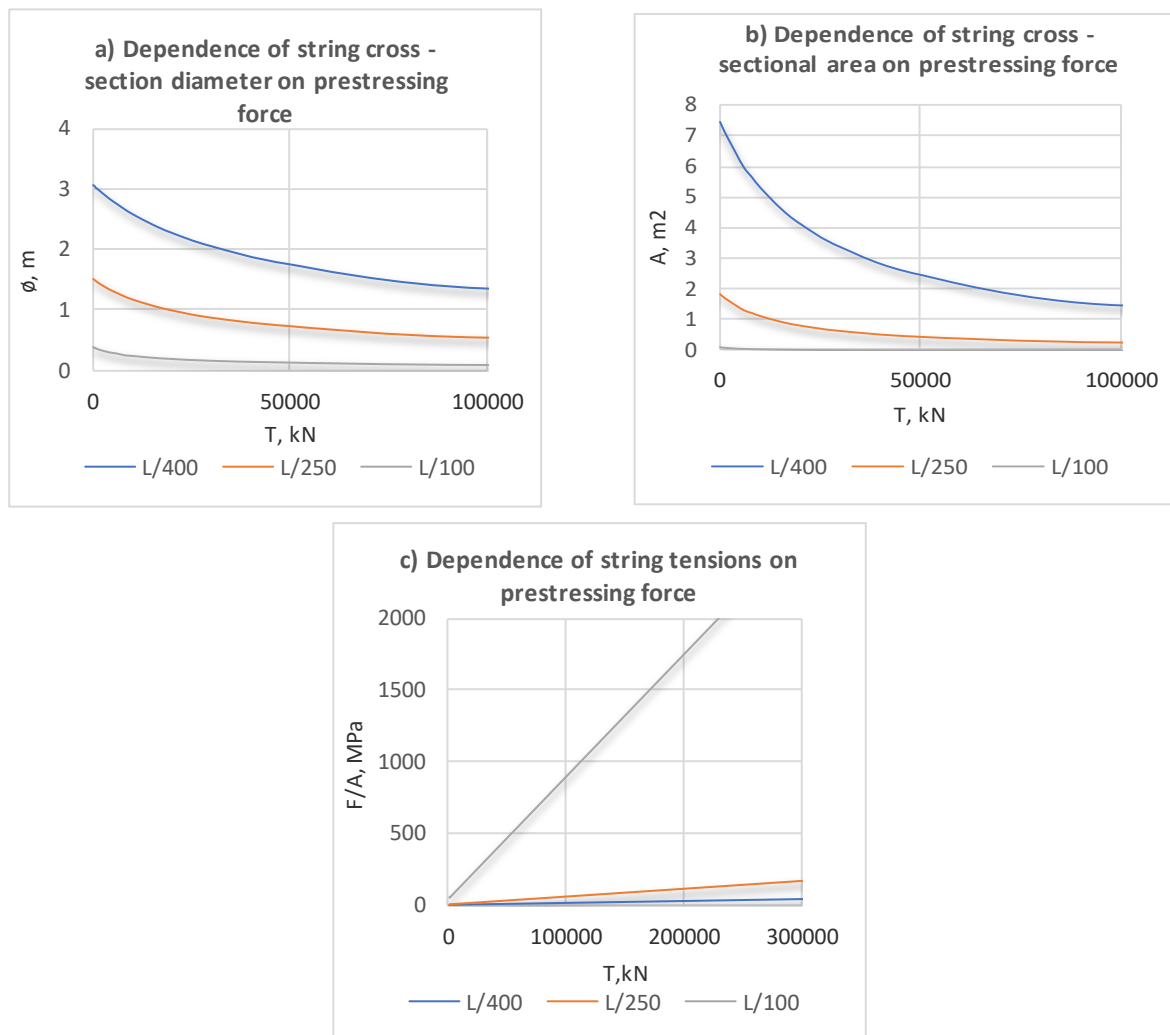**c) Dependence of string tensions on prestressing force**

Figure 3. Dependence of string and lower cable parameters on limit deflections and axial stiffness

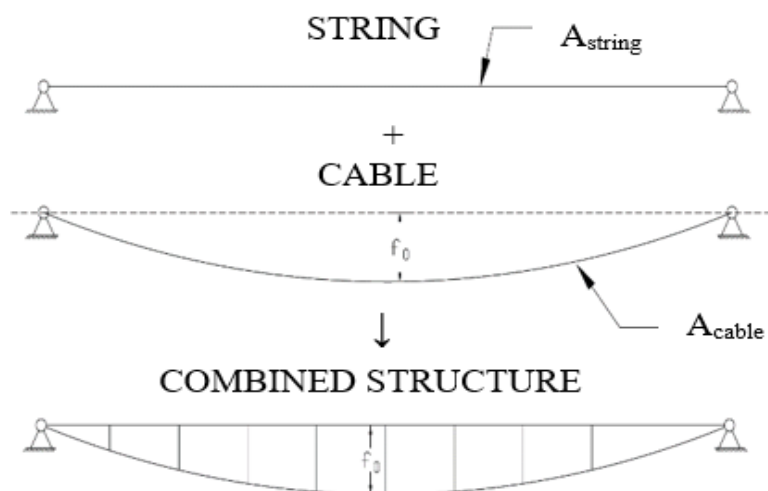**The Analysis of The Combined String Construction**

Figure 4. Combined string structure

The combined structure is a combination of a single-span and string structure. As seen in Figure 2, the string is supported by auxiliary cable using struts. This way the structure is combined into a joint operation. For the analysis of the combined structure, the familiar approximate calculation expressions are used (Beivydas, 2019).

$$\Delta f_{comb.} \cong \frac{3}{128} \cdot \frac{L^4}{E_{cable} \cdot A_{cable} \cdot f_0^2} \cdot (p+q)_{cable}; \quad (p+q)_{cable} = \sqrt[3]{\sqrt{\frac{1}{27} \cdot C^3 + \frac{1}{4} \cdot D^2} - \frac{1}{2} \cdot D} + \sqrt[3]{-\sqrt{\frac{1}{27} \cdot C^3 + \frac{1}{4} \cdot D^2} - \frac{1}{2} \cdot D};$$

Where:

$$C = \frac{32768}{9} \cdot \frac{E_{cable}^3 \cdot A_{cable}^3 \cdot f_0^6}{E_{string} \cdot A_{string} \cdot L^8};$$

$$D = (p+q) \cdot \frac{32768}{9} \cdot \frac{E_{cable}^3 \cdot A_{cable}^3 \cdot f_0^6}{E_{string} \cdot A_{string} \cdot L^8};$$

From these equations, we can notice what is required for the axial stiffness of the string and cable, depending on all parameters, i. e. the span length, the initial sag of the lower cable, the cross-sectional area of the string and the cross-sectional area of the lower cable.

$$A_{cable} \cong \frac{3}{128} \cdot \frac{L^4}{E_{cable} \cdot \Delta f_{Lim} \cdot f_0^2} \cdot \left[\sqrt[3]{\sqrt{\frac{1}{27} \cdot C^3 + \frac{1}{4} \cdot D^2} - \frac{1}{2} \cdot D} + \sqrt[3]{-\sqrt{\frac{1}{27} \cdot C^3 + \frac{1}{4} \cdot D^2} - \frac{1}{2} \cdot D} \right];$$

Table 8. Dependence of cross-sectional areas of combined structure on limit deflections.

Δf_{lim}	f_0	A, m² 10⁻⁴	n=3	n=1	n=0.5
L/100	L/10	A_s	22.53	11.38	8.55
		A_c	5.63	5.69	5.7
		A_{tot}	64.71	22.42	11.32
	L/20	A_s	86.28	44.84	33.96
		A_c	21.57	22.42	22.64
		A_{tot}	311.79	127.03	67.25
	L/50	A_s	415.72	254.06	201.75
		A_c	103.93	127.03	134.5
		A_{tot}	5.63	5.69	5.7
L/250	L/10	A_s	57	28.56	21.44
		A_c	14.25	14.28	14.29
		A_{tot}	169.86	56.98	28.54
	L/20	A_s	226.48	113.96	85.61
		A_c	56.62	56.98	57.07
		A_{tot}	1011.18	350.28	176.87
	L/50	A_s	1348.24	700.56	530.61
		A_c	337.06	350.28	353.74
		A_{tot}	16.9	5.69	2.851
L/400	L/10	A_s	68.49	22.86	11.43
		A_c	22.83	22.86	22.87
		A_{tot}	91.32	45.72	34.3
	L/20	A_s	273.36	91.35	45.71
		A_c	91.12	91.35	91.41
		A_{tot}	364.48	182.7	137.12
	L/50	A_s	1675.68	567.21	284.71
		A_c	558.56	567.21	569.42
		A_{tot}	2234.24	1134.42	854.13

Equations are used to calculate the cross-sectional areas of the string and the lower cable at the limit deflections at different axial stiffness ratios of the string and the lower cable. 3 options of the difference in axial stiffness are selected (the ratio of the cross-sectional areas of the string and the cable), i.e. when the axial stiffness of the string is 5, 1 and 0.5 times higher. In the same way 3 different limit deflections and 3 different lower cable displacements are selected. The axial stiffnesses of the cable, the axial stiffness of the string and the total axial stiffness are calculated separately to see the differences between the string and the lower cable. More details can be seen in fig. 5.

Figure 5. Dependence of the cross-sectional areas of the string and the lower cable on the ratio of the limit deflection and the axial stiffness. Where horizontal axis – String and lower cable cross-sectional area ratio (A_{st}/A_{cable}); Vertical axis – cross-sectional area; [L/x=1,2,3… + L/y=1,2,3…] – L/x=1,2,3… – limit of displacements, L/y=1,2,3… – initial sag ratio.

In Fig. 5, we see that almost in all the cases, only the strings and the total cross-sectional areas change as the axial stiffness ratio changes. Consequently, when the string is not pre-tensioned, almost the entire load is taken over by the lower cable, so the change in axial stiffness of the string is practically insignificant. Thus, if we have a non-tensioned string, it should be designed with the smallest possible cross-sectional area, transferring the entire load to the lower cable.
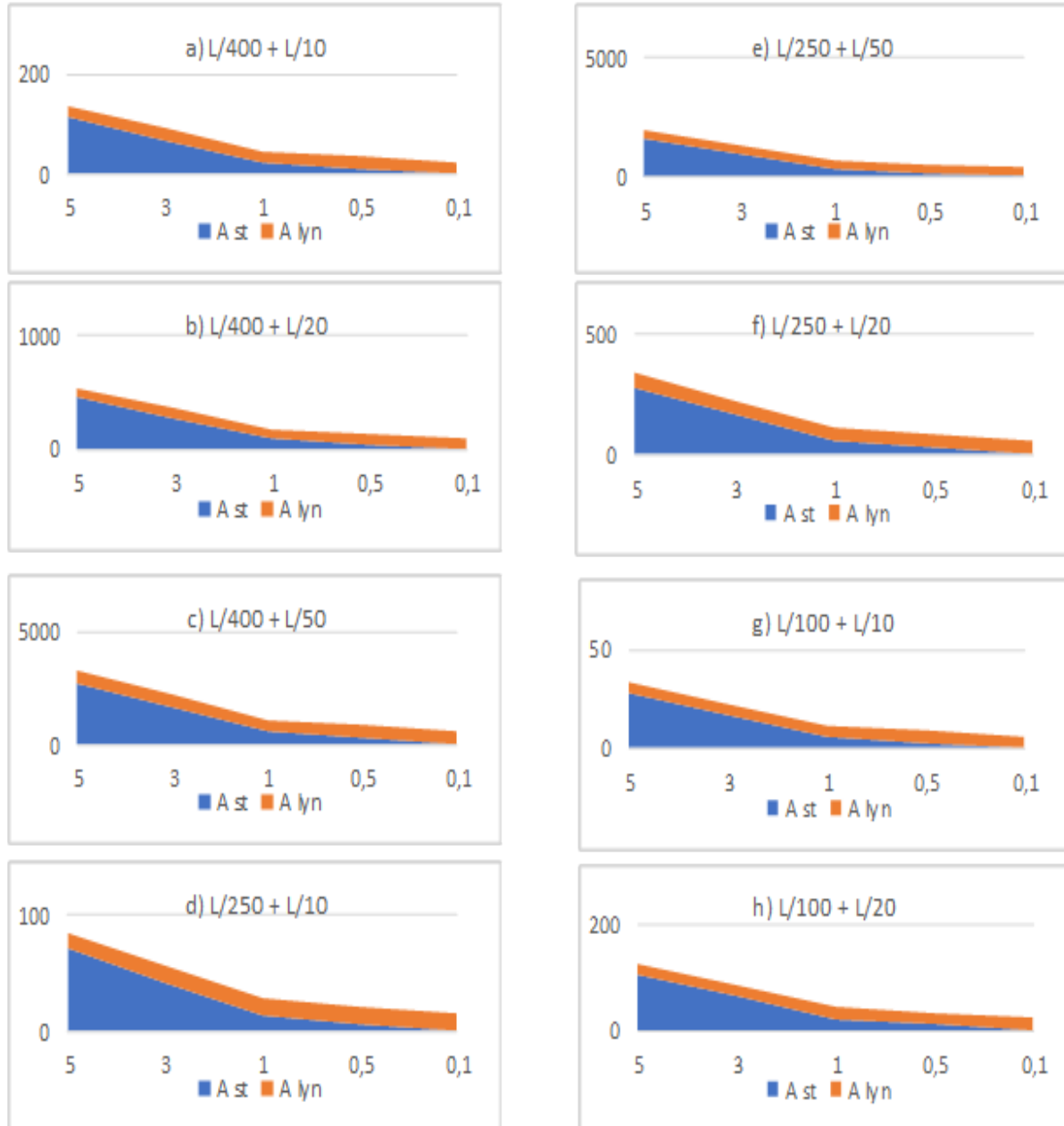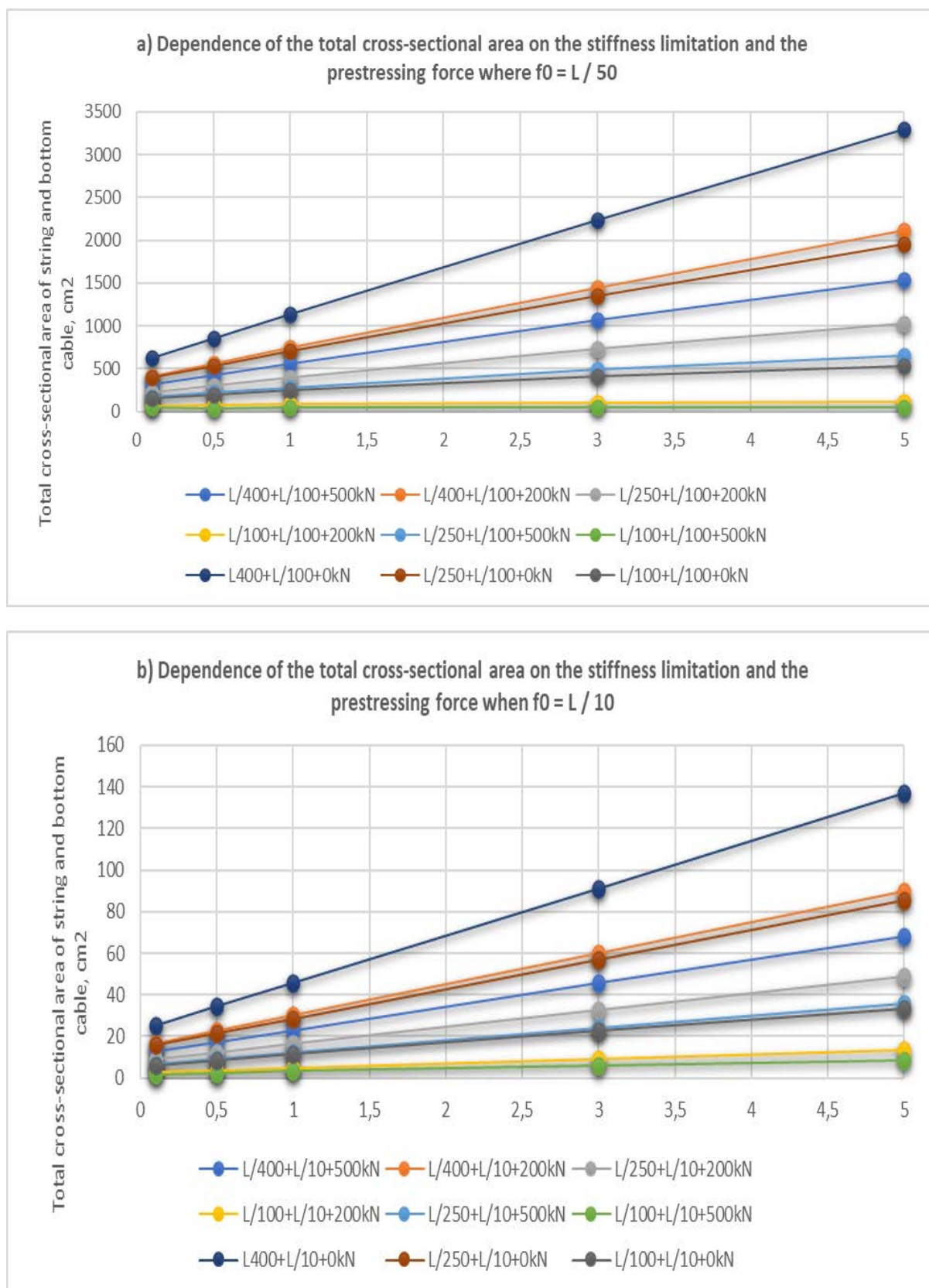
Figure 6. Dependence of the cross-sectional areas of the string and the lower cable on the ratio of the limit deflection and the axial stiffness. Where: [L/x=1,2,3… + L/y=1, 2, 3… + Z kN], L/x=1,2,3… + L/y=1,2,3…] – L/x=1,2,3… – limit of displacements, L/y=1,2,3… – initial sag ratio, Z – prestressing force.

The situation changes if the string is pre-tensioned. Very little additional prestressing force is required to express the advantages of the string. While comparing the option where the ultimate deflection is L/400 and the initial deflection of the lower cable is L/10, without prestressing with the option where the string is tensioned at 500 kN, when the ratio of axial stiffness is 5, the total cross-sectional area is reduced by 2 times; when the ratio of axial stiffness is 0.1, it decreases - 1.7 times. It is clear that regardless of the lower deflection of the lower cable, the pre-force gives the same result as the change in the mass of the structure.

Knowing that the prestress of a string has a significant effect on its axial stiffness when displacements is limited, the following are the results of the magnitudes of stresses in the string and the lower cable depending on the prestress of the string and the ratio of the axial stiffness of the string to the lower cable. The amount of the stresses indicates whether the main indicator is the safety limit state or the service limit state. Also, depending on the values of the forming stresses, it is possible to select the material used for both the string and the cable.
Tables 9 and 10 show that the string requires minimal stresses if it is not prestressed and how the stresses change after it is prestressed. Also, comparing the stresses and axial stiffnesses in the string and the lower cable, we see that the stresses are higher at a smaller cross-sectional area of the string and cable, which means that the element is used with higher efficiency.

Table 9. Dependence of stress in a string on limit deflection and prestressing (without pre-tension)

Δf_{lim}	f_0	σ, MPa	n=3	n=1	n=0.5
L/100	L/10	σ_s	0.41	0.27	0.18
		σ_c	95.30	277.52	550.88
	L/20	σ_s	0.41	0.27	0.18
		σ_c	546.70	546.61	546.65
	L/50	σ_s	0.41	0.27	0.18
		σ_c	218.67	218.67	218.67
L/250	L/10	σ_s	0.07	0.04	0.03
		σ_c	437.55	437.33	437.19
	L/20	σ_s	0.07	0.04	0.03
		σ_c	218.67	218.68	218.68
	L/50	σ_s	0.07	0.04	0.03
		σ_c	87.47	87.47	87.47
L/400	L/10	σ_s	0.03	0.03	0.03
		σ_c	273.51	273.32	273.24
	L/20	σ_s	0.03	0.03	0.03
		σ_c	136.67	136.67	136.66
	L/50	σ_s	0.03	0.03	0.03
		σ_c	54.67	54.67	54.67

Table 10. Dependence of stress in a string on limit deflection and prestressing (T=1000 kN).

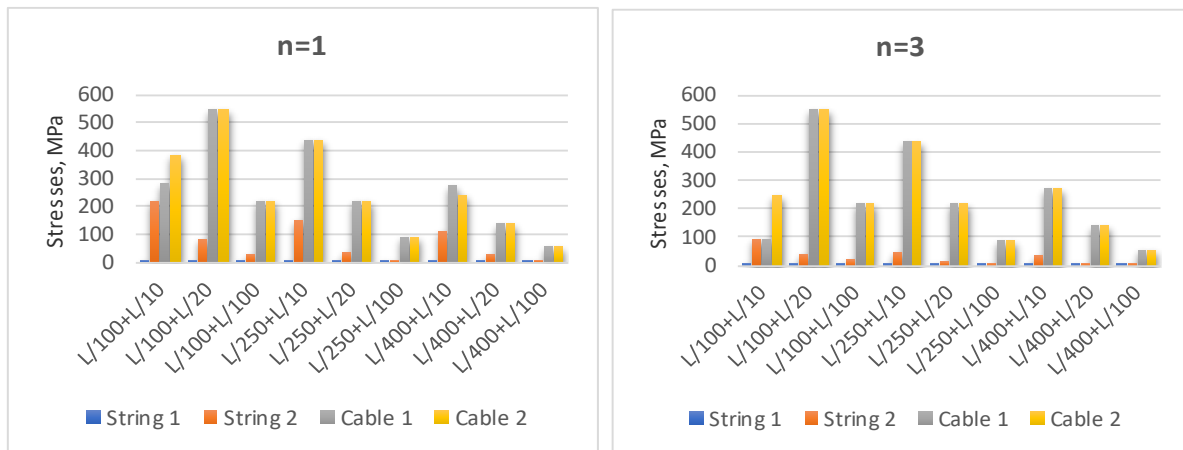| Δf_{lim}	f_0	σ, MPa	n=3	n=1	n=0.5
L/100	L/10	σ_s	93.26	217.95	403.46
		σ_c	243.84	380.92	470.37
	L/20	σ_s	37.39	81.56	146.86
		σ_c	546.72	546.61	546.90
	L/50	σ_s	17.53	25.39	36.48
		σ_c	218.69	218.67	218.67
L/400	L/10	σ_s	36.65	109.55	218.85
		σ_c	273.35	273.37	273.29
	L/20	σ_s	9.31	27.54	54.87
		σ_c	136.66	136.67	136.66
	L/50	σ_s	1.66	4.58	8.95
		σ_c	54.67	54.67	54.67

Figure 7. The dependence of the stresses in the string and the lower cable on the limit deflections of the structure when the string is additionally tensioned and non-tensioned. Where: [1] – string is not prestressed, [2] – string is bprestresssed, n – string ant lower cable cross-sectional ratio (A_{st}/A_{cable})

If we compare the differences between the string and the combined structure, we will see that the advantages of the combined structure are indisputable. However, it should be considered that the string fulfils its role in the functional way, and also all the advantages of the string are present with an asymmetrical load on the structure (Beivydas, 2018). Fig. 7 shows that regardless of whether the string is prestressed or not, in almost all the cases the stresses in the lower cable do not change, although the cross-sectional areas are reduced significantly.

Conclusions

The performed parametric analysis revealed the main advantages of the combined design compared to string and single-span constructions. When designing and composing a string structure, its main advantages are the definition of a straight line and the fact that it has only elastic displacements. The analysis of the parameters of the string through the ultimate stiffness shows that the string can be used only with small (up to 25 m) spans. When loading the string with a symmetrical load, the string must be pre-tensioned. Meanwhile, increasing the span of the string a problem appears where in order not to exceed the limit deflections, prestressing has to be increased immensely as well as the axial stiffness of the string. Although the stiffness of the string depends on the axial stiffness and the prestressing force, the actual problem is that by increasing the axial stiffness of the string, we increase the mass of the string, which consequently increases the load. This creates a dilemma in case of large spans. The more we increase the axial stiffness, the more the load will increase. The idea simply becomes irrational. In the case of single-span structures, in contrast to the string structures (depending on their initial sag) these absorb symmetrical loads perfectly and their elastic displacements are not large. However, in the case of asymmetric effects and taking into account that a single-span structure is not functional due to its shape definition, a single-span structure can be applied only to structures whose deformability is less limited and the shape of the structure is not particularly important functionally, i.e. in pedestrian bridges. Although in this case we can use larger spans (25-100 meters), the use of such a structure is strongly determined by functionality and usability. That is in the case of large spans, we will also have large initial sag, as a result of which such a structure will take up a considerable amount of space geometrically, thus, the field of application will be greatly reduced. Certainly small initial sag can be used, but this will cause the same problems as with the use of the string. By reducing the initial single-span sag, although we the kinematic displacements will be reduced, this will greatly increase the elastic displacements. When increasing the elastic displacements, we face the problem that the only way to increase the stiffness of a single span is to increase the cross-sectional area of the cable. The axial stiffness of the cable increases the mass of the structure, which becomes irrational. All these problems are solved by combining these two constructions into a joint operation. In order to limit the elastic displacements that are mainly taken over by the lower cable, we can increase the axial stiffness of the lower cable. In the case of asymmetrical effects, they are covered by the string. Also, not only in terms of deformations and stresses, such a structure can be used much more widely, due to its straight line.

Section 3 reveals that while using a non-prestressed string, almost all of the symmetrical loads are taken over by the lower cable, and when at least a little tension is applied, the string is also involved in the operation, immediately reducing the overall displacements of the structure. It can be concluded that when designing a structure, the axial stiffness of the string should be chosen to be the same as that of the lower cable or smaller, in

order to take advantage of the prestressing of the string. The string can be pretensioned to its safety limit state because the tensions of the lower cable do not change or have minimal changes as a result. When comparing the string, the single-span and the combined structures with the same mass, one can achieve 2-3 times larger spans with a combined structure.

Scientific Ethics Declaration

The author declares that the scientific ethical and legal responsibility of this article published in EPSTEM journal belongs to the author.

Acknowledgements or Notes

This article was presented as an oral presentation at the International Conference on Research in Engineering, Technology and Science (www.icrets.net) conference held in Baku/Azerbaijan on July 01-04, 2022.

References

Beivydas E. (2018). Vieno tarpatramio kabamosios kombinuotos stygines konstrukijos skaitine analize. *Journal Since – Future of Lithuania, 10.*

Beivydas, E., (2019) A simplified calculation method for symmetrical loading of a single-span composite string steel structure. *Journal Engineer structures and technologies, 11*(2), 70-73

Chen, Z., Cao H., Zhu H., Hu J., Li Sh. (2014). A simplified structural mechanics model for cable-truss footbridges and its implications for preliminary design. *Engineering Structures. 68*, 121–133.

Gimsing, N. J. (1997) *Cable supported bridges: concept and design. 2nd edition*. John Wiley & Sons.

Greco, L., Impollonia N., Cuomo M., (2014). A procedure for the static analysis of cable structures following elastic catenary theory. *International Journal of Solids and Structures 51,* 1521-1533.

Juozapaitis, A., Norkus A., (2005). Shape determining of a loaded cable via total displacements. *Technological and Economic Development of Economy, 9*(4), 283-291.

Juozapaitis, A., Vainiunas P., Kaklauskas G., (2006). A new steel structural system of a suspension pedestrian bridge. *Journal of Constructional Steel Research 62,* 1257–1263.

Katchurin, V. K., (1969). *Static design of cable structures*. Stroyizdat.

Kulbach, V. (1999). Half-span loading of cable structures. *Journal of Constructional Steel Research, .49*(2), 167-180.

Linkute, E. (2015). *Arrangement and behaviour analysis of prestressed string steel bridges*. (Master's thesis). Vilnius Gediminas Technical University.

Sandovic, G., Juozapaitis A., Kliukas R., (2011). Simplified engineering method of suspension two-span pedestrian steel bridges with flexible and rigid cables under action of asymmetrical loads. *The Baltic Journal of Road and Bridge Engineering. 6*(4), 267-273.

Schlaich, M., Bogle, A., Bleicher, A. (2011). *Entwerfen und Konstruieren Massivbau*. Institut fur Bauingenieurwesen Technische Universitat Berlin.

Strasky, J. (2005) *Stress-ribbon and supported cable pedestrian bridges*. Thomas Telford Ltd.

Author Information

Edmundas Beivydas
Department of Steel and Composite Structures, Faculty of
Civil Engineering, Vilnius Gediminas Technical
University, Sauletekio al. 11, LT-10223 Vilnius, Lithuania
Contact e-mail: *edmundas.beivydas@vilniustech.lt*

To cite this article:

Beivydas E. (2022). Parametrical analysis for symmetrical loading of a single-span composite string steel structure. *The Eurasia Proceedings of Science, Technology, Engineering & Mathematics (EPSTEM), 17,* 90-101.

ICRETS 2022: International Conference on Research in Engineering, Technology and Science

Technical, Economic and Environmental Comparison of Three Different Grid-Connected PV Tracking Systems Power Plant Under Kurdistan Region/Iraq Climate Condition

Veen Sagvan QADER
University of Zakho

Omar Mohammed ALI
University of Zakho

Nawfal Idrees HASAN
University of Mosul

Abstract: In this paper, a 1 MW grid-connected PV system was performed and simulated numerically in Zakho city, using hourly meteorological data for three systems; fixed, single-axis, and dual-axis tracking systems for solar module. The analysis of this study is based on technical, economic, and environmental feasibility. The analysis based on the actual 3 PV solar panels using different tracking systems which installed on the roof of the Engineering college of Zakho University. The evaluation findings suggest that PV technology is quite promising in this location, with annual yield factors of (1416 kWh/kW), (1694 kWh/kW), and (1902 kWh/kW) for the three systems, respectively. Furthermore, the proposed system's capacity factors are 16.2 percent, 19.3 percent, and 21.70 percent. The economic growth of a 1MW grid-connected photovoltaic (PV) system adjusted for meeting the daily peak load in Zakho is analyzed and compared based on the cost of electricity (COE), net present value (NPV), payback period (PBP), and the energy payback time (EPBT) for three systems in the present work. The COE for the three proposed systems, fixed, 1st axis, and dual axes solar tracking systems, was 0.0826 USD/kWh, 0.0489 USD/kWh, and 0.0441 USD/kWh, respectively, which indicated the tracking system is economically feasible. The findings indicate a favorable trend, implying that large-scale photovoltaics of dual-axis systems might be a feasible option for addressing future power needs.

Keywords: Grid-connected PV systems, Yield factor, Capacity factor, COE, NPV

Introduction

The utilization of renewable resources is the most effective way to achieve long-term solutions for energy sustainability, with various advantages such as being environmentally friendly and non-exhaustible (Salih et al., 2019). Solar energy is effective, inexpensive, and environmentally acceptable (Tsoutsos et al., 2005). In recent years, solar energy electricity has become very popular due to the low investment cost. A solar photovoltaic (PV) system converts the sun's irradiance into electrical power. The angle of incidence of sunlight determines the output power of solar energy. An optimum tilt angle for a fixed system may maximize output power (Chaturvedi et al., 2021; Fuke et al., n.d.; Xu et al., 2017). Due to the sun's site variation during the day, the angle of incidence changes, affecting the solar panel's performance. When the sun's rays are perpendicular to the solar panel's surface,

maximum electricity is produced (Saeedi & Effatnejad, 2021). The geographical conditions vary between locations, so different studies are required. Two basic types of sun-tracking systems, the single-axis tracking system, and the dual-axis tracking system are used which depend on the sun movement. The researchers developed different sun tracking systems, single-axis tracking (Roong & Chong, 2016; Zhao et al., 2016) and dual-axis tracking (Fathabadi, 2016; Hong et al., 2016; Njoku, 2016; Parthipan et al., 2016). The tracking system with a single axis is a mechanism for tracking the sun around one side of the rotation pivot(Fathabadi, 2016; Gupta et al., 2015; Hong et al., 2016; Njoku, 2016; Parthipan et al., 2016). The primary disadvantage of a single tracking system is that it follows the sun during its movement and does not follow the annual movement of the sun. The efficiency of tracking systems is decreased significantly during cloudy days due to the rotating around just one axis(Jamroen et al., 2020). A solar dual-axis tracker is a process that uses two pivot nodes to rotate in two separate axes of the sun. The active tracking system determines the sun's location using sensing elements throughout the day. These sensors drive the engine or actuator to drive the system to the sun all day long. Active tracking systems arranged with various control types, such as microprocessor-based, electrical-optical sensor-based approaches, date and time, and auxiliary PV cells (Ferdaus et al., 2014; Leon et al., 2014; Vermaak, 2014). Many studies are presented in the literature that deal with the tracking system. Fahad et al. (Fahad et al., 2019) demonstrated a performance comparison study of total incident solar energy on photovoltaic panels of the same size for three distinct tracking systems (fixed, single, and dual) during twelve months, with and without cloud cover in Bangladesh. The results reveal that there is no statistically significant variation in energy yield between single-axis and dual-axis trackers. F. Alfirjani (Abdulhamid & Alfirjani, 2021) designed three different tracking systems (fixed, single-axis, dual-axis) with identical solar panels of the same power and compared according to their efficiencies, the performance of three alternative systems is relatively near to each other across all parameters, however, it differs due to the locations. The findings display that the dual-axis solar tracker was 5.43 percent more efficient than a single-axis solar tracking system and 24.04 percent more efficient than a stationary solar panel. Tangi (Tangi, 2017) demonstrate that the dual-axis tracker is superior to any existing solar tracker, utilizing a microcontroller and motor drivers. The dual-axis sunflower tracker was cost-effective and fairly efficient and has the potential to make a significant difference in India's future of sustainable solar energy. Hoque et al. (Hoque et al., n.d.)presented two solar energy collection technologies, dual and single axes solar trackers are designed, fabricated, and tested. The power output and efficiency are increased by 69.85% for dual-axis solar tracker and 44.74% for single-axis solar tracker.

The tracking system significantly improves large-scale solar system's technical and economic performance in many solar applications. Tracking angles depend on the latitude of the place and the climate. Fuke et al. (Fuke et al., n.d.)investigated the technical performance and economic assessment of fixed, 1-axis, and 2-axis tracking orientations under geographical and climatic circumstances in Mumbai. During the summer, more power is obtained using a 1-axis tracking system compared to a fixed system. Furthermore, a 2-axis tracking system produces just 3-4% more electricity; as can be observed, there is no significant increase in producing power when using a 2-axis tracking system compared to a 1-axis system.

Several studies conducted in middle east countries deal with the technical performance and economic feasibility of PV solar energy power plants (Kazem et al., 2017; Allouhi et al., 2016; Audenaert et al., 2010; Drury et al., 2011; Vermaak, 2014) . Most of the studies which dealt with solar energy in Iraq which investigate the energy performance of the solar energy system (Ahmed & Ali, 2019; Ali & Jameel, (2011); Ali, 2020; Alomar & Ali, 2021; Alyousifi & Ali, 2019; Hussain & Mahdi, 2018; Bamisile et al., 2019; Chaichan & Kazem, 2018; Kazem & Chaichan, 2012; Khaled & Ali, 2020; Oudah, 2020; Salah, 2021; Zubeer & Ali, 2021, 2022). The studies that dealt with the technical and economic feasibility in Iraq is rare. Oudah and Salah (Salah, 2021) investigated theoretically the energy and economic performance of a proposed grid-connected PV Power Plant with a capacity 4 MW to produce the energy at AL- Mahmudiyah region. The results indicated the construction of the grid-connected PV Power Plant for electricity production is feasible due to its cost-effective. Also, the energy and economic feasibility studies for PV power plant using tracking systems are very little in Iraq. Hussein and Mahdi (Kazem et al., 2017)performed an environmental and economic feasibility study for a 10 MW sun-tracking PV power plant in the western region of Iraq. The total electrical power achieved using a dual-axis tracking system throughout the lifetime

In recent years, the shortage in electrical production and pollution problems of the power plants that uses fossil fuels are great challenges in Iraq. The improvement of the economic and technical performance of fixed PV solar panels has been the main priority of researchers because they need a huge installation area. The employment of the tracking system for PV solar energy power plant is one of the best methods to increase the energy production. From the

literature review, the studies which deal with the performance of solar systems using tracking systems is not considered and there are rare theoretical and experimental studies in Iraq which deal with this subject. Therefore, the present study aims to make a technical, economic, and environmental feasibility study to compare three different solar tracking systems fixed with constant tilt angle, single-axis, and dual-axis, to evaluate the impact of the factors on a grid-connected PV power plant in Zakho city using actual meteorological data. Simulation models are applied to design the planned PV power plant. The proposed grid-connected PV power plant has a 1 MWp system capacity. The system includes a grid-connected inverter, which is utilized to produce power from the grid. The PV power plant is compared with Iraq's available fossil fuel plants. This research is becoming earlier research done for northern Iraq, which compared three distinct solar systems and relied on real meteorological data to establish the feasibility of the intended power plant.

Zakho city Weather and Location Conditions

This section explains the yearly weather conditions in Zakho, Iraq. The actual data provided upon an hourly rate for 2019 includes the radiation from the sun intensity, temperature, and wind speed (*NREL Solar Spectra*, 2020), as seen in fig. 1. The ambient temperature in Zakho city varies from –4.9 to 46.7 °C, as illustrated in fig. 1(a), and the temperature reaches its highest during the summer. The radiation from the sun intensity, as illustrated in fig. 1(b) is an important factor in determining where to build PV systems. North Iraq as a whole has spectacular total solar insolation values that have reached 1050 W/m^2. Fig 1(c) depicts the city's local wind speed around an hourly rate over a year. The wind speed in the area fluctuates from 0.2 to 8.8 meters per second. Because the average wind speed in Zakho/Iraq is far less about 2 m/s, the influence of wind speed on PV systems is not as substantial as solar irradiation and ambient temperature.
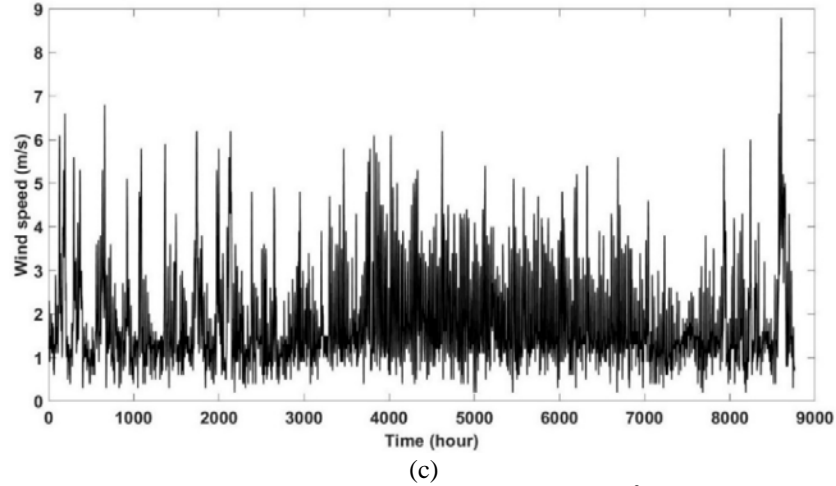

(a)

(b)

(c)
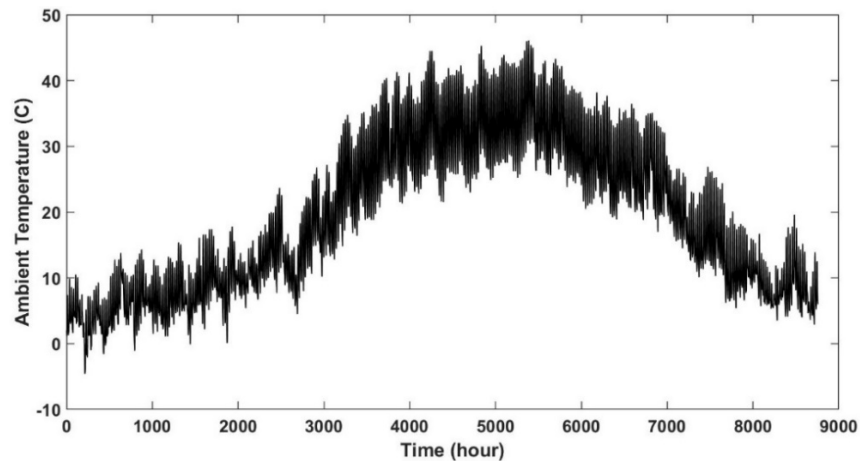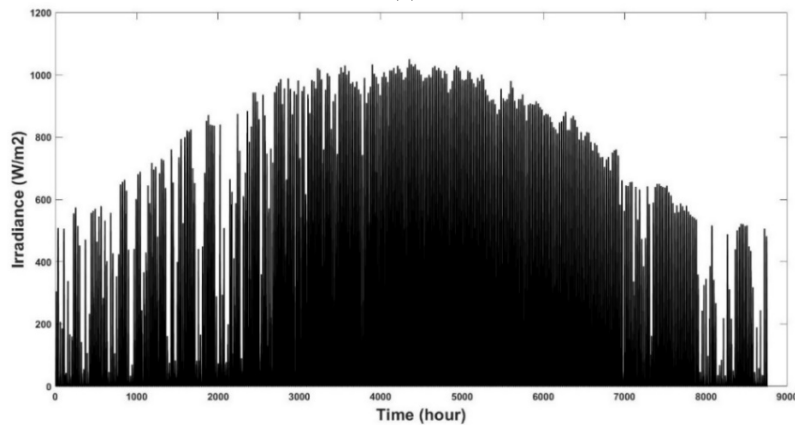
Figure 1: (a) Ambient temperature in °C, (b) Hourly solar insolation in W/m², (c) Wind speed in m/s for an entire year (2019).

Determining of Plant Output

Zakho is a bordering state in the northwestern part of Duhok Governorate, located at 37.15° north and 42.67° east. The city has around 1375 sq. km, which allows for installing PV panels (Wikipedia, 2021). The city of Zakho is located in a hilly environment, which is ideal for a PV plant because there is less concern about dust impacts. Considering the geographical situation, the PV capacity is on a stable foundation. However, the plant's design will produce excellent technological and economic outcomes.

Modeling of Grid-Connected PV Seystem

A photovoltaic solar panel and an inverter are the components of a grid-connected PV system. In Zakho, a 1 MWp PV system was recently simulated. As a result, this study assumed that a 1 MWp PV is developed in the Zakho area for research and development purposes. The same system is used for three types of power plants; fixed, single-axis, and dual–axes tracking solar systems. The present feasibility study depends on the actual solar panel installed in the Zakho city as displayed for the single and dual-axis case as shown in fig. (2). The specifications of the simulated PV system are shown in Table 1.

Table 1. Modelled PV system specification.

PV array (Multi-c-Si)	Canadian Solar Inc. CS6A-150PE
PV module rated power **(6720 modules)**	150W
Module Area	1.3 m²
Maximum Voltage	23.1V
Maximum Current	6.5A
Open circuit voltage Voc	28.8V
Short circuit current Isc	7.1A
Solar cells Efficiency	12%
Current temperature coefficient	0.006A/C
Voltage temperature coefficient	-0.107 V/C
Inverter	SunPower: SPR-15000m-3[480V]
Rated Power (4 inverters)	15kW

A sequence of hourly data of total solar radiation and ambient temperature provided by the National Renewable Energy Laboratory (NREL, 2020) is utilized to simulate the anticipated PV system. Furthermore, applying a PV array mathematical model, these data are utilized to compute the DC power provided by the PV panel. Additionally,

the Ac output is computed by taking the inverter efficiency into account (inverter mathematical model). Following that, the proposed system is evaluated by using the evaluation criteria that have been established.

Figure 2: Single and dual axis PV-panel systems of Zakho City

PV Array Model

The PV array's output power is determined by the obtainable solar radiation (G) and the ambient temperature (T). A PV array's output power rises proportionally as solar radiation rises and falls as ambient temperature rises(Wang et al., 2020). As a result, the instantaneous output of a PV array (Patel, 1999) may be calculated as,

$$P_{mp} = G\eta_m A_m (\frac{\gamma_{mp,ref}}{100})(T_c - 25) \tag{1}$$

Where G is the solar insolation, $\eta_m m$ is the efficiency of the module, $\gamma_{mp,ref}$ is the temperature coefficient of the PV panel power and T_c is the temperature of the cell, and it is given by,

$$T_c = T_a + \frac{G}{800}(T_{noct,adj} - 20)(1 - \frac{\eta_{ref}}{\tau\alpha})\frac{9.5}{5.7+3.8v_{w,adj}} \tag{2}$$

where NOCT is the nominal operating cell temperature, which can be measured practically at 800 W/m², 1.5 m/s wind speed and 20°C ambient temperature. However, considering Eq. (1), the hourly ambient temperature and solar radiation records for the chosen location have been gathered. The PV reference efficiency is obtained from:

$$\eta_{ref} = \frac{I_{mp}V_{mp}}{1000A_m} \tag{3}$$

Where I_{mp} is the module maximum power current rating, A, V_{mp} is the module maximum power voltage rating (V), and Am is the area of the module, m².

Inverter Model

The efficiency of an inverter (Khatib et al., 2012)is calculated by,

$$\eta(t) = \frac{P_{in}(t) - P_{Loss}(t)}{P_{in}(t)} \qquad (4)$$

Where $P_{Loss}(t)$ and $P_{in}(t)$, are the power loss and instantaneous input power during the conversion. The PV system's input power equals the PV module's output power, ignoring wiring losses. Calculating to be difficult, the PLoss is not constant and is affected by various factors. As a result, an alternate model for inverter efficiency must be established to determine the output power of the inverter. It is possible to acquire the input power (DC) as follows:

$$P_{dc,0} = \frac{P_{ac,0}}{\eta_{inv,0}} \qquad (5)$$

Fig. 3 depicts an efficiency curve derived from the datasheet for a commercial inverter. The graph depicts the inverter's efficiency (in percentage) in input and rated power. As a result, samples of the inverter's efficiency curve (illustrated in Fig. 3) should be collected for curve fitting.
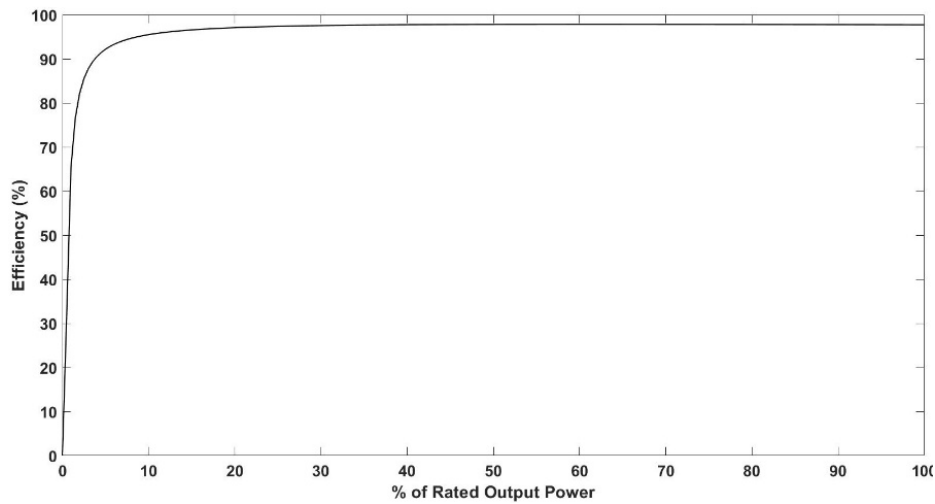

Figure 3: Typical efficiency curve for an inverter.

Criteria of PV grid-connected prodeucts for evaluation

Technical parameters

Technical and economic evaluation criteria can be utilized to determine the viability of a grid-connected PV system. Technical criteria, such as yield factor, capacity factor, and performance ratio, are considered in this research. The economic evaluation criterion and calculation methods are described in-depth in the following paragraphs. A yield factor YF is also defined as annually, monthly or daily net Electrical energy production of the system divided by the maximum output power of the PV array that is mounted under standard test conditions STC, and it is also provided by (Kymakis et al., 2009),

$$YF = \frac{E_{PV}(kWh/year)}{PV_{Wp}(kWp)} \qquad (6)$$

where E_{PV} is the system's energy yield, and PV_{WP} is the PV array's nominal power (P_{STC}). Under certain weather parameters, the above factor affects the production of a PV system. The capacity factor, on the other side, is defined as the ratio of actual yearly energy production to the quantity of energy a solar PV array would produce if it is maintained at full rated power for a year (Kymakis et al., 2009),

$$CF = \frac{Y_F}{8760} = \frac{E_{PV\ annual}}{P_R * 8760} \qquad (7)$$

This factor evaluates the usage of the PV array. The performance ratio P_R is the ratio of the actual energy output of a PV system to the theoretical standard test condition output for a given reporting period,

$$P_R = YF \frac{G_{STC}}{\sum G_t} \tag{8}$$

where G_{STC} is the amount of irradiance at standard test conditions, STC and $\sum G_t$ Are the accumulative irradiance on the plane of the PV array within a certain period (annual, monthly, or daily).

Economic Parameters

This factor rates the PV array's use. Life cycle cost (LCC), payback time, and cost factors can be utilized for the economic analysis. The total cost is defined by,

$$LCC = C_{capital} + \sum C_{O\&M} + \sum C_{replacement} - C_{salvage} \tag{9}$$

A project's capital cost ($C_{capital}$) must include the initial capital cost for instruments, system design, and operation. This cost is often viewed as a single fee paid during the first year of its project. Cost of maintenance ($C_{O\&M}$) is the total of all annual operation and maintenance expenditures. Operators' income, inspections, security, and local taxes are all examples of O&M costs. The replacement cost ($C_{replacement}$) is the total of all equipment repairs during the duration of the system. Typically, these expenditures happen in defined years, and the entire cost is incurred throughout those years. Eventually, a value of system salvage ($C_{salvage}$) is its net valuation in the final year of its life cycle. For mechanical devices that may be evacuated, it is usual practice to give a salvage rate of 20% of the initial cost. This rate can be adjusted based on other variables such as obsolescence and equipment conditions (Hong et al., 2016). Furthermore, the cost analysis is based on the actual solar panels placed in Zakho city. Note that installing grid PV systems comes with an additional cost for single and dual axes tracking systems which are often replaced after a certain period. Thus these higher costs are taken into consideration. After determining the LCC, the unit price of the energy may be determined as follows:

$$CoE = \frac{LCC}{\sum_1^n E_{PV}} \tag{11}$$

This model computes the power provided by an array and other system losses such as temperature inverter waste, wire damage, etc. Following that, the rating factors employed in this study are derived using Eqs. (5), (6), (7), and (9). The net present value (NPV) is critical in analyzing its economic viability since it indicates the net profit produced. A positive value of NPV shows that investing in the project would be productive. The net present value (NPV) is a difference between the current value of cash flows throughout the project's life and the original capital cost. The following formula can be used to calculate (Drury et al., 2011):

$$NPV = \sum_{t=0}^{N} \frac{Revenue}{(1+i)^t} - initial\ cost \tag{12}$$

where N denotes the number of years for the economic study, typically the project lifecycle, t represents the year, and I denotes the interest rate. The yearly income may be determined by multiplying the PV system's energy output by the energy price. The following equations can be used to compute annual revenue (Audenaert et al., 2010):

$$Revenue\ (year = i) =\ Energy\ produced \tag{13}$$

The payback period (PBP) calculates the time it takes for the system to return its initial investment. A shorter PBP time is preferable since the project returns its original cost in a shorter time. PBP is the amount of time necessary to reduce NPV to zero. To compute PBP, first determine if the project's overall NPV during its lifecycle is negative. If that is, it shows that the project is not possible. If the Net present value is positive, the parameter N in eq. (11) is decremented in 0.25-year stages, and the NPV is computed for every step till the NPV is equal to 0, at which point N equals PBP.

Environmental Impact

Various greenhouse gases, particularly CO_2, contribute to environmental contamination. CO_2 emissions are the major source of the potential issue of global warming. CO_2 is regarded as pollution when combined with power plants that use fossil fuels to generate electricity (Allouhi et al., 2016). The photovoltaic system is among the most environmentally friendly energy generation methods. In the current study, the environmental effect of each deployed technology is determined only by the embedded energy and CO_2 equivalent emissions. As a result, the current paper explores the possibility of lowering CO_2 emissions by installing such PV systems.

Validation of the Present Work

The cell temperature of the present work compares with theose of the available experimental results by Zubeer and Ali (Oudah, 2022)for a day of 24th September 2019 for Duhok city (it closer to Zakho city), as shown in figure (4). The agreement between two studies is good with a maximum error value of about 8% due to some difference in the climatic conditions.
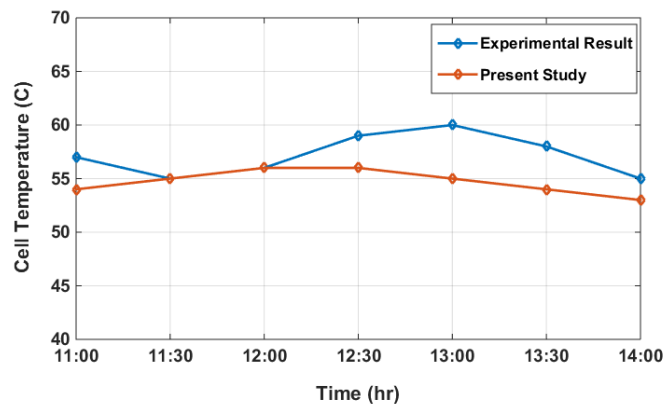

Figure 4:The cell temperature of the present work compared with another experimental work

Results and Discussions

According to the simulation findings, the system was tested for a year. Furthermore, the annual energy produced for three systems (fixed, single-axis, and dual-axis) for 1 MW power plants is around 1428466 kWh, 1709710 kWh, and 1919613 kWh. These results indicate an increase in the produced energy with 34% and 19.6% for power plants with dual and single axes tracking systems compared to the fixed system. The annual yielded energy produced by the PV power plant for Zakho city in the first year is approximately 1,416 kWh/kW, 1,694 kWh/kW, and 1,902 kWh/kW for three systems, respectively, which mean that the employment of the single-axis and dual-axes tracking systems for PV power plant increases the produced energy by 19.6% and 26% as compared with those of fixed panels. In contrast, the performance factors of the planned power plant are approximately 0.71, 0.71, and 0.69, respectively. The annual capacity factor for fixed, single-axis and dual-axes tracking systems are 16.2 percent, 19.3 percent, and 21.70 percent. The energy findings indicate that the employment of the tracking systems have a positive influence on the energy production. As illustrated in Fig. (5-6), the optimal tilt angles of the PV power plant/month are achieved. The monthly fluctuation in the ideal tilt angles is caused by the change in the altitude between the sun and earth, which changes the optimal values of the PV tilt angle regularly. A varied tilt angle delivers more output energy and peak power for the planned power plant every month. The average optimum tilt angle for each month is displayed in figure 6. To enhance the accuracy in determining the larger output energy and peak power that will be generated, a unique tilt angle equivalent to the recurring month tilt angles is selected. The optimum tilt angle is approximately equal to the latitude of Zakho city since it is the best tilt angle for five months. Therefore, the optimum tilt angle is selected for the fixed solar panel. Also, the simulations involve the cell temperature distribution for the PV panel, figure 7, which have an effect on the PV panel efficiency. The panel temperature increase with the increase of the ambient temperature and solar radiation intensity.
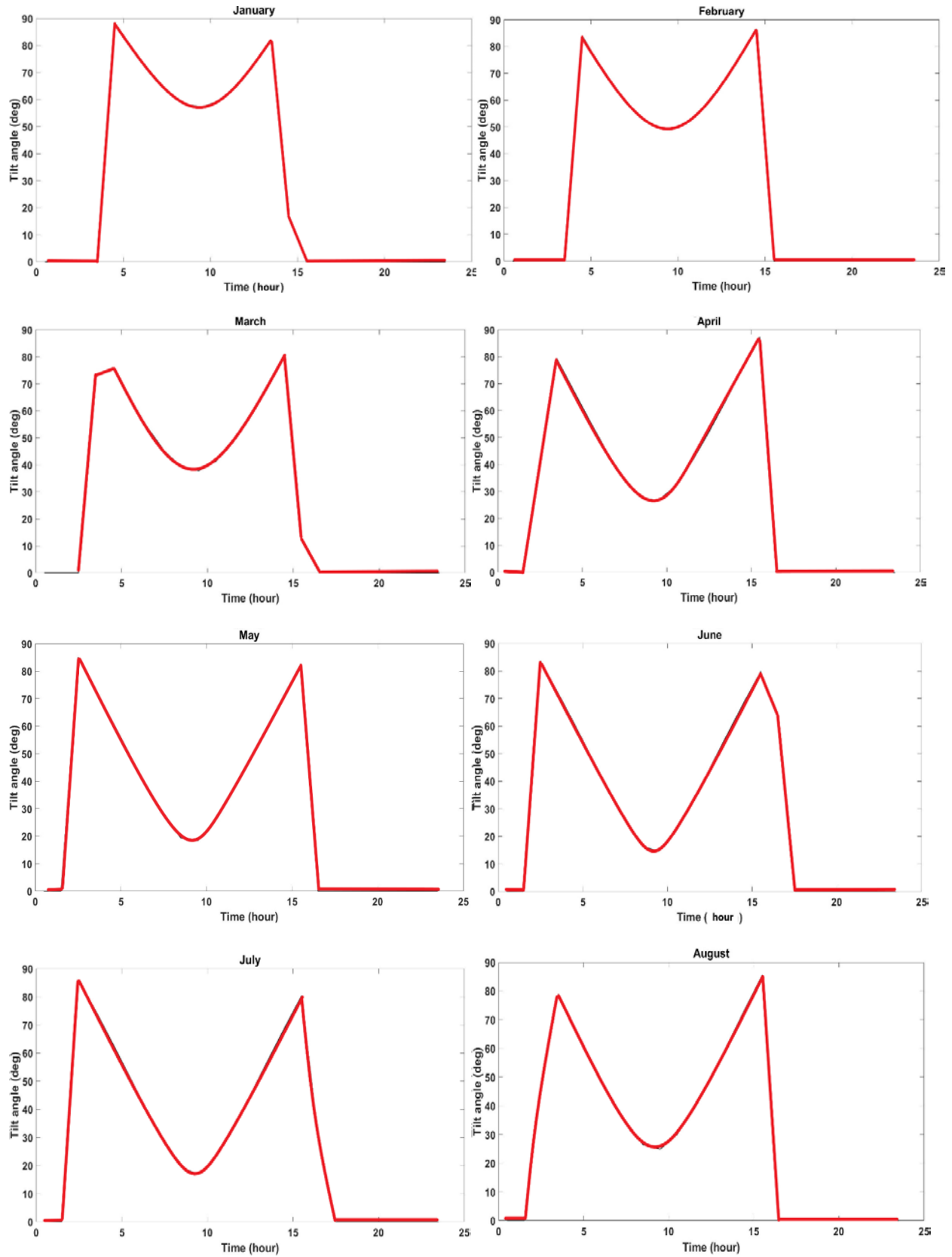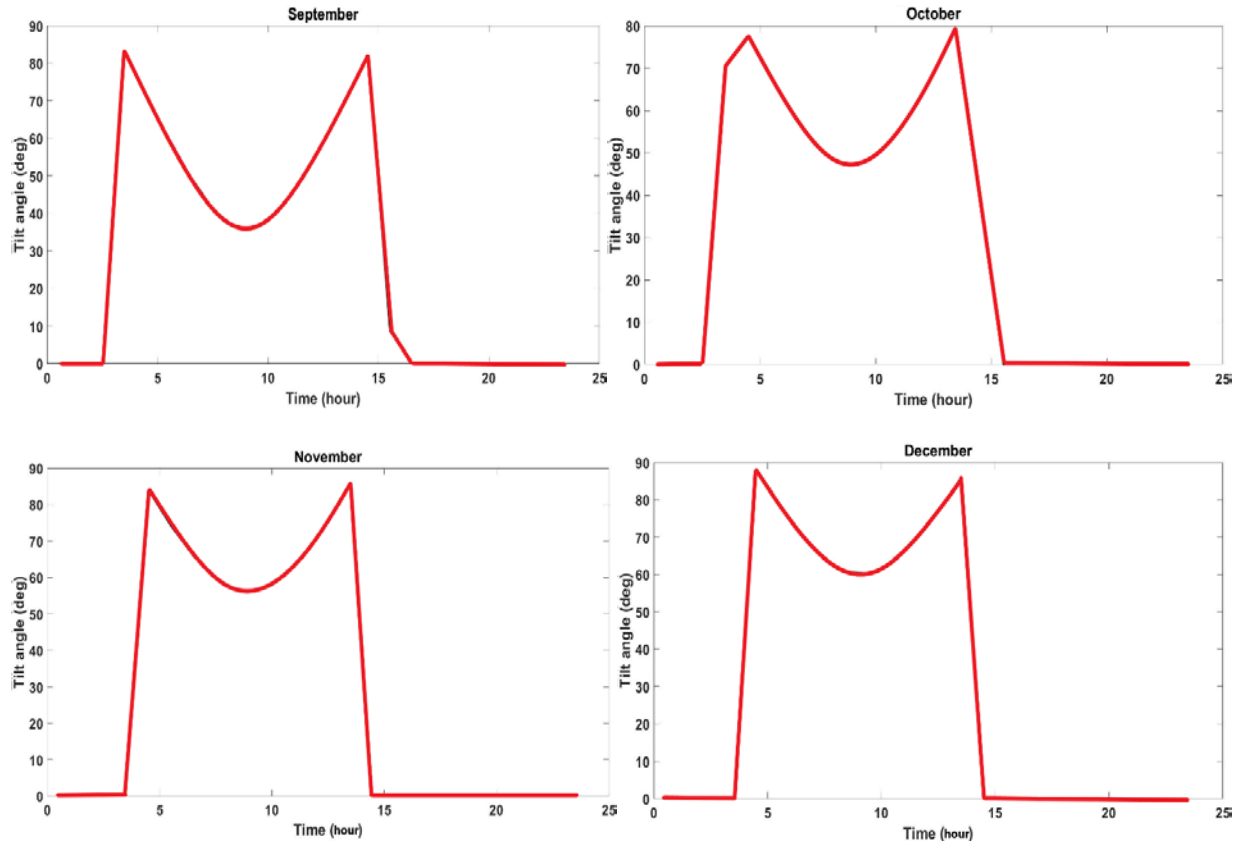
Figure 5: Optimum tilt angle for all months versus time
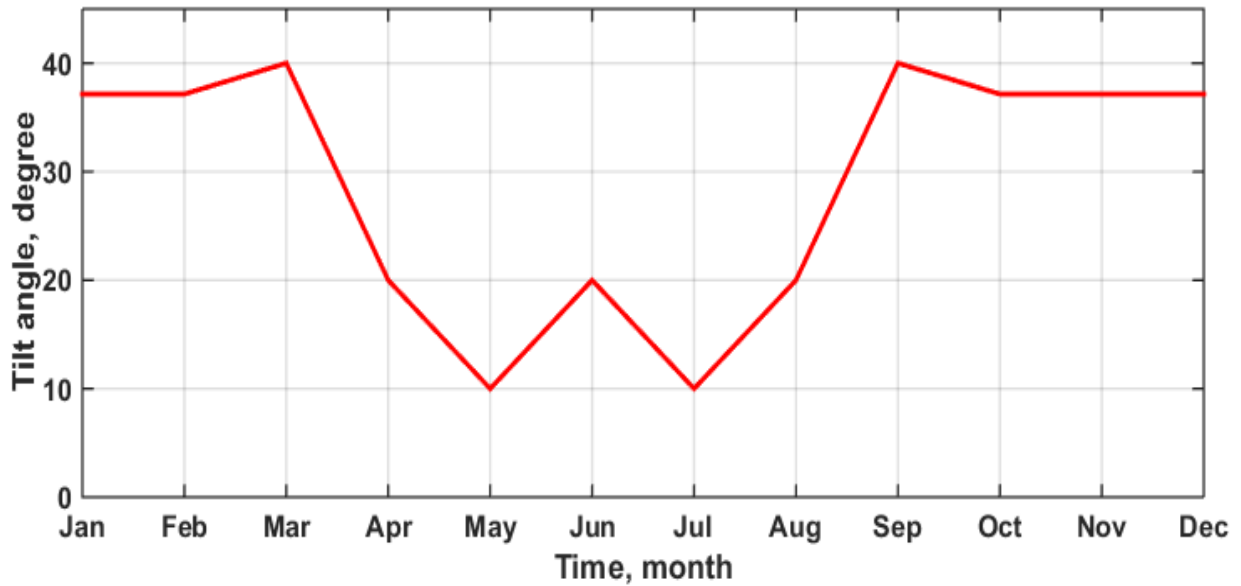
Figure 6: Monthly optimum tilt angle

The comparisons of generated energy, capacity factor, and yield factor for different 3 tracking systems are illustrated in figures 8 – 10. As seen in fig. 8, the energy production ranges for fixed, single-axis, and dual-axis systems are (62 – 150 MWh), (50 – 220 MWh), and (80 – 230 MWh), respectively with peak energy production for three systems is around 150 MWh, 220 MWh, and 230 MWh, respectively, showing an enhancement percentage with 31% and 34.7% for single and dual axis as compared with fixed panel system. Maximum enhancement for three systems are

obtained in May and July months while lowest energy output for these systems indicated in January and December months. The capacity factor of a suggested plant is depicted in figure 9, for three systems which ranged between 20-32 %, 22 – 48 %, and 23 – 50 %, respectively. This factor fluctuates between the lowest values in the winter and maximum values in the summer. Figure 10 display the the yield factor distribution for 3 tracking systems during 12 months' data. The highest results are reached for intended systems within the summer months of May – September due to the high ambient temperature and solar insolation. For some winter months, the yield factor for the PV power plant of 1-axis is more than those of 2-axis.
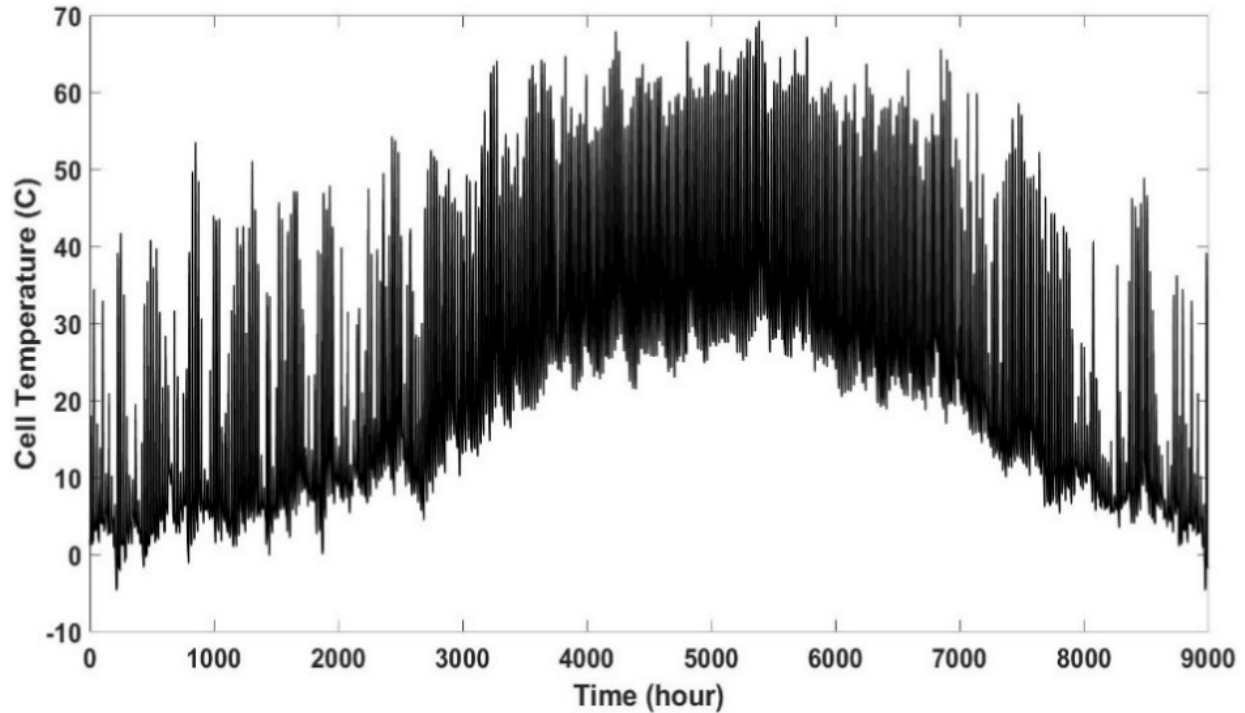

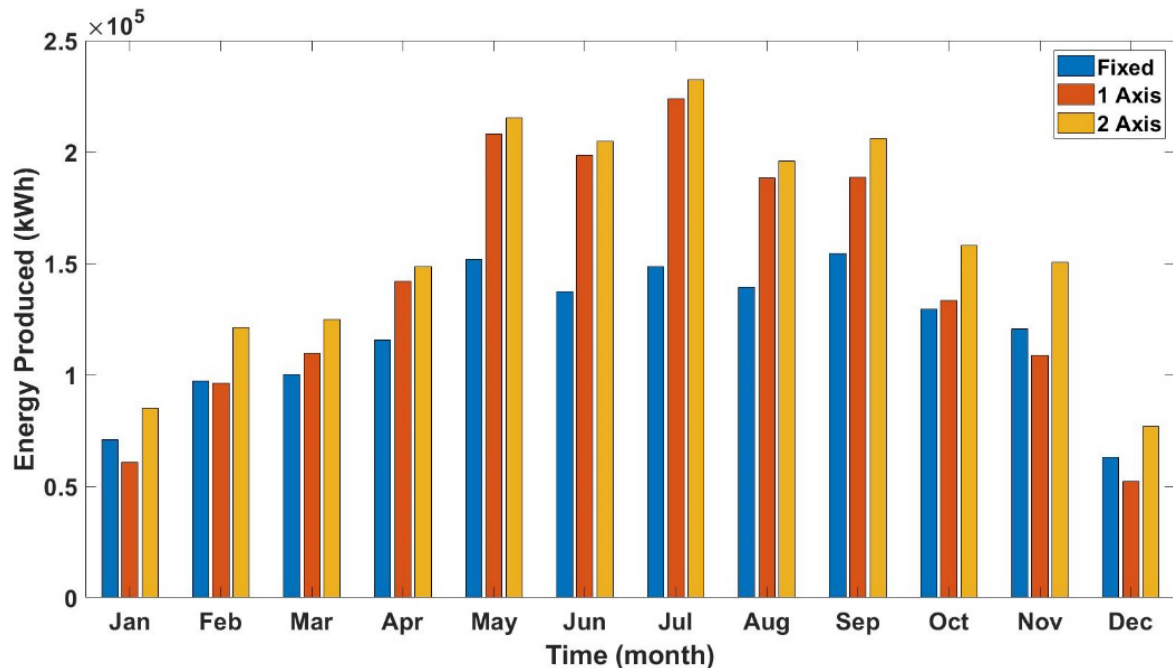Figure 7: Hourly cell temperature in ℃
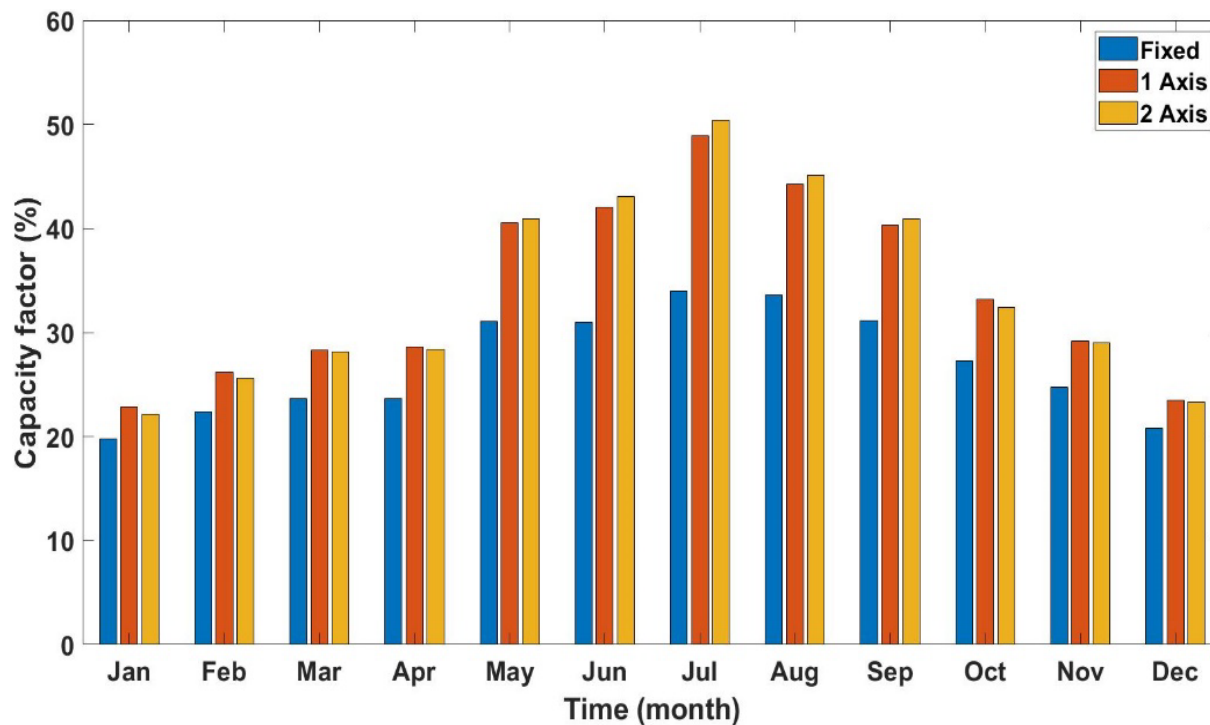

Figure 8: Monthly energy production, kWh
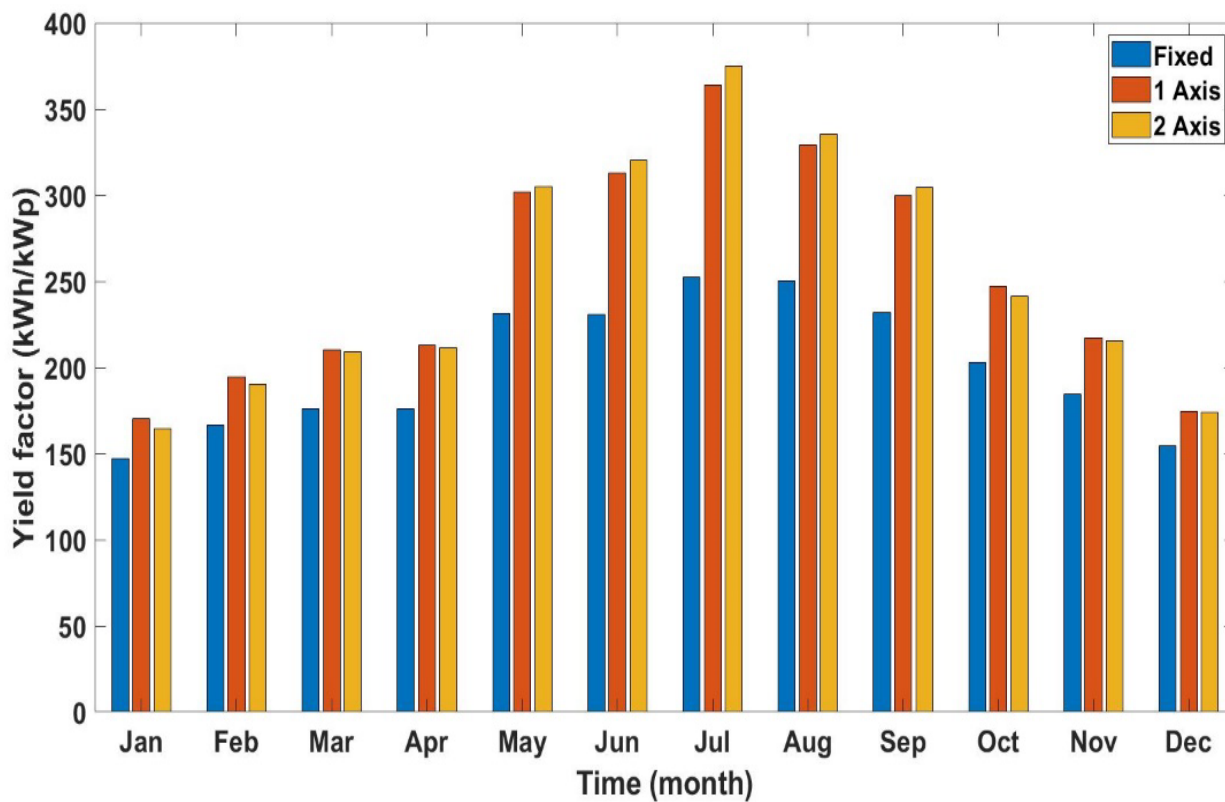
Figure 9: Monthly capacity factor

Figure 10: Monthly yield factor, kWh/kWp

Three PV solar panels are installed on the roof of the engineering college with the solar panel specification that displays in Table 1. The cost of the fixed PV solar panel includes the support structure and other accessories, while the single axis and dual axes tracking systems include the cost of the fixed panel plus additional cost due to the tracking systems. Therefore, the economic analysis depends on the actual prices in local Iraq markets.

The results of the economic analysis display in figure 11 and table 2. Figure 11 demonstrates that the PV power plant income increases and the cost of the intended power plant will be recovered after 9 years for a fixed system and about 15 years for the other two systems (single-axis and dual-axis). Table 2 displat briefly the comparison of the technical and economic results for three tracking systems of the PV power plants. The findings display that the CoE of a PV power plant for fixed, single, and dual-axis systems is 0.083, 0.049, and 0.044 USD/kWh, respectively, which displays that the tracking systems increase the energy production despite of the expensive installation costs. The NPV for 1 and 2 axes tracking systems is low, therefore, the payback period is long as compared with fixed panel. Due to government backing, the cost of energy in Iraq is lower than in other nations due to the government's minimal taxation (Kazem et al., 2017).
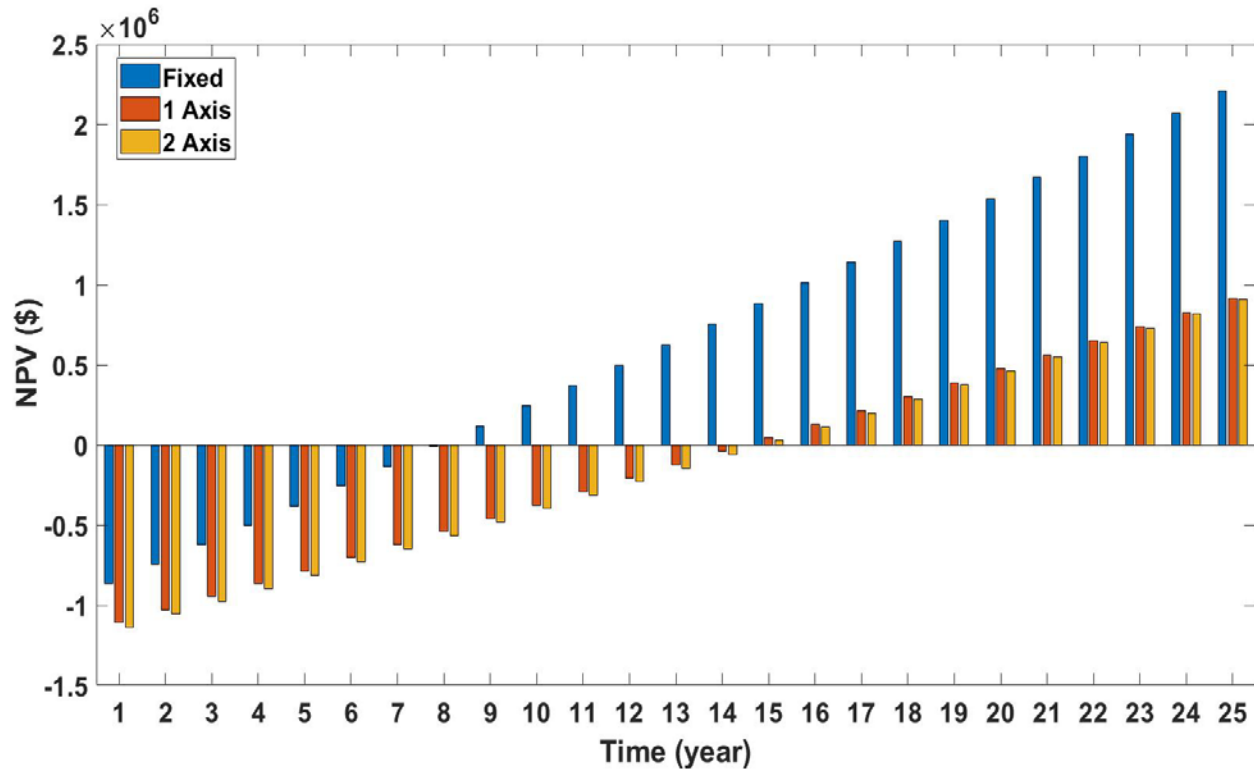
Figure 11: Net Present Value for PV power plant (1 MW) during its lifetime

The CO_2 emission analysis displays that the CO_2 emission is very low for PV power plant as compared with those of other power plants that employ fossil fuels, table 3. The fossil fuels in the table are selected because these fuels are used in Zakho city for central power plants and local generators. The CO_2 emission reduces when fixed PV power plants are used instead of Natural gas and gasoline with the values of 472.8 and 3292.6 tCO_2, respectively; 565.9 and 3940.8 tCO_2 for single-axis, and 635.4 and 4424.7 tCO_2 for Dual-axis. Table 4. Displays the generated energy, installation cost, fuel cost, O&M cost, and social cost for different power plants. The produced energy for a 1 MW power plant using gas turbine and steam turbine power plants are about four times of PV energy. Fossil fuels are very expensive compared with PV power plant costs. The running cost of PV power plants is very low, and the fuel is not required, while other power plants require fuels and expensive maintenance. Therefore, the running cost of the power plant is considered expensive. The CO_2 emission affects the community with a social cost in which each tCO_2 cost equals 50 USD (Rafaty et al., 2020). The employment of the tracking systems for PV power plant have not influence on the CO_2 emission.

Table 2: Technical and economic parameters results

Item	Unit Price			Value		
Type of PV System	Fixed	Single-Axis	Dual-Axis	Fixed	Single-Axis	Dual-Axis
PV array 6720X150Wp	0.38USD/Wp	0.38USD/Wp	0.38USD/Wp	383,423.03 USD	383,423.03 USD	383,423.03 USD
The support structure, circuit breakers, transformers, and cables	0.06 USD/Wp	0.06 USD/Wp	0.06 USD/Wp	201,801.59 USD	302,702.41 USD	332,972.62 USD
Inverter (15kW) × 220				60,540.48 USD	60,540.48 USD	60,540.48 USD
Installation and commissioning				110,990.88 USD	161,441.28 USD	161,441.31 USD
Total				756,756.00 USD	908,107.19 USD	938,377.44 USD
Salvage Value				19,372.95 USD	27,243.22 USD	28,151.32 USD
Operation and maintenance				13 USD/KW-	13 USD/KW-	13 USD/KW-
The total area of modules				8736m^2	8736m^2	8736m^2
Land area				87360 m^2	17470 m^2	17470 m^2
Energy Yielded				1,416 kWh/kW	1,694 kWh/kW	1,902 kWh/kW
System Lifetime				25 Years	25 Years	25 Years
Annual energy produced				1,428,466 kWh	1,709,710 kWh	1,919,613 kWh
Capacity factor				16.2%	19.3%	21.70%
Performance ratio				0.71	0.71	0.69
COE				8.26 cents/kWh	4.89 cents/kWh	4.41 cents/kWh
NPV				120,334 USD	22,354 USD	22,860 USD
IRR				11 %	11 %	11 %
PPA price				9.15 cents/kWh	5.03 cents/kWh	4.53 cents/kWh
Simple Payback period				9 years	15 years	15 years

Table 2. CO_2 emission factors, CO_2 emission results, and annual energy for some fuels and materials

	CO_2 Emission Factor, tCO_2/MWh		Annual Energy MWh	CO_2Emission, tCO_2	
	Natural gas	Gasoline		Natural gas	Gasoline
Fixed			1428.466	472.8	3292.6
Single-Axis	0.331	2.305	1709.71	565.9	3940.8
Dual-Axis			1919.613	635.4	4424.7

Table 3. Comparative between PV and fossil fuel power plants

Costs	Power Source		
	PV	Gas turbine	Steam turbine
Initial cost, USD	1800000	2,200,000	10,063,000
O&M cost, USD/ year	18000	133,000	396,500
Social cost, USD/ year	0	44,350	100,850
Fuel cost, USD/ year	0	235,725	279,000
Total cost, USD	1818000	2,613,075	10,839,350

Conclusion

In the present work, 1 MW_p PV power plants using fixed, single, and dual solar tracking systems for PV solar panel in Zakho city are evaluated and simulated depending on the actual metrological data and solar panels installed in Zakho city. The study's primary conclusions are explained in the following sections:

- The findings demonstrate that the power plant yield factor per year for the three recommended systems is 1,416 kWh/kW, 1,694 kWh/kW, and 1,902 kWh/kW, respectively.
- When compared to fixed panels, the use of single-axis and dual-axis tracking systems for PV power plants improves the produced energy by 19.6 percent and 26 percent, respectively. In comparison, the proposed power plant's performance factors are roughly 0.71, 0.71, and 0.69, respectively.
- The annual capacity factors for these systems are 16.2 %, 19.3 %, and 21.7 %, respectively.
- The PV system's potential as an energy-positive and sustainable source and a financially attractive investment was assessed using COE, NPV, PBP, and EPBT.
- The COE for the three anticipated systems was calculated to be 0.0826 USD/kWh, 0.0489 USD/kWh, and 0.0441 USD/kWh, which is less than the current actual cost of a kWh of production in Zakho city.
- The NPV value of the fixed PV system reached 120,334 USD which is undesirable compared to the single axis and dual axis which the NPV value is 22,860 USD and 22,354 USD, respectively. Since the NPV for 1 and 2 axis tracking systems is lower, the payback period is extended when compared to the fixed panel.
- The calculated PBP for three systems is nine years for the fixed system and fifteen years for single and dual-axis systems.
- This study also shows that achieving a sustainable energy transition is feasible while lowering carbon emissions by optimizing largescale PV installations in Zakho city for the system load curve.
- Indeed, according to the data, the dual-axis system was feasible and preferable to the other two systems.
- Currently, the authors are working on this study experimentally to expand this work more acceptable and efficient for practical applications.

Scientific Ethics Declaration

The author declares that the scientific ethical and legal responsibility of this article published in EPSTEM journal belongs to the author.

Acknowledgements or Notes

References

Abdulhamid, F., & Alfirjani, S. (2021). *Comparison of the Efficiencies of Dual-Axis, Single-Axis Solar Tracking Systems and Fixed Pv System in Karabuk*.

Ahmed, M. I., & Ali, O. M. (2019). Experimental investigation of flat plate collector system performance using galvanized steel absorber in Duhok climate. *Journal of Duhok University*, *22*(2), 49–56.

Ali, O., & Jameel, A. (2011). Performance analysis of the solar water heating system in Zakho City. *Polytechnic Journal, 1*(1).

Ali, O. M. (2020). An experimental investigation of energy production with a hybrid photovoltaic/thermal collector system in Duhok city. *Case Studies in Thermal Engineering*, *21*, 100652.

Allouhi, A., Saadani, R., Kousksou, T., Saidur, R., Jamil, A., & Rahmoune, M. (2016). Grid-connected PV systems installed on institutional buildings: Technology comparison, energy analysis and economic performance. *Energy and Buildings*, *130*, 188–201.

Alomar, O. R., & Ali, O. M. (2021). Energy and exergy analysis of hybrid photovoltaic thermal solar system under climatic condition of North Iraq. *Case Studies in Thermal Engineering*, *28*, 101429.

Alyousifi, S. O., & Ali, O. M. (2019). An experimental investigation of glazed flat plate PV/T hybrid solar collector system in Duhok city. *Journal of Duhok University*, *22*(2), 23–34.

Audenaert, A., De Boeck, L., De Cleyn, S., Lizin, S., & Adam, J.-F. (2010). An economic evaluation of photovoltaic grid connected systems (PVGCS) in Flanders for companies: A generic model. *Renewable Energy*, *35*(12), 2674–2682.

Bamisile, O., Olubiyo, F., Dagbasi, M., Adun, H., & Wole-Osho, I. (2019). Economic analysis and performance of PV plants: An application in Kurdistan region of Iraq. *International Journal of Renewable Energy Development*, *8*(3), 293–301. https://doi.org/10.14710/ijred.8.3.293-301

Chaichan, M. T., & Kazem, H. A. (2018). *Generating electricity using photovoltaic solar plants in Iraq*. Springer.

Chaturvedi, A., Tiwari, A., Binkley, D., & Chaturvedi, S. (2021). Service Evolution Analytics: Change and Evolution Mining of a Distributed System. *IEEE Transactions on Engineering Management*, *68*(1), 137–148. https://doi.org/10.1109/TEM.2020.2987641

Drury, E., Denholm, P., & Margolis, R. (2011). *Impact of Different Economic Performance Metrics on the Perceived Value of Solar Photovoltaics*. National Renewable Energy Lab.(NREL), Golden, CO (United States).

Fahad, H. M., Islam, A., Islam, M., Hasan, M. F., Brishty, W. F., & Rahman, M. M. (2019). Comparative analysis of dual and single axis solar tracking system considering cloud cover. *2019 International Conference on Energy and Power Engineering (ICEPE)*, 1–5.

Fathabadi, H. (2016). Novel high accurate sensorless dual-axis solar tracking system controlled by maximum power point tracking unit of photovoltaic systems. *Applied Energy*, *173*, 448–459.

Ferdaus, R. A., Mohammed, M. A., Rahman, S., Salehin, S., & Mannan, M. A. (2014). Energy efficient hybrid dual axis solar tracking system. *Journal of Renewable Energy*, *2014*.

Fuke, P., Yadav, A. K., & Anil, I. (n.d.). Techno-Economic Analysis of Fixed, Single and Dual-Axis Tracking Solar PV System. *2020 IEEE 9th Power India International Conference (PIICON)*, 1–6.

Gupta, M., Kumar, S., & Katyal, P. (2015). Experimental investigation of indirect solar cooker using evacuated tube collector with dual thermal storage unit. *International Journal of Thermal Technologies*.

Hong, T., Jeong, K., Ban, C., Oh, J., Koo, C., Kim, J., & Lee, M. (2016). A preliminary study on the 2-axis hybrid solar tracking method for the smart photovoltaic blind. *Energy Procedia*, *88*, 484–490.

Hoque, S. M. B., Das, B., & Al Askary, M. A. H. (n.d.). *Comparative Analysis of Dual and Single Axis Solar Tracker*.

Hussain, M. T., Mahdi, J. E. (2018). Assessment of solar photovoltaic potential in iraq. *Journal of Physics: Conference Series*, *1032*(1). https://doi.org/10.1088/1742-6596/1032/1/012007

Jamroen, C., Komkum, P., Kohsri, S., Himananto, W., Panupintu, S., & Unkat, S. (2020). A low-cost dual-axis solar tracking system based on digital logic design: Design and implementation. *Sustainable Energy Technologies and Assessments*, *37*, 100618. https://doi.org/10.1016/J.SETA.2019.100618

Kazem, H. A., & Chaichan, M. T. (2012). Status and future prospects of renewable energy in Iraq. *Renewable and Sustainable Energy Reviews*, *16*(8), 6007–6012.

Kazem, H. A., Albadi, M. H., Al-Waeli A. H. A., Al-Busaidi A. H., Chaichan M. T. (2017). Techno-economic feasibility analysis of 1 MW photovoltaic grid connected system in Oman. *Case Studies in Thermal Engineering*, *10*, 131–141.

Khaled, S., & Ali, O. (2020). Numerical and experimental investigation for hybrid photovoltaic/thermal collector system in Duhok city. *Journal of Environmental Engineering and Landscape Management*, *28*(4), 202–212. https://doi.org/10.3846/jeelm.2020.13691

Khatib, T., Mohamed, A., Sopian, K., & Mahmoud, M. (2012). An iterative method for calculating the optimum size of inverter in PV systems for Malaysia. *Electrical Review*, *88*(4a), 281–284.

Kymakis, E., Kalykakis, S., & Papazoglou, T. M. (2009). Performance analysis of a grid connected photovoltaic park on the island of Crete. *Energy Conversion and Management*, *50*(3), 433–438.

Leon, N., García, H., & Ramírez, C. (2014). Semi-passive solar tracking concentrator. *Energy Procedia*, *57*, 275–284.

Njoku, H. O. (2016). Upper-limit solar photovoltaic power generation: Estimates for 2-axis tracking collectors in Nigeria. *Energy*, *95*, 504–516.

NREL, (2020). *Solar Spectra*. https://www.nrel.gov/grid/solar-resource/spectra.html

Oudah, S. S. and M. A. S. (2020). Numerical and experimental investigation for hybrid Photovoltaic/thermal collector system in Duhok city. *Journal of Environmental Engineering and Landscape Management*, *28*(4), 202–212.

Oudah, S. S. and M. A. S. (2022). Experimental and numerical study of low concentration and water-cooling effect on PV module performance. *Case Studies in Thermal Engineering*, *34*, 102007.

Parthipan, J., Raju, B. N., & Senthilkumar, S. (2016). Design of one axis three position solar tracking system for paraboloidal dish solar collector. *Materials Today: Proceedings*, *3*(6), 2493–2500.

Patel, M. R. (1999). *Wind and Solar Energy*. CRC Press LLC London.

Rafaty, R., Dolphin, G., & Pretis, F. (2020). *Carbon pricing and the elasticity of CO2 emissions*.

Roong, A. S. C., & Chong, S.-H. (2016). Laboratory-scale single axis solar tracking system: Design and implementation. *International Journal of Power Electronics and Drive Systems*, *7*(1), 254.

Saeedi, M., & Effatnejad, R. (2021). A New Design of Dual-Axis Solar Tracking System with LDR sensors by Using the Wheatstone Bridge Circuit. *IEEE Sensors Journal*.

Salah, O. and. (2021). Performance analysis and electrical production of photovoltaic modules using active cooling system and reflectors. *Ain Shams Engineering Journal*, *12*(2), 2009–2016.

Salih, M. M. M., Alomar, O. R., Ali, F. A., & Abd, H. M. (2019). An experimental investigation of a double pass solar air heater performance: A comparison between natural and forced air circulation processes. *Solar Energy*, *193*, 184–194. https://doi.org/10.1016/J.SOLENER.2019.09.060

Tangi, S. (2017). Comparative study of Solar panel positioning system using single-axis and dual-axis tracking system. *Journal of Electrical Engineering*, *17*(2), 5.

Tsoutsos, T., Frantzeskaki, N., & Gekas, V. (2005). Environmental impacts from the solar energy technologies. *Energy Policy*, *33*(3), 289–296.

Vermaak, H. J. (2014). Techno-economic analysis of solar tracking systems in South Africa. *Energy Procedia*, *61*, 2435–2438.

Wang, G., Wang, B., Yao, Y., Lin, J., Chen, Z., & Hu, P. (2020). Parametric study on thermodynamic performance of a novel PV panel and thermal hybrid solar system. *Applied Thermal Engineering*, *180*, 115807.

Wikipedia. (2021). *Zakho city*. https://En.Wikipedia.Org/Wiki/Zakho.

Xu, R., Ni, K., Hu, Y., Si, J., Wen, H., & Yu, D. (2017). Analysis of the optimum tilt angle for a soiled PV panel.

Energy Conversion and Management, *148*, 100–109.

Zhao, D., Xu, E., Wang, Z., Yu, Q., Xu, L., & Zhu, L. (2016). Influences of installation and tracking errors on the optical performance of a solar parabolic trough collector. *Renewable Energy*, *94*, 197–212. https://doi.org/https://doi.org/10.1016/j.renene.2016.03.036

Zubeer, S. A., & Ali, O. M. (2021). Performance analysis and electrical production of photovoltaic modules using active cooling system and reflectors. *Ain Shams Engineering Journal*, *12*(2), 2009–2016. https://doi.org/10.1016/j.asej.2020.09.022

Zubeer, S. A., & Ali, O. M. (2022). Experimental and numerical study of low concentration and water-cooling effect on PV module performance. *Case Studies in Thermal Engineering*, *34*. https://doi.org/10.1016/j.csite.2022.102007

Author Information

Veen Sagvan Qader
University of Zakho
Zakho, Kurdistan Region, Iraq
Contact e-mail:*Veensagvan96@gmail.com*

Omar Mohammed Ali
University of Zakho
Zakho, Kurdistan Region, Iraq

Nawfal Idrees Hasan
University of Mosul
Mosul, Iraq

To cite this article:

Qader, V. S., Ali, O. M., & Hasan, N. I. (2022). Technical, economic and environmental comparison of three different grid-connected PV tracking systems power plant under Kurdistan region/Iraq climate condition. *The Eurasia Proceedings of Science, Technology, Engineering & Mathematics (EPSTEM), 17,* 102-119.

Implementation of Essence Practice into Bayesian Networks

Lidiya IVANOVA
Tomsk State University

Denis ZMEEV
Tomsk State University

Oleg ZMEEV
Tomsk State University

Abstract: Modern project management in software engineering still lacks a commonly accepted applicable formal model of projects that can be used for accumulating experience or for developing applied optimization methods that can potentially help IT companies to reduce risks and deliver software in a more efficient way. The Essence language which was developed by SEMAT initiative can potentially work as such a formal model for software projects, but current Essence practitioners mostly focus on methodology work for describing different approaches to perform tasks for software projects. In this work, we propose a way to develop a prototype of a decision support system based on the Essence kernel and language in combination with an applied optimization model. In order to do this, we firstly design how to include Essence practice in an applied math model and then modify a Bayesian network that finds false-positive manager mistakes. As an example of implementation of the achieved results, we present the current state of the plugin for the software project management system Redmine that uses our approach to help managers of projects.

Keywords: Bayesian network, Essence, Project Management, Redmine, SEMAT

Introduction

Statistics provided by the Standish Group in the new CHAOS Report (Portman 2020: Beyond infinity», 2021) show that only about 31% of projects succeed, 50% cause difficulties, and 19% fail, with this value barely changing in recent years. Statistics collected from sources (Project Smart, 2009; Wojewoda & Hastie, 2015) are shown in Table 1. From these data, it can be concluded that the IT industry is an area with a high proportion (about 70%) of outcomes that cannot be called completely successful. Given the rapid growth of the industry and its impact on the economy, the need to increase the proportion of successful projects, and hence the scope of works devoted to the study of this problem, is relevant.

Table 1. Project success statistics from CHAOS reports

	2011	2013	2015	2020
Successful	29%	31%	29%	31%
Challenged	49%	50%	52%	50%
Failed	22%	19%	19%	19%

Over the past 10 years, many tools have appeared in the field of software development that facilitate the technical component of the development process: new versions of integrated development environments, automatic code analysis and refactoring tools, new programming languages with concise syntax, various frameworks and libraries that can significantly increase the speed of software development and its quality.

However, the technological breakthrough apparently did not affect the percentage of successful completion of projects, and therefore it can be assumed that the main reason for failures is not in the technical component of the process. According to the author of Software Conflict 2.0: The Art and Science of Software Engineering (Glass, 2006), the reasons for failures in the computer industry are: inability to estimate (project deadlines, costs) due to a lack of understanding of the process, instability of requirements for the software being developed, as well as "whims and delusions" – the desire of managers and developers to find universal solutions to all emerging problems. In the field of project evaluation and planning, as well as in the field of risk management in software development, significant changes have not occurred over the past decade. The results of various scientific studies on these topics have not found their application in business, or have not been widely disseminated.

A few years ago, our team started research in the field of application of mathematical models for project management. The result of this research is a prototype of the AI assistant for software management, which uses Bayesian networks as a basic mathematical model (Ivanova et al., 2021; Zmeev, 2022). Alpha state game allows manager to evaluate current status of the project. However, our approach allows us to find internal conflicts between statements about the status of the project. The manager must indicate which checkpoints are completed in his opinion, and the tool calculates the probability of the truth of the hypothesis that these checkpoints are completed. The prototype is developed as a plugin for the Redmine project management system.
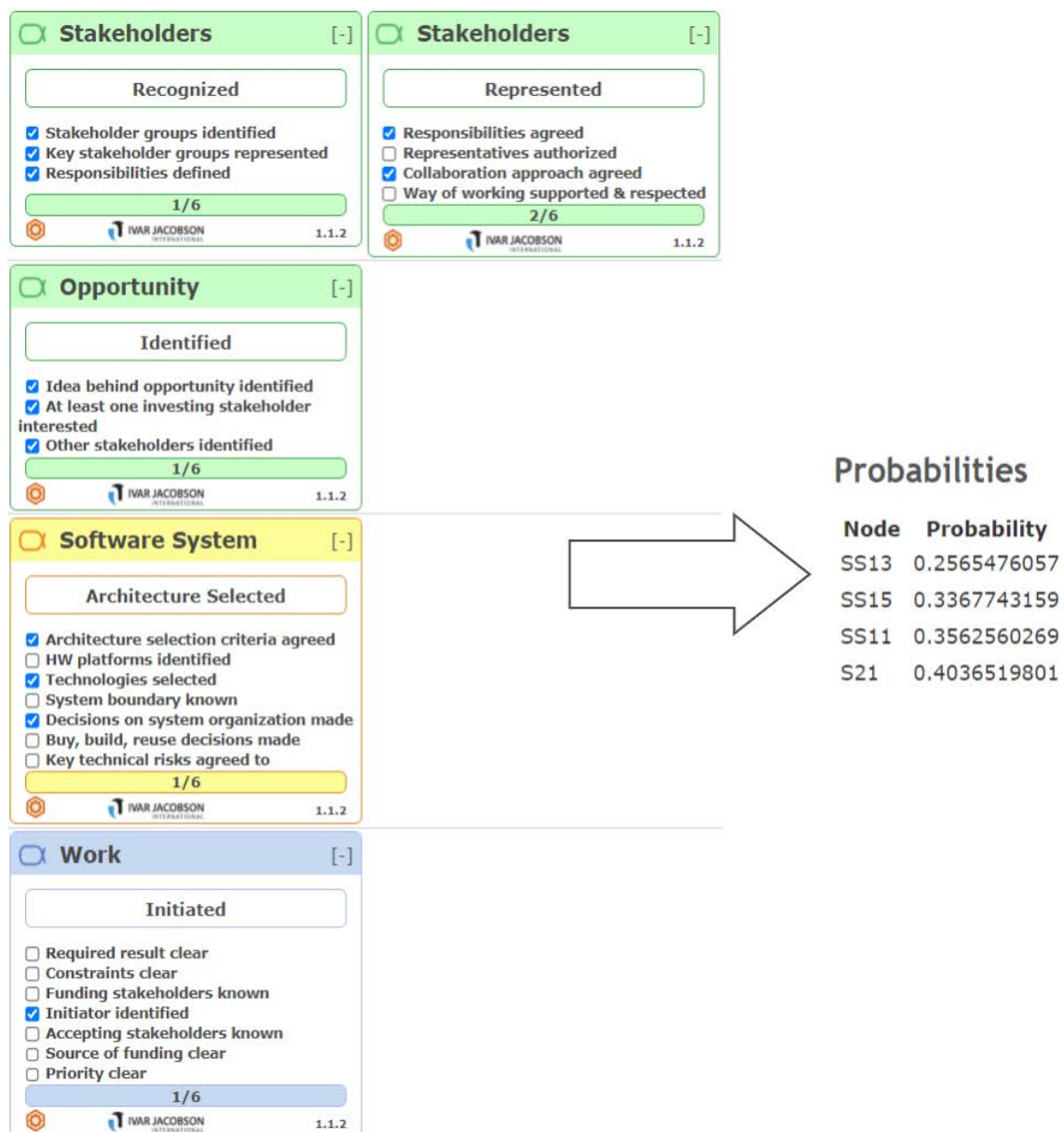

Figure 1. Prototype first version working results

Since the first version of the prototype uses only a subjective assessment – the manager's opinion in form of checkboxes from alpha state cards (Figure 1). In order to determine the probability of a manager's false-positive mistake more accurately, we decided to add accounting for objective evidence of the project progress – different work products that had been developed in the process of work. Examples of work products are source code, documentation, mockups, and so on. It should be noted that the impact of work products can be both positive and negative, since work products can be, for example, reports of errors, which has negative meaning. Adding new functionality will allow expanding the set of Essence language entities supported by the prototype.

This paper presents a method for accounting for work products in a Bayesian network and the probabilistic inference counting algorithm for determining the probability of the truth of a hypothesis corresponding to a statement about the state of a software development project. Section 2 presents a Bayesian network configuration designed to account for the presence of work products and their levels of details. Section 3 contains the algorithm developed for conditional probability counting, which takes into account both the positive and negative impact of the evidence, as well as the number of instances of work products corresponding to the evidence. Section 4 presents the results of calculations for a project that is at the initial stage of development.

Accounting Work Product in a Bayesian network

Work products, their number, and levels of detail change throughout the life cycle of a project, so it is necessary to dynamically rebuild the Bayesian network at each iteration. As an example, consider a project in which 4 work products «Antipattern Report» were created. This work product is evidence of an antipattern in the system – a common inefficient solution to a commonly occurring design and/or implementation problem. The levels of detail achieved are shown in Figure 2. Achieved levels of detail are marked with a checkmark.
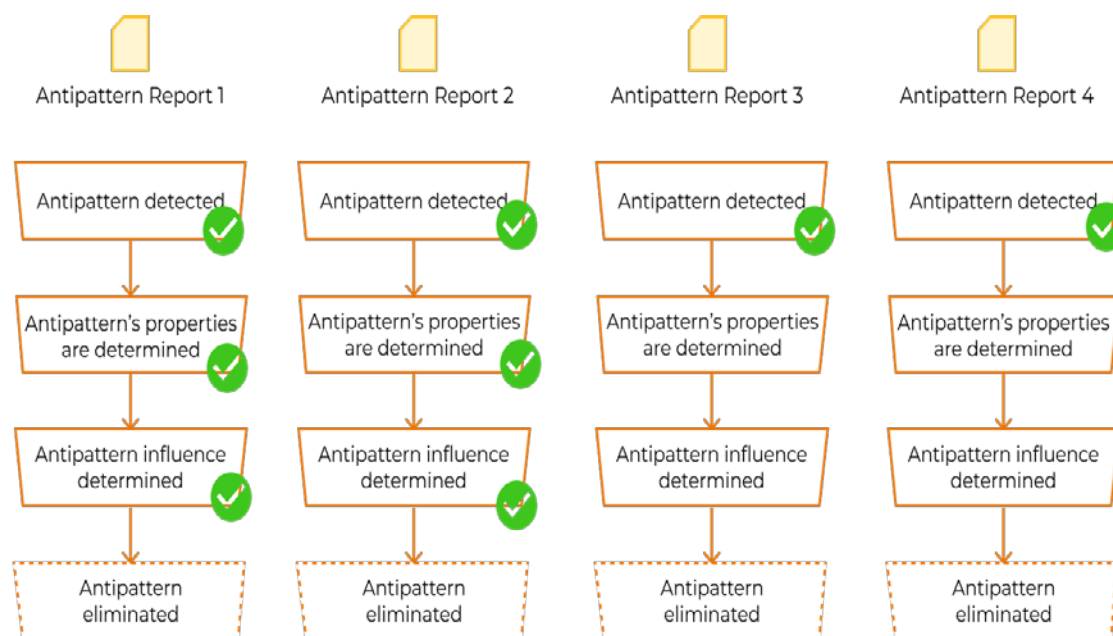
Figure 2. Work products and their levels of detail

The presence of such work products affects the statement about the Software System «Key technical risks are agreed», and the strength of evidence and its sign depends on the level of detail. In the first level of detail, Antipattern Report has a negative meaning because it is a potentially future technical risk. However, if antipattern influence determined Antipattern Report become positive evidence because we have more information about this part of the code.

In the process of research, various configurations of nodes and edges were considered to display information about work products. Figure 3 shows the resulting Bayesian network configuration for the above example. This configuration involves creating a node for each level of detail that affects a specific state node and the corresponding dependency.

Figure 3. Bayesian network nodes and edges for Antipattern Reports accounting

This configuration has the following advantages:

- slow increase in the number of nodes when adding new work products and practices. Since nodes are being created for the levels of detail, the rate of increase in their number and the number of dependencies will be rather low;
- a small number of edges to the state nodes of the project. The experience of using the prototype has shown that if a node has more than 40 pare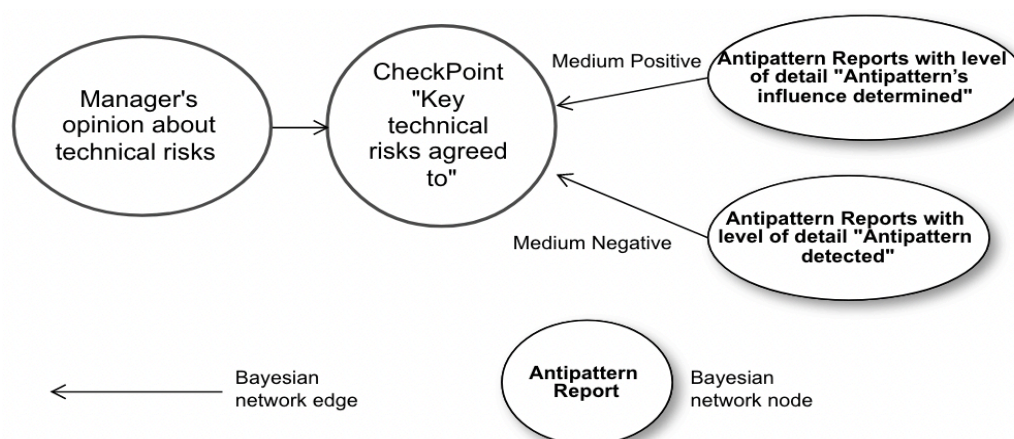nt nodes, the calculation of a probabilistic inference takes several hours. In this regard, it is necessary to reduce the number of dependencies as much as possible. At the moment, there are nodes in the system that have 15 parent nodes.

The disadvantage of this configuration is the need to determine the strength of the evidence of the added nodes since it is necessary to take into account the number of work products that have reached the appropriate level of detail. Dynamic rebuilding of the Bayesian network creates a problem of obtaining and storing conditional probabilities. In the first version of the prototype, conditional probabilities were predetermined and stored as a probability vector. The fact is that with a large number of practices, the size of the vector increases very quickly, which negatively affects both performance and the memory used. In addition, the vector cannot be predetermined because the set of practices may change during project development. Because work products can have a negative impact on the project progress, handling for this impact needs to be added. Also, keep in mind that work products are not unique. For example, requirements analysis creates many use case diagrams. Therefore, it is necessary to take into account the number of work products of a certain type.

Conditional Probability Counting Algorithm Modification

The main difficulty is the determining conditional probabilities. When adding practices supported by the team, it is not possible to build a vector in advance, since the number of work products, and their levels of detail change with each iteration of the project. In addition, the team can combine several practices. Therefore, it was decided to abandon the storage of conditional probabilities and calculate them during the operation of the main algorithm.

Consider the case shown in Figure 2. It is necessary to determine the probability that the node corresponding to the Software System «Key technical risks agreed to» alpha checkpoint is true, that is, the probability that the hypothesis that all key technical risks of the project are agreed is true. Let us denote this hypothesis as H, and denote the opposite hypothesis that this checkpoint is false, denote it as $\neg$H. The presence of work products with a level of detail is evidence that can affect the likelihood of our hypothesis being true. Let us denote the evidence corresponding to the level of detail «Antipattern detected» as e_1, the evidence corresponding to the level of detail «Antipattern's influence determined» as e_2. There is an interpretation of the influence of evidence on the change in the ratio of conditional probabilities of mutually exclusive hypotheses H and $\neg$H, presented in the form of a line, the center corresponds to the ratio of equiprobability of these two hypotheses (Bayes, n.d.). The appearance of evidence shifts the pointer toward the hypothesis favored by the evidence by an amount corresponding to the strength of the evidence's influence.

Figure 4 shows an example from the specified source, in which the ratio of prior probabilities of hypotheses is 1, the circles indicate the occurrence of evidence with a 2:1 chance in favor of hypothesis H. It was decided to use this approach to determine the conditional probabilities for the Bayesian network nodes instead of storing the conditional probabilities as a probability vector.
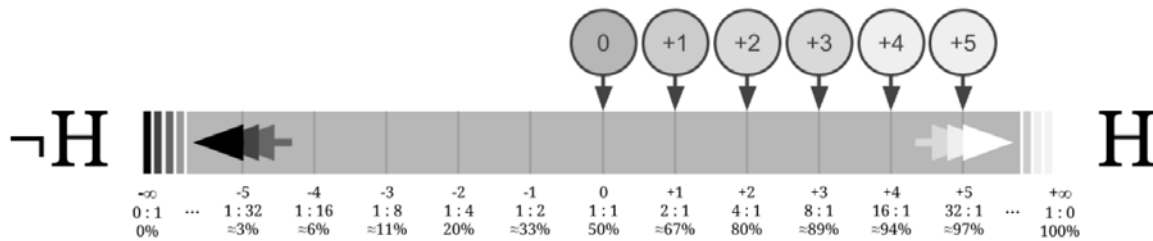

Figure 4. Log-odds line («Bayes' rule: Log-odds form», n.d.)

For the convenience of calculations, we represent the change in the ratio of conditional probabilities as a power of two, that is, 2^k, where k is the strength of the influence of the evidence. Thus, stronger evidence will change the ratio more than weaker evidence. If evidence has a positive impact on the project (evidence is a positive factor in the development of the project), there are two possible cases: the true value of the evidence in favor of H will increase the conditional probability of the hypothesis H. A false value for evidence will decrease the probability of hypothesis H.

Since some work products, such as an antipattern report, can have a negative impact on the project, it is necessary to consider the appropriate cases:

1. Evidence affects negatively. The evidence is the truth. The probability that hypothesis H is true decreases.
2. Evidence affects negatively. The evidence is false. The probability of hypotheses does not change, since the absence of fixed problems or risks in the project does not mean that there is progress, nor that there are any obstacles to development.

With the approach described above, we can determine the conditional probability for positive and negative evidence. However, as mentioned earlier, the chosen Bayesian network configuration gives rise to the problem of determining the strength of influence. The strength of influence, in this case, should depend on the number of work products that have reached these levels of detail. At the same time, it is necessary to remember such indicators as the size of the project (small, medium, large), as well as some norms for the number of work products adopted by the creators of practices.

To account for project size and recommendations for the number of work products it's necessary to define new coefficients:

- project scale – a coefficient reflecting a subjective assessment of the ratio of the project size in relation to a typical project for a set of practices used. This parameter was introduced to ensure further scaling of the mathematical model for various projects.
- norm – the number of instances of the work product, characteristic of a typical project, according to the author of a particular practice.

These concepts have already been encountered in the software engineering literature. For example, A. Jacobson argues that « A really large system might have seven use cases» (Cockburn, 2016). The authors of (Jacobson et al., 1999) speaking of use-case models, state that «at the end of the design phase, these models are less than 10% complete. Standing apart are use-case and analysis models, which … can include significantly more (up to 80% in some cases)». Thus, the researchers also point to the existence of some standards that determine the number of work products for projects, depending on the scope of the project. Over fulfillment of such a «norm» is considered redundant, since the creation of an additional work product instance in excess of the «norm» does not make a major contribution to the project. Let N be the number of work products of a particular type with the level of detail being considered. The following situations are possible:

1. N = 0. The strength of evidence does not change.
2. N < norm * scale. It is necessary to reduce the strength of evidence.

3.   N = norm * scale. The strength of evidence does not change.
4.   N ≥ norm * scale. The power of evidence is increasing. In the case of exceeding the product of the norm by the scale, the increase in the strength of evidence should be insignificant, since the excess of the number of work products of the recommended standards is more likely evidence of overengineering and formalism than the basis for a significant increase in the strength of evidence.
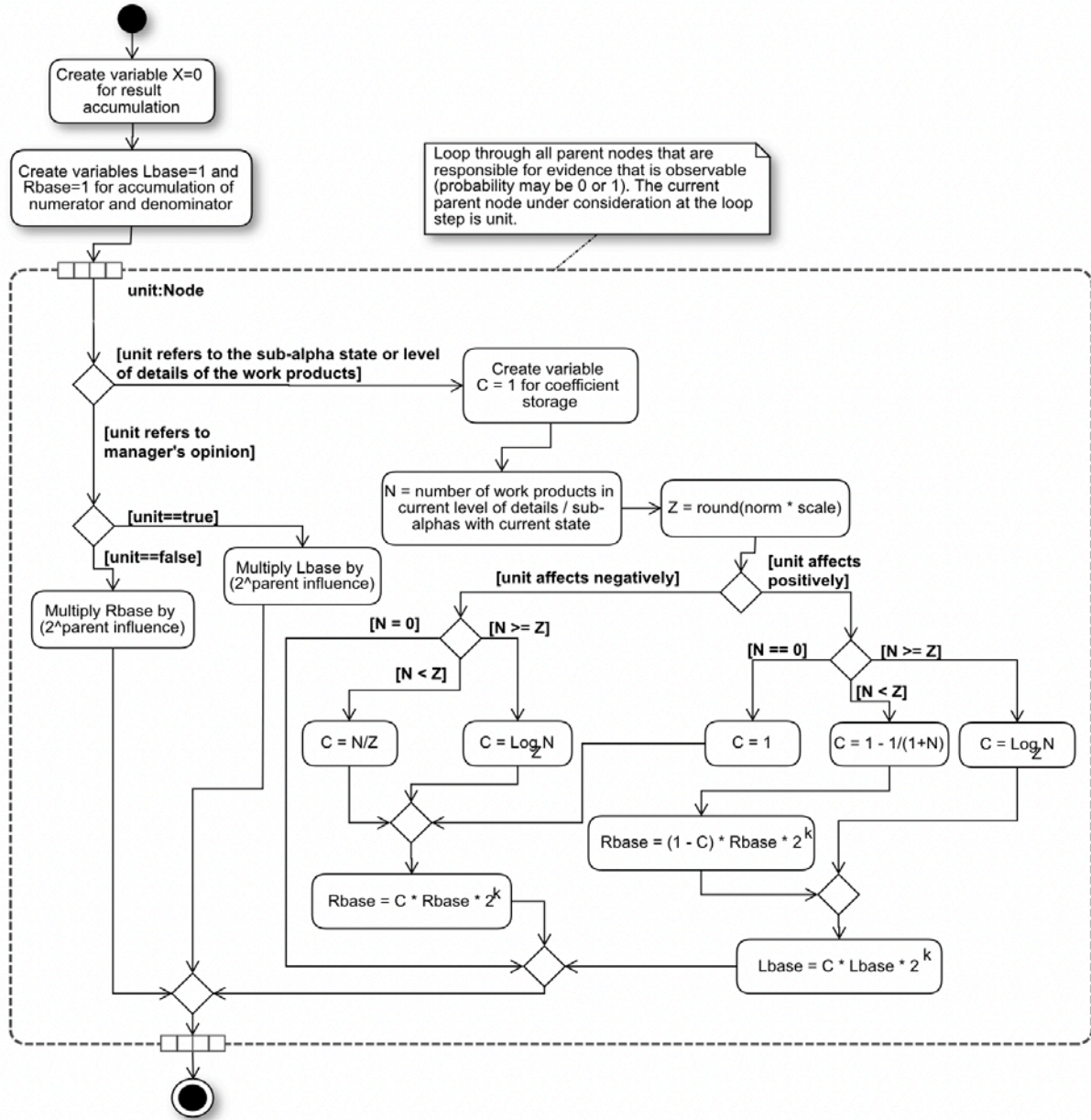
Figure 5. Parents corresponding to work products and sub-alphas

Let us designate the coefficient of change in the strength of influence as C. The value of C for evidences with positive impact is determined by the formula (1):

$$C = \begin{cases} 1, & if\ N = 0 \\ 1 - \dfrac{1}{1+N}, & if\ N < norm * scale \\ 1, & if\ N = norm * scale \\ log_{norm*scale}N, & if\ N > norm * scale \end{cases}$$

(1)

The value of C for evidences with negative impact is determined by the formula (2):

$$C = \begin{cases} 1, if\ N = 0 \\ \dfrac{N}{norm * scale}, if\ N < norm * scale \\ 1, if\ N = norm * scale \\ log_{norm*scale}N, if\ N > norm * scale \end{cases} \quad (2)$$

Since all aspects related to the addition of work product accounting have been determined, it is necessary to consider modifying the algorithm for calculating conditional probability. The algorithm can be divided into two steps. In the first stage (Figure 5), all parent nodes that correspond to work products and sub-alphas are processed. The second one (Figure 6) considers the parent nodes corresponding to the alphas of the project.

Figure 6. Parents corresponding to alphas

Prototype Working Results

Figure 7 shows the results of calculations made using the new version of the evolutionary prototype for one iteration in the absence of data on antipatterns. At the same time, the manager believes that the «Key technical risks agreed to» checkpoint is set to «true». The value of the checkpoint «Decision on system organization

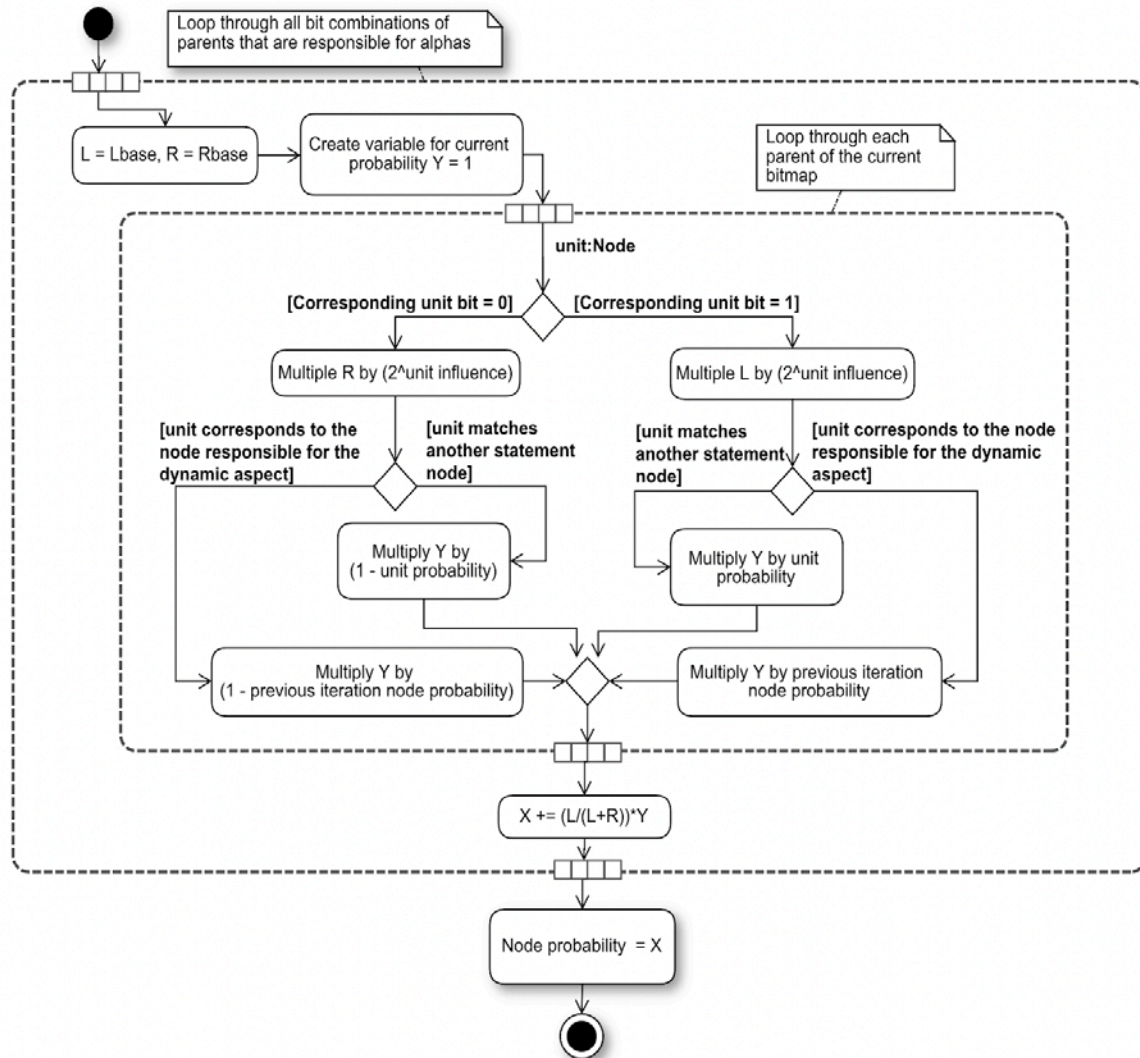made» is highlighted in red, because, according to the manager, it has the value «true», however, according to calculations, the probability of the system being in this state is less than the threshold value of 0.5.

SS12
HW platform identified — 0.9642030079856995

SS13
Technologies selected — 0.9292076292467458

SS14
System boundary known — 0.37379982672146667

SS15
Decision on system organization made — 0.486922066859319

SS16
Buy, build, reuse decisions made — 0.5671586499695527

SS17
Key technical risks agreed to — 0.8414990475820213

SS21
Key architecture characteristics demonstrated — 0.00034260709771812323

SS22
System exercised &perfomance measured — 0.012925077001684044

SS23
Critical HW configurations demonstrated — 0.007732808408702965

SS24
Critical interfaces demonstrated — 0.005017596635103755

Figure 7. Results of calculations in the absence of data on antipatterns

Table 2 shows the values of the probability of truth for the Software System «Key technical risks agreed to» checkpoint, which can be affected by the presence of antipatterns in the system. The test project is at the initial stage of development.

Table 2. Probability values for checkpoint «Key technical risks agreed to»

Case	«Key technical risks agreed to» probability
Information about work products is not counted	0,841499
4 work products with a negative impact	0,662517
2 work products with a negative impact, 2 with positive impact	0,88555
4 work products with a positive impact	0,90467
16 work products with a negative impact	0,629207

The results of the calculations demonstrate the impact that the presence of work products has on the probability of the project being in a certain state. This information adds an objective dimension that helps improve the accuracy of the estimate given by the prototype.

Conclusion

The second version of the system allows us to take into account objective evidence of project progress. Thus, the manager does not need to constantly check which work products have appeared in the system and what their status is. The applied method for determining conditional probabilities made it possible to abandon the storage of probability vectors, which had a positive effect on the memory used.

We see the following directions of development for the proposed approach: the dependence functions of the strength of the influence of evidence on the number of evidence can have a different form, and it is necessary to take into account the degree of the formalism of the method used. For example, the Unified Process is a more

rigorous method than Scrum. In addition, the development of the tool requires the creation of a repository of practices, as well as additional research on the issue of Bayesian network learning based on statistical data.

Scientific Ethics Declaration

The authors declare that the scientific ethical and legal responsibility of this article published in EPSTEM journal belongs to the authors.

Acknowledgements or Notes

References

Bayes (n.d.) *Bayes' rule: Log-odds form.* Arbital. Retrieved March 1, 2022, from https://arbital.com/p/bayes_log_odds/

Cockburn, A. (2016). *Writing effective use cases*. Addison-Wesley.

Glass, R. L. (2006). *Software conflict 2.0: The art and science of software engineering*. Developer.

Ivanova, L. S., & Rafikova, R. R., & Zmeev, D. O. (Eds.). (2021). *Presenting the progress of a software development project in the form of a dynamic Bayesian network*. Information technologies and mathematical modelling (ITMM-2020). Proc. of the ninth international conference named after A.F. Terpugov, 291–297.

Jacobson, I., Booch, G., Aguilar, J. L., Pimentel, E., Rumbaugh, J., & Sánchez Salvador. (1999). *The Unified Software Development process*. Addison-Wesley.

Portman, H. (2021). *Review Standish Group – Chaos 2020: Beyond infinity*. Retrieved July 1, 2022, from https://hennyportman.wordpress.com/2021/01/06/review-standish-group-chaos-2020-beyond-infinity/

Project Smart (2009). *The curious case of the chaos report.* Retrieved March 1, 2022, from https://www.projectsmart.co.uk/it-project-management/the-curious-case-of-the-chaos-report-2009.php

Wojewoda, S., & Hastie, S. (2015, October 4). *Standish Group 2015 chaos report - Q&A with Jennifer Lynch.* InfoQ. Retrieved February 1, 2022, from https://www.infoq.com/articles/standish-chaos-2015/

Zmeev, D. O. (2022). *Decision support system prototype for project management based on OMG Essence Standard and Bayesian networks.* [Candidate's dissertation]. Tomsk State University.

Author Information	
Lidiya Ivanova	**Denis Zmeev**
Tomsk State University	Tomsk State University
36, Lenin Avenue, Tomsk, 634050, Russia	36, Lenin Avenue, Tomsk, 634050, Russia
Phone.: +7 (382-2) 52-97-93	Phone.: +7 (382-2) 52-97-93
Contact e-mail: *lidiya.ivanova@persona.tsu.ru*	Contact e-mail: *denis.zmeev@accounts.tsu.ru*

Oleg Zmeev
Tomsk State University
36, Lenin Avenue, Tomsk, 634050, Russia
Phone.: +7 (382-2) 52-97-93
Contact e-mail: *ozmeyev@gmail.com*

ICRETS 2022: International Conference on Research in Engineering, Technology and Science

Identifying the Antecedents of Public Trust in the Citizen-Centric E-Governance

Seyed Mohammadbagher JAFARI
University of Tehran

Sara NIKBAKHSH
Islamic Azad University

Parvane KOMIJANI
University of Tehran

Fatemeh KARIMI
University of Tehran

Abstract: For the success of e-governance, its focus must shift to a value-oriented and citizen-informed approach that is called citizen-centric e-governance. Trust is one of the most important issues that lead citizens to use a citizen-centric e-governance system. However, its role in accepting and using e-governance systems has not been investigated enough. The primary purpose of this study is to explore and identify the antecedents of public trust in citizen-centric e-governance. By reviewing related literature, the antecedents of public trust were extracted and tested via the survey method. Information accessibility, system quality-security, and regulation and policy environment were identified as the antecedents of public trust. Using the data of 356 questionnaires, the developed hypotheses in the research were tested via the structural equation modeling (SEM) technique. The results confirmed that the relationship between system quality-security and regulation and policy environment with public trust were significant. However, the influence of information accessibility on public trust was not significant among the research population.

Keywords: Citizen-Centric, E-Governance, Public Trust

Introduction

The rapid evolution of new technologies has created challenges for all governments, and citizens are becoming electronic communities that formulate, influence, and contribute toward their own "public value" (Riley, 2003). E-governance has been located between two global shifts, the governance revolution and the information revolution. Both of these shifts are changing the way that society is governed and the way society works (Heeks, 2001). Basically, the political debate now considers that the Internet and the Web will play a crucial role in transforming relationships between the state and citizens. Therefore, it can be considered that e-governance is the next step for e-government development (Kolsaker & Lee-Kelley, 2007). According to Kašubienė, and Vanagas (2007, p. 70), citizens are more likely eager to use e-government portals that are designed to address their needs and are indeed citizen-centric. According to Singh and Singh (2018), by automating and accelerating the government-citizen relationship with ensuring governance transparency, e-governance has the capacity of a package of benefits to citizens. However, despite the global diffusion of e-governance programs, the claimed benefits of e-governance have not been easily attained for various organizational and technological causes (Saxena, 2005). Several studies have shown that e-governance in realism has been unsuccessful in reaching what it promises before (Liu et al., 2008; Madon, 2004; Reichheld and Markey, 2000). There are many reasons

for failure, and according to Heeks (2001), a major reason is a mismatch between the new system and the present reality. The implementers fail to recognize the difference between the social context, including people, culture, politics, etc., it operates and the real technology (Dada, 2006). Saxena (2005) has emphasized that the reason for the high rate of failure in e-governance initiatives is often a techno-centric concentration rather than a citizen-centric one. For the success of e-governance, the focus of it must shift to a value-oriented and citizen-informed approach (Kolsaker & Lee-Kelley, 2007). However, much of the research on e-governance focuses on the technical and practical factors, and this approach obscures an important and significant factor, the needs of users that here are citizens (Bertot & Jaeger, 2006). One of the most important subjects that lead citizens to use e-governance systems is trust. Therefore, the antecedents of public trust in a citizen-centric e-governance system should be identified to provide more insight into citizens' usage of e-governance systems.

Review of Related Literature

Public Trust

As Pavlou (2003) indicated, citizens need to be certain that their online communication with the government is safe since they use an open technological infrastructure, like the Internet. According to Belanger and Carter (2008), citizens will only use the e-government if they are certain it is reliable. Roy (2005) has claimed that public trust and public assurance are key factors of e-governance success. Several studies debated the citizens' needs for trust of e-government or e-governance and its effect on the success, usage, adoption, and satisfaction of these systems (Belanger & Carter, 2008; Shareef et al., 2011).

Service Quality-security

Security is typically one of the key aspects of e-governance systems (Murthy & Kumar, 2003) that citizens need. The definition of service quality-security is "support of citizens in their needs for security in e-governance systems."

Regulation and Policy Environment

There are several features that affect the citizens' intention to use and, in fact, actual usage of e-governance systems. Dawes (2008) and Paskaleva-Shapira (2006) have highlighted the significance of policies and regulations and their effect on e-governance success. Chauhan et al., (2008) have reported that legislation for driving and regulating e-governance has recently been enacted by various countries. UNDP (2010) called for public investments to provide the implementation and creation of e-governance regulations, policies, and legislation. The protocols, policies, and data management mechanisms will balance each citizen's privacy protection with efficient and effective usage of that information by the government (Dawes, 2009). Then, the readiness of these regulations and policies more assures those citizens to advance trust in using e-governance systems.

Information Accessibility

UNDP (2010) defined Information accessibility as "promoting the digitalization and dissemination of public information among the overall population." It also refers to promoting the formation of national regulation on Information accessibility, i.e., freedom of information acts. The dissemination and digitalization of public information among the whole population is one of the cross-cutting parts of an e-governance environment. There are a number of studies that support this notion (Dawes, 2008; Jaeger & Bertot, 2010; Jiang & Xu, 2009; Saxena, 2005; Shareef, et al., 2010). The governments have to promote the creation of national regulation on Information accessibility (A2I), which is critical for the success of e-governance systems since the accessibility makes the citizens trust the systems (Paskaleva-Shapira, 2006).

Theoretical Framework and Hypotheses Development

Public Trust and Service Quality-Security

Several studies have highlighted the role of security as an antecedent of citizens' trust in the e-governance or e-government systems (Akkaya et al., 2011; Belanger & Carter, 2008; Lean et al., 2009; Park, 2008; Shareef, et al., 2011). Better quality of e-governance services shapes better trust in citizens (Bhatnagar & Singh, 2010). Akkaya et al. (2011) indicated that when the government is the service provider, skepticism increases among the citizens. Principally, citizens have a tendency to suspect that the government lookouts everything and collects data about citizens through several channels (Belanger & Hiller, 2006). Consequently, citizens do not trust the government if they do not exactly recognize in what way the data collected is used by the public authorities (Akkaya et al., 2011). Therefore, the security features of e-governance systems are very important for building trust among citizens. According to Shareef et al. (2011), security issues are one of the potential providers in developing trust among citizens for the usage of e-governance systems. Based on these arguments, we posit the following hypothesis:

H1: Service quality-security will have a positive relationship with public trust in e-governance systems.

Public Trust and Information Accessibility

One of the aspects that increase the trust and confidence of the citizens in e-governance systems (Paskaleva-Shapira, 2006) is the dissemination and digitalization of public information among the whole population and the provision of specific conditions and rules for sharing, gathering, protecting, and using information by individuals, government, and the private sector via e-governance systems (Dawes, 2008, 2009). As it has been noted by the Pacific Council on International Policy (2002), more public Information accessibility via e-government makes the government more accountable to its citizens. Therefore, it enhances public trust. A study by Isaac (2007) shows that the availability of government information to citizens is one of the enablers of public trust in e-governance systems. Therefore, we posit the following hypothesis:

H2: Information accessibility will have a positive relationship with Public trust in e-governance systems.

Public Trust and Regulation and Policy Environment

Chen and Hsieh (2009) noted that the availability of regulation and policy on e-governance would encourage citizens to use these systems by attracting their trust. Actually, it occurs since citizens will feel much safer and more confident conducting online transactions with the government (Wong et al., 2007). Therefore, if citizens feel that they are not protected by laws and regulations and are exposed to misuse by e-governance systems, they will not use these systems. Consequently, the availability of policy and regulation is necessary for building public trust in e-governance. Therefore, we posit the following hypothesis:

H3: Regulation and policy environment will have a positive relationship with Public trust in e-governance systems.

The conceptual framework of the research can be drawn as Figure 1 based on the above discussion.
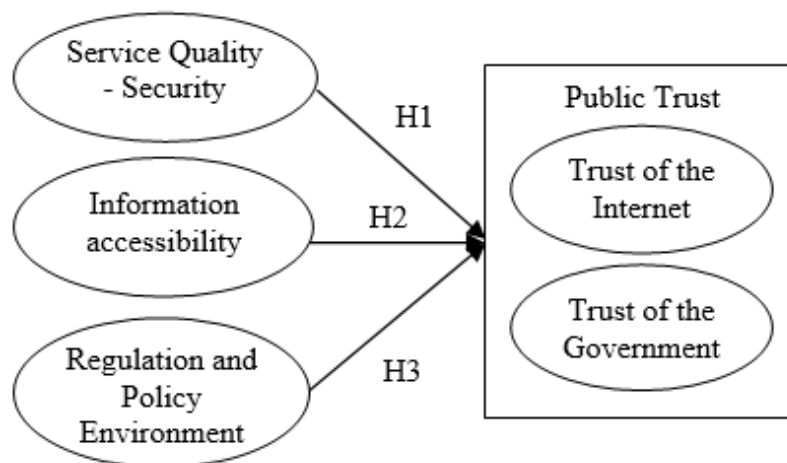

Figure 1. Conceptual framework

Method

The population of this research was the citizens who were familiar with government online services. Using the convenience sampling method, 356 questionnaires were collected. The measures used to evaluate variables are shown in Table 1.

Table 1. Measures

Variable	Dimension	No. of Items	Sources
Service Quality – Security	---	6	Dawes (2009), Kolsaker and Lee-Kelley (2008), Verdegem and Verleye (2009)
Information accessibility	---	3	Dawes (2009), Jiang and Xu (2009), Park (2008)
Regulation and policy environment	---	3	Chen and Hsieh (2009), Wong et al. (2007)
Public Trust	Trust of the Internet	3	Belanger and Carter (2008)
	Trust of the Government	4	Belanger and Carter (2008)

In order to measure each item in the questionnaire, a 5-point Likert scale that measures from "strongly agree" to "strongly disagree" has been used. The reliability test showed that the Cronbach alpha values for all the constructs were in the acceptable range, as shown in Table 2.

Table 2. Cronbach's Alpha for The Measurement Scales

Scale	Cronbachs' alpha
Service Quality – Security	0.786
Information Accessibility	0.722
Regulation and Policy Environment	0.876
Public Trust	0.865

Results

Descriptive Statistics

The characteristics of the respondents are: (1) 46% were males, and 54% were females, (2) 50% had used the applications of e-governance systems for more than three years, (3) 60% had a bachelor's degree or higher qualifications and (4) 51% were 30 years old or younger. Descriptive statistics (mean, standard deviation), composite reliability (CR), and average variance extracted (AVE) of all constructs are given in Table 3.

Table 3. Mean, standard deviation, composite reliability (Cr), average variance extracted (Ave)

Construct	Mean	Std. Deviation	CR	AVE
Service Quality-Security	4.6325	.50923	0.89	0.59
Information accessibility	4.1732	.69175	0.84	0.64
Policy Environment & Regulation	4.3408	.66709	0.91	0.78
Public Trust	3.2604	.92177	0.90	0.75

Testing of Hypotheses

The hypotheses were tested by running the SEM structural model using Amos software. The testing results (with significant relationships) are given in Figure 2. All hypotheses have been supported except the following. The hypothesis that links Information accessibility and public trust has not been supported. These imply that citizens do not consider Information accessibility as a key to enhancing public trust and increasing user satisfaction.
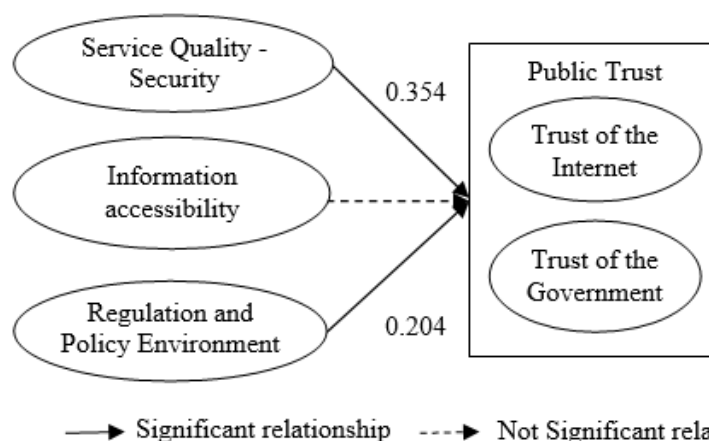
Figure 2: Research Framework with Hypothesized and Significant Relationships

Discussion

Our research has several significant findings. First, the positive relationship (β=0.354, p-value= 0.001) between service quality (security) and public trust is established. This relationship indicates that the more secure the e-governance systems are the more trust is developed by the citizens on these systems. The role of security as one of the antecedents of citizens' trust in e-governance systems has been emphasized by previous studies (Belanger & Carter, 2008; Lean et al., 2009; Park, 2008; Shareef, et al., 2011). The trust-building mechanisms are necessary for government agencies to make citizens feel confident about the security functions resulting in increased usage of e-governance systems. Second, the relationship between regulation and policy environments and public trust (β = 0.204, p-value = 0.019) is supported. The availability of policy and regulation on e-governance encourages citizens to have trust in the e-governance systems and use these systems. Dawes (2008) and Paskaleva-Shapira (2006) have highlighted the importance of regulations and policies for e-governance systems and their effect on system success. Wong, et al. (2007) has stated that the availability of policy and regulation makes citizens feel safer and more confident in performing online transactions with the government. The availability of privacy and security laws makes citizens feel confident with the authorities' intention to prevent criminal activities in cyberspace regarding privacy attacks or security violations of any e-governance system through unauthorized access by hackers. Facilitating laws and regulations on e-governance is also necessary to further encourage citizens to participate and interact online with the government.

Conclusions

This study has identified and analyzed the antecedents of public trust in the citizen-centric e-governance. Based on the result, the relationship between system quality-security and public trust, and regulation and policy environment and public trust were significant. Nevertheless, the influence of Information accessibility on public trust was not significant among the research population. It is recommended that this study be conducted in different countries with different e-governance systems to provide more insight into the antecedents of public trust in different contexts. If the policymakers and the government agencies that design and implement the e-governance systems notice the recommendations given in this study, the citizens' trust will increase, resulting in enhanced citizen satisfaction.

Scientific Ethics Declaration

The author declares that the scientific ethical and legal responsibility of this article published in EPSTEM journal belongs to the author.

Acknowledgements or Notes

References

Akkaya, C., Obermeier, M., Wolf, P. & Krcmar, H. (2011). Components of Trust Influencing eGovernment Adoption in Germany, In M. Janssen, H. Scholl, M. Wimmer & Y.-h. Tan (Eds.), *Electronic Government* (6846, 88-99): Springer Berlin / Heidelberg.

Belanger, F. & Carter, L. (2008). Trust and risk in e-government adoption, *The Journal of Strategic Information Systems*, *17*(2), 165-176.

Belanger, F. & Hiller, J. S. (2006). A framework for e-government: privacy implications, *Business Process Management Journal*, *12*(1), 48-60.

Bertot, J. C. & Jaeger, P. T. (2006). User-centered e-government: Challenges and benefits for government Web sites, *Government Information Quarterly*, *23*(2), 163-168.

Bhatnagar, S.C. & Singh, N. (2010). Assessing the impact of e-government: a study of projects in India, *Information Technologies and International Development*, *6*(2), 109–127.

Chauhan, R., Estevez, E. & Janowski, T. (2008). A model for policy interventions in support of electronic governance, Proceedings from *the 2nd International Conference on Theory and Practice of Electronic Governance*, Cairo, Egypt.

Chen, Y. C. & Hsieh, J. Y. (2009). Advancing E-Governance: Comparing Taiwan and the United States, *Public Administration Review*, *69*(1), 151-158.

Dada, D. (2006). The failure of e-government in developing countries: A literature review, *The Electronic Journal of Information Systems in Developing Countries*, *27*(6), 1-14.

Dawes, S. S. (2008). The evolution and continuing challenges of e-governance, *Public Administration Review*, *68*(s1), S86-S102.

Dawes, S. S. (2009). Governance in the digital age: A research and action framework for an uncertain future, *Government Information Quarterly*, *26*(2), 257-264.

Heeks, R. (2001). Understanding e-Governance for Development, *i-Government Working Paper Series: Institute for Development Policy and Management*, University of Manchester.

Isaac, W. C. (2007). Performance measurement for the e-Government initiatives: A comparative study, PhD, *Nova Southeastern University*, Fort Lauderdale, FL.

Jaeger, P. T. & Bertot, J. C. (2010). Designing, Implementing, and Evaluating User-centered andCitizen-centered E-government, *International Journal of Electronic Government Research*, *6*(2), 1-17.

Jiang, M. & Xu, H. (2009). Exploring Online Structures on Chinese Government Portals, *Social Science Computer Review, 27*(2), 174-195. doi: 10.1177/0894439308327313.

Kašubienė, L. & Vanagas, P. (2007). Assumptions of e-government services quality evaluation, *Engineering economics*, *5*(55), 68-74.

Kolsaker, A. & Lee-Kelley, L. (2007). Mind the Gap II': E-Government and E-Governance. In M. Wimmer, J. Scholl & Å. Gronlund (Eds.), *EGOV 2007. LNCS* (4656, 35-43): Springer Berli/Heidelberg.

Lean, O., Zailani, S., Ramayah, T. & Fernando, Y. (2009). Factors influencing intention to use e government services among citizens in Malaysia, *International Journal of Information Management*, *29*(6), 458-475.

Liu, J., Derzsi, Z., Raus, M. & Kipp, A. (2008). E-governance project evaluation: an integrated framework, *Electronic Government Lecture Notes in Computer Science*, 5184, 85–97.

Madon, S. (2004). Evaluating the development impact of e-governance initiatives: an exploratory framework, *The Electronic Journal on Information Systems for Developing Countries*, *20*(5), 1–13.

Murthy, D., & Kumar, R. (2003). Software architectural design model for e-governance systems. Proceedings from *the TENCON 2003 Conference on Convergent Technologies for Asia-Pacific Region*, Bangalore.

Pacific Council on International Policy. (2002). *Roadmap for E-government in the Developing World*, Los Angeles, CA.

Park, R. (2008). Measuring Factors that Influence the Success of E-Government Initiatives, Proceedings from *the 41st Annual Hawaii International Conference on System Sciences (HICSS 2008)*, Hawaii.

Paskaleva-Shapira, K. (2006). Transitioning from e-Government to e-Governance in the knowledge society: the role of the legal framework for enabling the process in the European union's countries, Proceedings from *the Proceedings of the 2006 international conference on Digital government research*, San Diego, California.

Pavlou, P. A. (2003). Consumer acceptance of electronic commerce: Integrating trust and risk with the technology acceptance model, *International Journal of Electronic Commerce*, *7*(3), 101-134.

Reichheld, F.F. & Markey, J.R.G. (2000). E-customer loyalty – applying the traditional rules of business for online success, *European Business Journal*, *12*(4), 73–179.

Riley, T. B. (2003). E-Government vs. E-Governance: Examining the Difference in a Changing Public Sector Climate, Ottawa: The Commonwealth Secretariat and Government Telecommunications and Information Services, *Public Works and Government Services*.

Roy, J. (2005). Service, Security, Transparency & Trust: Government Online or Governance Renewal in Canada?, *International Journal of Electronic Government Research*, *1*(1), 40.

Saxena, K. B. C. (2005). Towards excellence in e-governance, *International Journal of Public Sector Management*, *18*(6), 498-513.

Shareef, M. A., Kumar, V., Kumar, U. & Dwivedi, Y. K. (2011). e-Government Adoption Model (GAM): Differing service maturity levels, *Government Information Quarterly*, *28*(1), 17-35.

Shareef, M. A., Kumar, V., Kumar, U., Chowdhury, A. H. & Misra, S. C. (2010). E-Government Implementation Perspective: Setting Objective and Strategy, *International Journal of Electronic Government Research*, *6*(1), 59-77.

Singh, V., & Singh, G. (2018). Citizen centric assessment framework for e-governance services quality. *International Journal of Business Information Systems*, *27*(1), 1-20.

UNDP. (2010). *Mapping of UNDP e-governance Activities*. Retrieved May 28, 2010, from www.sdnp.undp.org/e-gov/mapping.

Verdegem, P. & Verleye, G. (2009). User-centered E-Government in practice: A comprehensive model for measuring user satisfaction, *Government Information Quarterly*, *26*(3), 487-497.

Wong, K., Fearon, C. & Philip, G. (2007). Understanding egovernment and egovernance: stakeholders, partnerships and CSR, *International Journal of Quality and Reliability Management*, *24*(9), 92.

Author Information

Seyed Mohammadbagher Jafari
Faculty of Management and Accounting,
College of Farabi,
University of Tehran, Tehran, Iran
Contact e-mail: *sm.jafari@ut.ac.ir*

Sara Nikbakhsh
Faculty of Humanities,
Qom Branch,
Islamic Azad University, Qom, Iran

Parvane Komijani
Faculty of Management and Accounting,
College of Farabi,
University of Tehran, Tehran, Iran

Fatemeh Karimi
Faculty of Management and Accounting,
College of Farabi,
University of Tehran, Tehran, Iran

To cite this article:

Centrifugal Pump Design: An Optimization

Van Thanh Tien NGUYEN
Industrial University of Ho Chi Minh City

Thi Minh Nhut VO
Thu Dau Mot University

Abstract: A centrifugal pump is an efficient piece of machinery that is often used in the activities of our everyday lives as well as the production of industrial goods. Due to the ever-increasing demands of our contemporary lifestyle, the process of designing a pump is becoming more authoritarian and demanding. In order to assist designers in overcoming these limits, an optimization algorithm would be suggested. This algorithm would help designers use optimum design methodologies and reduce risk throughout the manufacturing stage. ANSYS's Computational Fluid Dynamics (CFD) tool was used to develop numerical models for simulation. These models were created using ANSYS. For the purpose of the multi-objective optimization design, the simulation's best-chosen model was taken into consideration. This algorithm was used throughout the process of designing the ideal solution. Several design models were created by selecting characteristics such as the size of the pump volute casing section, the tongue's length, and the tongue's angle. The findings demonstrate that the provided strategy is viable for resolving the issue with the optimal design. These findings have the potential to serve as an encouraging reference for companies that manufacture centrifugal pumps, as well as researchers who are interested in applying their invention and development to the pump design sector in the future.

Keywords: Centrifugal pump, Optimal design, Volute casing tongue, Intelligent algorithms for design

Introduction

It is safe to say that centrifugal pumps are integral to any system designed to regulate the built environment. Little has changed in the underlying physics and mechanics of pumps in the previous century. However, in recent years, the technology for using pumps has significantly advanced. Pumps are a popular area of focus in projects because of the potential for considerable energy savings that may be uncovered via field inspection and testing of pumps' performance, which is typically underutilized. Energy can be saved by adjusting pump flow rates closer to the load requirements or doing away with redundant pressure drops. Below is an illustration of how decisions made during the design process might affect the building's operation for decades. Centrifugal pumps (Abdolahnejad et al., 2022; Bamberger et al., 2020; Bellary et al., 2016)are essential gear in water treatment plants since they are the ones in charge of transferring water from one section of the plant to another. Therefore, the readers may make the most educated choice regarding the design of their pumping system (Elkholy & Fathy, 2016; Esmaeilian et al., 2019; Jegha et al., 2020). Besides, the authors determined to examine this study's various kinds of pumps and their associated efficiencies. Pumps are devices that transport something from one location to another by directing a flow of fluid via a pipe in order to do so.

A pump may be used for a variety of uses, including the circulation of fluids (Liu et al., 2013; Shim et al., 2018), such as water, oil, gas, and others. Many pump designs are available (Bamberger et al., 2020; Shim et al., 2016). Still, they all have one crucial characteristic: they are highly effective devices that can transfer a large volume of fluid in a short amount of time. The centrifugal pump is among the most efficient (Capurso et al.,

2022; Parikh et al., 2022). The circular motion of this sort of pump is used to generate a force that either propels or retracts items as they are moving through a fluid. Centrifugal pumps are used to move a lot of liquids and gases about, but they are beneficial for transporting liquids since they are able to do it swiftly and quietly. Centrifugal pumps are used to move a lot of liquids and gases around. The inability of centrifugal pumps to effectively move solids is one of the drawbacks of using these types of pumps. This is because they do not have sufficient torque to push solid items through the fluid, and as a result, they often need additional equipment to move materials such as earth or boulders. However, despite their drawbacks, centrifugal pumps remain one of the most effective types of pumps that can be purchased. They are an excellent choice for applications that require the rapid transport of liquids or gases.

A pump with its motor is referred to as a tubular pump. Because the tubular pump's input and outlet channels run in parallel, it may be used for emergency mine drainage, water lifting for large-scale water conservation projects, and water supply for tall structures. Because of the intricate nature of the pump's internal flow arrangement, its efficiency (Capurso et al., 2022; Derakhshan & Bashiri, 2018; Derakhshan et al., 2013; Latifi et al., 2021; Lu et al., 2021; Mitrovic et al., 2021)is often poor. The issue of energy consumption (Derakhshan & Bashiri, 2018; Wu et al., 2022; Yildiz & Vrugt, 2019)is gaining more attention due to the fast expansion of the economy and the ongoing rise in the world's population. At this time, the global community is working on a solution to the issue of an inadequate supply of energy (Elkholy & Fathy, 2016; Wu et al., 2022; Zeidan & Ostfeld, 2022; Zhang et al., 2021); excessive use of energy will always result in problems with the environment. The objective of reaching the global carbon peak requires the implementation of many essential strategies, including energy saving and emission reduction. Pumps, which are considered to be multi-purpose pieces of equipment, find widespread use in a variety of economic-related disciplines. According to the available data, the percentage of the world's total power consumption (Yildiz & Vrugt, 2019)that is accounted for by the pumps' electricity is around twenty percent. Therefore, increasing the pump's efficiency is of utmost importance if one wants to achieve energy savings, a decrease in consumption, and relief from energy shortages, due to the fact that they have a high flow pumping capacity. The research objectives of this study are diving tubular pumps. It is of considerable worth to find a strategy that can optimize its performance since there are times when emergency rescue operations need electricity that is in low supply (Wu et al., 2022; Zeidan & Ostfeld, 2022; Zhang et al., 2021).

The study of the creation of entropy that is presented in this article is used to examine the flow loss (Anagnostopoulos, 2009; Ghorani et al., 2020; Lu et al., 2021; Shim et al., 2016)of the first pump. This problem is done to identify the areas of the original pump (Wang et al., 2020; Wang et al., 2017; Wu et al., 2022). As a result, it is possible to disregard the vicious impact dissipation and entropy formation has on flow loss (Anagnostopoulos, 2009; Ghorani et al., 2020; Shim et al., 2016; Wu et al., 2022; Zhang et al., 2021)that diving tubular pumps experience. Production of entropy at the wall and the entropy of turbulent kinetic energy generation are two significant contributors to the flow loss that diving tubular pumps participate in. The ensuing investigation concentrates its primary attention primarily on wall entropy formation as well as turbulent kinetic energy entropy creation. The purpose of this kind of optimal design for pumps is to give an analysis of possible future applications or future research areas.

Efficiency, Head, And Output Power Theory

The Efficiency of the Centrifugal Pump

There are pump efficiency η = 65.5%, volume efficiency $\eta_v = 94\%$, hydraulic $\eta_h = 80\%$ and

machinery efficiency $\eta_m = 83\%$

$$\eta = \frac{\rho g H Q}{T . \omega}$$

where is:

η: efficiency (%)

gH : specific energy of the centrifugal pump ($m^2 s^{-2}$)

ρ : fluid density (kg/m^3)

Q: flow rate (kg/s)

T: torque (Nm)

ω: angular velocity(rad/s)

$$Q_t = \frac{Q}{\eta_v} = \frac{1}{(60 \times 0.94)} = 0.018 m^3 / \sec$$

Head And Output Power of the Centrifugal Pump

$$H_{th} = \frac{H}{\eta_h} = \frac{33}{0.84} = 39.3 m$$

$P = T.\omega$

Specific speed

$$n_s = \frac{n\sqrt{Q}}{H^{3/4}} = \frac{1750\sqrt{1}}{33^{3/4}} = 127(m, m^3 / \min, rpm)$$

$$n_s' = k n_s = 6.67 \times 127 = 847(ft, gpm, rpm)$$

Angular velocity

$$\omega = \frac{2\pi n}{60} = \frac{2\pi \times 1750}{60} = 183.16 rad / \sec$$

Pump shaft diameter

$$d = k \sqrt[3]{\frac{L_m}{n}} = 125 \sqrt[3]{\frac{11}{1750}} = 23.1 mm$$

k=125, d =38mm, $D_s = 35\ mm$

Impeller boss diameter

$$D_b = 1.4 d_s = 1.4 \times 35 = 50 mm$$

Impeller inlet velocity

$$k_{mo} = 0.1 + 0.00023 n_s = 0.1 + 0.00023 \times 127 = 0.129$$

$$v_{mo} = k_{mo}\sqrt{2gH} = 0.129\sqrt{2 \times 9.8 \times 33} = 3.29 m / \sec$$

Empirical equation

$$v_{mo} = \frac{\sqrt[3]{Qn^2}}{60}$$

$$v_{mo} = \frac{\sqrt[3]{1 \times 1750^2}}{60} = 2.42 m / \sec$$

Impeller outlet velocity

$$D_s = \sqrt{\frac{4Q_t}{\pi v_{mo}} + D_b^2} = \sqrt{\frac{40 \times 0.018}{\pi(3.29 \sim 2.42)} + 0.05^2} = 0.097 \sim 0.109m$$

Choose

$D_s = 100\ mm$, Area at impeller outlet position

$$A = \frac{\pi}{4}(D_s^2 - D_b^2) = \frac{\pi}{4}(0.1^2 - 0.05^2) = 0.006m^2$$

$$v_{mo} = \frac{Q}{A} = \frac{0.018}{0.006} = 3m/\sec$$

Impeller discharge dimensionless

$$\psi = \frac{gH}{u_2^2}, \beta_e = 27^0, n_s = 127, \psi = 0.57$$

⇨ Select Ψ =0.52

where Ψ is Head coefficient, a dimensionless parameter; β_e is average outlet angle.
The necessary impeller peripheral velocity and the impeller outlet diameter were calculated from

$$u_2 = \sqrt{\frac{gH}{\psi}} = \sqrt{\frac{9.8 \times 33}{0.52}} = 24.9m/\sec$$

$$D_2 = \frac{60u_2}{\pi n} = \frac{60 \times 24.9}{\pi \times 1750} = 0.272$$

➔ $D_2 = 0.272\ m$

Impeller outlet width

$$H_{th} = a\frac{u_2^2}{g}\left\{h_0 - h_v \frac{v_{m2}}{u_2}(\cot\beta_e + \cot\alpha_1)\right\}$$

where is a = 0.95, $\alpha_1 = 90^0, u_2 = 24.9\ m/\sec, \beta_e = 27^0$,

Busemann factor number is 7, $\beta_2 = 27^0, h_0 = 0.805, h_v = 1$

Thus,

$$39.3 = 0.95 \frac{24.9^2}{9.8} \left\{ 0.805 - 1\frac{v_{m2}}{24.9}(\cot 27^0) \right\}$$

$$v_{m2}^{'} = 1.918 m/\sec$$

$$t_2 = \frac{272\pi}{7} = 122 mm,$$

$$\frac{t_2}{t_2 - s_2} = 1.1$$

$$\delta_2 = s_2 \sin \beta_2 = 11 \sin 27^0 = 5mm$$

The impeller outlet width was given by

$$b_2 = \frac{Q_t t_2}{(t_2 - s_2)(2\pi r_2 v_{m2}^{'})} = \frac{0.018 \times 0.122}{(0.122 - 0.011)(2\pi 0.136 \times 1.918)} = 0.012m$$

Impeller profile

Table 1. Impeller profile of the designed pump

D(mm)	D×b(mm^2)	b (mm)	D (mm)	D×b(mm^2)	b (mm)
272	3264	12.00	160	2474	15.46
260	3179	12.23	140	2333	16.66
240	3038	12.66	120	2192	18.27
220	2897	13.17	100	2051	20.51
200	2756	13.78	80	1910	23.88
180	2615	14.53	75	1875	25.00

Methodology

Design Structures and Unstructured Models

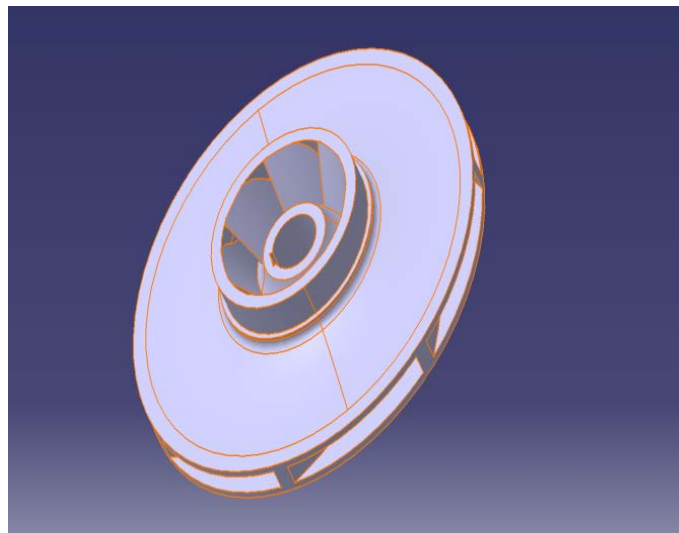The geometry model was designed following the parameters calculated above by using CATIA.

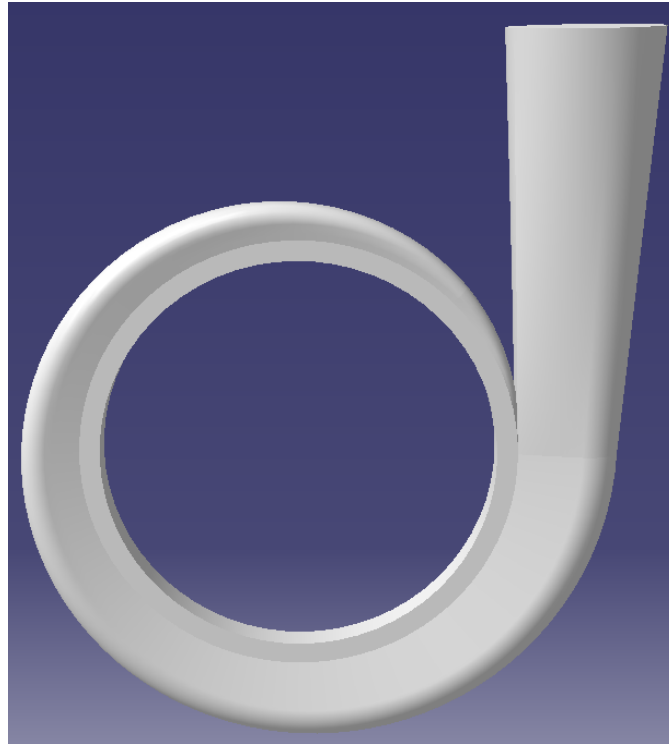Figure 1. Designed impeller by using Catia

Figure 2. Unstructured designed volute by using Catia

Table 2. Boundary conditions

Specification	Option
Working fluid	water
Turbulence model	SST
Boundary condition	Inlet: total pressure
	Outlet: Mass flow
Interface type	Fluid-Fluid
Analysis type	Steady-state
Frame change/mixing model	Frozen Rotor and None
Residual target	10^{-5}

Numerical Methods

It looked at how "the solution of the three-dimensional incompressible Navier-Stokes" equation affects the pressure and flow fields via the impeller (Anagnostopoulos, 2009; Bellary et al., 2016; Derakhshan & Bashiri, 2018; Shim et al., 2016; Wang et al., 2017). İn addition, the disturbance is simulated using the standard k-model (Bamberger et al., 2020; Farokhzad et al, 2012). This equation's solution leads to the formation of the pressure and flow fields. The simulations are carried out with the help of the commercial CFD code (Benini & Cenzon, 2010; Capurso et al., 2022; Fracassi et al., 2022; Siddique et al., 2022)known as Fluent®, which has a history of successful use in the field of turbine engineering. The pressure-velocity coupling is carried out with the use of an algorithm (Anagnostopoulos, 2009; Bellary et al., 2016; Capurso et al., 2022; Derakhshan, Mohammadi, & Nourbakhsh, 2009; Derakhshan et al., 2013; Elkholy & Fathy, 2016)known as SIMPLE.

Quadratic wind arbitrary is used for convection and central difference for diffusion. There is only one slab in the computational domain (Bamberger et al., 2020). The logarithmic-based wall functions are used on all solid walls and periodic boundary conditions (Luan et al., 2016; Myrzakhmetov et al., 2020) are implemented. It is ensured that there will be no slip circumstances at any stable, stationary, or rotating surface and that there will be uniform inflow conditions as well as free-flow conditions at the inlet and outflow of the flow, respectively. The computational grid (Bamberger et al., 2020; Peng et al., 2022)is structured, and the Fluent preprocessor Gambit is the tool used to construct it. This is made possible by the fact that the domain as a whole is divided into multiple domains or subregions. The precision and the computing cost are considered. And an alphanumeric grid with around 4.5 million cells is deemed sufficient for the computations. Figure 2a depicts an image that

suggests the mesh around the blade, and Figure 2b depicts a close-up view of the blade's leading edge. The algorithm (Abdolahnejad et al., 2022; Almasi et al., 2022; Bamberger et al., 2020; Bellary et al, 2016; Derakhshan et al., 2009)begins with a modest rotational speed and progressively increases it until it achieves its nominal speed of 3000 rpm. This is done for stability reasons. Box and Wilson presented the Reaction Surface Methodology (RSM) in 1951; it is a technique for estimating the combined effect of several independent variables that do not require the performance of factorial design experiments for all of the independent variables at each level. RSM (Liu et al., 2019; Meng et al., 2022)is a technique that can be found in the field of chemical engineering.

There are at least two different categories of variables that are being looked at, and an estimation of the functional relationship that exists between the response variables and the independent variables is being used to make a prediction about the variation that occurs in response to changes in the values of the independent variables. from data. An optimization procedure (Benini & Cenzon, 2010; Derakhshan & Bashiri, 2018; Fracassi et al., 2022)is used to determine the values of the independent variables for which the response should be optimized. This is based on the information provided above. Among the various kinds of reaction surfaces, experiments are the two-level factorial arrangement method and the three-level factor arrangement method, both of which are utilized when the estimation equation for the reaction surface is a first-order equation. Other types of reaction surface experiments include the factorial arrangement method. the design approach and the Box-Behnken method (Meng et al., 2014)are used in the estimation process. estimated is a quadratic, central composite. Within the scope of this investigation, an optimization strategy that makes use of central synthesis was implemented. Carrying out the job of impeller optimization (Abdolahnejad et al., 2022; Bamberger et al., 2020; Bellary et al., 2016; Derakhshan & Bashiri, 2018; Derakhshan et al., 2013; Ghadimi, Nejat, Nourbakhsh, & Naderi, 2019) was studied. The goal value and the column of the pump were set to 33 meters. And the efficiency was set to the utmost value possible while considering the significant margin and the loss because the pump being studied has a current that fits the intended specification. Figures 1-2 depict the unstructured models for the centrifugal pump which was employed for predicting the optimal propeller model that satisfies the selected target value. In this case, a numerical analysis is done on the optimization model, and the performance of the optimized model is compared with the performance of the basic model, as shown in Figures 1-2 and Tables 1-2; this allows for an accurate evaluation of the performance of the propeller optimization model. The performance result value for this propeller-optimized model is raised by around 0.5 meters compared to the standard model, but the efficiency is decreased by about 0.1 percent. When beta two is raised to meet the goal value for the head, as shown by the findings of the impact analysis of the design variable, it is expected that the efficiency would suffer a minor drop in order to accommodate the new value. On the other hand, the impeller optimization model (Abdolahnejad et al., 2022; Bellary et al., 2016; Fang et al., 2020; Ghorani et al., 2020) was created using specified response surface engineering since it was determined that this efficiency drop quite tinily and does not substantially impair the pump performance. is the most comprehensive model for the optimization of impellers.

Results and Discussion

The numerical model first determines the flow field in a 3000-rpm conventional impeller, and this impeller has regular-height blades with a single casing. Therefore, the nominal flow rate and other impeller properties follow the lab model pump, showing informative numbers. Figures 3-4 present the design variables of x_1 (variable angle) and x_2 (impeller-tongue gap, which is the gap between the impeller and the volute casing). Besides, Figure 5-6 shows the design variable ignored for the above variables mentioned in Figures 3-4. It could be seen how a leading-edge affects the intake radius. This study discusses non-twisted blade geometry. The impeller with a blade edge angle of 30° has 11% poorer hydraulic efficiency but better BEP flow rates. In the context of this investigation, we try to construct the area of the cross-section. The Stepanoff hypothesis is used in the execution of horizontal arcs.

As a consequence of this, the rate of flow inside the chain was determined to be 12.5 meters per second, and the distribution of the cross-sectional area. The constant value used in calculating the internal flow rate of the voltage is practical, and it is impossible to identify which deal is the best one to use to compute the flow rate. This was explained before. Four more cross-sectional area distributions were picked on top of the cross-sectional area distributions computed using Stepanoff's theory as the center. In this case, the open duct connecting to the impeller output is 90 millimeters in width—additional considerations for the design. Final answer is x(0.0; -1.0)
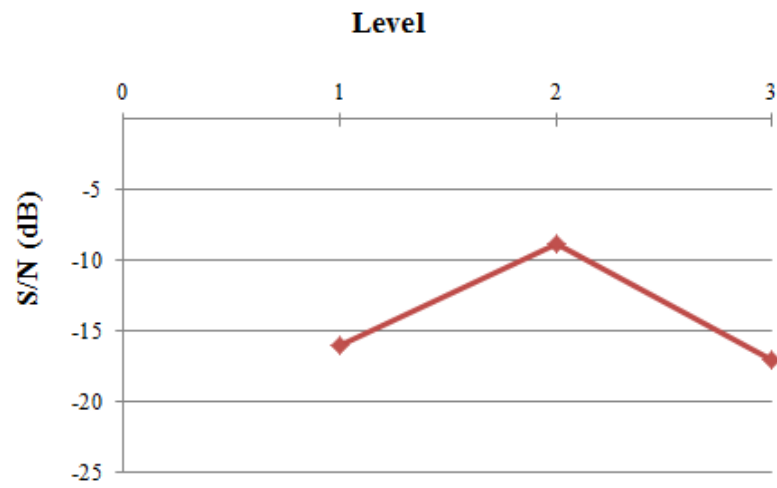
Figure 3. Design variable x_1
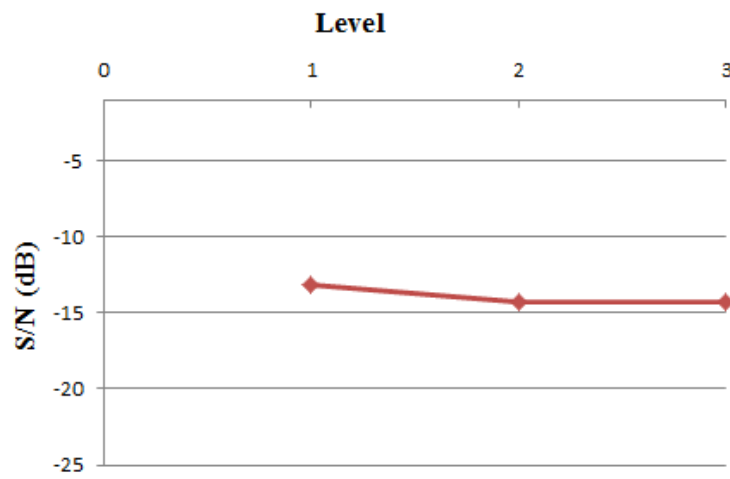
Figure 4. Design variable x_2
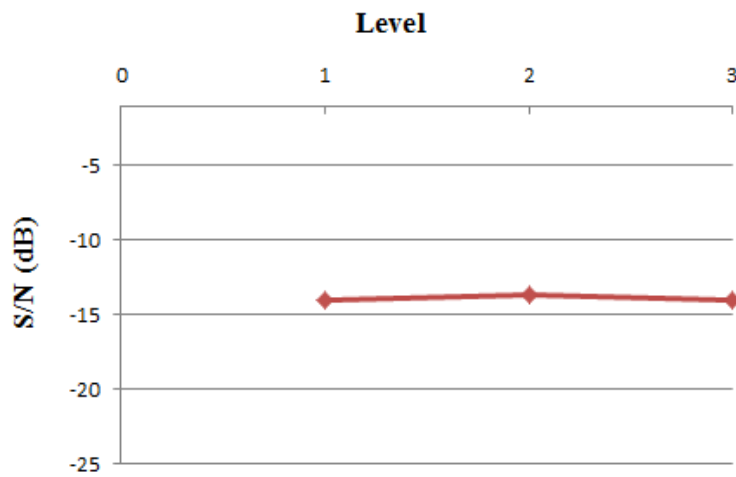
Figure 5. Design variable Ignored 1
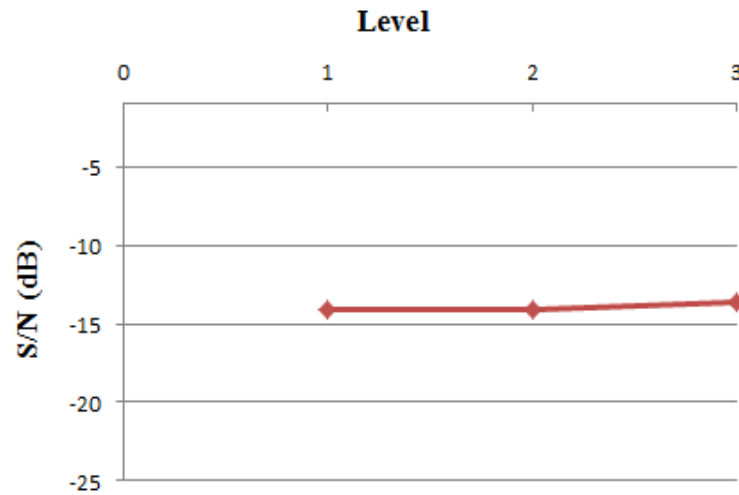
Figure 6. Design variable Ignored 2

From the results, it is easy to see that the optimum values of factors and their levels selected are x (0; 2.7) $x_1 = 0^0, x_2 = 2.7\%$. After optimization, the variable angle and impeller-tongue gap are $X_1 = 0^0$ $X_2 = 3.67\ mm$, respectively. These are the best parameters for centrifugal pump design, particularly volute tongue length.
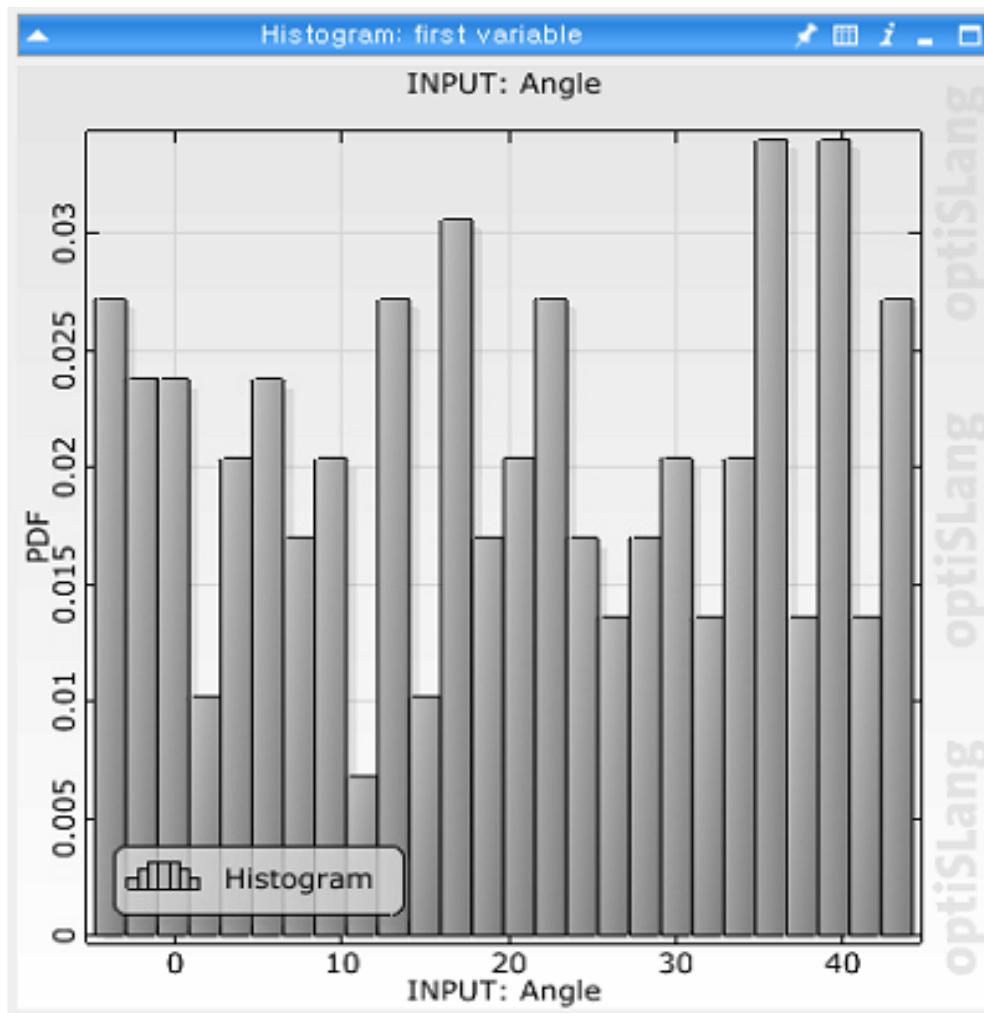
Figure 7. Histogram of first variable
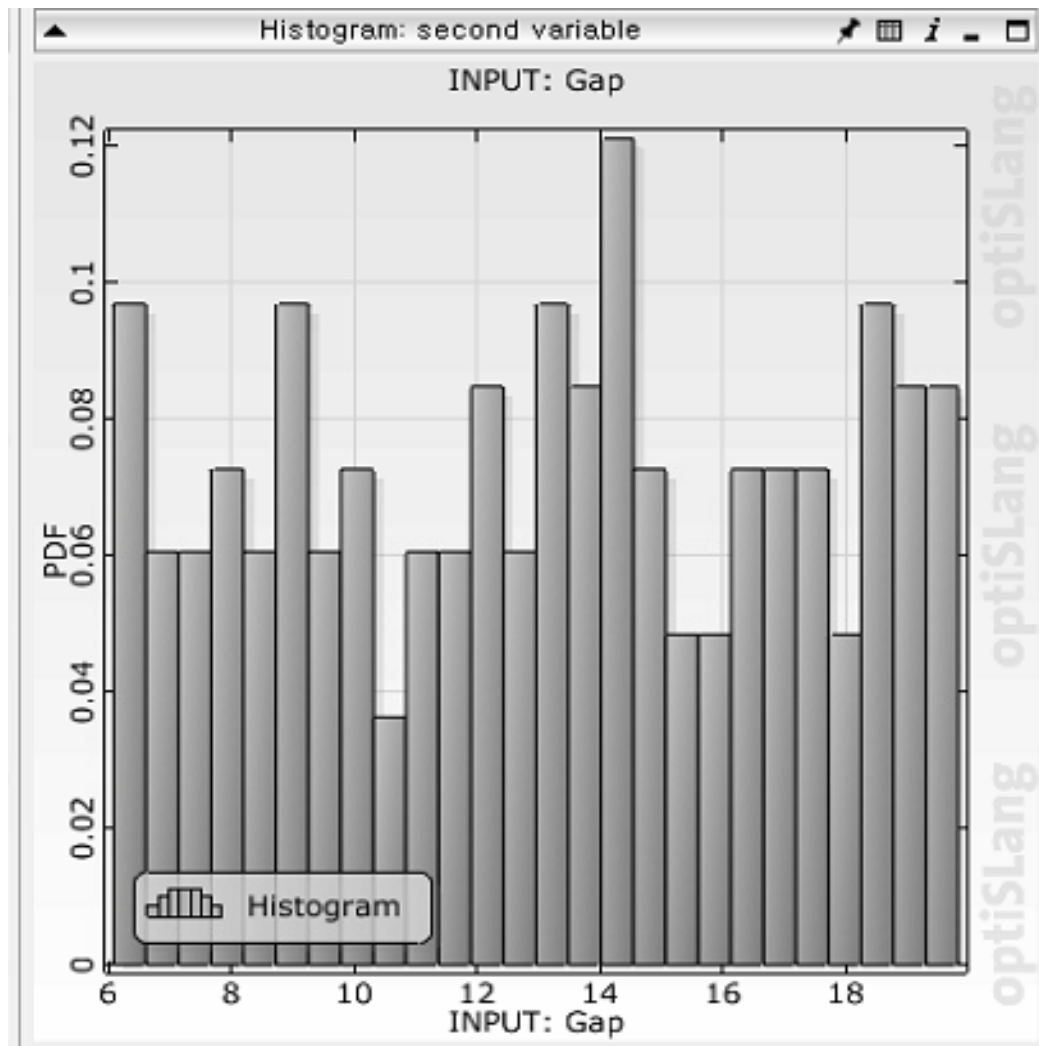
Figure 8. Histogram of the second variable
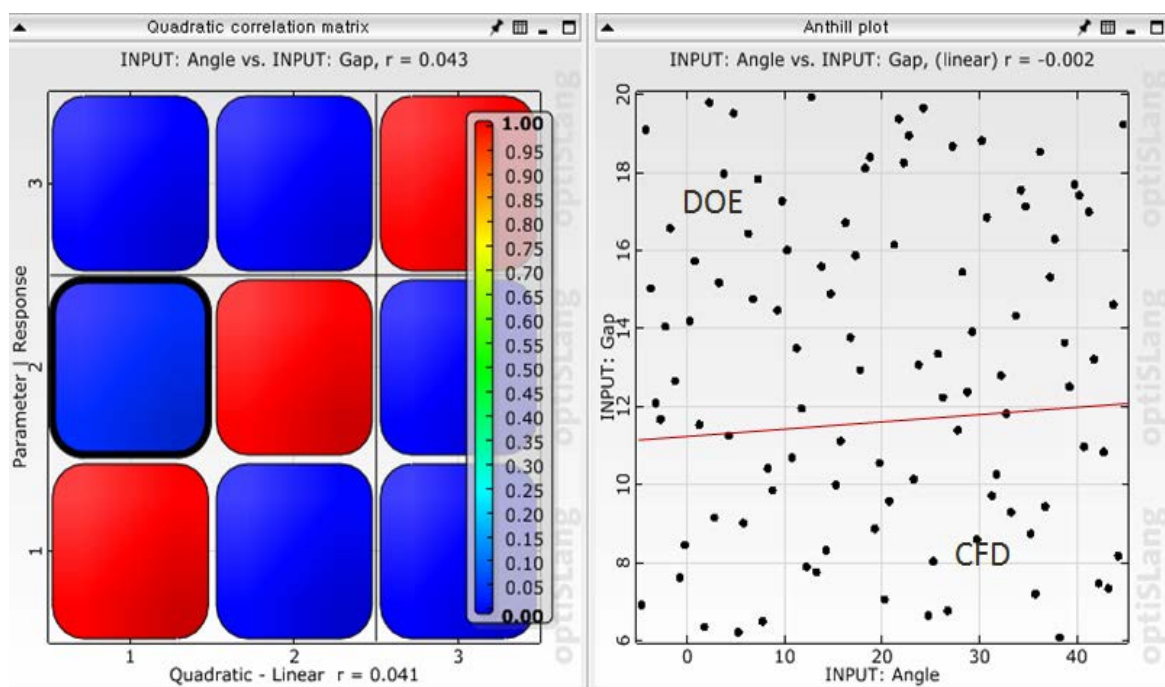
Figure 9. Quadratic correlation matrix
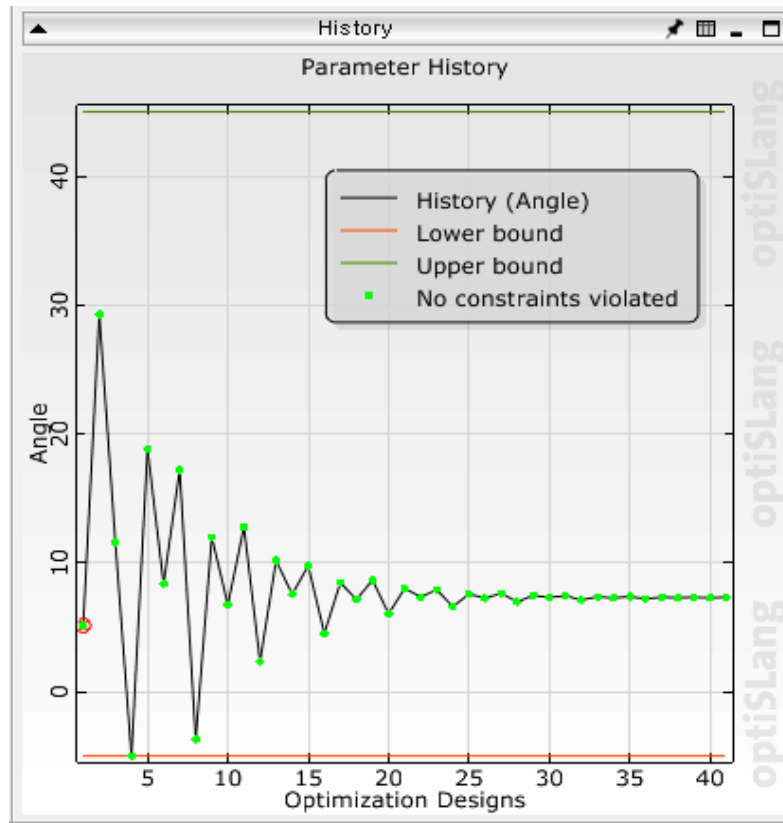
Figure 10. Parameter history
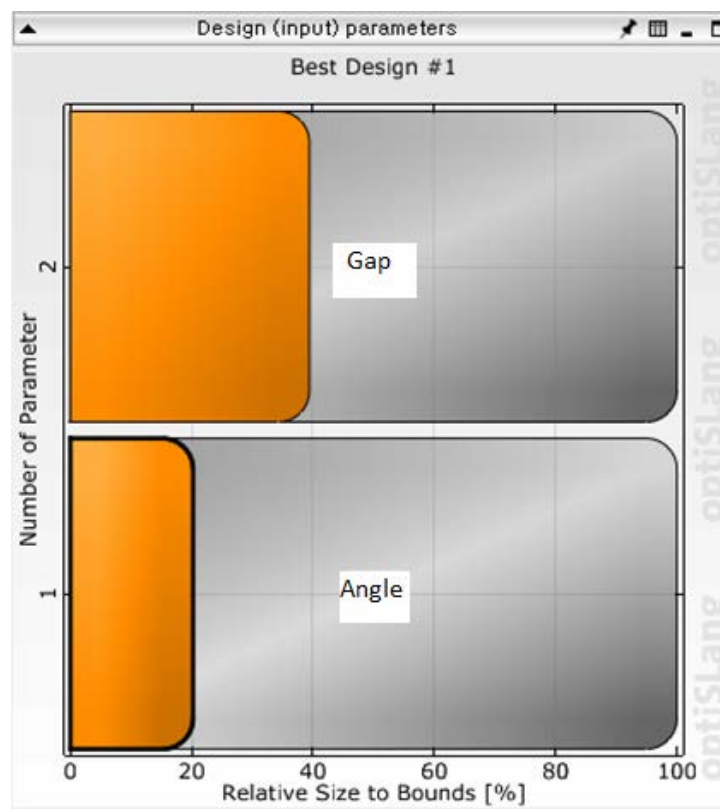
Figure 11. Design input parameters (Best Design #1)
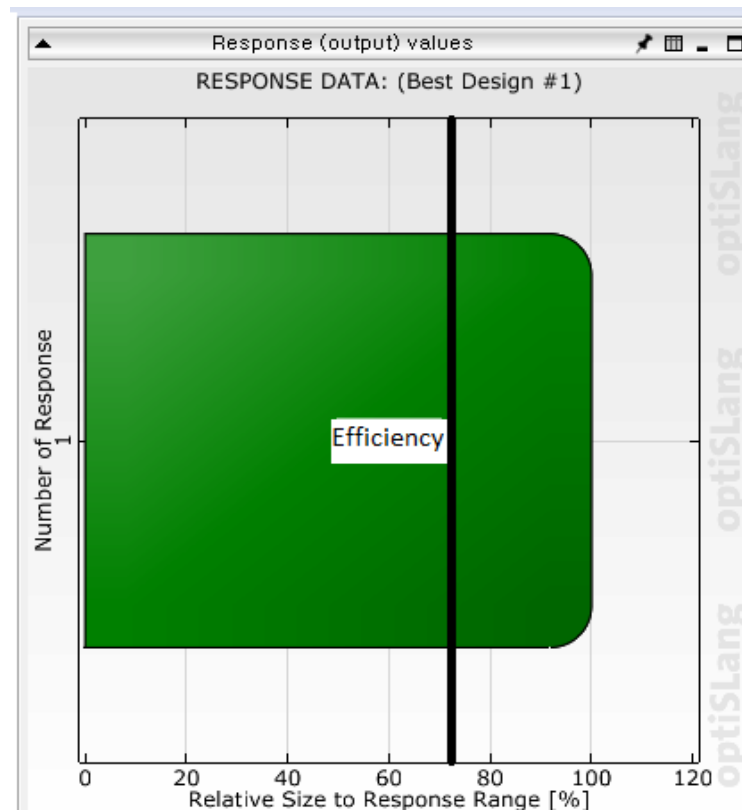
Figure 12. Response data (Best Design #1)

Optimal Design Stage

In order to discover the optimal blade form that maximizes, the two geometric parameters discussed before make up the free design variables. These geometric parameters may be adjusted within certain constraints. This research resulted in the presentation of a centrifugal pump design that was capable of meeting the desired parameters. In order to accomplish this objective, the propeller's optimum design work was carried out using response surface engineering and CFD. Additionally, a voltage matching proposal for optimally designed propellers was developed via the application of Stepanoff's theory. 1) Based on the study's findings that analyzed each variable's impact, it was discovered that the exit angle of the impeller has the most significant impact on the life force and the efficiency of the impeller. 2) The response surface method calculates the propeller optimization model. The performance of the calculated optimization model was compared to the performance of the basic model. As a consequence of this comparison, the performance of the computed optimization model was slightly lowered (about 0.3 percent) to 98.2 percent, but the top of 64.5 m, approximately 2.5 m. Elevate to a level that will fulfill the goal value. As a consequence of this, the final propeller optimization model will be the target model that was chosen. 3) As a result of carrying out a performance assessment through numerical analysis and establishing each design voltage in the vane optimization model, it was determined that it should be built with the internal cross-sectional area distribution. When the chain model is used, it can be shown that the head is around 32 meters, and the efficiency is improved, demonstrating that the model produces the best results. As a result, the target curve model is provided as an alternate line design appropriate for the impeller optimization model. Figures 7-8 present the histograms of the first variable (x_1) and the second variable (x_2). The chart image shows that in variable 1, the concentration amplitude deviates to the right, tends to increase from low to high, and has an average value of about 0.018. Figure 8 shows that the highest values are concentrated in the center on the left and right sides (with an average value of 0.06). Figure 9 depicts the quadratic correlation matrix shown to be highly correlated in optimization with r=0.043. The red line divides the two experimental domains, DOE and the CFD simulation domain, and the selected experimental values are arranged fairly evenly in these two domains. Figure 10 shows the convergence history of parameters with lower bound, upper bound, and no constraints violated for the first variable. In this study, our preliminary results are drawn and presented in Figures 11-12. These two figures illustrate design input parameters (Best Design #1) and response data (Best Design #1). In this result, the optimal value is chosen for the designed pump at 74%. However, the optimization problem is to solve the problem by a trade-off. This result may not be very high, but it is consistent with the hypothesis.

Production Process Development

In developing the processes of production, based on the assumption of small and medium-sized organizations, three ideas were kept in mind, casting philosophical foundations, namely

✓ While the principles and language of design may be universal, their application in the redesign of goods cannot be. The miniaturized variant of a substantial marketable item
✓ The success or failure of a company cannot be attributed to the quality of its production system; nonetheless, a system that is insufficient or gives the wrong impression might prevent even the most promising enterprise from reaching its full potential.
✓ It is preferable to be roughly accurate in redesign procedures than precisely incorrect. In other words, the design was carried out to achieve target performance requirements (Head H and Discharge Q for a contemplated speed N)

Design for manufacturing and assembly was the approach taken in the design of this product. It includes considerations of manufacture and assembly during the design stage. Less time is needed to get the product to market, a smoother transition to the market, fewer parts in the final product, easier assembly, lower production costs, a better product, and happier customers. The resulting sized parts were then tested for assembly. With the tolerances specified, the designs were assembled using CATIA software to check if it was possible to create the product. The dimensions were adjusted to ensure a good design consistent with the design requirements for assembly. Moreover, material properties were also checked.

Conclusions

The current technique can readily manage more free design factors, and it is anticipated that integrating these variables would enhance the impeller design differently. Multi-objective optimization is also a possibility. Right now, it is planned to make an impeller that improves performance and efficiency while being built in a way that costs less. This study found that changing the shape of the volute tongue makes pumps work better. The velocity vector density and the vortex core region of case studies are lower than in previous designs. The smaller the gap between impeller and volute, the better the pump's performance. The impeller outlet blade angle strongly affects the pump performance; the pump performance was improved the most with $\beta_2=34^o$.

Initial research has yielded many exciting results. However, the results presented in this paper are subject to further examination and study in the future. The optimization just stopped at the initial development stage. We have many phases of research in-depth, and that will change, but results are uncertain when the empirical analysis is conducted. The limitations of this study are that the final results have not been finalized, the research time is limited, the equipment has not been manufactured and tested, and the funding for the research is relatively modest and self-sufficient. We will complete the CFD simulation steps in the following research direction and conduct careful optimization based on machine learning with optimization algorithms. Then we will collect the optimal result based on the initial design of the CFD data value. After choosing the best model, we will proceed to fabricate the centrifugal pump sample and bring it to the test. The pump manufacturer will verify the experimentally collected deals and suggest future improvements.

Scientific Ethics Declaration

The authors declare that the scientific ethical and legal responsibility of this article published in EPSTEM journal belongs to the authors.

Acknowledgements or Notes

References

Abdolahnejad, E., Moghimi, M., & Derakhshan, S. (2022). Optimization of the centrifugal slurry pump through the splitter blades position. *Proceedings of the Institution of Mechanical Engineers Part C-Journal of Mechanical Engineering Science, 236*(1), 191-207. doi:Artn 0954406221102760810.1177/09544062211027608

Almasi, S., Ghorani, M. M., Haghighi, M. H. S., Mirghavami, S. M., & Riasi, A. (2022). Optimization of a vacuum cleaner fan suction and shaft power using Kriging surrogate model and MIGA. *Proceedings of the Institution of Mechanical Engineers Part a-Journal of Power and Energy, 236*(3), 519-537. doi:Artn 0957650921104961310.1177/09576509211049613

Anagnostopoulos, J. S. (2009). A fast numerical method for flow analysis and blade design in centrifugal pump impellers. *Computers & Fluids, 38*(2), 284-289. doi:10.1016/j.compfluid.2008.02.010

Bamberger, K., Carolus, T., Belz, J., & Nelles, O. (2020). Development, Validation, and Application of an Optimization Scheme for Impellers of Centrifugal Fans Using Computational Fluid Dynamics-Trained Metamodels. *Journal of Turbomachinery-Transactions of the Asme, 142*(11). doi:Artn 11100510.1115/1.4048022

Bellary, S. A. I., Adhav, R., Siddique, M. H., Chon, B. H., Kenyery, F., & Samad, A. (2016). Application of computational fluid dynamics and surrogate-coupled evolutionary computing to enhance centrifugal-pump performance. *Engineering Applications of Computational Fluid Mechanics, 10*(1), 172-182. doi:10.1080/19942060.2015.1128359

Bellary, S. A. I., Samad, A., Couckuyt, I., & Dhaene, T. (2016). A comparative study of kriging variants for the optimization of a turbomachinery system. *Engineering with Computers, 32*(1), 49-59. doi:10.1007/s00366-015-0398-x

Benini, E., & Cenzon, M. (2010). Development of a multi-objective optimization method for aerospace turbopump design. *International Journal of Turbo & Jet-Engines, 27*(3-4), 219-250.

Capurso, T., Bergamini, L., & Torresi, M. (2022). A new generation of centrifugal pumps for high conversion efficiency. *Energy Conversion and Management, 256*. doi:ARTN 11534110.1016/j.enconman.2022.115341

Derakhshan, S., & Bashiri, M. (2018). Investigation of an efficient shape optimization procedure for centrifugal pump impeller using eagle strategy algorithm and ANN (case study: slurry flow). *Structural and Multidisciplinary Optimization, 58*(2), 459-473. doi:10.1007/s00158-018-1897-3

Derakhshan, S., Mohammadi, B., & Nourbakhsh, A. (2009). Efficiency Improvement of Centrifugal Reverse Pumps. *Journal of Fluids Engineering-Transactions of the Asme, 131*(2). doi:Artn 02110310.1115/1.3059700

Derakhshan, S., Pourmahdavi, M., Abdolahnejad, E., Reihani, A., & Ojaghi, A. (2013). Numerical shape optimization of a centrifugal pump impeller using artificial bee colony algorithm. *Computers & Fluids, 81*, 145-151. doi:10.1016/j.compfluid.2013.04.018

Elkholy, M. M., & Fathy, A. (2016). Optimization of a PV fed water pumping system without storage based on teaching-learning-based optimization algorithm and artificial neural network. *Solar Energy, 139*, 199-212. doi:10.1016/j.solener.2016.09.022

Esmaeilian, H., Mohammadi, E., Fadaeinedjad, R., Bakhshai, A., & Rahnama, M. (2019). Design methodology to optimise induction machines based stand-alone electrical wind water pumping systems. *Iet Electric Power Applications, 13*(12), 2058-2069. doi:10.1049/iet-epa.2019.0210

Fang, H., Ma, J. F., Zhang, W., Yang, H., Chen, F., & Li, X. J. (2020). Hydraulic Performance Optimization of Pump Impeller Based on a Joint of Particle Swarm Algorithm and Least-Squares Support Vector Regression. *Ieee Access, 8*, 203645-203654. doi:10.1109/Access.2020.3036913

Farokhzad, S., Ahmadi, H., Jaefari, A., Abad, M. R. A. A., & Kohan, M. R. (2012). Artificial neural network based classification of faults in centrifugal water pump. *Journal of Vibroengineering, 14*(4), 1734-1744.

Fracassi, A., De Donno, R., Ghidoni, A., & Congedo, P. M. (2022). Shape optimization and uncertainty assessment of a centrifugal pump. *Engineering Optimization, 54*(2), 200-217. doi:10.1080/0305215x.2020.1858075

Ghadimi, B., Nejat, A., Nourbakhsh, S. A., & Naderi, N. (2019). Multi-Objective Genetic Algorithm Assisted by an Artificial Neural Network Metamodel for Shape Optimization of a Centrifugal Blood Pump. *Artificial Organs, 43*(5), E76-E93. doi:10.1111/aor.13366

Ghorani, M. M., Haghighi, M. H. S., & Riasi, A. (2020). Entropy generation minimization of a pump running in reverse mode based on surrogate models and NSGA-II. *International Communications in Heat and Mass Transfer, 118*. doi:ARTN 10489810.1016/j.icheatmasstransfer.2020.104898

Jegha, A. D. G., Subathra, M. S. P., Kumar, N. M., & Ghosh, A. (2020). Optimally Tuned Interleaved Luo Converter for PV Array Fed BLDC Motor Driven Centrifugal Pumps Using Whale Optimization

Algorithm-A Resilient Solution for Powering Agricultural Loads. *Electronics, 9*(9). doi:ARTN 144510.3390/electronics9091445

Latifi, M., Moghadam, K. F., & Naeeni, S. T. (2021). Pressure and Energy Management in Water Distribution Networks through Optimal Use of Pump-As-Turbines along with Pressure-Reducing Valves. *Journal of Water Resources Planning and Management, 147*(7). doi:Artn 0402103910.1061/(Asce)Wr.1943-5452.0001392

Liu, H. L., Wang, K., Yuan, S. Q., Tan, M. G., Wang, Y., & Dong, L. (2013). Multicondition Optimization and Experimental Measurements of a Double-Blade Centrifugal Pump Impeller. *Journal of Fluids Engineering-Transactions of the Asme, 135*(1). doi:Artn 01110310.1115/1.4023077

Liu, X. W., Li, H. C., Shi, X. X., & Fu, J. F. (2019). Application of biharmonic equation in impeller profile optimization design of an aero-centrifugal pump. *Engineering Computations, 36*(5), 1764-1795. doi:10.1108/Ec-08-2018-0378

Lu, R., Yuan, J. P., Wei, G. J., Zhang, Y., Lei, X. H., & Si, Q. R. (2021). Optimization Design of Energy-Saving Mixed Flow Pump Based on MIGA-RBF Algorithm. *Machines, 9*(12). doi:ARTN 36510.3390/machines9120365

Lu, Y. M., Wang, X. F., Liu, H. R., & Li, Y. Y. (2020). Investigation of the effects of the impeller blades and vane blades on the CAP1400 nuclear coolant pump's performances with a united optimal design technology. *Progress in Nuclear Energy, 126*. doi:ARTN 10342610.1016/j.pnucene.2020.103426

Luan, H. X., Chen, Q. G., Weng, L. Y., Luan, Y. Z., & Li, J. (2016). Numerical computation of the flow noise for the centrifugal pump with considering the impeller outlet width. *Journal of Vibroengineering, 18*(4), 2601-2612. doi:10.21595/jve.2016.16656

Meng, F. N., Dong, Q. L., Wang, P. F., & Wang, Y. (2014). Multi-objective Optimization for the Impeller of Centrifugal Fan Based on Response Surface Methodology with Grey Relational Analysis Method. *Advances in Mechanical Engineering*. doi:Artn 61458110.1155/2014/614581

Mitrovic, D., Morillo, J. G., Diaz, J. A. R., & Mc Nabola, A. (2021). Optimization-Based Methodology for Selection of Pump-as-Turbine in Water Distribution Networks: Effects of Different Objectives and Machine Operation Limits on Best Efficiency Point. *Journal of Water Resources Planning and Management, 147*(5). doi:Artn 0402101910.1061/(Asce)Wr.1943-5452.0001356

Myrzakhmetov, B., Sultabayev, A., & Toktamissova, S. (2020). Substantiation of the methodology for modeling and calculating the optimal operating modes of a tandem pumping installation when mining uranium. *Mining of Mineral Deposits, 14*(4), 59-65. doi:10.33271/mining14.04.059

Parikh, T., Mansour, M., & Thevenin, D. (2022). Maximizing the performance of pump inducers using CFD-based multi-objective optimization. *Structural and Multidisciplinary Optimization, 65*(1). doi:ARTN 910.1007/s00158-021-03108-6

Peng, C. C., Zhang, X. D., Gao, Z. G., Wu, J., & Gong, Y. (2022). Research on cooperative optimization of multiphase pump impeller and diffuser based on adaptive refined response surface method. *Advances in Mechanical Engineering, 14*(1). doi:Artn 1687814021107294410.1177/16878140211072944

Shim, H. S., Afzal, A., Kim, K. Y., & Jeong, H. S. (2016). Three-objective optimization of a centrifugal pump with double volute to minimize radial thrust at off-design conditions. *Proceedings of the Institution of Mechanical Engineers Part a-Journal of Power and Energy, 230*(6), 598-615. doi:10.1177/0957650916656544

Shim, H. S., Kim, K. Y., & Choi, Y. S. (2018). Three-Objective Optimization of a Centrifugal Pump to Reduce Flow Recirculation and Cavitation. *Journal of Fluids Engineering-Transactions of the Asme, 140*(9). doi:Artn 09120210.1115/1.4039511

Siddique, M. H., Samad, A., & Hossain, S. (2022). Centrifugal pump performance enhancement: Effect of splitter blade and optimization. *Proceedings of the Institution of Mechanical Engineers Part a-Journal of Power and Energy, 236*(2), 391-402. doi:Artn 0957650921103740710.1177/09576509211037407

Wang, W. J., Li, Y. P., Osman, M. K., Yuan, S. Q., Zhang, B. Y., & Liu, J. (2020). Multi-Condition Optimization of Cavitation Performance on a Double-Suction Centrifugal Pump Based on ANN and NSGA-II. *Processes, 8*(9). doi:ARTN 112410.3390/pr8091124

Wang, W. J., Yuan, S. Q., Pei, J., & Zhang, J. F. (2017). Optimization of the diffuser in a centrifugal pump by combining response surface method with multi-island genetic algorithm. *Proceedings of the Institution of Mechanical Engineers Part E-Journal of Process Mechanical Engineering, 231*(2), 191-201. doi:10.1177/0954408915586310

Wu, T. X., Wu, D. H., Ren, Y., Song, Y., Gu, Y. Q., & Mou, J. G. (2022). Multi-objective optimization on diffuser of multistage centrifugal pump base on ANN-GA. *Structural and Multidisciplinary Optimization, 65*(6). doi:ARTN 18210.1007/s00158-022-03278-x

Yildiz, V., & Vrugt, J. A. (2019). A toolbox for the optimal design of run-of-river hydropower plants. *Environmental Modelling & Software, 111*, 134-152. doi:10.1016/j.envsoft.2018.08.018

Zeidan, M., & Ostfeld, A. (2022). Hydraulic Ram Pump Integration into Water Distribution Systems for Energy Recovery Application. *Water, 14*(1). doi:ARTN 2110.3390/w14010021

Zhang, R. H., Chen, X. B., & Luo, J. Q. (2021). Knowledge mining of low specific speed centrifugal pump impeller based on proper orthogonal decomposition method. *Journal of Thermal Science, 30*(3), 840-848. doi:10.1007/s11630-020-1356-5

Author Information

Van Thanh Tien Nguyen
Industrial University of Ho Chi Minh City
12, Nguyen Van Bao, Go Vap, Ho Chi Minh City, Vietnam
Contact e-mail: *thanhtienck@ieee.org*

Thi Minh Nhut Vo
Thu Dau Mot University
Binh Duong, Vietnam

To cite this article:

Artificial Intelligence in HR: Practices and Prospects of the Spread in Ukraine

Svitlana TSYMBALIUK
Kyiv National Economic University

Alla VASYLYK
Kyiv National Economic University

Olga BILYK
Kyiv National Economic University

Abstract: The main purpose of the study is to assess the use of Artificial Intelligence (AI) in HR in Ukrainian organizations practice and the prospects of the AI spread in HR. The results of the survey confirmed the first working hypotheses that the spread of AI in HR is a natural process; and partially confirmed the second hypothesis that the use of AI in HR has both positive and negative consequences. Due to the spread of AI in HR today, one of the most important competencies of HR professionals is the ability to perform various HR functions and processes using AI technologies, which requires appropriate training and experience.

Keywords: Artificial intelligence, Human resources management, HR practices

Introduction

The modern world is hard to imagine without digital technology and Artificial Intelligence (AI). All spheres of human life and the functioning of the economy make extensive use of scientific and technological progress. There are more and more applications of Artificial Intelligence in such areas as finance, e-commerce, marketing, communications, etc. For a long time, Artificial Intelligence seemed a distant reality for the field of personnel management, until now. Automation of such traditionally routine HR functions as search and selection of candidates, resume processing, correspondence with candidates, interview planning, evaluation of professional performance, feedback collection helps to reduce the time spent on these processes and increase their efficiency. The huge potential of AI-based software for automating HR functions and cloud tools necessitates their implementation in the personnel management system of the enterprise. That is why monitoring the level of implementation of Artificial Intelligence in HR is relevant.

Literature Review

The expediency of introducing Artificial Intelligence in HR practice is confirmed by the research of theorists and the experience of practitioners. O'Connor (2020) defines Artificial Intelligence (AI) as a technology that allows computers to learn from previously collected data and to draw conclusions or recommend actions. Saxena (2020) defines AI in HR as a means of providing human resources with advanced tools for consistent decision-making to solve human resources business problems by automating repetitive tasks. Jatobaa et al (2019) conducted research on the evolution of the use of Artificial Intelligence in human resource management (HRM) over the past 18 years. The authors divide the process of implementation of Artificial Intelligence in HR into three periods: First decade, Reduction Period and Period of Growth. The first period (2000-2010) the

authors associate with the general development of Artificial Intelligence, the emergence of interest in the use of AI in various fields and the first attempts to implement it in the field of human resource management. The second period (2011-2017) is called the "Reduction Period", as there was a decline in interest in research on the application of AI in HR, which was manifested in the absence of comprehensive targeted research and development. According to the authors, the "Period of Growth" of AI in HR implementation started in 2018. The promoters of this are the countless possibilities of automation due to the advanced achievements in the field of Artificial Intelligence, and the new requirements of companies for human resource management, which stimulate new research.

So, the results of a study conducted Matsa and Gullamajji (2019), published in the International Research Journal of Engineering and Technology, showed that the integration of artificial intelligence, which can quickly and efficiently analyze, diagnose and predict, allows more objective justification of personnel decisions and, consequently, significantly increases the efficiency of personnel management. "Integration of HR practices with AI based applicants definitely have a stronger impact in enhancing the organizational performance. Even though AI applications may not possess the abilities like humans the emotional and cognitive abilities, but these powerful AI based HR applications can analyze, predict, diagnose, and it is powerful resource for any kind of organization." stated the report (Barboza, 2019). The results of the study showed that "66% of the respondents believed that the use of AI in management systems will give rise to more transparent meritocracy in the workplace. 74% opined and predicted that within the next 10 years, AI will be standard practice for measuring the employee performance" (Barboza, 2019).

Varallyai and Hmoud (2020) conducted research on the factors influencing the intention to use personnel systems that use AI. Scientists have found that a significant impact on the intention to use AI in HR is influenced by awareness of the possibilities of using artificial intelligence in personnel management and confidence in technological innovations or new technological solutions. In addition, the study showed that HR professionals generally have a positive attitude and trust in new AI technologies to maintain the effectiveness of personnel management in organizations.

Baakeel (2020) conducted research on the relationship between the use of Artificial Intelligence in personnel management and the effectiveness of personnel processes in the company. The author proves that there is a statistically significant association between the effectiveness of personnel management functions, in particular the selection and recruitment of personnel, the analysis of talent acquisition, and the use of AI in these processes. In addition, the author substantiates that the correlation between the effectiveness of HRM functions and the use of AI is strong.

It should be noted that there is a growing trend of commitment to the implementation of AI in HR by companies. Research conducted Hmoud (2021) confirms this dynamic to the growing desire of managers to use AI in HR. The author also substantiates that technologies based on Artificial Intelligence will continue to appear, develop and offer advanced services that radically change the field of personnel management. The presence of such trends requires managers to be well-informed about the trends and innovations of AI in HR in order to keep the company in a specific environment. AI has a number of uses in HR. Berhil, Benlahmar and Labani (2020) consider the use of AI in HR in the following areas: Recruitment, Jobs & Skills Management; Employee Attrition Prediction; Employee's Turn Over; Improve human resources talents, productivity, effectiveness and performance. Barboza (2019) claims that today Artificial Intelligence (AI) is reshaping the way companies manage their workforce and considers the following uses of AI in HR: AI in Talent Acquisition; AI in Organizational Adaptation; AI in Succession Planning; AI in Training; AI in Performance appraisal; AI in Human Capital Management (HCM); AI in Retention.

Based on the generalization of the approaches of different scientists, we have formulated important theoretical and methodological principles for studying the use of AI in HR. In the dynamic information world, technology has changed approaches to enterprise management, and personnel management in particular. Artificial intelligence technologies have enabled organizations to enhance their existing performance by effectively performing personnel management functions on a day-to-day basis.

We have identified a number of factors that affect the spread of AI in HR:

- awareness of HR managers with modern technologies and the possibilities of their use in HR;
- development of AI use in HR in various areas of personnel management;
- economic feasibility of using specific AI systems in HR;
- substantiated positive and negative results of AI use in HR.

Summarizing the best practices of AI implementation in HR, we have compiled a list of the main areas of use of AI in human resource management. In particular, AI is used in the following HR functions (tasks, processes):

- preparation of a job description (requirements for a candidate for a vacant position);
- search for candidates (work with resume databases);
- professional selection (removal of resumes of candidates who do not meet the requirements of the position and/or corporate values of the company);
- correspondence with candidates, in particular with the use of chatbots;
- study of candidates' resumes;
- evaluation of candidates (based on video interviews, results of professional and psychological online testing, questionnaires, etc.);
- consulting new employees during onboarding and accompanying newly hired employees during the adaptation period;
- performance of functions of management and control of efficiency of professional activity of employees (delivery of the purposes, tasks, development of KPI);
- ensuring fairness and transparency of the remuneration system through electronic recording of employees' achievements in professional activities;
- evaluation the behavior of employees to identify their socio-psychological destructive (conflict) behavior or intentions to leave the company (reduced loyalty to the company);
- modeling, forecasting and drawing up a plan of professional and career growth for employees;
- employee engagement management;
- study of the effectiveness of working time and violations of labor behavior;
- establishing feedback with the company's staff and answering standard HR-questions of employees;
- study of the reasons and motives for dismissal.

The positive consequences of using AI in HR are:

- reduction of time spent on certain HR functions, which in turn helps to speed up the process of personnel decisions;
- accelerating the analysis of large amounts of data;
- impartiality, objectivity and transparency of personnel decisions made on the basis of the conclusions of artificial intelligence systems;
- minimization of errors related to the human factor (bias, inattention, ignorance, incompetence, etc.);
- optimization (reduction) of costs for the implementation of certain HR functions.

The negative consequences of using AI in HR are:

- partial replacement of human labor by technology, which inevitably leads to a decrease in the need for HR professionals in the labor market (rising unemployment among workers in this sector);
- lack of emotional component, namely the use of AI does not allow to take into account emotional intelligence when making personnel decisions;
- decisions made on the basis of conclusions and recommendations of artificial intelligence programs are rarely subject to critical analysis and doubt (high confidence in the machine brain);
- probability of loss of personal data and confidential information.

The main purpose of the study is to assess the use of AI in HR in Ukrainian organizations practice and the prospects of the AI spread in HR.

Methodology

The working hypotheses of the research are: the first one – the spread of AI in HR is a natural process (H1); the second one – the use of AI in HR, has both positive and negative consequences (H2). To confirm or disprove the working hypotheses, the authors have conducted quantitative research (a survey) during April - June 2021. The research aims to assess the use of AI in HR in Ukraine, to determine the prospects for its spread and the expected consequences.

The objectives of the research are the next:

- to assess the level of awareness of HR managers with the possibilities of using AI in HR;
- to define the directions of use of AI in HR;
- to substantiate the expediency of use and prospects of the spread of AI in HR;
- to determine positive and negative consequences of using AI in HR.

88 HR managers from Ukrainian companies undertook the survey. A score scale from 0 to 5 was used to assess the level of awareness of respondents with the possibilities of using AI in HR and the practicability of using AI in HR, where 0 is not advisably at all, 5 is quite advisably. A standard symmetrical scale of answers was used to determine the directions (functions, processes, tasks) of using AI in HR: "yes", "no", "difficult to answer".

In order to assess the spread of using AI in HR, the positive and negative consequences of its usage it was used a scale: "completely agree", "rather agree", "rather disagree", "disagree completely", and "difficult to answer". The analysis of the respondents' assessment of the level of their awareness of the possibilities of using AI in HR and the practicability of using AI in HR was carried out based on the following statistical indicators – average (arithmetic average, median, mode), coefficients of variation and asymmetry, excesses, etc. The coefficient of variation was calculated by the formula (1)

$$V_\sigma = \frac{\sigma}{\overline{x}} \cdot 100\% \qquad (1)$$

where σ – means square (standard) deviation;
$\overline{x}$ – arithmetic average value.

Results

Statistical indicators of the respondents' assessment of the level of their awareness of the possibilities of using AI in HR are shown in Table 1.

Table 1. Statistical indicators of the respondents' assessment of the level of their awareness of the possibilities of using AI in HR

Statistical indicators	Value
Arithmetic average	3.43
Standard error	0.08
Median	4
Mode	4
Standard deviation	0.78
Sample dispersion	0.62
Excess	-0.51
Asymmetry	-0.35
Interval	3
Minimum	2
Maximum	5
Total	302
Score	88

The average statistical indicators indicate a high level of respondents' awareness of the possibilities of using AI in HR. The coefficient of variation is 22.7% (less than 33%). It indicates that the assessments of the HR managers of their awareness of the possibilities of using AI in HR are homogeneous. The asymmetry coefficient has a negative value (see Table 1) and more (by module) than 0.25 ($|A| > 0.25$), which indicates a left-sided high asymmetry in the distribution of respondents' awareness of the possibilities of using AI in HR are homogeneous. The negative value of the excess ($Ek > 0$) indicates that the distribution is flat-topped. The distribution of respondents based on the assessment of their awareness of the possibilities of using AI in HR is presented in Figure 1.

Figure 1. Distribution of respondents based on the assessment of their awareness of the possibilities of using AI in HR

Thus, the research results indicate a high rate of respondents' assessment of their awareness of the possibilities of using AI in HR. The distribution of respondents' answers to the question about using AI in HR in organizations is shown in Figure 2. According to Figure 2, 36.4% of respondents said that the organization uses AI in HR. Regarding the prospects for the spread of AI in HR, 52.3% of respondents indicated that the organization plans to use/expand the AI use in HR. This confirmed the first hypothesis (H1): the spread of AI in HR is a natural process.
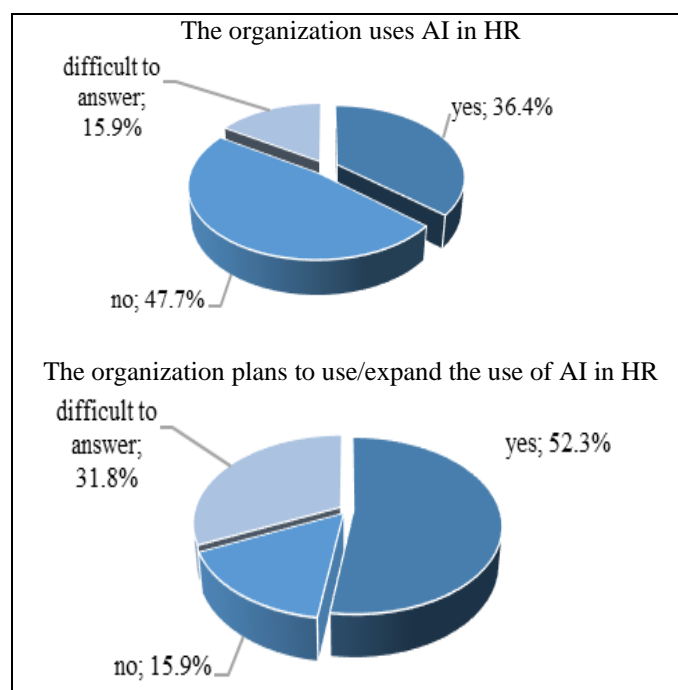
Figure 2. Using AI in HR in organizations

The survey results on using AI in HR (in organizations where AI is used in HR) are given in Table 2. According to Table 2, the most common functions of using AI in HR are search for candidates, consulting new employees during onboarding and adaptation, correspondence with candidates, in particular using chatbots, and answers to HR questions of employees.

Statistical indicators of the respondents' assessment of the practicability of using AI in HR are shown in Table 3. The average statistical indicators indicate a high level of respondents' assessment of the practicability of using AI in HR. The coefficient of variation is 26.8% (less than 33%). It indicates that the assessments of the HR managers of their awareness of the possibilities of using AI in HR assessments of the HR managers of the practicability of using AI in HR are homogeneous.

Table 2. The survey results on using AI in HR

Functions (tasks, processes)	Answers, %		
	yes	no	difficult to answer
Preparation of job description	19.0	59.5	21.4
Search for candidates	52.4	35.7	11.9
Correspondence with candidates, in particular using chatbots	45.2	45.2	9.5
Study of candidates' resumes	35.7	54.8	9.5
Evaluation of candidates (based on video interviews, test results, questionnaires, etc.)	26.2	61.9	11.9
Consulting new employees during onboarding and adaptation	52.4	38.1	9.5
Track employees' behaviour to identify their intentions to leave the company	23.8	61.9	14.3
Answers to HR questions of employees	40.5	52.4	7.1
Performing functions of control over the activities of employees	28.6	52.4	19.0
Employee performance management (set up goals and objectives, KPI development)	35.7	45.2	19.0
Compensation management	31.0	47.6	21.4
Customizing professional and career development offers for employees	35.7	47.6	16.7
Employee engagement management	23.8	54.8	21.4
Revealing abnormal behaviour, which may indicate inefficient use of time, corruption or other violations of employees	14.3	64.3	21.4
Conducting an exit interview with dismissed employees	14.3	71.4	14.3

The asymmetry coefficient has a negative value (see Table 3) and more (by module) than 0.25 ($|A| > 0.25$), which indicates a left-sided high asymmetry in the distribution of respondents' assessment of the practicability of using AI in HR are homogeneous.

Table 3. Statistical indicators of the respondents' assessment of the practicability of using AI in HR

Statistical indicators	Value
Arithmetic average	4.11
Standard error	0.12
Median	4.5
Mode	5
Standard deviation	1.1
Sample dispersion	1.2
Excess	0.88
Asymmetry	-1.19
Interval	4
Minimum	1
Maximum	5
Total	362
Score	88

The positive value of the excess ($Ek > 0$) indicates that the distribution is peaked.The distribution of respondents based on the assessment of the practicability of using AI in HR is presented in Figure 3. The results of the resp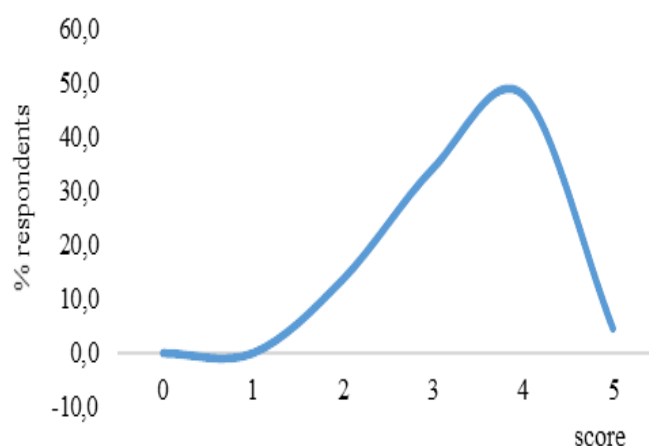ondents' assessment of the prospects of the AI spread in HR are given in Table 4. According to the survey results, the vast majority of respondents (81.9%) negatively assess the prospects of complete replacement human resources by AI to perform all HR functions. Respondents' assessment of the complete replacement of human resources by AI to perform some HR functions are positive: 59.1% completely supported this idea. Respondents consider that replacement of human resources by AI to perform some HR processes is promising: 93.2% gave positive answers. The vast majority of respondents (93.2%) believed that only people can perform some HR functions and, accordingly, AI cannot replace these functions.
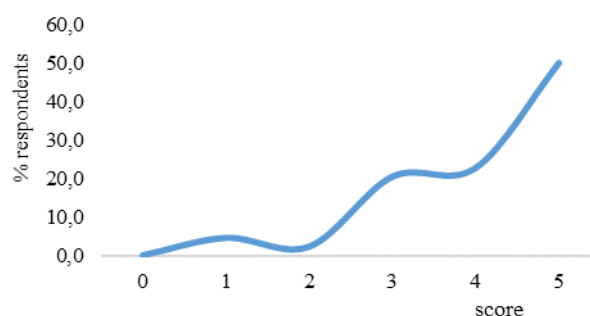
Figure 3. The distribution of respondents based on the assessment of the practicability of using AI in HR

Table 4. The results of the respondents' assessment of the prospects of the AI spread in HR

Statements	Answers, %				
	completely agree	rather agree	rather disagree	disagree completely	difficult to answer
AI can completely replace human resources to perform all HR functions	2.3	15.9	36.4	45.5	0.0
AI can completely replace human resources to perform some HR functions	15.9	43.2	27.3	11.4	2.3
AI can replace human resources to perform only some HR processes	31.8	61.4	6.8	0.0	0.0
Some HR functions can only be performed by people	75.0	18.2	6.8	0.0	0.0

Respondents' assessments of the positive consequences of using AI in HR are given in Table 5.

Table 5. Respondents' assessments of the positive consequences of using AI in HR

Statements	Answers, %				
	completely agree	rather agree	rather disagree	disagree completely	difficult to answer
Using AI saves time for HR professionals	61.4	36.4	0.0	0.0	2.3
Using AI allows you to quickly analyze large amounts of data	81.8	13.6	4.5	0.0	0.0
Using AI allows you to increase the objectivity of personnel decisions	31.8	31.8	34.1	0.0	2.3
Using AI reduces the number of errors caused by the human factor	40.9	43.2	13.6	0.0	2.3
Using AI can speed up the personnel decision-making process	27.3	29.5	13.6	4.5	2.3
Using AI reduces costs	34.1	36.4	15.9	6.8	6.8
Using AI has a positive impact on efficiency	31.8	52.3	6.8	0.0	9.1

According to the survey, the most significant positive consequences of using AI in HR are the following:

— using AI saves time for HR professionals (97.8% of respondents gave affirmative answers);
— using AI allows you to quickly analyze large amounts of data (95.4%);
— using AI reduces the number of errors caused by the human factor (84.1%);
— using AI has a positive impact on efficiency (84.1%).

Respondents' assessments of the negative consequences of using AI in HR are given in Table 6.

Table 6. Respondents' assessments of the negative consequences of using AI in HR

Statements	Answers, %				
	completely agree	rather agree	rather disagree	disagree completely	difficult to answer
The use of AI reduces the need for HR professionals and, consequently, increases unemployment	15.9	29.5	40.9	13.6	0.0
The use of AI does not allow emotional intelligence to be taken into account when making decisions	50.0	29.5	13.6	4.5	2.3
It is difficult to find errors in AI-based decisions	15.9	25.0	45.5	4.5	9.1
The use of AI complicates the process of personal data protection	2.3	27.3	38.6	18.2	13.6
The use of AI leads to intrusion into privacy	0.0	31.8	40.9	15.9	11.4
Using AI increases the likelihood of loss of confidential information	4.5	31.8	34.1	15.9	13.6
Using AI can negatively impact corporate culture	11.4	29.5	36.4	11.4	11.4

Among the most significant negative consequences identified by respondents:

-       the use of AI does not allow emotional intelligence to be taken into account when making decisions (79.5% of respondents gave affirmative answers);
-       the use of AI reduces the need for HR professionals and, consequently, increases unemployment (45.5%);
-       it is difficult to find errors in AI-based decisions AI (40.9%);
-       using AI can negatively impact corporate culture (40.9%).

Regarding the other negative consequences, less than 40% of respondents gave affirmative answers, and some negative consequences were refuted. The respondents' assessment of the consequences of using AI in HR showed that HR specialists have a positive attitude to the spread of AI technologies in HR. The respondents' assessment partially confirmed the second hypothesis (H2) that the use of AI in HR has both positive and negative consequences as respondents identified more positive effects than negative ones, and assessments of positive results far exceed the negative ones.

Since the spread of AI in HR is a natural process, as confirmed by the survey, and this process has many obvious positive consequences, managers and HR professionals must objectively assess the prospects of implementing AI technologies in HR practices bearing in mind the specifics of the organization. It is significant to find ways to minimize the negative consequences of the spread of AI in HR.

The main disadvantage of implementing AI in HR is the inability to make decisions using emotional intelligence. In this regard, it is necessary to identify decisions where emotional intelligence is critical, and people have to make such decisions. As AI use can reduce the need for HR professionals, they must prepare to retrain and master competencies to perform functions and processes that need human participation.

Conclusion

The results of the survey confirmed the first working hypotheses that the spread of AI in HR is a natural process; and partially confirmed the second hypothesis that the use of AI in HR has both positive and negative consequences. According to the survey results, the vast majority of respondents negatively assess the prospects of complete replacement human resources by AI to perform all HR functions. Respondents' assessment of the complete replacement of human resources by AI to perform some routine HR functions are positive. Respondents consider that replacement of human resources by AI to perform some HR processes is promising. The vast majority of respondents believed that only people can perform some HR functions and, accordingly, AI cannot replace these functions. Due to the spread of AI in HR today, one of the most important competencies of

HR professionals is the ability to perform various HR functions and processes using AI technologies, which requires appropriate training and experience.

Scientific Ethics Declaration

The authors declare that the scientific ethical and legal responsibility of this article published in EPSTEM journal belongs to the authors.

Acknowledgements or Notes

This article was presented as an oral presentation at the International Conference on Research in Engineering, Technology and Science (www.icrets.net) conference held in Baku/Azerbaijan on July 01-04, 2022.

References

Baakeel, O. A. (2020).The association between the effectiveness of human resource management functions and the use of artificial intelligence. *International Journal of Advanced Trends in Computer Science and Engineering. 9 (1.1),* 606-612. https://doi.org/10.30534/ijatcse/2020/9891.12020

Barboza, D.C. (2019). Artificial intelligence and hr: the new wave of technology. *Journal of Advances in Social Science and humanities JASSH, 5 (4),* 715–720. https://doi.org/10.15520/jassh54429

Berhil, S., Benlahmar, H. & Labani, N. (2020). A review paper on artificial intelligence at the service of human resources management. *Indonesian Journal of Electrical Engineering and Computer Science. 18.(1),* 32-40. http://doi.org/10.11591/ijeecs.v18.i1.pp32-40

Hmoud, B. (2021) The adoption of artificial intelligence in human resource management and the role of human resources. *Forum Scientiae Oeconomia. 9 (1),* 105-118. https://doi.org/10.23762/FSO_VOL9_NO1_7

Jatobaa, M., Santosa, J., Gutierriza, I. & Moscon, D. (2019). Evolution of artificial intelligence research in human resources. *Procedia Computer Science. 164,* 137-142. DOI: https://doi.org/10.1016/j.procs.2019.12.165

Matsa, P. & Gullamajji, K. (2019). to study impact of artificial intelligence on human resource management. *International Research Journal of Engineering and Technology (IRJET),* 1229-1238. Retrieved from https://www.irjet.net/archives/V6/i8/IRJET-V6I8226.pdf

O'Connor, S. W. (2020). *Artificial intelligence in human resource management.* Retrieved from https://www.northeastern.edu/graduate/blog/artificial-intelligence-in-human-resource-management/

Saxena, A. (2020). The growing role of artificial intelligence in human resource. *EPRA International Journal of Multidisciplinary Research (IJMR). 6 (8),* 152-158. https://doi.org/10.36713/epra4924

Varallyai, L., & Hmoud, B. (2020). Artificial intelligence in human resources information systems: investigating its trust and adoption determinants. *International Journal of Engineering and Management Sciences (IJEMS). 5 (1),* 749-765. https://doi.org/10.21791/IJEMS.2020.1.65

Author Information

Svitlana Tsymbaliuk
Kyiv National Economic University named after V. Hetman
54/1 Prospect Peremogy 03057 Kyiv Ukraine
Contact e-mail: *tsymbaliuk_svitlana@ukr.net*

Alla Vasylyk
Kyiv National Economic University named after V. Hetman
54/1 Prospect Peremogy 03057 Kyiv Ukraine

Olga Bilyk
Kyiv National Economic University named after V. Hetman
54/1 Prospect Peremogy 03057 Kyiv Ukraine

To cite this article:

Tsymbaliuk, S., Vasylyk, A. & Bilyk, O. (2022). Artificial intelligence in HR: practices and prospects of the spread in Ukraine. *The Eurasia Proceedings of Science, Technology, Engineering & Mathematics (EPSTEM), 17,* 152-160.

ICRETS 2022: International Conference on Research in Engineering, Technology and Science

The Effectiveness of Kindergarten Buildings in Jordan: Shaping the Future toward Child-Friendly Architecture

Shaden ABUSAFIEH
Al-Ahliyya Amman University

Nouran MUWAHID
Al-Ahliyya Amman University

Rawan MUWAHID
Al-Ahliyya Amman University

Lama ALHAWATMAH
Al-Ahliyya Amman University

Abstract: From a sociology perspective, schools and kindergartens are society's primary institutions. Hence, safety in schools and especially kindergartens is essential for society. Moreover, due to the increasing number of working mothers in Jordan, the demand for safe and reliable kindergarten design has become extremely important. Child safety from injury, especially within the age group 4 to 6 years, is a crucial issue in architectural design. Moreover, there is a lack of interest in this age group compared to nurseries or primary schools. Therefore, this study aims to conduct a systematic field study to reveal to what extent Kindergartens in Amman city, as a case study, have achieved the fundamental criteria of a safe and child-friendly environment. The case study analytical approach was applied to a random sample of Amman kindergartens to generate an in-depth evaluation of the inner and outer built environment and its features based on the UNICEF evaluation checklist for the child-friendly environment. In addition, a triangulation method (interviews, questionnaires, and field visits) was used to ensure the credibility and reliability of the collected data. Results revealed that kindergartens achieved only 40% of the benchmark criteria for a safe, child-friendly environment. This percentage rings the bell for a real problem that must be considered and brought to the attention of the responsible authorities to find the necessary solutions to create a safe, healthy, child-friendly environment. The research proposed a framework consisting of proposals and practical solutions to the various kindergarten design problems. More large-scale studies are required to evaluate kindergartens in other cities in Jordan to develop national sustainable standards that consider the child's psychological, physical, and intellectual aspects, with the participation of government sectors, universities, experts, and students of architecture colleges.

Keywords: Architecture engineering, Civil engineering, Child-friendly architecture, Sustainable design, Design for safety

Introduction

Every child has the right to a safe environment, protected from injury and violence. Any facility or institution caring for the child is responsible for providing the necessary protection and care, regardless of the difficulty in achieving this task (WHO, 1986). Despite this, around 2,400 children worldwide die from unintentional or intentional injuries (Peden et al., 2008). Injury is a common reason for children to visit the emergency room or be admitted to the hospital. According to the National Safety Council, the National Center for Injury Prevention

and Control, and other sources, injury is the primary cause of death in children and young adults. Moreover, over 40% of deaths among children aged 1 to 14 are caused by injuries (UNICEF, 2001).

Schooling is the one shared experience that most children have around the world, and it is the most common way for societies to educate their children for the future. More than a billion youngsters attend schools or kindergartens on any given day. They share the experience of learning, developing their potential, and enhancing their lives in permanent or temporary facilities. But on the other hand, schooling is not always a joyful experience for children.

The Convention on the Rights of the Child (CRC) emphasizes fundamental human rights principles: the access that allows for learning; the quality that promotes cognitive and affective growth; and the respect that values the individual's language, culture, religion, and point of view (Convention on the rights of the child, 1989). These principles played an essential role in the schools, ensuring a child's overall development and child-friendly environments. As a result, many nations' educators have been looking for ways to implement the CRC in schools. The child-friendly school action (CFS) takes a rights-based education approach and is one of the best initiatives (Clarke et al., 2001).

The United Nations Children's Fund (UNICEF) sought to create an education model aimed at helping schools achieve safe, healthy, and preventative environments that meet the needs of children. UNICEF was the first to employ the concept of child-friendly settings to improve interaction and engagement, but it was later expanded to include educational settings. This idea has been adopted and focused on by many countries. In the last decade, these approaches have been advocated in primary schools, and UNICEF's "Child-Friendly Schools Manual" has been used to transfer child-friendly surroundings to schools (Wright et al., 2009).

Child-friendly Schools

Fulfilling the education goals is not only ensuring that all children attend school. Its comprehensive mission ensures that all schools work in the children's best interests. This entails creating safe and secure schools that are appropriately staffed with trained teachers, supplied with sufficient resources, and blessed with conducive learning environments.

Learning environments should support students' and teachers' physical, psycho-socio, and emotional health. Child-friendly schools (CFS) use a multidimensional approach to quality that considers the whole child's needs as learners. According to UNICEF, the CFS model aims to move schools and education systems closer to quality standards over time (Almazeedi, 2019). In other words, they allow children to attain, at the very least, the knowledge and skills required by the curriculum and assist children in developing their ability to think and reason. Moreover, CFS helps children develop self-respect and respect for others and realize their full potential as individuals, community members, and global citizens (Mohidin et al., 2015).

CFS is a model that encourages schools to work in child-centered environments where children provide context that allows children to learn and develop; respect their identities, interests, and needs. The child-friendly schools manual proposed by UNICEF addressed all factors that affect the child's well-being and rights as a learner REF. Moreover, the CFS manual emphasizes a critical principle of a safe, healthy, and protective environment. According to CRC, children in the school environment should be away from violence, abuse, and injury. This learning setting benefits all children's physical and mental health.

Child-friendly School Manual by UNICEF

As the leading developer of various CFS models, UNICEF took responsibility for presenting a cohesive overview of them, summarizing their key aspects to establish a template that can build national capabilities that design and develop CFS in various countries. This manual introduces the child-friendly idea, its underlying ideology, and the essential concepts that can be used to derive the major characteristics of a child-friendly school in many settings. Moreover, it provides practical guidance on designing, constructing, and managing child-friendly schools as safe, welcoming learning spaces, focusing on community connections, educational concerns, cost-effectiveness, and sustainability (Wright et al., 2009). Table 1 explores how new CFS spaces are planned and designed, considering the location, design, building construction, operation, and maintenance.

Table 1. Basic planning and design standards for school facilities (Wright et al., 2009)

Essential Elements and Criteria for CFS	Characteristics
Structure	The structure must be waterproof following local environmental conditions, climatically comfortable, quickly exited in an emergency, and well-integrated with the surrounding environment and culture.
Administrative Office	Separate space for teaching and administrative workers provides privacy for students and teachers. To monitor students' activities and create safety through transparency,' proximity between classrooms and administrative offices is recommended. Increases classroom space to allow staff to work independently from students.
Safe Water	Within the school, children should have access to fresh, potable water. The provision of safe water is made possible by proper plumbing infrastructure. A borehole/well should be included in the school compound if such a setup does not exist. As needed, this can be supplemented by a roof-mounted rainwater collection system.
Hygiene Facilities	For youngsters to wash their hands, a separate area with water, soap, or another cleaning agent should be provided.
Toilets	For girls and boys, separate toilets should be available. Regarding facility location and design, privacy, cleanliness, and safety are essential factors. Separate bathrooms for boys and girls within or near the classrooms are the most practical and safest arrangement for students. However, to protect younger children, these facilities can be constructed and placed so they are shared among clusters of classrooms.
Environmental Conditions: Light, air, sun, dust, glare, reflection, humidity, noise, and odor	Classrooms require sufficient fresh-air circulation To minimize heat and excessive humidity. A minimum of 20% of the classroom floor's area should be a window area to ensure adequate daylight. Electricity is required to give light and run the equipment. Direct sunshine, glare, and reflection must be adequately shaded in classrooms (indirect light). Schools should not be built near sources of excessive noise (traffic, railways, industry, or informal sector activities), pollution, or odors (waste belts, abattoirs). If this isn't possible, design treatments to reduce the impact of these issues should be used.
Color	Warm natural hues (reds, oranges, maroons, ochres, and linen/khaki/off-white) guided by local cultural tastes should be selected in harmony with the light, natural colors of the building materials. Materials like transparent varnish can be applied to maintain the material's natural beauty and warmth. Play corners, decks, corridors, and furniture can benefit from brighter colors. Learning environments should be light and airy, not gloomy, dull, or dark.
Power and Electric	A power supply should be available at the school to provide illumination and connectivity for communication equipment (computers, radios, and televisions) and other appliances (refrigerators, stoves). Alternative energy sources (solar, wind, and biogas) can be integrated into school design.
Safety Provisions	The design process and the school curriculum must include fire fighting and emergency evacuation plans. Flammable materials should not be used for construction unless treated to resist fire. Construction materials should be free of dangerous components or elements. All fluid, solid, and gaseous wastes should be removed from school sites once construction is completed. Industrial or other hazards should not be near schools.
Health Provisions	Schools should provide a first-aid kit or medicine cabinet for basic emergencies or accidents. Schools should be close to a clinic, so health personnel can visit the school regularly, and children can be taken to the clinic to treat health problems. Many developing countries achieve this proximity by clustering the primary social services in the exact location.
Library	Learning and teaching activities require a particular space where books and learning resources may be found in a comfortable reading environment. The library or resource room should be strategically positioned within the school to allow for convenient access while remaining quiet.
Landscaping	School grounds create an integrated, comprehensive unity between school buildings and their users. Trees are necessary for the filtration of sunlight, dust, and noise and for beautifying the school. Indigenous trees, shrubs, flowers, and edible plants

	should be planted on the school grounds to teach children about food production and sustainability. The learning environment and its users are also softened and calmed by trees. Planning the landscaping for the school is an excellent method to involve children in creating a child-friendly environment.
Flexible Spaces	Flexible spaces provoke student participation in class and enable teachers to create a more dynamic learning and teaching environment. Group activities, rooms for manual work, and easy access to open spaces are all available in such spaces. All students should be able to access their classrooms; ramps and broad doorways should be provided for less-mobile children.
Relaxation Rooms	Rooms -where children can relax- are ideal in the design of child-friendly schools at the nursery and kindergarten levels. In general, homelike aspects near learning places create a welcoming, friendly environment for this age group.
Individual Spaces	Individual-learning spaces should be offered in addition to flexible learning spaces for large and small groups (project-based learning/teamwork) because children have different learning styles, and some will need room to study or reflect on their own.
Open Spaces	Easy access to open spaces from classrooms grants direct contact for children with their environment and allows them to participate in physical activities. Sports fields, school gardens and orchards, decks or verandas for outdoor learning activities, open performance spaces, broad corridors and courtyards, trellises, canopies, shaded pavilions, nooks, alcoves, play lofts, and enclosed backyards are all examples of open spaces. After school, the community may use these spaces for neighborhood gatherings and other events.
Kitchen	Food should be kept fresh and away from flies and other pests that degrade food quality in school lunch preparation spaces, which should be constructed and furnished with appropriate equipment and furniture.
Clinic	Having the school near a clinic and health services helps children with general health services and allows for treating children who require constant monitoring of their health issues. This would establish a link between school, community, and family, all of which revolve around the child's well-being.
Protective	There are two critical aspects to the protective feature of child-friendly school design: -Teachers and parents must be trained in nonviolent, child-based disciplining tactics and interventions to combat bullying and abuse. Child abuse can be prevented by designing schools and other spaces to make actions visible from the outside. -The enclosure and limits of schools can vary in form and function depending on location and environment. The idea is to strike a balance where a fence can protect a child from outside factors (such as traffic and animals), set boundaries to keep students within the school, and separate an area for gardening and orchards.

Children should have the chance to get a beautiful, challenging, and interactive built environment from their early childhood (kindergarten) that helps them shape their sense of aesthetics and play as the bedrock for their knowledge and personalities. Moreover, an unrestricted environment consolidates a creative and innovative approach that establishes an evoking and renewable future vision. Therefore, CFS must balance the child's need for challenge exploration and safety. This research concentrates on the critical built-environment features highlighted in the CFS manual and related to child physical safety.

Early Childhood- Kindergarten Settings

Childhood is a distinct physical, mental, and cognitive stage that ranges from one and a half to sixteen years (Dudek, 2005). Dudek defined kindergarten (early childhood between the ages of four and six) as the children's garden, in which the child blooms and grows like a plant. From a sociological perspective, schools from early childhood (kindergartens) are the fundamental institution for society ((Parsons, 1966). Therefore, kindergarten is one of the most critical stages in forming a child's personality and education; it deals with the most critical years of a human's life that affect his mental, psychological, and emotional development (Anbari & Soltanzadeh, 2015).

At the age of four, a child is full of energy, talkative and curious, asks many questions, and desires to test his environment and explore his surroundings (Anbari & Soltanzadeh, 2015). In his theory of cognitive development, Piaget called this stage the pre-operational stage, where the child builds and develops his

knowledge through experience and exploring his surrounding environment (Piaget, 2013). Kindergartens are available worldwide, providing preschoolers with early education and care (Watson & White, 2001). However, with the significant increase in working mothers in the workforce, the demand for kindergarten childcare has increased significantly over the past few years (Chen, 2013). Children in kindergarten spend 2.5 hours on average in Finland. In comparison, it rises to 4 hours per day in Germany (Kong & Kumpulainen, 2018), while in Jordan, it ranges from 5 to 7 hours per day (in the case of the waiting system after official working hours). Therefore, the demand for safe and reliable kindergarten schools has become extremely important.

Based on the above facts, the child-safe environment in kindergarten is an important topic that needs exploration and research, noting that injuries and accidents in kindergartens are not given attention, and data for these injuries are not recorded so far. Only severe injuries among children were reported in the media or social media, including deaths. Thus, the importance of this research comes with the increasing concerns about the safety of children and injury prevention, especially in the age group 4 to 6 years, and with the lack of interest in this age group compared to nurseries or primary schools.

The main objective was to conduct a systematic field study to reveal to what extent Kindergartens in Amman, as a case study from Jordan, achieved the factors related to a safe and child-friendly environment according to the CFS manual by UNICEF. This would help improve the environment's physical safety and highlight the need for innovative technological and sustainable solutions within indoor and outdoor kindergartens' built environments. To provide a child-friendly environment in kindergartens, Leinonen and Vetiand emphasized that four main factors must be considered in the design: comfort, movement, efficiency, and control (Leinonen & Venninen, 2012). Furthermore, to achieve comfort, great attention was paid to the appropriate scale for the child, such as the dimensions of the classroom and classroom furniture, the ceiling height, the floor height, and the texture of the finishing materials. The movement also represents one of the leading design requirements in kindergarten and is the cornerstone of every intellectual child's development as he learns life experiences through play (Anbari & Soltanzadeh, 2015). Therefore, the architectural elements in the interior spaces, such as educational classrooms, and the outdoor spaces, such as playgrounds, must provide a child-friendly environment that allows them to move freely and safely without being subjected to physical injuries.

Stating the Problem

Currently, very few studies evaluate safety practices related to the built environment in kindergartens. For example, Davison revealed that 85% of school injuries occurred during rest and physical education, accounting for about a third of school time (Davison & Lawson, 2006). While in Germany, 47% of school injuries were related to sports, 30% to playtime, and 17% to classroom lessons for all school-age children (Scherer et al., 2006). In addition, other research has shown that injuries among children in childcare settings are increasing exponentially over time (Canadian Pediatric Society, 2009). Consequently, this problem has become a growing concern due to the increasing injury rates among children. Furthermore, despite a QIS checklist designed for kindergartens to help assess safety standards and children's well-being, many kindergartens are often reluctant to assess themselves, making the implementation of this checklist ineffective as it should be (Chiam, 2008).

Therefore, as a case study, this research aimed to explore and evaluate the physical risk factors and causes of injuries related to Amman's kindergartens' built environment structure, considering various indoor and outdoor elements. The reference point was the CFS manual which reported all the risk factors children might be exposed to at school and recommended several interventions to prevent these risks.

Methods

By analyzing the physical environment of kindergartens and linking them to cases of minor to severe injuries among children, we can understand and identify the elements that affect safety and safety in kindergartens. Thus, effective strategies can be developed to provide a safer environment, prevent future injuries, and eliminate physical environmental hazards. According to the Ministry of Education, there are 848 kindergartens in Amman, the capital of Jordan, distributed over seven different directorates. The Directorate of Education for the University Brigade was chosen to be the study population. Fifty kindergarten quota sample was selected with proportions related to the distribution of kindergartens among the University Brigade, excluding ten kindergartens who refrained from participating. That made the study sample more representative since the University's Directorate's economic and social factors are uneven.

Table 1. Evaluation questionnaire for testing child-friendly criteria at kindergartens

Pivots	Essential Criteria for CFS	Questions	1	2	3	4	5
Structural and Environmental Features	Structure	Paved roads to facilitate access to the kindergarten.					
		The building's proximity to an inhabited neighborhood					
		The kindergarten site is far away from the main streets.					
	Environmental Conditions: Light, air, sun, dust, glare, reflection, humidity, noise, and odor	Humidity and damp wall treatment in classrooms					
		The convenient temperature inside the building					
		The kindergarten building is exposed to sunlight and air.					
		The kindergarten site is far away from pollution sources.					
	Power and Electric	Kindergarten is provided with alternative power supplies					
		Electricity sockets are located far from children's reachability					
Design and Functional Features	Toilets	There are separate toilets for boys and girls					
	Flexible Spaces	Kindergartens are designed to consider less-mobile children					
		Different spaces in the kindergarten supported various activities for children					
	Relaxation Rooms	There is a relaxing room for children					
	Individual Spaces	There is an individual space for special needs children to learn and reflect					
	Kitchen	There is a kitchen and its appliances					
	Anthropometrics and Ergonomics	classroom seating is suitable and comfortable for children					
		Toilet seats of the bathroom suitable for children					
	Entrances	The distance between the main entrance of the kindergarten and the street shouldn't be less than 3 meters					
Open Spaces and Landscape features	Landscaping	Trees and plant allergies are considered in kindergarten					
	Open Spaces	Playground sharp edges are treated against injuries The swimming pool's edges and floor are treated against slippery accidents					
Health and Safety features	Safe Water and Hygiene Facilities	Fresh potable water is available for children					
	Clinic	There is a clinic and first aid kit					
		Ease of entering the building in case of emergency					
	Safety Provisions	Fire alarms and extinguishers are located in a conspicuous place					
		Emergency exits are located in clear and appropriate places					
		Children are trained for emergency evacuations					
		Treatment of doors against injury in case of a sudden close					
		Evacuation plans are hanging in clear and visible places					
		Corners and sharp edges are treated against injuries					
		There are surveillance cameras					

		The main entrance opens to the outside				
		Outdoor playground furniture is safe for children				
	Protective	Kindergarten is designed in a way that can watch classrooms				
		Kindergarten has a fence (at least 1.5 meters) and architectural features to protect children from streets hazards				

The research relies on qualitative and quantitative methodology by collecting measurable and nonmeasurable data that help draw results and conclusions. For credibility and objectivity issues, the triangulation method was used for data collection during all stages of the research. Data collection tools were interviews (56 teachers and 25 principals), direct observation with documentary evidence and checklists, and online questionnaires targeting parents of children in the chosen kindergartens. The questionnaire was designed based on the data collected from principals' and teachers' interviews and the observation results (Table 2). One hundred fifty online questionnaires were collected, while Fifty questionnaires were excluded because they were filled by patients whose children are attending kindergarten outside the chosen directorate. The research developed an evaluation tool based on the CFS manual to evaluate the kindergartens' physical environments. Table 2 elucidates the research evaluation tool built on a 5-points Likert scale providing five alternative responses (1= Very Poor, 2= Poor, 3= Fair, 4= Good, 5= Excellent), allowing parents to indicate the level of quality for the evaluated criteria.

Results and Findings

The questionnaire was the primary measurement tool used for data collection. It was designed to evaluate the safety and the effectiveness of kindergartens' built environment based on the CFS manual through field visits and online google forms. It consisted of five main pivots: Structural and Environmental Features, Design and Functional Features, Open Spaces and Landscape features, and Health and Safety features. In addition, SPSS was used to process and analyze the frequency and correlation ratios. Following are the results found from all data collection methods:

Online Questionnaire Findings

Figure 1 represents the questionnaire results from various study areas affiliated with the University Directorate at Amman. Results showed that the correlation between economic-social levels and the score of CFS criteria is (r=.89), indicating a solid positive correlation.
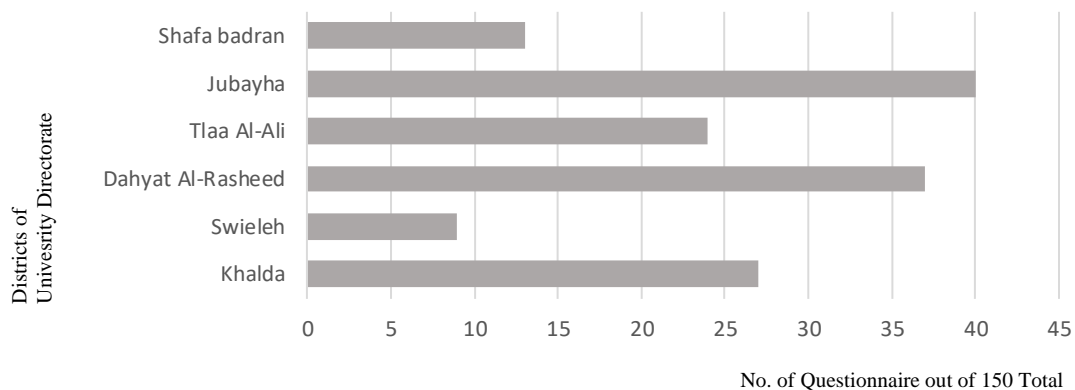
Figure 1 The number of questionnaires answered distributed over various study areas

Results related to anthropometrics and ergonomics showed that furniture inside classrooms, bathrooms, and courtyards took child dimensions into high consideration. 65.3% of participants evaluated this factor as an excellent treatment. However, this consideration disappeared regarding the protection from reaching electrical sockets; on average, 66% consider it poor treatment; this causes a high probability of danger (Table 3).

Table 3. The most critical causes of danger resulting from the built environment of kindergartens

		Very Poor	Poor	Fair	good	Excellent	Total
Q26: Treatment of doors against injury in case of a sudden close	Frequency	62	49	15	14	10	150.0
	Percentage	41.33	32.67	10.00	9.33	6.67	100%
	Mean	*2.07*					
Q19: Swimming Pool tools for emergencies	Frequency	5	8	12	55	17	97
	Percentage	5.15	8.25	12.37	56.70	17.53	100%
	Mean	*3.73*					
Q15: Furniture and toilets furniture suits children's scale	frequency	5	9	18	20	98	150
	percentage	3.3	6	12	13.3	65.3	100%
	Mean	*4.3*					
Q8: Electricity sockets are located far from children's reachability	Frequency	43	57	22	11	17	150
	Percentage	28.67	38.00	14.67	7.33	11.33	100%
	Mean	*2.3*					
Q20: The swimming pool's edges and floor are treated against slippery accidents	frequency	11	13	24	33	16	97
	percentage	11.34	13.40	24.74	34.02	16.49	100%
	Mean	*3.4*					
Kindergartens are designed to consider less-mobile children	frequency	64	34	30	13	9	150
	percentage	42.67	22.67	20	8.67	6	100%
	Mean	*2.1*					
Kindergarten is provided with alternative power supplies	frequency	73	42	15	11	9	150
	percentage	48.67	28.00	10.00	7.33	6.00	100%
	Mean	*1.94*					
Emergency exits are located in clear and appropriate places	Frequency	62	38	22	15	13	150
	Percentage	41.33	25.33	14.67	10.00	8.67	100%
	Mean	*2.2*					
Playground sharp edges are treated against injuries.	Frequency	69	51	15	8	7	150
	Percentage	46.00	34.00	10.00	5.33	4.67	100%
	Mean	*1.88*					

The results in the outdoor playing area showed an apparent deficiency in the safety treatments; the percentage of suitable treatments of exterior features against risk and hazard was 5.33% (Table 3). The answers differed about the cause of harm caused by playing in these yards to address the most critical causes of severe injuries in the outdoor yards and playing areas, which included: falling from games, falling from stairs, sharp edges in the gaming hall, wounds and fractures from falling on asphalt yards, in addition to stinging Insects in sandy yards. In addition, the results showed that allergies to trees and plants affect, to varying degrees, the health and safety of the child in kindergarten.

Table 4. The most critical causes of danger resulting from the built environment of kindergartens

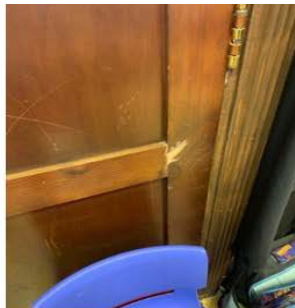| Questions about availability	No	Yes	Remarks
Are the doors handled in a way that prevents children's hands from getting hurt in case of sudden closing?	%80	%20	High Danger
Have dangerous sharp corners in the indoor environment and classrooms been treated?	%65	%35	High Danger
Are there surveillance cameras?	%35	%65	Moderate Danger
Are fire exits clear?	%67	%33	High Danger
Are fire exits located in a suitable place?	71%	29%	High Danger
Are there fire extinguishers in sufficient number and a clear place?	%45	%55	High Danger
Are children trained to evacuate buildings?	%58	52%	Moderate Danger

The last part of the questionnaire aimed to study the state of kindergartens' outdoor and indoor environments and the extent to which they fulfill the essential principles and conditions of safe and child-friendly environments. In addition, it explored the essential emergency standards and treatments for a safe-physical environment at kindergartens. Table 4 shows the most important results related to this part of the questionnaire:

Field Visits and Direct Observations Findings

Observation is used in the social sciences to collect data about people, processes, and situations. It is the systematic description of events and behaviors in a social environment. (Fry et al., 2009). In this research, direct observation was made by visiting the selected kindergartens. In addition, information was collected through interviews, observation, blogging, and photos. The concentration was on the built environment features and their effect on child physical safety. Figure 2 depicts some of the poor features of the kindergartens' observations. The total score for all of the visited kindergartens was 2.06, which indicates a bad situation and rings the bell to the kindergartens' conditions related to safe environments and child-friendly schools criteria and the required criteria.

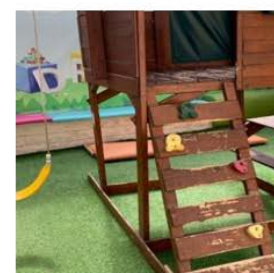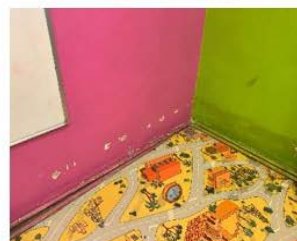|		
Uncovered radiators pipes	Dangerous sharp edges	Door with no treatment for sudden close
The dangers of exposed wires	Outdoor materials with rough finishes and sharp edges	Electricity sockets that can be reached by children
Door Steps that causes hamper	Furniture with sharp edges	Children playroom unmaintained
Untreated clomons corners	Treated corners with soft materials	Damped wall

Figure 2. Features that do not Match CFS Criteria

Interviews Findings

During the field visits, interviews were conducted with twenty-five principals, 54 teachers, and some parents. The interviews show that the level of safety and security of kindergartens in Amman is "acceptable" in general. Still, some of the studied pivots lack the minimum requirements for security and child-safety features. The interview questions were developed based on previous studies and the UNICEF manual of the CFS. Data collected from the interview participants are summarized into four main aspects: sharp edges, outdoor and landscape furniture, emergency exits and evacuation plans, and obstacles of high-cost treatments that prevent injuries and accidents. A summary of these results is presented in Table 5.

Table 5 Interviews and direct observation findings and results

			Observations
Interviews and Direct Observation Finding and Results	Sharp Edges Risk	-	Sharp edges are located at step doors, corridors, windows, furniture, and the playing area
		-	Heating pipes are uncovered most of the time
		-	Trees, playground floor finishing, landscape furniture, and plants container are poorly treated to avoid falls and accident injuries
		-	Heating must be covered to ensure the safety of children.
		-	Doors pose a danger to children if they are closed incorrectly
	Emergency Exits and Evacuation Plans	-	Fire extinguishers and alarm devices are available most of the time
		-	The location of fire exits is in the kitchen most of the time
		-	There was no concern about the dimensions and Specifications of emergency doors
		-	No fire evacuation plans were hanging in viewable places
		-	Children training for evacuation is rarely conducted
	Outdoor and Landscape Furniture Risk	-	Trees stems are covered with poor materials that need high maintenance (most of the time torn and ruined)
		-	Playground floors are unsuitable for children (asphalt, broken tiles, slippery)
		-	The playing field is not shaded.
		-	Insects and reptiles in the sandy playground (In the summer, children are often exposed to the danger of pinching by poisonous insects)
		-	Trees and plants that cause allergies are not taken into consideration
	Financial obstacles	-	Financial constraints hinder the desire of some schools to provide safe buildings that consider children's safety.
		-	Design solutions for risk considered expensive and hard to achieve

Analysis and Discussion

The previous results showed an apparent defect in understanding the child-friendly environment in most kindergartens in the chosen area. In addition, many features of the built environment appeared to be related to danger and put children at risk of injuries. Through inductive observation, there was an attempt to explain results and search for causes that turn kindergartens into risky built environments. Following is a summary of the current situations assessment and kindergartens evaluation according to the designed tool used by this research:

1. The external environment analysis showed an apparent deficiency in the treatments related to the safety of the yards and the games they contain. The percentage of the number of unsafe kindergartens was 80% of the total sample studied.

2. The analysis of the results related to the internal environment of the kindergarten showed shortcomings in the treatments related to the general safety of the classrooms according to the furniture and equipment they contain.

3. UNICEF emphasized in its manual the importance of choosing a site far from noise, pollution, main streets, and industrial areas. In comparison, the results showed that approximately 56.3% of the kindergartens did not adhere to this item and did not take into account healthy and safe sites.

4. It was noted that 68.7% of the study sample had an entrance that was not higher than the outside street level. And based on climatic changes, especially after the increase in rainfall rates in recent years in Jordan, attention should be paid to raising the level of kindergartens on the street to avoid the damage caused by the flow of rain.

5. UNICEF emphasized that Child-Friendly Schools should use trellises and trees to create shaded places to protect children from the sun's direct rays. The results showed that designed shaded areas at outdoor yards were 31.3%. At the same time, only 12.5% of kindergartens used trees for shading. It is a poor percentage and shows

an imbalance concerning the essential environmental treatments related to sunlight. Note that the trees' quality and the possibility of causing allergic reactions for children were not considered.

6. 19% of kindergartens did not consider ease of movement and freedom of movement, which is especially necessary when children scramble inside the kindergarten building. Moreover, there were many obstructing objects and furniture in the corridors.

7. Floor treatment to reduce the possibility of life-threatening head injuries is one of the most critical items to consider, whether in indoor or outdoor yards (Martinsen, 2015). However, it was noticed that the internal floors were only concerned with using rubber or foam for kindergarten floors, while the playgrounds lacked appropriate treatments. Furthermore, the percentage of asphalt coverage was 59% of the kindergartens, which is a high percentage that shows the risk of potential injuries. In comparison, only 18% of kindergartens used sand for outdoor yards.

8. Regarding outdoor toys, 10% of iron toys and 18% of mixed toys (iron and plastic) were used. This poses a clear danger to children because iron toys contain dangerous sharp corners, and iron may cause burns due to its high temperature and friction with the child's skin while playing.

9. The kindergartens contained 75% of the furniture with untreated sharp corners, which constituted an essential cause of wounds and injuries ranging from simple to severe.

10. 43.7% of the kindergartens studied suffer from moisture problems, and the presence of the child for nearly six hours a day in such environments leads to many diseases, the most important of which are various respiratory diseases.

11. 43.7% of the kindergartens studied suffer from moisture problems, and the presence of the child for nearly six hours a day in such environments leads to many diseases, the most important of which are various respiratory diseases.

12. 75% of the kindergartens did not treat the sharp corners of the columns, which posed a real danger to the child.

13. 68.8% of kindergartens had games with sharp angles and designs that posed a danger to the child while playing or jogging in the outdoor yards.

14. One of the most critical factors in child-friendly schools is the presence of ramps for people with special needs. The field visits showed that 97.3% of kindergartens do not have these ramps.

15. Emergency doors that do not open to the outside according to security and public safety requirements represented 68% of the kindergarten study sample.

16. It was noted that 56.7% of electrical sockets are within reach of children, and we can attribute this to the fact that most of the kindergartens that were visited were houses or villas that were reused as kindergartens; This situation makes kindergartens unsuitable in terms of function and environment for the child.

17. The physical aspects were sometimes an obstacle to the periodic maintenance of some treatments for the physical environment.

These solutions are considered impractical due to the need for permanent and expensive maintenance that prevents some kindergartens from achieving them.

Conclusions and Recommendations

Schools in Jordan have achieved some child-friendly school standards by 32%. This percentage was extracted from the various results and observations during the study. Therefore, it enables us to predict a real problem that must be considered and highlighted before the responsible authorities to find the necessary solutions to create a safe, healthy, and child-friendly environment.

Kindergartens should have a good quality environment to enhance children's self-confidence and create safe and free exploration spaces. However, the economic aspects hindered this in terms of the difficulty financing or sustaining maintenance of the physical environment. In addition, the prevailing idea of converting any house or apartment into a kindergarten, ignoring the special requirements and needs of such an environment, increased the risk and the rate of injuries. Figure 3 shows some of the research's suggestions to find solutions for a child-friendly environment as economical and inexpensively as possible. Through the analysis and discussion of the results, it was possible to reach proposals and practical solutions to the problems of kindergartens and the natural and built environment to create an appropriate child-friendly environment per international standards and requirements. Figure 3 shows some of these subjected solutions. As a healthy, civilized society, we must recognize the importance of preventing or mitigating danger in its many forms in childhood. In light of the results of this study, it was found that although kindergartens in Jordan are concerned with the child's safety, there are still some matters that are not concerned attention despite their importance and danger to the child's life or health. This research has tried to highlight the risks children are exposed to that result from indoor and outdoor environments at kindergarten, shedding light on conducting studies of broader scope that include other

areas of Amman and extend to all parts of the Hashemite Kingdom of Jordan. These studies must consider the child's psychological, physical, and intellectual aspects. We could benefit from these studies in developing special codes for kindergartens that take care of safety and public safety to create a child-friendly environment and find solutions to risks with intense cooperation between different authorities and official and private departments.
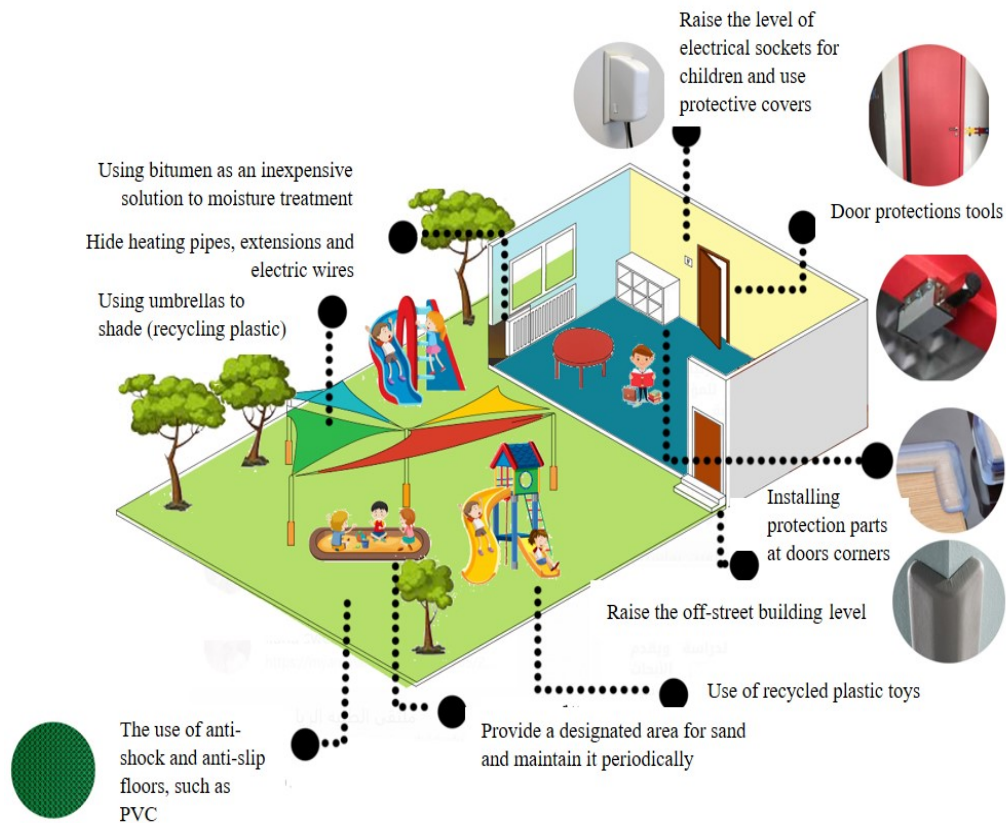

Figure 2 Economic and technological solutions to some kindergartens design shortening

There is a high need to encourage cooperation between kindergartens and the industrial sectors in the country (paper and plastic recycling companies). For example, water bottles, plastic bags, damaged plastic toys, and paper from children's waste could be collected and recycled to obtain indoor furniture such as chairs, tables, and shelves, and outdoor furniture such as outdoor toys (Figure 4). These products are low-cost, environmentally friendly in terms of their components, and child-friendly in their final finishes. The researchers also recommend expanding the circle of interest in the subject by stimulating interdisciplinary studies and research within different university disciplines to create child-friendly design and environmental solutions. Comprehensive and continuous training programs and seminars must be increased in the field of awareness of the risks that affect the safety and security of the child, that wealth The future that we are investing in since childhood for a prosperous pioneering future in all areas of life

Figure 3. The HDPE plastic is cleaned, processed, and molded into 100% recycled toys.

Believing in the Jordanian Ministry of Education in the significant role that early childhood plays, which is reflected in the family and society, it has established and equipped many kindergartens in government schools. To ensure the quality of services provided to this category, whether governmental or private, the Ministry, in cooperation with the National Council for Family Affairs, developed a proposed document, "Standards for Kindergarten Accreditation" (National Council for Family Affairs, 2016). However, after an extensive study of the criteria related to the built environment, the research found that they need more detail in some items and greater clarification, in addition to some modifications in dimensions and design ideas. This is to ensure that the best is achieved in the kindergarten environment and to formulate the future of child-friendly architecture with standards, standards, and codes that serve the nurturing environment for our children in whom we invest in building a better tomorrow.

References

Almazeedi, H. M. (2019). The impact of kindergarten on children's socio-emotional development. *International Journal of Education, Learning and Development, 7*(5), 59–70.

Anbari, M., & Soltanzadeh, H. (2015). Child-oriented architecture from the perspective of environmental psychology. *European Online Journal of Natural and Social Sciences, 4*(3), 137-144.

Canadian Pediatric Society. (2009). Health implications of children in child care centres Part B: Injuries and infections. *Paediatrics & Child Health, 14*(1), 40. https://doi.org/10.1093/PCH/14.1.40

Chen, J. H. (2013). Multiple childcare arrangements and health outcomes in early childhood. *Maternal and Child Health Journal, 17*(3), 448–455. https://doi.org/10.1007/S10995-012-1016-9

Chiam, H. K. (2008). International journal of child care and education policy. *International Journal of Child Care and Education Policy, 2*(2).

Clarke, D., Bundy, D., Lee, S., Bank, W., Celia Maier, U., McKee, N., Becker, A., Birdthistle, I., Gudyanga, S., Widdus, D., Kimzeke, M., Buckland, P., Furniss, E., Skinner, N., Guerrero, A., Haregot, A., Koopmans, O., King, E., Ulkuer, N., … Health, A. (2001). *Skills for Health*. The World Health Organization's.

Convention on the rights of the child. (1989). *Convention on the rights of the child*. United Nations Treaty Series.

Davison, K. K., & Lawson, C. T. (2006). Do attributes in the physical environment influence children's physical activity? A review of the literature. *International Journal of Behavioral Nutrition and Physical Activity, 3*(1), 1–17. https://doi.org/10.1186/1479-5868-3-19/TABLES/2

Dudek, M. (2005). *Children's spaces*. Architectural Press Elsevier.

Fry, H., Ketteridge, S., & Marshall, S. (2009). *A handbook for teaching and learning in higher education: enhancing academic practice* (3rd ed.). Routledge Taylor and Francis Group.

Kong, H., & Kumpulainen, K. (2018). Australia Singapore Evolving a Harmonized Hybrid System of ECEC: A Careful Balancing Act Respecting Children and Families A Case Study of the Finnish Early Childhood Education and Care System.

Leinonen, J., & Venninen, T. (2012). The 5th Intercultural Arts Education Conference: Design Learning Designing learning experiences together with children. *Procedia-Social and Behavioral Sciences, 45*, 466–474. https://doi.org/10.1016/j.sbspro.2012.06.583

Martinsen, M. T. (2015). Structural conditions for children's play in kindergarten. *Tidsskrift for Nordisk Barnehageforskning, 10*. https://doi.org/10.7577/NBF.1426

Mohidin, H. H. B., Ismail, A. S., & Ramli, H. B. (2015). Effectiveness of Kindergarten Design in Malaysia. *Procedia - Social and Behavioral Sciences, 202*, 47–57. https://doi.org/10.1016/J.SBSPRO.2015.08.207

National Council for Family Affairs. (2016). *Kindergarten accreditation standards*. National Council for Family Affairs. http://haqqi.info/ar/haqqi/research/معايير-اعتماد-رياض-الاطفال

Parsons, T. (1966). *Societies; evolutionary and comparative perspectives*. Prentice-Hall.

Peden, M., Oyegbite, K., Ozanne-Smith, J., Hyder, A. A., Branche, C., Rahman, A. F., Rivara, F., & Bartolomeos, K. (2008). World report on child injury prevention.

Piaget, J. (2013). *Child's conception of space: selected works*. Routledge. https://www.routledge.com/Childs-Conception-of-Space-Selected-Works-vol-4/author/p/book/9780415846462

Scherer, K., Mausner-Dorsch, H., & Kemeny, P. (2006). Surveillance-based injury epidemiology in schools in Germany. International Journal of Injury Control and Safety Promotion, 13(3), 159–169. https://doi.org/10.1080/17457300600725317

UNICEF. (2001). Innocent report card issue no:2. www.unicef-icdc.org

Watson, M., & White, J. (2001). Accident prevention activities: A national survey of health authorities. *Health Education Journal, 60*(3), 275–283. https://doi.org/10.1177/001789690106000309

WHO. (1986). Ottawa Charter for Health Promotion.

Wright, C., Mannathoko, C., & Pasic, M. (2009). *The child friendly school manual. in manual* (pp. 1–244). UNICEF Division of Communication.

Author Information

Shaden Abusafieh
Al-Ahliyya Amman University, Jordan
Amman/ Jordan
Contact e-mail: *arch_shaden@yahoo.com*

Nouran Muwahid
Al-Ahliyya Amman University, Jordan
Amman/ Jordan

Rawan Muwahid
Al-Ahliyya Amman University, Jordan
Amman/ Jordan

Lama Alhawatmah
Al-Ahliyya Amman University, Jordan
Amman/ Jordan